MIT Skywalker: A Novel Robot for Gait Rehabilitation of Stroke and Cerebral Palsy Patients
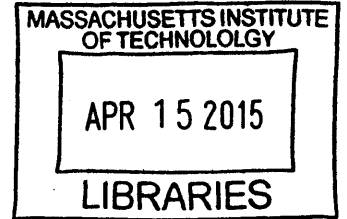
by

Tyler Gregory Susko

Submitted to the Department of Mechanical Engineering
in partial fulfillment of the requirements for the degree of

Doctor of Philosophy

at the

MASSACHUSETTS INSTITUTE OF TECHNOLOGY

February 2015

© Massachusetts Institute of Technology 2015. All rights reserved.

Signature redacted

Author...
Department of Mechanical Engineering
January 23, 2015

Signature redacted

Certified by.......................................
Hermano Igo Krebs
Principal Research Scientist and Lecturer
Thesis Supervisor

Signature redacted

Accepted by..
David E. Hardt
Chairman, Department Committee on Graduate Students

MIT Skywalker: A Novel Robot for Gait Rehabilitation of Stroke and Cerebral Palsy Patients

by

Tyler Gregory Susko

Abstract

Every two minutes, 3 people in the United States will have a stroke and every hour an American baby is born with cerebral palsy. The only method available to recover from motor impairments associated with these brain injuries is time-consuming labor intensive physical and occupational therapy. Upper extremity rehabilitation robotics is well established and recommended by the American Heart Association, the Veterans Administration, and the Department of Defense; however, lower extremity rehabilitation robots are still in their infancy, so far leading to inferior results when compared to manual methods in the only available sizable randomized control trials. Thus, there exists an urgent need for novel methods to augment gait rehabilitation. This thesis outlines the design and development of a novel gait rehabilitation robot, the MIT-Skywalker, that enables the exploration of new methods of gait rehabilitation based on current understanding of the neuroscience of motor control.

Because each patient's impairment is unique, the MIT-Skywalker system creates a flexible environment that accommodates a wide spectrum of pathological gaits. It can operate in three unique modes. The first promotes the rhythmicity of walking by removing the floor constraint during the swing phase of walking. The second mode fosters discrete start and stop movements and focuses on the accuracy of heel placement. Finally, a balance program perturbs gait in the frontal plane to engage balance mechanisms. A one-month feasibility study with the MIT-Skywalker demonstrated positive outcomes for two adults with impairments due to cerebral palsy and one person with chronic stroke and proved the safety and viability of each training mode.

Acknowledgments

This work has been my life's greatest challenge to date. It has pushed me to my limit and I was able to feel pure mental exhaustion at the end of long days or weeks but in writing this thesis, I feel much like a painter, finally able to admire a small recreation of something beautiful. I came to MIT and joined the Newman lab in search of a greater sense of fulfillment from my work, something I found to be absent in the corporate world. Not a day passed that I found myself counting hours as I used to, instead, I always felt I was chasing them. I feel proud of the work that I have done and I feel honored to be in the presence of the great minds that helped to shape my work.

First, I must express my deepest gratitude to my advisor Dr. Hermano Igo Krebs whose guidance and support enabled all of the work in this thesis. No matter how full his schedule became, he always made time to meet when I needed to vet ideas. His mentorship and candid discussions allowed me to see through the fog which seemed blinding, especially when trying to define the direction of my PhD. I truly benefited from his seemingly unending knowledge of rehabilitation robotics both technically and clinically.

Another consistent supporter and contributor to my work has been Neville Hogan. His guidance and detail-oriented criticism has made me a better engineer and his insightful teaching as one of the leaders in the field of human-machine interaction and the neural control of movement has inspired me to join this area of research. I am exceeding grateful to Professor Dagmar Sternad, whose extensive knowledge of the human motor control system planted seeds into my mind. Her one-on-one time with me over the summers helped to shape the direction of my thesis. I must also thank Professor David Trumper whose teaching built my foundation in controls from which I was able to develop the Skywalker robot. I am grateful for his mentorship and guidance, especially with the mechatronics involved with Skywalker. Last, but certainly not least, having worked as his teaching assistant, I must thank Professor Derek Rowell, from whose example of pedagogy I will eternally benefit. His unending sense of

humor wrapped around a core of brilliance inspired me to become an instructor.

I had the privilege of advising 9 undergraduate researchers (Fareeha Safir, Marta Krason, Thuan Doan, Joyce Chen, Alex Lukas, Krithika Swaminathan, Camille Henrot, Simon Okaine, and Aya Suzuki) during this project. Without their hard work and dedication, the Skywalker would never have been completed. I also would like to acknowledge Brenda Hyland-Miller for donating her time as the therapist for the participant evaluations and Mark Belanger for all of his wisdom in the Edgerton student shop. Even though I am unable to acknowledge their names in this document, I must thank the three participants that donated time to be in our study. Additionally, I must thank all of my peers that have worked with me in the Newman Lab including Yunseong Song, Hyunglae Lee, Dan Klenk, Jooeun Ahn, Mo Rastgaar, Panagiotis Artemiadis, Seung-jae Kim, Konstantinos Michimizos, Will Bosworth, Julie Ochoa, Michael Farid and Lucille Hosford for their thought-provoking conversation and collegiality.

Aside from the professional side of this thesis, this work was supported by the many friends and family that stuck by me though the long process. First, I must thank my first and current role model, my father, who never let me be satisfied with mediocrity and constantly pushed me to be my best. My mother has always been my emotional support from the day I was born. Her heart broke with mine in times of distress and rejoiced in successes and I owe her everything. I am fortunate to have the support of two sisters (Jennifer and Lori), four brothers (Chris, Jon, Dan and Drew) and wonderful second set of parents (Jim and Mary).

Finally, I dedicate all of this work to my heart and soul, my wife Dana and my son John Tyler (Butch). Dana, you are the most empathetic and selfless person I've met, putting the well-being of others far in front of your own. Your support of my work in the past 5 years has taught me the meaning of love and I could not have done it without you. We did it baby! And to my son, the silly little man, I thank you for the giggles and wubb wubbs every day to greet me. Watching you grow up has been the most joyous experience of my life.

6

Contents

List of Figures

15

17

List of Tables

21

Chapter 1

Introduction

The work outlined in this thesis describes the design and feasibility of a novel robotic tool, the MIT Skywalker, to be used to deliver locomotion rehabilitation to an adult population with a static brain injury.

Injuries of the Central Nervous System often affect the victims ability to move. This thesis is focused on two types of injuries, cerebral palsy and stroke. Cerebral palsy is a catch-all term for brain irregularities or injuries resulting in a movement abnormality that occur before the age of two. It is caused by a developmental defect or by trauma. Of every 1000 children born, 2-3 will have cerebral palsy [11], which accounts for about 8,000 cases per year in the United States. Low birth-weights are associated with much higher rates of cerebral palsy and it is postulated that as medical care is able to save more very-low-birth-weight infants, the number of surviving people with cerebral palsy will increase [12].

Stroke, like cerebral palsy, is a static (non-progressive) brain injury. Each year, 795,000 Americans will suffer a stroke and it is estimated that 6.4 million stroke survivors reside the US [13]. The prevalence of stroke increases with age and thus, as the average age in the US will increase in the next 20 years due to the baby boomer generation, so will the number of stroke victims and stroke survivors. The mean lifetime cost due to an ischemic stroke is above $140,000 and the total direct and indirect cost of strokes in the US was estimated at $73.7 billion per year in 2010 [13]. Thus the need for efficacious and economical methods to treat stroke patients is

self-evident. Presently there is a scientific thrust for pharmaceutical neuro-protection following an ischemic stroke but to date, none promote neuro-recovery [14]. Hence, rehabilitation is the only available method to attempt to ameliorate motor deficiencies associated with stroke, resulting in a degree of recovered motor abilities for most patients [15].

Rehabilitation literature associated with cerebral palsy gait rehabilitation is generally focused on minors. Very little research is available for gait rehabilitation of adults with Cerebral Palsy. Thus, rehabilitation studies presented in this chapter focus exclusively on stroke patients, however, the theory extends to adults with cerebral palsy.

1.1 Stroke Etiology and Symptoms

A stroke's etiology is limited to either ischemia or hemorrhage. The former is defined as the insufficient blood flow to the brain and the later refers to ruptured blood vessels in the brain. The primary mechanisms of ischemic stroke include an embolism (a blockage that travels to the brain, often a blood clot, fat globule or gas bubble), decreased perfusion (problem delivering blood to capillaries, often due to abnormal narrowing of an artery) and thrombosis (formation of a blood clot inside of an artery that blocks blood flow to the brain)[16]. Hemorrhages stem primarily from an aneurysm (a blood-filled bulge in a blood vessel wall) or arteriovenous malformation (an abnormal connection between arteries and veins). Ischemia accounts for between 80 and 90% of strokes while hemorrhagic strokes account for the remainder. Of the ischemic strokes, the most common mechanism is thrombosis[17].

Both etiologies of stroke result in a loss of brain cells and thus the loss of brain function. The most prevalent impairment due to stroke is of motor function (77-80% of surviving stroke patients)[18][19]. Other common afflictions include urinary incontinence, impaired consciousness, dysphagia, dementia and impaired cognition[18][20]. The motor impairments due to stroke primarily manifest in hemiplegia (right or the left half of the body will be impaired). This is in contrast to Cerebral Palsy patients

who are primarily diplegic (having symmetrical impairment primarily of the lower extremities)[21].

1.1.1 Early intervention

When a person suffers a stroke, the first step is to assess if the stroke is ischemic or hemorrhagic via a CT or MRI scan. If the patient reaches the hospital quickly after the onset of stroke, medical professionals can use emergency treatments to lessen the severity of the stroke. For ischemic stroke, this may involve a tissue plasminogen activator (a blood clot dissolving medicine) or aspirin. If the stroke was determined to be hemorrhagic, efforts will be taken to control bleeding and reduce pressure to the brain and in emergency situations, surgery will be performed to repair ruptured tissue. It is important to note that damage occurs to the brain at the onset of stroke and while these procedures are able to minimize damage to the brain by stopping the ailing agent, brain function that is affected will be lost. Once stabilized in the hospital, patients will receive some form of rehabilitative therapy until released.

1.2 Motor Function Rehabilitation Post Stroke

While common outpatient movement rehabilitation treatments vary (eg. range of motion therapy, mobility training, constraint-induced movement therapy, electrical stimulation and robotic therapy), rehabilitative treatments after stroke are efficacious for the vast majority of patients[15]. The success of stroke rehabilitation treatments lies in the brains ability to reconfigure itself after injury. In 1949, Donald Hebb outlined the concept of neural plasticity, summarized by the popularized phase, "neurons that fire together wire together", suggesting that the brain is capable of restructuring itself by altering synaptic connections [22]. Prior to Hebbs work, the brain was believed to be hard-wired, with little plastic capacity. Countless studies have corroborated Hebbs theory. Randy Nudo showed that squirrel monkeys with targeted cortical lesions affecting hand control could regain the control of the affected hand with some targeted rehabilitation training. The result of the training showed the control area

of the motor cortex for the hand expanded into regions of the brain that previously controlled the elbow and shoulder, explicitly showing the effects of plasticity in neurorecovery [23][24]. The same effect of plasticity is seen in humans post stroke by use of neuroimaging [25][26].

The mechanisms of supraspinal neural plasticity can be activated only if the proper efferents (decending neuronal signals) match the proper afferents (ascending signals from the periphery). In other words, to regain motor control, it seems that a person must attempt to send motion commands to the subcortical feedback loop in order for the network to reconnect. For effective rehabilitation, this means that patient intention plays a key role in redeveloping motor control. A patient must intend to move, activating the cerebral cortex at the same time that the movement occurs. If a limb is passively moved without cerebral effort, no motor control network will be developed and the activity will only have the benefits of stretching the muscle such as improved joint stability[27]. Successful motor rehabilitation paradigms work by gently assisting the patient to the motor goal without creating the motion for the patient[28].

1.2.1   Upper Extremity Stroke Rehabilitation

Upper extremity therapy is well established and efficacious. The benefits observed far outweigh the risks of treatment if done properly[29]. Constraint-induced movement therapy (CIMT) is one of the most straightforward and beneficial ways to treat upper extremity motor impairments due to mild stroke[30][31]. It works by constraining the non-affected limb of hemiparetic stroke patients and forcing them to use the impaired arm. Another prominent method of rehabilitation is therapist assisted movement therapy which employs the help of a therapist for movement recovery. For example, a patient will be instructed to reach to a certain location and the therapists job is to guide (but not to define) the patients movement to the location. This type of therapist assisted movement therapy was the basis for the creation of upper extremity rehabilitation robots.
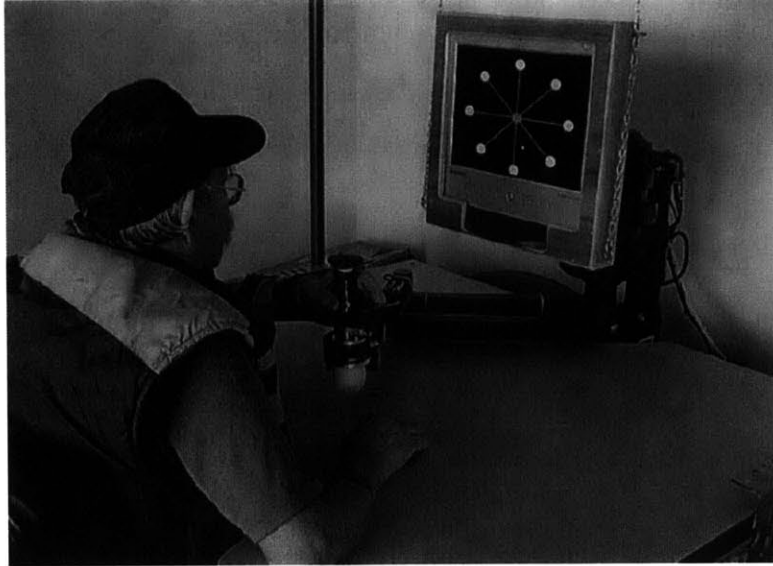
Figure 1-1: MIT-Manus: figure from [1]

1.2.2 Upper Extremity Rehabilitation Robots

The advantage of the robots lies in their ability to work without tiring. This allows patients to use the robot continuously for far more movements in a given training session than with a human therapist. In a recent study, therapist assisted UE rehabilitation sessions consisted of 23 movements in the inpatient setting and 45 movements in the outpatient setting[32]. This compares with 1024 movements in a recommended robotic session[33]. An additional benefit of robotics is real time visual feedback given to the patient during training.

The MIT-Manus is an upper extremity planar rehabilitation robot that was developed to replace the therapist in the therapist assisted movement therapy. The robot (seen in figure 1-1) uses impedance control to either assist or provide resistance to challenge a patient during a motion[1]. Performance based assistive mode uses a slot controller. When presented with a target on the screen, the computer will set up a movement slot between the current position and the final position. If the patient deviates from this slot, the robot will gently move the hand back to the slot. If the subject is not moving, the back of the slot will begin to move the joystick towards the target by moving the back of the slot. In the progressive-resistance mode, the robot

is set up to provide a force opposing the motion using an adaptive algorithm that changes with the strength of the patient. The MIT-Manus has been tested extensively with stroke patients in both the acute (< 6 months after stroke) and chronic (> 6 months after stroke) phases and has shown significant motor control improvements that have been shown to be long lasting after therapy[32][33][34].

Upper extremity rehabilitation robotics encompasses more than the horizontal plane. Interactive Motion Technologies (IMT)[1], Watertown, MA developed commercial versions of the MIT rehabilitation robots. This includes a version of the MIT-manus, called InMotion ARM, the InMotion WRIST, the InMotion Hand and the InMotion Anti-gravity. A large randomized study showed that the use of these four robots yielded motor outcomes exceeding usual care and even an intensive comparison therapy (defined to mimic operation of robots using therapists) at 36 weeks after the onset of therapy[33]. This, among other studies, leads to a strong American Heart Association recommendation for the use of robotics for upper extremity stroke rehabilitation [29].

1.2.3   Lower Extremity Stroke Rehabilitation

The overarching goal of lower extremity stroke rehabilitation is to restore gait and to allow patients to accomplish daily mobility tasks. The most popular method of treatment for locomotion impairments following stroke has changed over time. Developed by Karel Bobath, neurophysiological treatment concepts dominated the international methods by which people received therapy until the 1990s[35]. This method intended to restore the most physiological gait pattern by applying tone-inhibiting exercises and motor tasks while in a seated, standing or lying position. At the same time, a new paradigm (task-specific repetitive concepts) began to emerge. This paradigm, as applied to stroke locomotion, asserts that those who wish to walk must walk. And thus, body weight supported treadmill therapy (BWSTT) was created. BWSTT (see figure 1-2) suspends the patient in a harness over a treadmill while two therapists take their positions, one sitting adjacent to the paretic leg and the other behind the

---

[1]http://interactive-motion.com/

Figure 1-2: Body-weight supported treadmill therapy (BWSTT): figure from [2]. The picture does not depict the physical demands of the therapists, specifically the therapist on the leg of the patient.

patient. The therapist at the leg assists in the swing phase of gait to ensure initial heel strike, prevents knee hyperextension and attempts to control the symmetry of step lengths between the two legs. The therapist to the rear assists in shifting the weight properly between stance and swing phase while also encouraging hip extension and supporting the trunk. In a landmark study, Hesse et. al showed that treadmill training with partial body weight support compared favorably with the Bobath method in improving both gait ability and walking velocity[36]. Today, BWSTT is a benchmark of gait rehabilitation. A review of 21 randomized controlled trials (RCTs) showed that both gait speed and walking distance improved after gait-oriented training[37]. Increased brain activity has been observed after BWSTT in fMRI scans of stroke patients making ankle movements, indicating that the intervention has a cortical effect for stroke patients[38].

The next logical question becomes: is BWSTT the best way to rehabilitate stroke

patients to walk? The answer to this question is unclear. Meta-analysis indicated that there were no statistically significant differences between BWSTT and other interventions for walking dependent participants in multiple studies[39]. The confusion regarding the advantages of BWSTT lies in the small size and differences in protocol between all of these studies, most of which assess less than 30 patients. In order to add substance to this question, a large RCT known as the Locomotor Experience Applied Post-Stroke (LEAPS) trial was conducted. The LEAPS study was run with 408 patients across the country at multiple facilities to provide an answer to two critical questions:

1. Is a locomotion program superior to a home-based exercise (placebo) program?

2. Does sub-acute phase training provide greater results than chronic phase training?

To assess these questions, the patients were divided into three groups, an early (2 mo. post stroke) locomotor training group (LTP-early), a late (6 mo. post stroke) locomotor training group (LTP-late) and a home based exercise group (HEP-early). The locomotor training group training was meant to be the state of the art method for locomotion rehabilitation and consisted of 20-30 minutes of step training using the BWSTT method followed by 15 minutes of overground ambulation training. The home exercise program was designed to improve upper and lower extremity strength, balance while sitting and standing and coordination. It was expected to have little effect on gait speed and its design was meant such that it appeared as a credible training program with equal number of sessions and duration as the locomotor training group to avoid the placebo effect for the locomotor groups. Heart rate was determined to be equal in both types of interventions to negate the effect of exercise and intensity. Each of the groups received therapy 3 times per week for 12 weeks[40]. Surprisingly, at one year after stroke, there were no significant differences in improvement between either of the groups. 52% of all participants had increased functional walking ability. All groups had similar improvements in not only walking speed but balance and quality of life[41]. The findings dispelled common beliefs that training in the acute phase

of stroke would provide superior results to the chronic phase and more importantly showed that the locomotor training paradigm is not as well understood as was once thought. The result of the LEAPS study presents an opportunity for researchers to develop the next generation of locomotion rehabilitation therapy.

1.2.4   Lower Extremity Rehabilitation Robots

As BWSTT's popularity grew among the therapy community, interest was taken by researchers on mechanizing the treatment. The strenuous supporting movements of therapists during BWSTT spawned the development of robotic-assistive step training (RAST) devices that could offer the therapy without the occupational hazards to therapists. Two major classes of rehabilitation robots were originally developed: exoskeletons and foot plate robots.

Exoskeletons

Among the exoskeletons, one of the first and certainly the most commercially successful locomotion robot to date is the Lokomat[42]. The Lokomat (figure 1-3) uses actuators at the hip and knee to move the patient through a neurologically healthy kinematic path while walking with body-weight support. Initial clinical trials used a PD controller within a position loop of exoskeleton joint angles which strictly defined the kinematics of the limbs. This type of control ignores the activity of the human subject, thereby bypassing Hebbs law of the requirement of supraspinal interaction in motor recovery. In fact, allowing for variation in stepping has been seen to increase the kinematic coordination (defined as the consistency of intralimb movements of the paretic limb) of stroke patients[43]. Force sensors have been implemented into Lokomat and control schemes that follow the MIT Manus slot controller have been developed to implement more forgiving control architectures that allows patients to influence the timing of their leg movements[44][45]. Additionally, visual feedback has been incorporated into the system. Initial pilot studies suggested the potential for efficacy[46][47], however, two recent large multicenter RCTs that compared a Lokomat

33
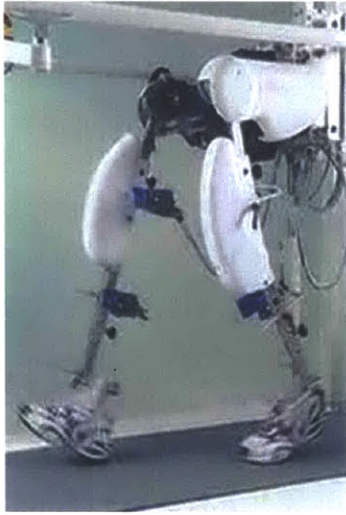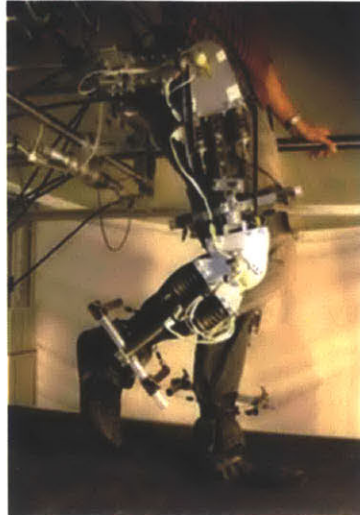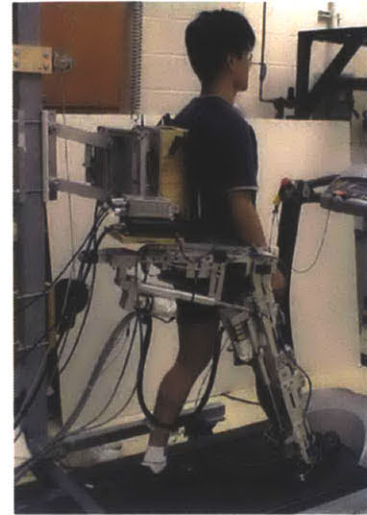
A. Lokomat   B. LOPES   C. ALEX

Figure 1-3: Exoskeletons

training group to a conventional gait training group, found the conventional group experiencing significantly greater gains in walking speed and distance that lasted at a 3 month follow up examination in both subacute and chronic stroke groups[48][49].

Other exoskeletons include LOPES[50], ALEX[51] and the HealthSouth AutoAmbulator [2]. The LOPES is the newest of these and uses series elastic actuators in an effort to apply natural feeling impedance control at the joints. There are not sufficient RCTs to properly evaluate the efficacy of these machines. It is important to note that each of these exoskeletons ignore or simply constrain the ankle, arguably the most important joint for propulsion during human locomotion.

Foot plate robots

End effector robots include Lokohelp [3], Gait Trainer I[52][53], Haptic walker[54] and the G-EO system[4][55] (figure 1-4). The later three were developed in Germany under direction of Stefan Hesse. These systems stay with the foot during the full cycle of

---

[2]http://www.healthsouth.com/experience-healthsouth/the-healthsouth-difference/leading-technology/autoambulator

[3]http://www.fysiomed.cz/eng/medical-technologies/neurologic-stimulation/lokohelp-pedago-gait-trainer/

[4]http://www.rehatechnology.com/en/home.html

A. Gait Trainer I   B. Haptic Walker   C. G-EO system
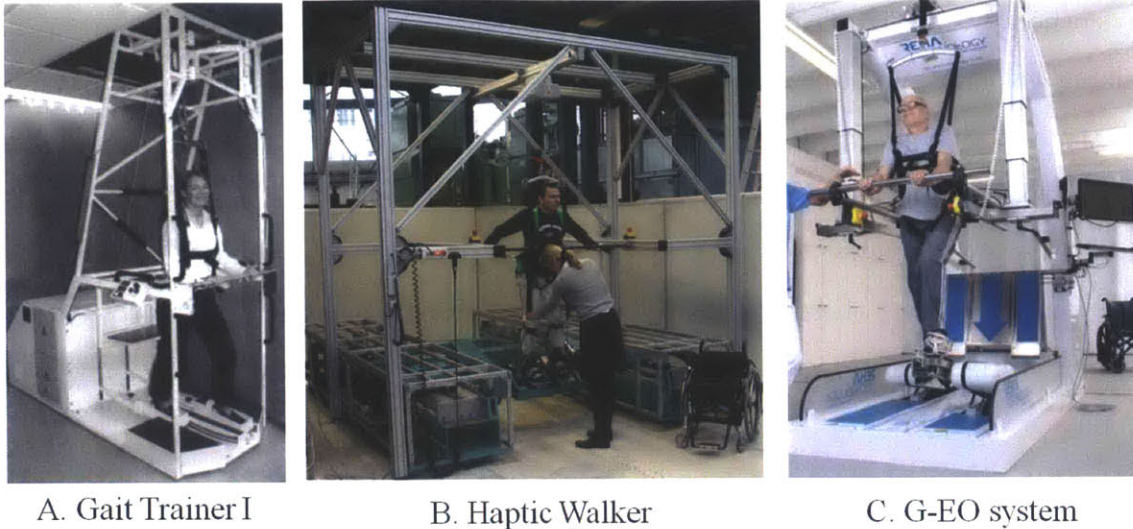
Figure 1-4: Foot plate robots

walking to simulate walking. The early systems such as the original gait trainer were directly taken from an elliptical exercise machine but since have gotten much more advanced. The Lokohelp system prescribes a motion trajectory but allows for foot contact onto a treadmill, however, it does not resemble proper heel strike. The Haptic Walker is a massive machine that allows precise control over the footplates, capable of simulating different walking parameters such as walking up stairs in addition to normal overground walking. The sheer size precluded it from use in the clinic. The G-EO system is the newest of the machines listed here and it is meant to be a smaller version of the Haptic Walker capable of being used in a medical setting and can simulate stair climbing as well as walking.

For years, there were only small patient trials using the end effector type robots[56][57], however, in 2007, the DEGAS study showed that a group receiving locomotor training with the Gait Trainer I along with physiotherapy improved significantly more in walking speed among other clinical scales over the group receiving only physiotherapy[58]. The G-EO system which was released to the public in 2010 has began the process of testing with patients. In the first patient study, thirty patients were broken into two groups. The first group received 30 minutes of training on the G-EO in conjunction with 30 minutes of physiotherapy where the control group received 60 minutes of

physiotherapy. A significantly larger improvement was seen by the robot group in walking velocity and stair climbing ability among other measures tested[59]. While this study is the first on this device, it was not randomized and the raters were team members. The authors acknowledge that a larger multicenter RCT is in order to evaluate efficacy. It is important to note that in contrast to the large multicenter RCTs done with Lokomat, these studies included physiotherapy in combination with the locomotor group. There were no large studies that compared an end effector machine vs. physiotherapy.

Other types of lower extremity robots

While the focus of locomotion robots has been on exoskeletons and end effector robots, other machines have been developed that take new approaches to locomotion therapy. Balance systems such as the CAREN have been developed to train locomotion while perturbing balance[60].

The MIT Anklebot was developed in the Newman Lab at MIT. The system can be used both during walking and in a seated position. In the seated position, an assortment of games have been developed to train dorsi-plantarflexion as well as inversion-eversion movements. As a low impedance device, the MIT Anklebot is capable of providing impedance controlled slot controller training similar to the MIT-Manus for toe pointing exercises. A pilot study showed that seated training with the Anklebot alone was enough to increase the walking speed in stroke patients[61][62]. Despite a significant weight (3.6 kg), it was shown that kinematics are only slightly disturbed while healthy or stroke subjects don the device[63]. This allows for novel methods of rehabilitation by actuating the Anklebot to modify gait via entrainment[64]. Only small studies used the anklebot while walking to determine its efficacy.

1.2.5 Potential Design Shortcoming of Current Walking Robots

Lower extremity robots seem to have been designed to follow BWSTT in an effort to decrease the heavy load on therapists. In doing so, the exoskeletons seem to violate

the most important principle identified in upper extremity rehabilitation training, the idea of self directed movements. The focus of exoskeletons is to move patients towards a hypothetical healthy set of joint kinematics and in doing so, the exoskeleton must be guided by a path (similar to the slot defined in the upper extremity robots). It is widely known that no step is identical in healthy walking, thus it is impossible to predict the exact motion and timing of the leg. Defining joint kinematics will inherently interfere with self directed movements in an unpredictable way at unpredictable phases of gait. Developing softer robots via series-elastic actuators or force feedback controllers will likely help but will always distort self-directed movement. The primary difference here between the undertakings of the upper extremity robot is that the upper extremity movements are discrete in nature, such that there is no disturbance of timing or natural rhythmic mechanisms.

Force plate robots, do not prescribe individual joint kinematics but they do prescribe heel trajectories, potentially limiting self-directed movement. Additionally, these robots stay with the foot through the whole walking cycle, disallowing an ecological swing phase and heel strike (an important afferent to walking kinematics [65][66]).

1.3 Economic Considerations

Despite a large initial investment, robots have the potential to lower medical costs associated with rehabilitation because they require less personnel resources. A large study, done with three different upper extremity robots showed greater efficacy than usual care [33] while decreasing overall healthcare costs [67]. To be economical, it was estimated that a hospital needs to recruit more than 131 patients to offset the initial investment. As technology matures and economies of scale are leveraged, the break-even point will likely decrease.

1.4 A Working Theory of the Sensorimotor Control of Walking

Human gait is an evolving field of research. We can observe kinematics, muscle activity or end effector kinetics but for the understanding of how the nervous system generates walking, we must rely on scientifically supported theories. One of the most comprehensive theories is outlined by Hogan and Sternad, asserting that sensorimotor control may be comprised of three building blocks: oscillations, submovements and mechanical impedances [68]. In order to theorize the neural mechanisms behind walking, we are interested in how the primitives combine to create discrete movements, rhythmic movements and how the associated kinetics are generated.

Discrete movements, in their most basic form, can be defined as movements with a definitive posture at the beginning and end. It has been shown that discrete movements can be further simplified as the superposition of submovement profiles[69]. Submovements are defined as a smooth sigmoidal end effector movement from one position to another. We can define $X = [x_1, x_2, \ldots, x_n]^t$ as a vector of foot positions, in a Cartesian coordinate system. Each submovement has the same speed profile $\dot{x}_j(t) = \hat{v}_j \sigma(t), j = 1 \ldots n$ where $\hat{v}_j$ is the peak velocity of the element j and $\sigma(t)$ is the stereotyped velocity profile. Combining m submovements with independent start and end times (b_k, d_k) results in a discrete movement with the speed profile defined in equation 1.1.

$$\dot{x}_j(t) = \sum_{k=1}^{m} \hat{v}_{jk} \sigma(t|b_k, d_k), j = 1 \ldots n \tag{1.1}$$

In biological systems, precise repeatability is scarce, thus our definition of rhythmic movements is quasi-periodic. Letting ϵ_j and δ represent small constants, we can define a rhythmic movement via equation 1.2.

$$|x_j(t) - x_j(t + \Delta t + lT)| < \epsilon_j \forall t, l = 0, 1 \ldots, j = 1 \ldots n \tag{1.2}$$

where T is the average period and Δt is a small deviation from T s.t. $|\Delta t| < \delta$.

Note, that these definitions deviate from [68] only for clarity. The theory further suggests that rhythmic and discrete movements are combined to form a virtual trajectory denoted by x_o such that $x_o = x_d + x_r$ where x_d and x_r represent discrete and rhythmic trajectories respectively. Anatomically, the virtual trajectory represents a time dependent set of coordinates $[x_{o1}, x_{o2}, \ldots, x_{on}]^t$ determined by the CNS. Finally, the theory holds that kinetics are determined via the interaction between the virtual trajectory (x_o), the actual trajectory (x_a) and mechanical impedances $Z(\alpha, \gamma, \theta_1, \theta_2, \ldots, \theta_n)$ as shown in equation 1.3. Mechanical impedance is represented as a nonlinear function function where α represents CNS muscle innervation, γ represents muscle spindle levels and θ_j represents the joint angles. Equation 1.3 represents the lowest order definition of force derived from mechanical impedance, in this case behaving as a spring.

$$F = Z(x_a - x_o) \tag{1.3}$$

1.4.1 Implications for Rehabilitation

When relearning to walk, highly impaired stroke patients resemble infants, using discrete steps (steps with a definitive starting and stopping point). This contrasts with healthy walking which seems to resemble pseudo-periodic oscillations (rhythmic motion). It would be easy to estimate that these two types of movement are one in the same; yet, brain scans clearly show the distinct brain mapping of these two breeds of human motion [70]. Current methods of robotic walking therapy focus on rhythmic walking but we can hypothesize that discrete stepping is a separate skill that could allow patients to develop walking in a more natural way. Furthermore, motor learning literature has shown that an adaptation to a discrete task was nearly fully transferred to rhythmic movements. The same study found that the reverse was not true, which suggests another potential benefit to discrete training [71].

1.5 Thesis Goals and Organization

The goal of this thesis is to push the state-of-the-art in robotic gait rehabilitation for stroke and cerebral palsy patients through the development of a novel rehabilitation robot. Chapter 2 examines the front-end design process of concept generation and the development of functional requirements. Chapter 3 outlines the detailed design and features of our system. Chapter 4 details the design of the power electronics. Chapter 5 explores the vision system hardware and algorithms. Chapter 6 outlines the controls and characterization of the robotic system via models, dynamic system analysis and step responses. Chapter 7 details the rehabilitation program algorithms and the results of a month long feasibility study with three patients. Finally, in chapter 8, we summarize the the thesis and make recommendations of future work based on data collected from individual training sessions.

Chapter 2

Skywalker Front-End Product Design Process

The Skywalker system is very much a product and was seen as such during the design process. This means that a full product development process was used such as the one defined in [72] with slight modifications. Specifically, the general methods for developing customer needs (or functional requirements) were unique to this product. Interviews, focus groups or observing end-users were exchanged for a literature review due to the novelty and uncertainty involved in the design.

Our goal was to define a set of user needs (see table 2.1) based on a set of scientifically grounded hypotheses. Body weight supported treadmill therapy (BWSTT) is successful just over half the time with stroke patients but as seen in the LEAPS study [41], home-based strength and balance training yields similar results. Further, it seems that exoskeletons are inferior when compared to manual body weight support treadmill training (BWSTT) [48][49]. The reasons can only be hypothesized. In determining the functional requirements of our system, we are relying on the hypothesis that balance is vital to walking and that current exoskeletons interfere with self-directed rhythmic motions.

Skywalker-γ is tasked with pushing the state-of-the-art in neural rehabilitation, thus we based our design on state-of-the-art human movement theories. Discrete movements recruit a larger portion of the brain [70] and learning is unidirectionally

transferred to rhythmic movements[71]. Additionally, some humans learning to walk (infants to stroke patients[1]) seem to take individual steps when learning to walk, so it is a reasonable hypothesis that discrete stepping is important to normal walking.

Finally, it has been said that stroke patients are like snowflakes, each is different. It is important that the system is flexible to many major pathologies of impaired gait outlined in table 2.2.

Table 2.1: Research Driven Functional Requirements

#	Research	Hypothesis	Functional Requirement
1	Exoskeleton outperformed by manual BWSTT	Exoskeletons interfere with movements	System not capable of interfering with self-directed movement
2	Plasticity Neurons that fire together, wire together	Use repetitive movements	System to match efferent and afferent signals
3	Strength and balance training = BWSTT	Balance is vital to walking	System to offer balance training
4	Discrete and rhythmic movements are distinct	Discrete movement skill vital to walking	System to offer modes to train both movement primitives
5	Many different gait pathologies	Single machine can train all pathologies	Training modes must support common gait pathologies

Table 2.2: Post stroke control impairments and resulting pathologies: collected from [8],[9]and[10]

Control Impairments	Gait Pathologies
Spasticity	Drop Foot
Selective Control	Equinovarus
Primitive Locomotor Patterns	Genu Recurvatum
Inappropriate Phasing	Stiff Knee Gait
Proprioception	Asymmetric Gait
	Balance Problems
	Slow Gait Speed

---

[1]evidence from Youtube of stroke patients and infants https://www.youtube.com/watch?v=iszPQK2_vOo, https://www.youtube.com/watch?v=qzWHgT66Tks

2.1 Skywalker-γ Mantra, concepts and specifications

2.1.1 Terminology

Skywalker-γ is the most recent embodiment of the Skywalker machine at the time this thesis is written. We refer to the device made by Bosecker [73] as the α prototype or Skywalker-α. The β prototype of Skywalker was very similar to the γ and was used for an inter-limb coupling experiment. From that experiment, it was clear that more frontal plane torsional support (section 3.3.2) was needed and once added, we chose to name the system Skywalker-γ.

2.1.2 Design of an environment

Summarizing all of the needs into a single statement, the mantra of Skywalker-γ became: to design an environment that fosters the redevelopment of self-directed movement in three distinct modes (rhythmic, discrete and balance). This mantra encompassed all user needs defined in table 2.1. The focus of the design mantra was to encourage self-directed ecological movement while minimizing interference.

Susko and Krebs [3] describe the general methods of training to fulfill each of the functional requirements (figure 2-1). Chapter 7 details the 3 modes and the feasibility study with stroke and cerebral palsy showing the flexibility of the system to train patients at different levels of impairment.

2.1.3 Concept Generation

Bosecker and Krebs developed the α prototype of the Skywalker (figure 2-2(a)) and showed its promise as a horizontal implementation of a passive walker [74] via tests with a wooden mannequin [73]. The α prototype was limited by underpowered actuators and a design that was far too high off the ground (figure 2-2(b)) for patient use, but it proved the rhythmic concept. The Skywalker paradigm (shown in figure 7-2) provided a method to actuate rhythmic walking without attaching to the limb, thus
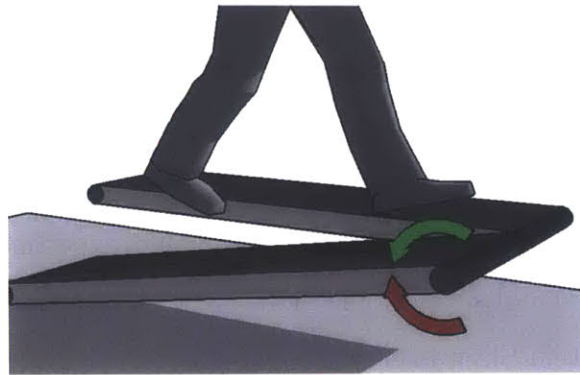
(a) Rhythmic Training

(b) Discrete Training
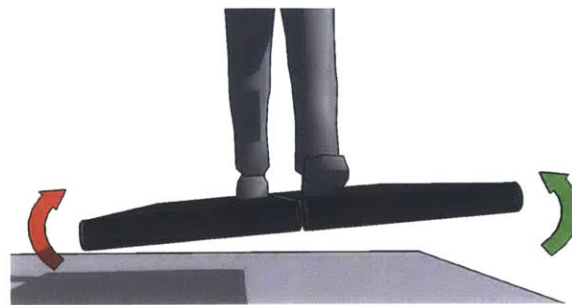
(c) Balance Training

Figure 2-1: Proposed Training Paradigms from [3]
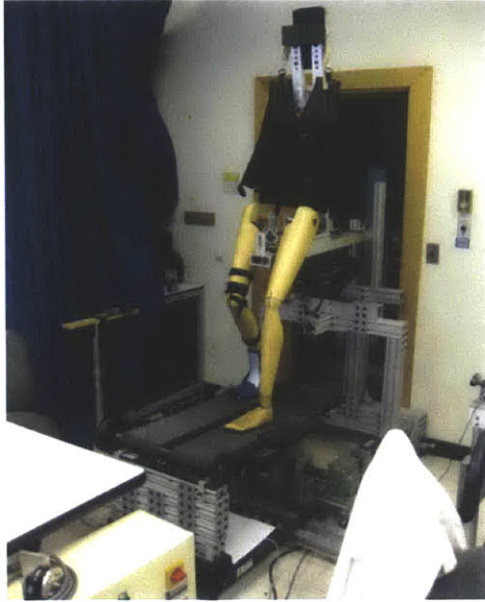
(a) Skywalker α prototype
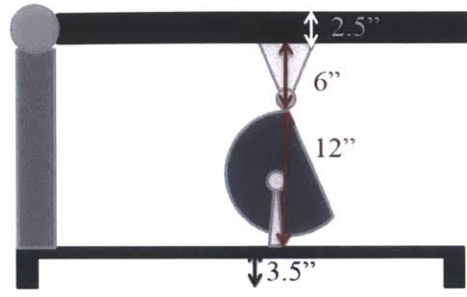
(b) Height measurements of system with radial cam

Figure 2-2: Skywalker α prototype and height measurements

being incapable of interfering with the patients' movement. In developing the next prototype of the Skywalker, we wished to use the same track-dropping paradigm.

The next task involved a look at some different configurations to produce the same dropping effect (figure 2-3). Vertical actuation was initially attractive due to the prospect of bringing the system all the way to the floor (some early concepts seen in figure 2-4). The crank-rocker concept had the advantage of being able to conserve energy through a continuous movement. The lever concept was ultimately chosen because it was a tested design with the α model and had the advantage of lower vertical velocities during heel strike with higher vertical velocities and accelerations during toe-off as a consequence of the foot positioning in relation to the fulcrum.

Once the lever configuration choice was made, actuation methods were considered (see figure 2-5). Skywalker-α used a radial cam which led to a system that was too high off the ground. For this reason, I considered locating the actuator outside of the tracks (see figure 2-5). This solves the height problem but induces a significant frontal plane moment (figure 2-6(a)). In order to exploit the available geometry, I considered having a wedge move underneath the tracks (figure 2-6(b)). The wedge

Vertical Actuation   Rocker   Lever

Linear Joint

Actuation

Rotational Joint
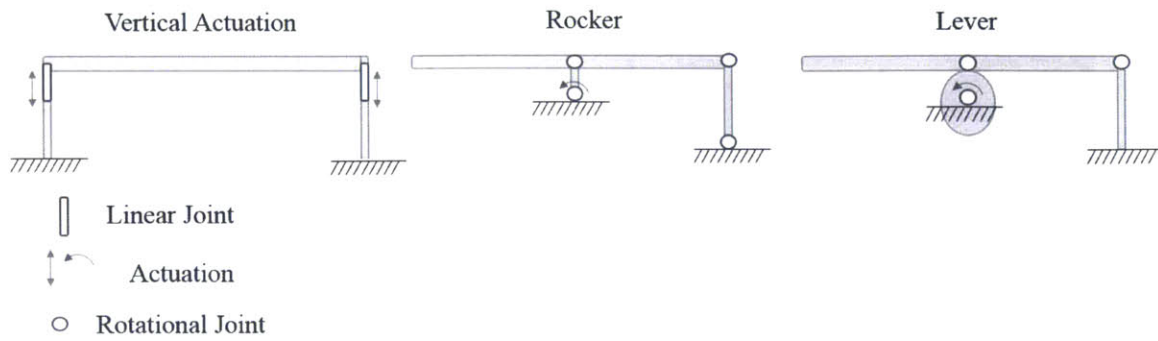
Figure 2-3: Concepts for track dropping
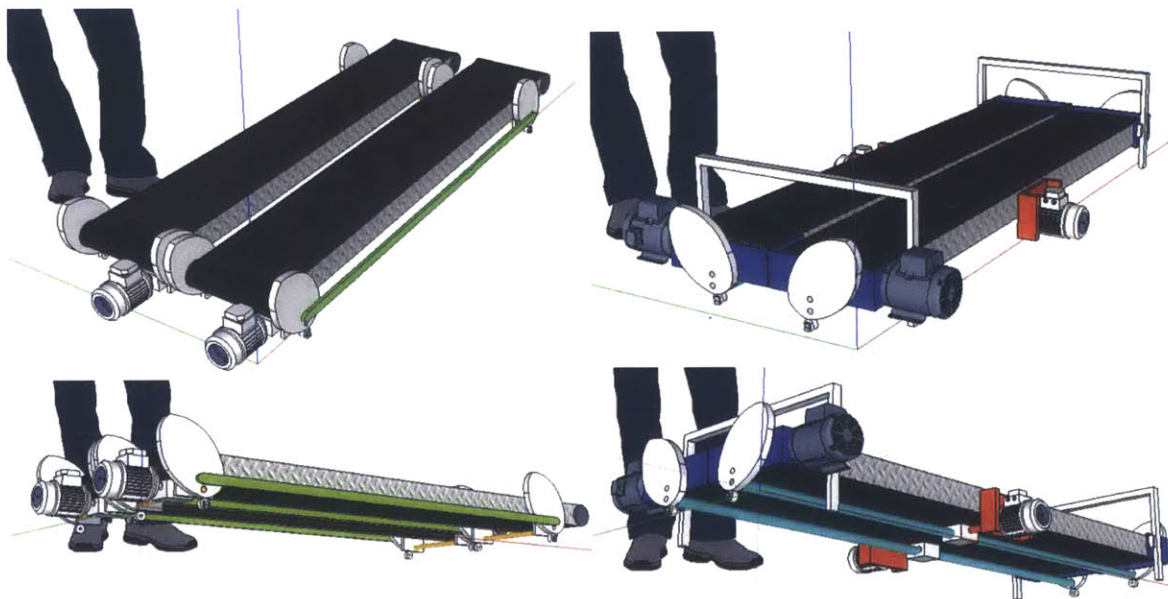
Figure 2-4: Vertical Concepts
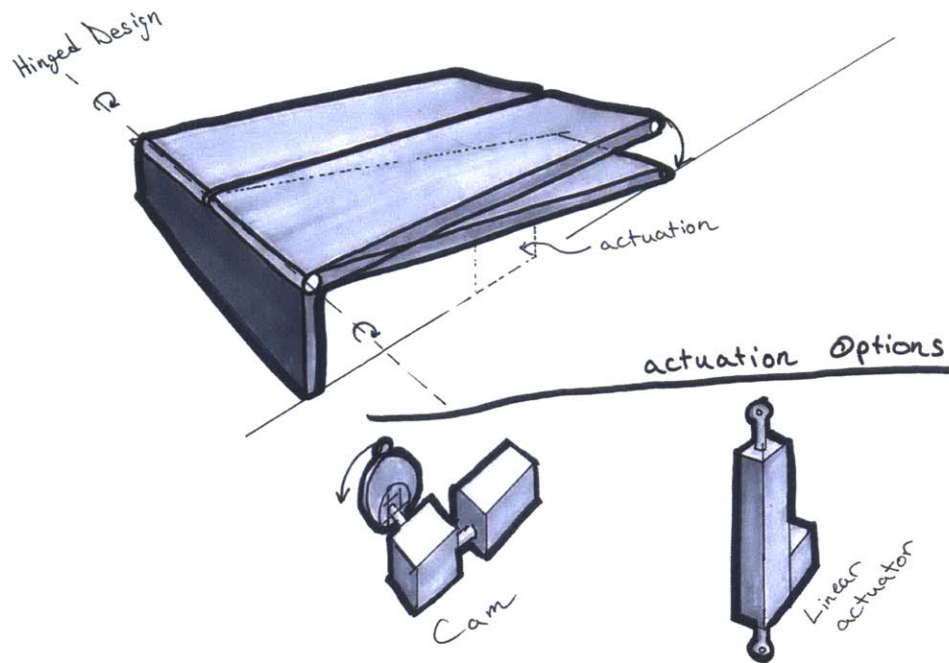
Figure 2-5: Outside actuation options

allows us to solve both the height and moment problems by fitting within the space provided by the system in both the horizontal and fully lowered position. The wedge idea fully developed into a linear cam drive as shown in figure 2-7.

2.1.4 Target Specifications

The specifications set for the new design in comparison to the measured final Skywalker-γ parameters are shown in table 2.3. Skywalker-α had a maximum drop of 1.5 inches underneath the foot after it was modified with its final trilobular cam, which operators noted as being too shallow. The new maximum drop specification for our machine was set at 6 inches to attempt to accommodate the 95% man [75] with healthy knee and hip kinematics [76] and drop foot (limp ankle angle found to be 40 degrees in a small lab experiment of healthy subjects), as seen in figure 2-8. Equation (2.1) represents the necessary track drop (d) in this extreme case. During our feasibility study, outlined in chapter 7, we never needed to drop more than 2.6" underfoot (defined as the medium drop in figure 7-3).
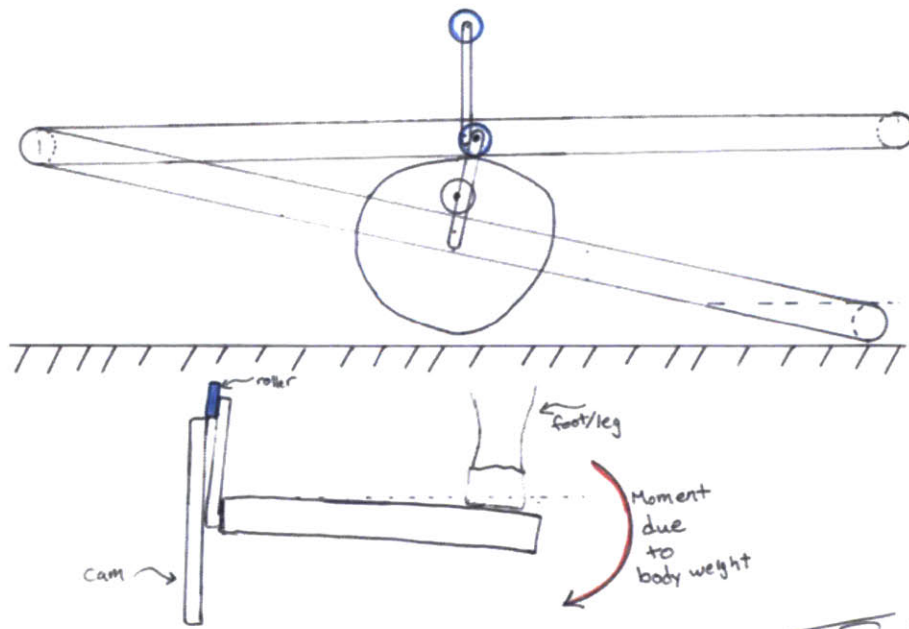
(a) Radial cam with raised roller
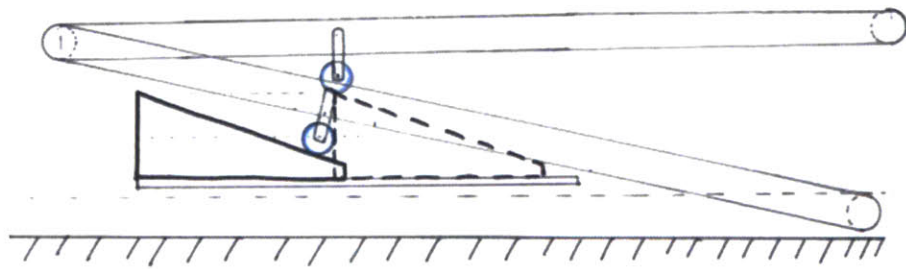
(b) Initial wedge drawing

Figure 2-6: Cam Exploration
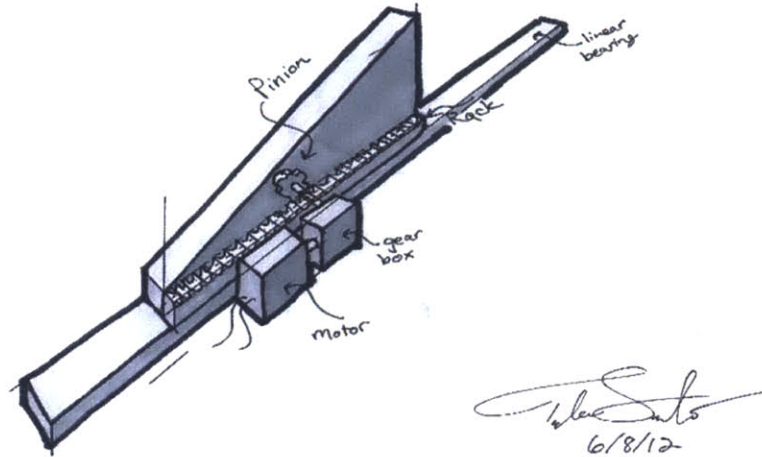
Figure 2-7: Linear cam drive sketch

$$d = 36.4 + 12sin(40) - [18.4cos(15) + 18cos(40) + 12sin(57)] = 5.84 inches \quad (2.1)$$

Table 2.3: Skywalker-γ specifications

Metric	Design Specifications	Skywalker-γ measurements
Treadmill Tape Width	20	20
Treadmill Tape Length	60	59.5
Distance Between two tracks	1.9	1.8
Low Sagittal Plane drop	6	6.15
Low Sagittal Plane angle	11.3 degrees	11.6 degrees
Hi Sagittal Plane angle	2	1.82
Hi Sagittal Plane angle	2.7 degrees	2.5 degrees
Frontal Plane max angle	5 degrees	6 degrees
Time from horizontal to low position	0.2s	0.2s
Time from low to horizontal position	0.2s	0.2s
Frontal Plane horizontal to 5 deg and back	0.5s	0.45s
Minimum Treadmill Speed	0.2 mph	0.05 mph
Maximum Treadmill Speed	2 mph	4 mph

Artemiadis and Krebs first published the idea of adding a vertical displacement to the leg prior to swing [77] and Osaki [78] shows that the toe raises approximately 2 inches in the early swing phase. The desired drop and return time was chosen to

49

15°

18.4 in

36.4 in

18 in

25°

8 in ·17°

d

12 in 40°
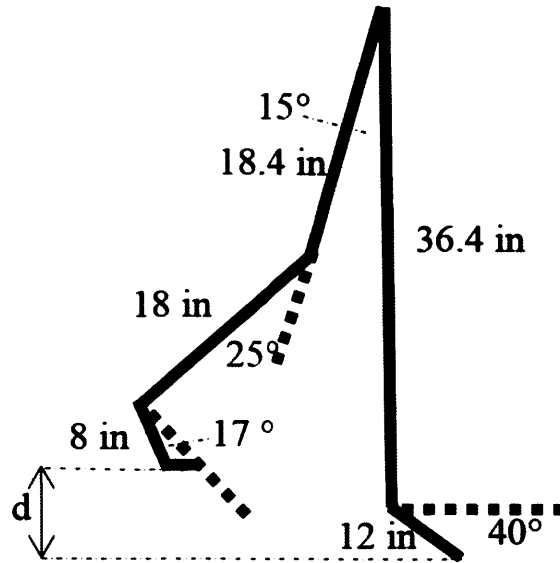
Figure 2-8: Diagram to calculate drop depth specification

be 0.4 seconds because this is the approximate healthy swing time. The minimum treadmill speed was selected to be as slow as possible to support slow discrete steps and the maximum treadmill speed was selected to be faster than healthy treadmill walking (self-selected treadmill speeds are between 2-3 mph for healthy subjects).

Skywalker-α is 40" in length, which made subjects wary that the foot would exceed the treadmill surface. For this reason, it was desired to create a much longer surface. The most common treadmills on the market measure 60" in length and 20" in width and because we wished to use a standard treadmill belt, each track was made to be the common size. In a future design of Skywalker, I recommend a 55" long, 18" wide track if the belt can be easily purchased.

As a long term vision, the Skywalker would allow patients in wheelchairs to ascend Skywalker's tracks from the rear with a wheelchair (figure 2-9). The American disabilities act[2] requires curbs and doorways to be at a minimum width of 32" which will allow access for most wheelchairs. Spacing between tracks was minimized to 1.8" and thus the standard sized treadmill tapes provide a surface that is much wider than the disabilities guideline for wheelchair access and in fact will accommodate even the widest wheelchair on the market. Section 3.2.2 details the design of the treadmill

[2]http://www.ada.gov/regs2010/2010ADAStandards/2010ADAstandards.htm

50
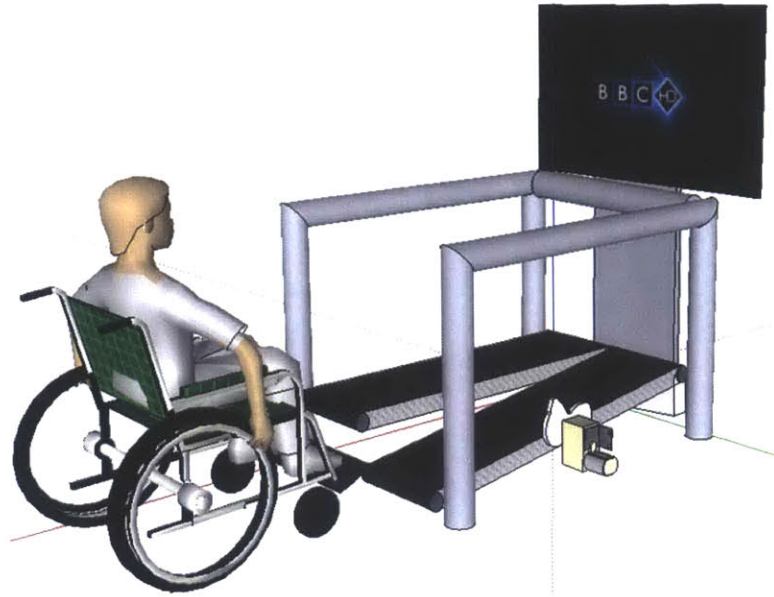
Figure 2-9: Wheelchair access to hinged system

motors. Care was taken to ensure that the treadmill motor torque was sufficient to carry a person to the top on its sharpest incline (11.6 degrees).

The toe off occurs at about 30cm behind the center of the gait or 41.8 inches behind the axis of rotation. Thus, as a specification, we may determine the High sagittal plane angle to be $\arctan(2/41.8) = 2.7 degrees$.

The frontal Plane range of motion (ROM) was chosen as a feasible degree of rotation with the geometry of the rest of the system. The Skywalker's ROM does not match the 18 degrees of the CAREN[60] system but is capable of both disrupting balance and creating a noticeable tilted walking environment.

2.2 Body Weight Support Design

2.2.1 Functional Requirements

The body weight support became an important piece of the system design. Typical body weight support systems support the patient from above (see figure 2-10(a)[3]).

---

[3]Biodex Medical Systems, Shirley, New York http://www.biodex.com/physical-medicine/products
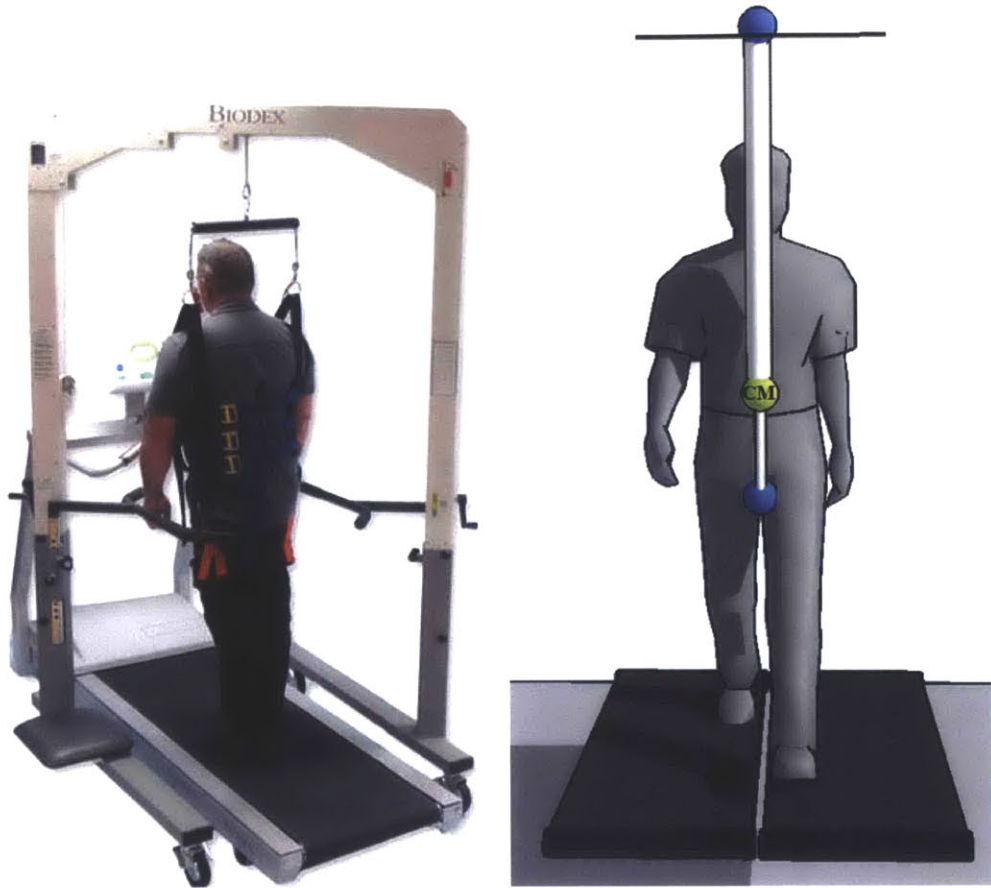
(a) Typical overhead body weight support   (b) Desired point of support below the center of mass (from [3])

Figure 2-10: Body weight support concepts

This type of support violates our design mantra by creating an artificially stable condition. If the person is to deviate by any angle, the overhead support creates a stable pendulum. For this reason, we developed a design target to support the weight in a location that would maintain the natural inverted pendulum type dynamics of the standing human (seen in figure 2-10(b)). Of course, for safety, a separate device is needed to prevent falls. We set the maximum patient weight at 300 pounds for the design of the body weight support and the Skywalker and attempted to work with a 1.5 factor of safety.

(a) Stroke patient using the body weight support

(b) Detailed BWS seat

Figure 2-11: Body Weight support features

2.2.2 Design Concept

The Skywalker body weight support system was completed by a series of undergraduate researchers (specifically, Fareeha Safir, Marta Krason, Thuan Doan, and Simon Okaine) under my supervision. All machine design calculations and models can be found in Simon Okaine's undergraduate thesis (June 2015). This section will serve to explain its function and overall structure rather than to detail structural calculations.

Figure 2-11(a) shows a stroke patient using the body weight support system during training. Notice that the vest fits loosely. Its only function is to catch the subject in the event of a fall. A more detailed view of the seat can be found in figure 2-11(b). The harness adjusts at the top to accommodate different heights. Body weight is unloaded on a bicycle seat (rigidly attached to a shaft) which rides on a spring. The motion of the seat shaft is guided by a linear bearing. The seat is allowed to vertically translate and can rotate around the shaft axis. A linear potentiometer tracks the position of the seat shaft, thereby creating a spring scale. The displacement readings can be interpreted as a force due to the linear relationship via the spring constant (112 pounds/inch). The subject is held onto the seat with a standard seat belt.

2.2.3 Structure

Figure 2-12(a) shows the sagittal plane view of the body weight support. It was important that the seat shaft and the back support maintain a vertical position, so that readings from the potentiometer represented true force being offset from the participant and to ensure comfort. A linear actuator is used to adjust the vertical position of the boom, thereby increasing the preload on the spring (equal to the force being offloaded from the subject). The data wire feeds into the PXI control box as an analog signal between 0 and 5 volts to relay the information to a real time display as the system is adjusted.

The linear actuator [4] utilizes a lead screw type of transmission. The nut serves as the actuator carriage and sits below the boom. There is no rigid connection between the actuator carriage and the boom. The boom simply rests on the carriage. Linear bearings installed on the rear end of the boom resist the moment generated from the subject's force multiplied by the distance to the fulcrum. Detailed calculations were done to ensure the moments could be supported by the bearings. Transverse plane moments are offset via the two t-slot linear bearings on either side of the linear actuator (see figure 2-12(b))

2.2.4 Operation

Operation is very simple. The linear actuator moves at a single (very slow) speed and is operated by the black remote control seen in figure 2-12(b). The remote control contains only two buttons, up and down.

2.2.5 Modifications

During the study, our most severe participant (P2) used two canes to walk on the machine. His canes did not allow us to drop the tracks because the drops would perturb his canes as well. For this patient, we added hand rails (see figure 2-13(a)). The hand rails simply slide into the vertical back support brace for easy setup. Tennis

---

[4]Firgelli Automations FA-450-TR-24-30 `www.firgelliauto.com`

54
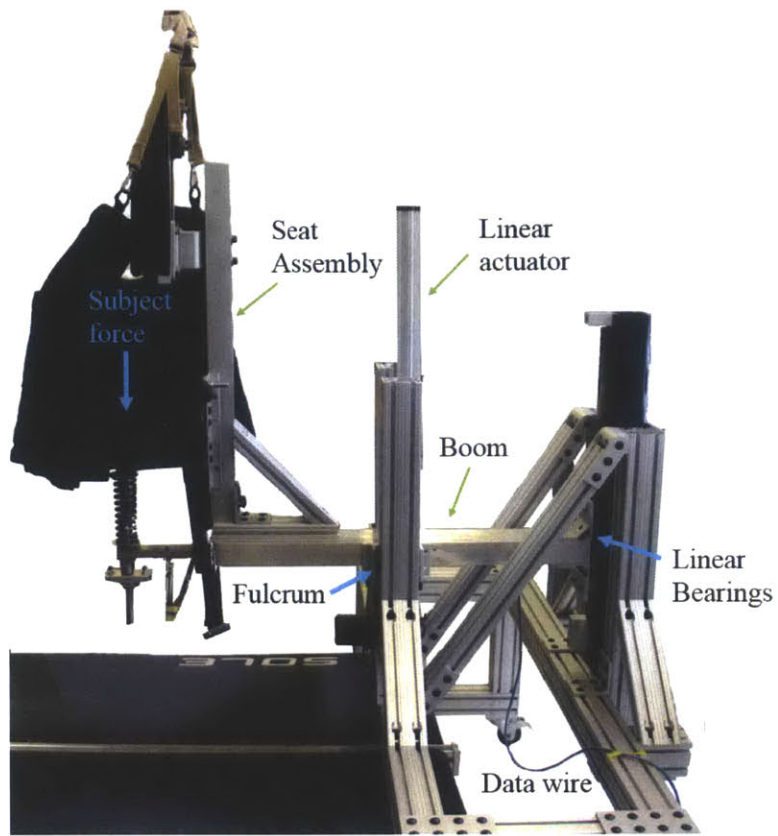
(a) Body weight support structure
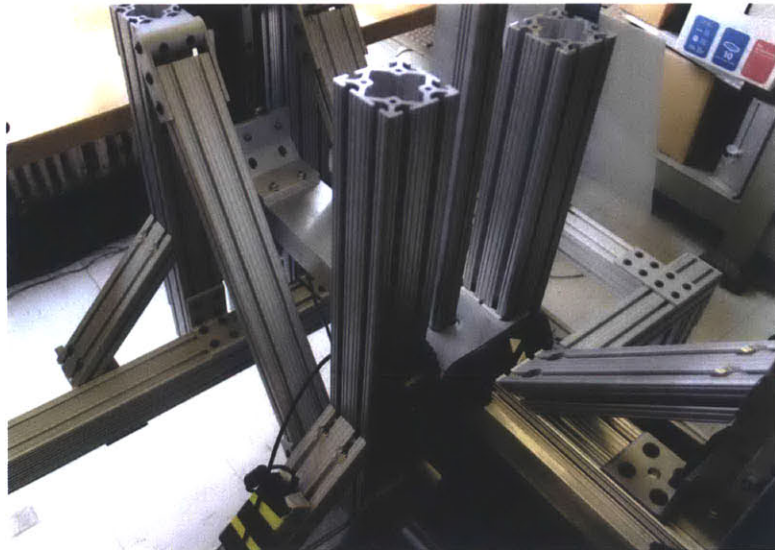
(b) View of vertical control and transverse supports

Figure 2-12: Body weight support structure

(a) Body weight support with rails   (b) Rail assembly with tennis tape
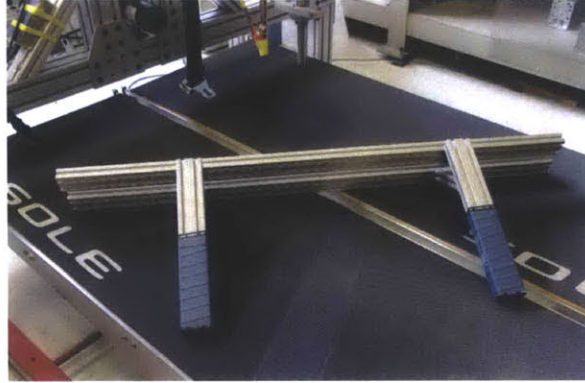
Figure 2-13: BWS rails

racket grip tape was used to pad the ends of the hand rails (figure 2-13(b)). Before installing the tape, P2 complained of the bare aluminum hurting his hands. The tape solved the problem.

2.2.6 Kinematics changes induced by the BWS system

2.2.7 Patient feedback

An exit survey was given to our study participants. The full survey documents can be seen in appendix F. We asked participants to rate the body weight support on comfort and to assess the ease of mounting the robot.

P2 rated the body weight support as a 2 of 5 citing that it elicited spasticity for him. Our stroke patient (P3) rated the comfort a 3 out 5, neither finding it comfortable or uncomfortable. Our least impaired individual (P1) found it to be extremely comfortable.

Mounting the device was a problem only for P2. Mounting should be considered on the next version, focusing on the most impaired patients.

Chapter 3

Skywalker-γ Detailed Machine Design

3.1   Skywalker Mechanical Configuration

3.1.1   Frame

Figure 3-1(a) shows a full view of the Skywalker frame. All red pieces are made of steel and are powder coated to prevent rust. The frame is bolted together using a series of thick aluminum brackets. Slots allowed for the adjustment of members to give freedom to adjust the location of the ring gear seen in figure 3-1(c). The front ring gear is bolted to the frame and was chosen to provide the desired 90:1 gear ratio for the frontal plane drive. A custom fabricated partial circle ring gear costs three times that of the standard full ring gear chosen, and while we could cut the ring gear, the look of a full ring gear was pleasing and cutting hardened steel is not trivial. Plastic shields were laser cut to prevent injury on the exposed gear teeth. A notched shaft was press-fit into the front of the frame to mount the front-end bearing of the base assembly (figure 3-2(b)).

Two heavy duty cam-followers (figure 3-1(b)) were attached to the rear of the frame to support the rear end of the base assembly (figure 3-2(c)). Removable aluminum track rests (figure 3-1(d)) support the tracks in the lowest position to allow

(a) Full frame view

(b) Cam follower

(c) Front frame view showing ring gear, pressed shaft and aluminum brackets

(d) Rear view showing the removable track rests
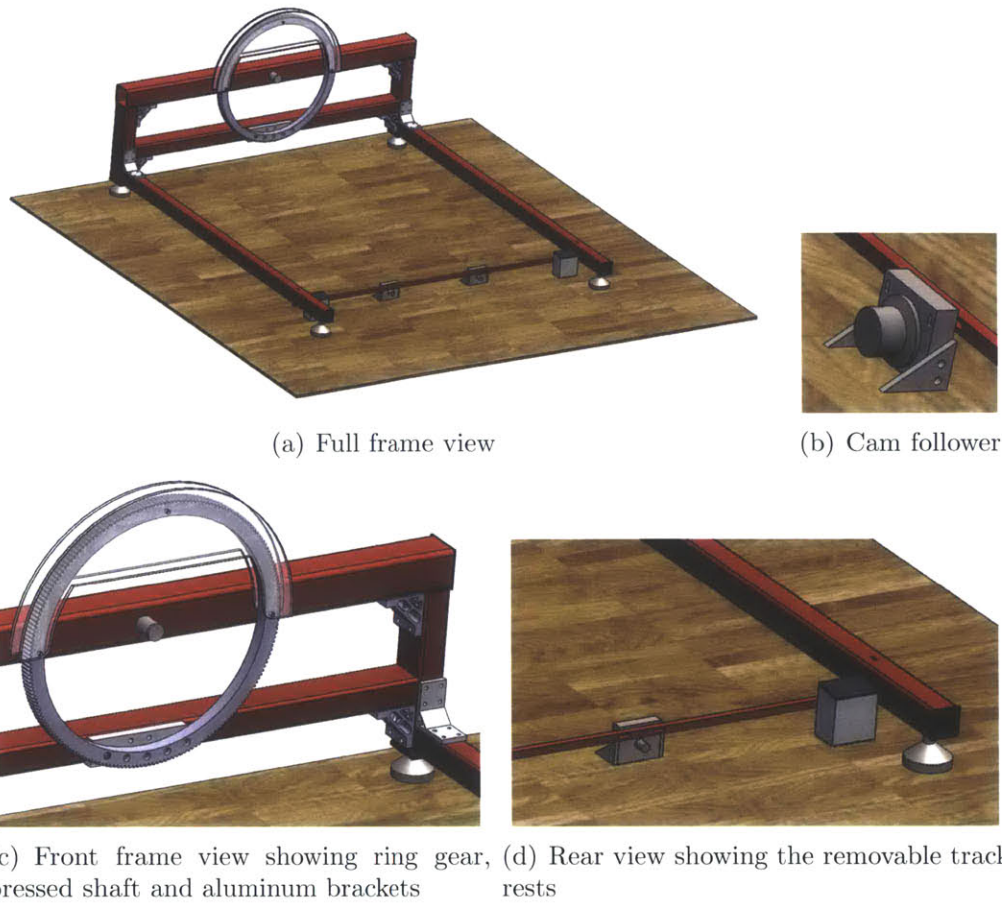
Figure 3-1: Frame CAD images

the system to convert into a ramp for patients to mount the machine from the rear as shown in figure 2-9.

3.1.2 Base assembly

Figure 3-2(a) shows the base assembly attached to the frame. The parts encompassing what we term the base assembly include all 5 motors with appropriate pinion gears or pinion pulleys (for the treadmill transmission belts). The belts, seen in figure 3-2(b), are J-section V-ribbed belts which mate with the standard front rollers used in the track assembly and provide proper torque and speed requirements for our use [79]. Figure 3-8 shows a close up of the motor-belt interaction and details the method used for tensioning the belts. The sagittal plane motors (which actuate the track drops)

are fastened to mounting plates. A helical pinion gear is pressed onto a keyed shaft. To ensure even greater hold, a radial mechanical clamp is used to further clamp the pinion gear onto the shaft. Helical gears offer quieter motion and higher load capacity when compared to straight cut gears [79]. Linear bearing guide rails are fastened to the outside of the base plate to locate the linear bearing carriages that are attached to the linear cams (figure 3-3(c)). Figure 3-2(b) highlights the front bearing that mates with the frame shaft and the pinion gear of the frontal plane actuator. The frontal plane motor is attached to a 10:1 planetary gear box. The pinion gear is pressed onto the gear box's output shaft. This gear mates with the large ring gear on the frame.

The rear end of the base assembly (figure 3-2(c)) shows a partial circle. This arc rests on the frame's cam followers to support frontal plane motion. The virtual center of the arc aligns with the center of the front bearing to ensure frontal plane system alignment.

3.1.3 Sagittal plane actuation assembly

Figure 3-3(a) shows the linear wedge assemblies installed on the base assembly. The linear wedge is fastened to a helical rack gear. FEA was conducted on multiple designs of the wedge. Thinner wedges with the cam path cut through the wedge was attractive because it lowered the weight, however, the FEA showed stresses above yield for loads occurring during quick drop profiles. For this reason, the wedge was made slightly wider with material that closes the back of the cam path. Figure 3-3(b) shows the sagittal plane motors mating with the rack. A clear view of the linear bearing carriages (in green) can be seen in figure 3-3(c). Notice here that we also introduce a torsion restraint linkage that mounts behind the motor. The purpose of this linkage is to resist frontal plane torques that are created when subjects load the inner portion of the treadmill. It attaches to the center support beam of the treadmill assembly (figure 3-4(c)). Without these linkages, there is noticeable frontal plane rotational deflection on the tracks with a 150 pound person loading the center of the track. When installed, the deflection is unnoticeable. Detailed design and calculations for the linear cams and linkages can be found in sections 3.2.3 and 3.3.2.
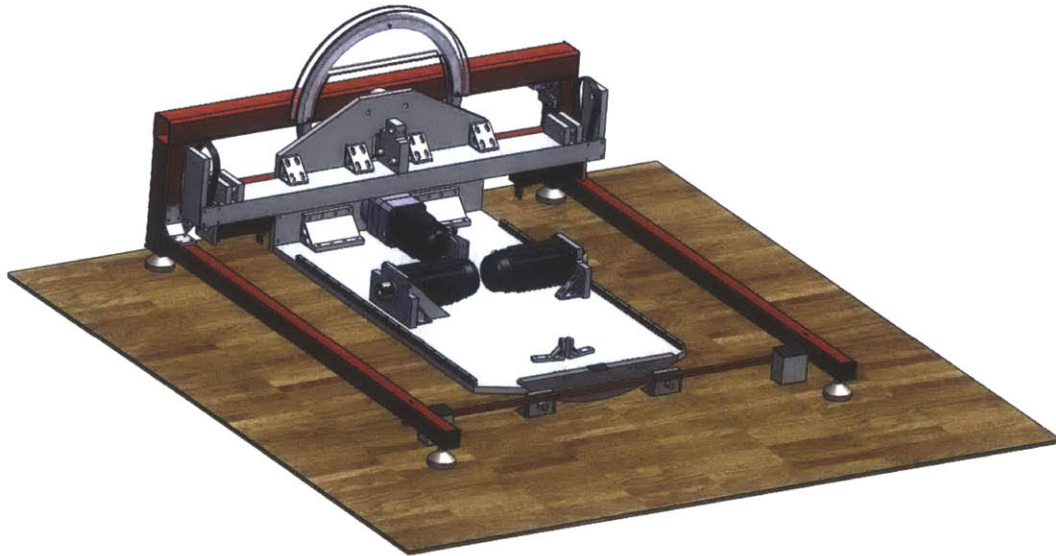
(a) Base assembly mounted onto the frame
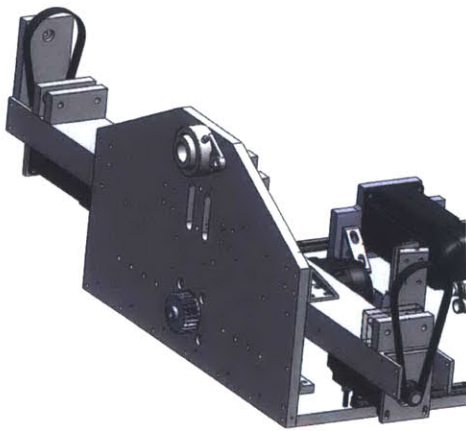
(b) Front end of the base assembly
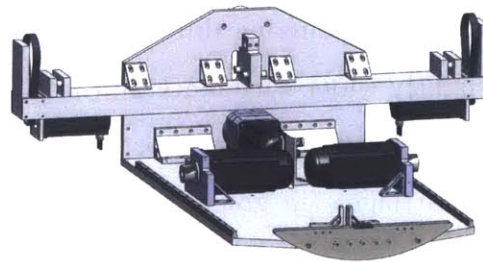
(c) Rear view of the base assembly

Figure 3-2: Base assembly
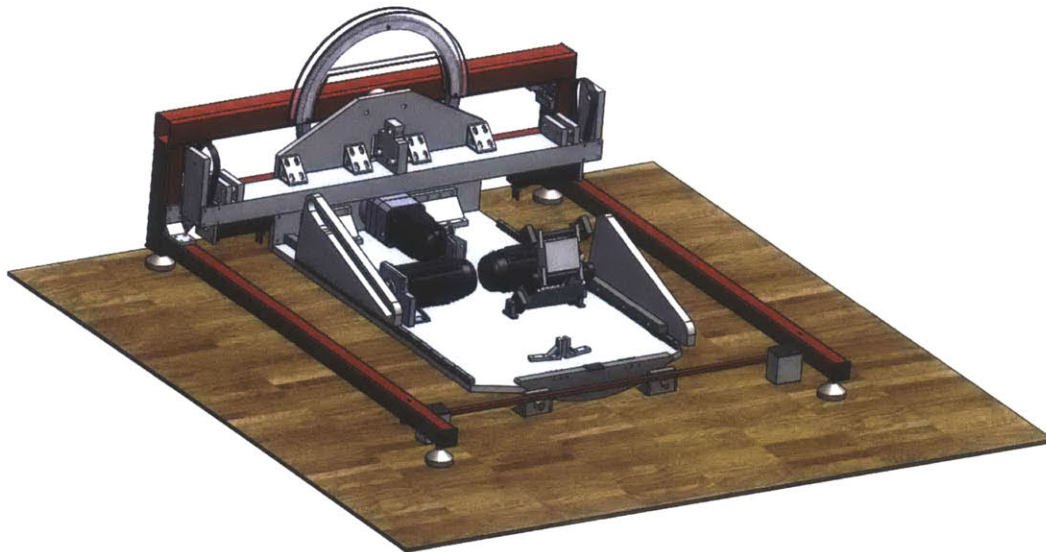
(a) Linear cam assemblies and one torsion restraint linkage assembled to the Base assembly
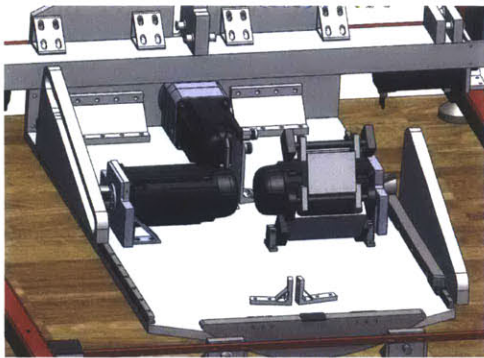
(b) Rear view
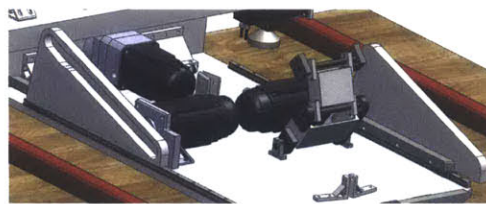
(c) Side view

Figure 3-3: Sagittal plane actuation assembly

3.1.4 Tracks

Completing the Skywalker assembly, the tracks are added to the model as shown in figure 3-4(a). The treadmill tracks are custom built. Unlike standard treadmills, the Skywalker treadmills must be as light as possible to accommodate high accelerations during the sagittal plane motion. The only standard part on this treadmill is the front roller. Standard treadmill frames are made of steel and the decks are made of a 1" thick type of particle board. The Skywalker's track frame is constructed of 6061 aluminum and the deck is made of 3/4" thick Okoume (a light type of hardwood plywood). The Okoume track weighs only 15 pounds per deck, which saves 2 pounds over the standard Oak and Birch plywood sold at common home improvement stores. To obtain a smooth, low friction surface, a piece of adhesive-ready Teflon was laid over the Okoume. The Okoume track was cut on a CNC router to ensure the necessary tight tolerance, within 0.020".

The front of the track employs "offset" bearings, 1/2" thick pieces of stainless steel that are carved with slots that are concentric with the axis of the front rollers. Graphite impregnated journal bearings fit inside of these slots and form the hinge. This configuration was chosen to minimize the width of the track assemblies, due to the design specification limiting the space between the two treadmill tapes.

To improve frontal plane rigidity, aluminum cross-members were inserted to the underside of the treadmill tracks to "close-the-box" and increase the second moment of area of the structure in the frontal plane (figure 3-4(b)). The central beam transfers most of the subject's weight to the base assembly via the cam follower. The central beam also mates with the torsional restraint linkage. This beam was studied with FEA (seen in figure 3-33) because of its importance to the structure of the system.

The treadmill tape tension is adjusted by two screws that set the position of the rear roller similar to a standard treadmill.
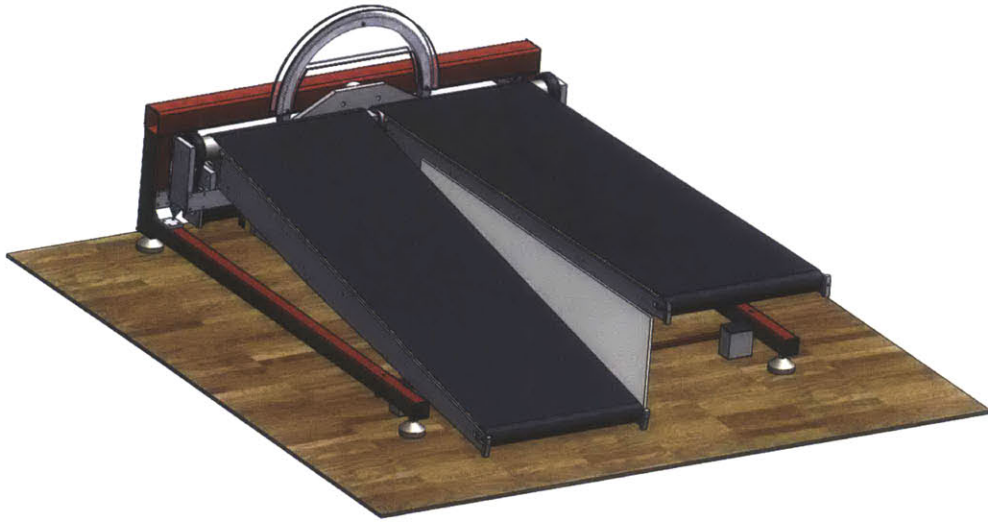
(a) Full assembly with tracks installed onto the base and actuation assembly
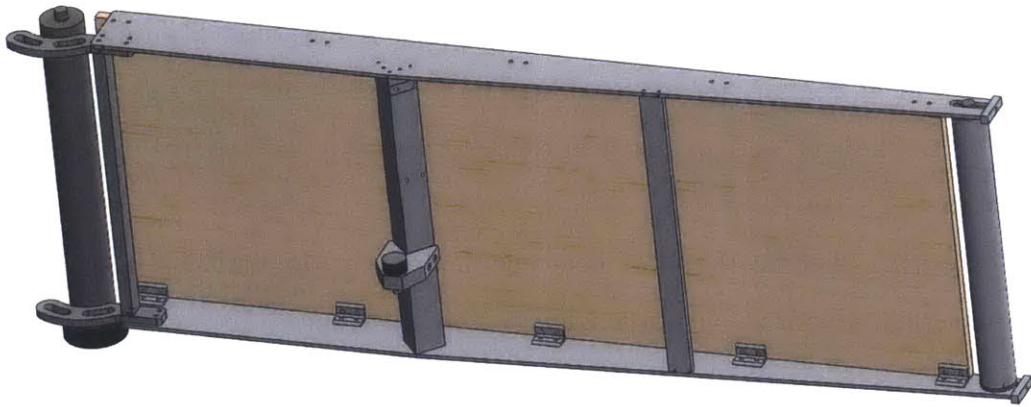
(b) Track structure without treadmill tape
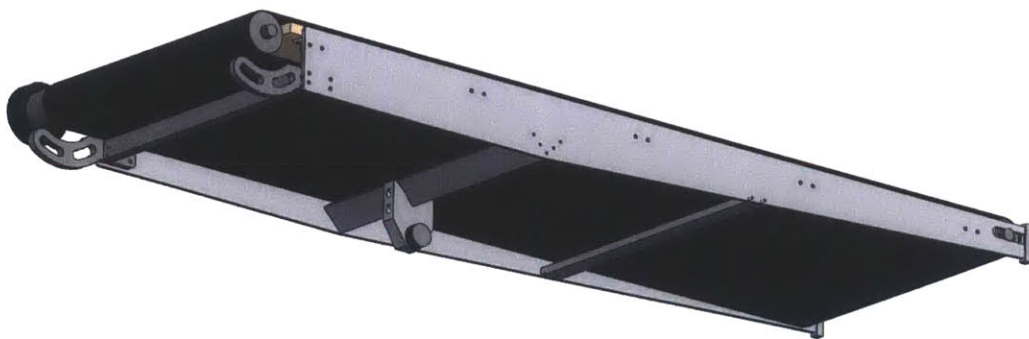
(c) Treadmill tape installed

Figure 3-4: Treadmill track assemblies

3.2 Mechanical Drive Design

3.2.1 A Generalizable Mechanical Drive Design Guide

We will define a mechanical drive as the combination of a mechanical transducer and a transmission to create useful motion for a given mechanical design application. The Skywalker-γ uses servomotors as the mechanical transducers and uses cams, gears and pulley systems as the transmissions. The following section details the full design process taken to determine proper motor specifications for Skywalker. A large portion of this thesis focuses on the design of Skywalker-γ and thus, the learnings encountered along the way will be documented. In popular mechanical engineering design textbooks, there is little or no information on designing mechanical drives [80, 81]. The best book I have found in this area is Precision Machine Design by Slocum [82] but it is really meant for designing machine tools. The following method is easier to implement and will enable the selection of a mechanical drive for most applications.

In developing specifications for a mechanical drive, the end goal is to generate three quantities: required output torque (τ), angular speed (ω) and their product, power (P).

$$P = \tau * \omega \tag{3.1}$$

The output of a machine may very well be translational in which case:

$$P = F * v \tag{3.2}$$

The process below was used to design of each drive in Skywalker-γ and can be adapted to many other machines in order to define these three important specifications.

Determination of Drive Specifications

1. Generate a rough conceptual model (a drawing, a physical model, CAD, etc.)

2. Think through the major types of mechanical impedances present

   (a) Masses or rotational inertias are the easiest to consider because they are easily measurable, linear time invariant and predictable. If masses are the only impedance present or they are dominant during normal operation, simulations can be run with masses only.

   (b) Stiffnesses are the next simplest impedance that may exist. If a design has a spring in it, chances are that there will be a published spring constant. If there is a flexure, CAD packages can be used to estimate the stiffness. Once the stiffnesses are known, the parameters can simply be added to a simulation.

   (c) Damping components can be simple to estimate if the item is a precision damper but friction is nearly impossible to estimate without access to materials and running conditions. If a system has a significant amount of friction, testing should be done to simulate the environment. Section 3.2.2 illustrates an example of determining the force of friction via tests with a standard treadmill.

3. Consider external loads.

4. Create an analytical model OR in cases of high friction, generate a test, remembering that the end goal in either case is to determine the desired output torque, speed and power.

Drive Selection

The system drive selection is often an iterative process, but iterations can be limited if the designer considers first the types of transmissions available and suitable for use before looking at transducers. This will give the designer certain limits to then browse mechanical transducer options. The drive selection process should look as follows:

1. Search through transmission options (it is recommended to engage in a concept generation / concept selection process such as the process described in [72].

Specific questions specific to transmissions are:

(a) Can the system tolerate backlash? If not, consider preloaded, friction or other commercially available transmissions as outlined in [83].

(b) How much force and at what speed must the transmission operate? This information should be now available from the specifications developed above.

(c) What are the geometrical constraints? Drawings and models help to understand space.

(d) Does the machine need to be backdrivable?.

2. Generate limits of transmission ratios available from the chosen solution(s). It will then be possible to define limits that the transducer needs to operate within.

3. Search for acceptable transducers

(a) Mechanical transducers all have a torque-speed relationships. In brushed electromechanical motors, this relationship is often inverse and linear. Brushless motors, however, can have an intermittent duty zone, shown in figures 3-7, 3-14, and 3-25 during which max torque is available. Based on the transmission ratios being considered, choose a motor that can output more than the desired Torque / Speed requirements at all required operating conditions. It is generally recommended that chosen motor power stays at least 25% higher than the specification value [82].

A Note on Brushless Servomotors and Motor Drivers

When designing a servo system, it is important to consider not only the motor but also the motor driver (see section 4.1.1). Each driver will operate with a bus voltage or in other words, the DC voltage accessible by the motor. Skywalker-α was flawed because the design was done without consideration of this voltage, thus the drive was speed limited by the back EMF generated during motor operation. The motor specs were assumed at the listed value of 640 Volts when only 60 Volts were accessible by the motor [73]. The motor bus voltage accessible by Skywalker-γ's motors reads 324

+/- 0.5 VDC. All motor curves were generated using this voltage and the current limit of the selected motor drivers. Without these considerations, the designer can be creating something that will not perform as expected.

Skywalker Motors and Transmissions

All motors used in Skywalker are from the Kollmorgen AKM series of servomotors[1]. Motors for the sagittal plane and frontal plane actuation were chosen based on simulations (section 3.2.3 & section 3.2.4). The treadmill track motor requirements were established by studying a Sole F80 treadmill as seen in section 3.2.2. The process outlined in section 3.2.1 was used to determine the proper transmission requirements of the system. In a commercial version of Skywalker, consideration may be taken to study the efficiencies but for the purposes of a prototype machine, it was omitted.

3.2.2   Treadmill Drive

Specifications

In determining specifications for a treadmill motor, simulation is a fairly difficult method to use because estimating friction in a treadmill belt is challenging and friction is a large component of the system impedance. The following procedure was a based on experiments and commercial motor data. A Sole F80 treadmill[2] available in the lab was studied to generate the treadmill motor specifications. It is equipped with a large 3hp brushed dc motor with a sizable flywheel attached to the output shaft (see figure 3-5(a)). The reason for the high power motor is that these treadmills are equipped to support running up to 12mph. The treadmill was run in a loaded condition (160 lb adult walking on the belt) and an unloaded condition at various speeds while monitoring the voltage and current reaching the motor. Current and voltage data was recorded using a magnetic current probe and a voltage probe. The

---

[1]AKM series motor information available at: www.kollmorgen.com/en-us/products/motors/servo/akm-series/akm-series-ac-synchronous-motors/akm-series/

[2]Treadmill specifications available at www.soletreadmills.com/treadmills/f80-treadmill-2013

RMS value of the data was computed by a Lecroy Waverunner LT224[3] oscilloscope. The data is shown in the table 3.1. The peak amperage was always approximately 1.5x the RMS value during loaded condition tests.

Table 3.1: Sole F80 test data at various track speeds

Treadmill Speed (mph)	Voltage (V)	Unloaded RMS Current (A)	Loaded RMS Current (A)	Loaded RMS Elec. Power (W)	Loaded RMS Mech. Power (W)
0.5	5	7.5	15	75	63
1	10	9.0	16	160	127
2	20	9.75	17.5	350	276
3	30	10.5	17.5	525	428
4	40	11	20	800	638

The Sole treadmill motor was marked and thus discoverable online as a motor from Ya Cheng Electrical Engineering Co.[4]. The Ya Cheng motor curve can be seen in figure 3-5(b). The motor curve shows a value of torque at each level of current, however, knowing the speed of the motor, the level of torque that is shown in figure 3-5(b) would be creating mechanical energy so it is unusable. In order to tease out the estimated torque from the motor, first electrical power was computed using the recorded voltage and current and equation (3.3). The electrical power for each track speed is listed in table 3.1.

$$P_e = V * I \tag{3.3}$$

It was then possible to convert the electrical power into mechanical power by using the efficiency curve at the specified current level in figure 3-5(b). While we know the motor diagram is incorrect, these charts usually embellish actual behavior. Being that we are concerned with the amount of torque being delivered by the motor, using a high value for the efficiency (η) will give us a conservative number for the mechanical power and thus a high torque estimate. The last column in table 3.1 shows the estimated mechanical power in the system using equation (3.4).

---

[3]Specifications can be found at http://www.tequipment.net/LecroyLT224Specifications.html

[4]Curve taken from http://yacheng.imb2b.com/
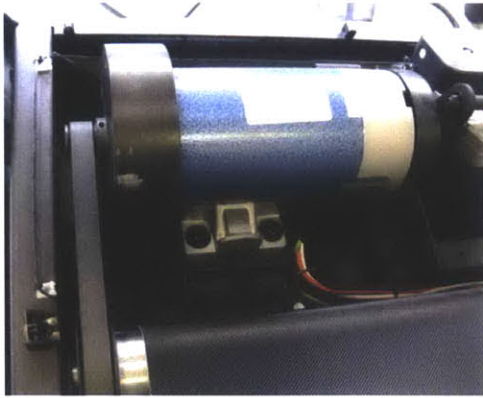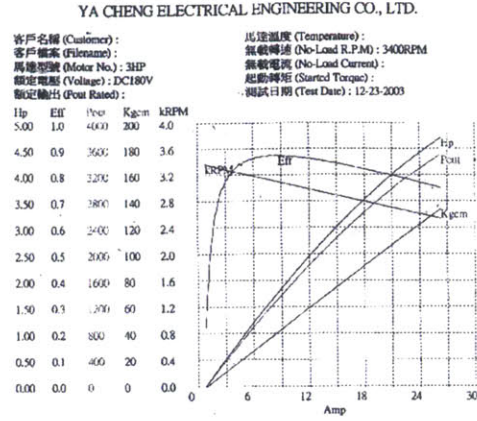
(a) Sole F80 drive   (b) Published motor curve

Figure 3-5: Ya Cheng 3hp motor

$$P_m = \eta * P_e \tag{3.4}$$

It was determined that the front roller of the Sole F80 would be used in Skywalker and thus the output power of concern was the speed and torque at the front roller (seen in figure 3-5(a)). The speed of the roller was computed by using a stopwatch to time 60 rotations of the front treadmill roller. Speed of the front roller (ω_r) was simply:

$$\omega_r = 2 * \pi * 60/t \tag{3.5}$$

Finally, now that we have speed of the front roller and the mechanical power of the system, the roller torque (τ_r) was calculated as:

$$\tau_r = P_m/\omega_r \tag{3.6}$$

As a simplification, the belt transmission was assumed to be 100% efficient being that belts typically have 98% efficiency. The mechanical power, speed and torque at the front roller of the treadmill are shown in table 3.2. Peak torques were assumed to be 1.5x the RMS torque value because peak current was 1.5x the RMS current level.

The system max speed specification (table 2.3) was originally set at 2mph. The

69

Table 3.2: Front roller speed and torque requirements at various treadmill speeds

Treadmill Speed (mph)	Mech RMS Power (W)	Roller Speed (rad/s)	Roller Torque (Nm) RMS/Peak
0.5	63	6.1	10.3/15.4
1	127	12.3	10.4/15.6
2	276	24.5	11.3/16.9
3	428	36.8	11.6/17.4
4	638	49.0	13.0/19.5

summary of the drive specifications can be seen in table 3.3.

Table 3.3: Treadmill drive design requirements at the front roller

Mech Power RMS/Peak (W)	Roller Speed (rad/s)	Roller Torque RMS/Peak (Nm)
276/414 peak	24.5	11.3/16.9

Transmission Design

The majority of standard treadmills use a belt transmission from the motor to one of the treadmill rollers. Some medical grade treadmills such as the Woodway [5] are chain driven, but for the purpose of Skywalker, weight was a driving factor and thus a belt drive was chosen. The transmission ratio (R) of belt transmissions can be approximated by equation (3.7) where D_m refers to the diameter of the motor pulley and D_r refers to the front roller pulley diameter. However, in a real belt system, it is necessary to use equation (3.10).

$$R = D_r/D_m \tag{3.7}$$

D_r is fixed because Skywalker will be using the Sole F80 front roller. The variation in the transmission ratio arises from only the motor pulley. Figure 3-6 shows the geometry of the drive. The belt needs to fit between the vertical struts of the front beam and thus the motor pulley has a maximum diameter of approximately 50mm. The lower limit of the motor pulley was defined by Machinerys Handbook[79] as 0.8 inches, however, due to the motor shaft size, the minimum outer diameter of the

---

[5]medical.woodway.com/gait_rehab/

70
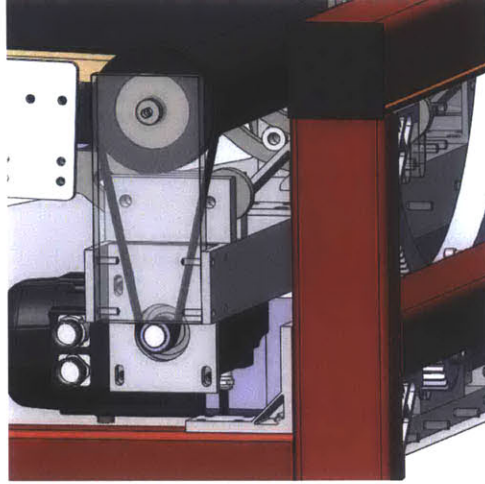
Figure 3-6: Skywalker treadmill drive

motor pulley was deemed to be 1 inch. Table 3.4 shows the limits of the transmission ratios based on these constraints.

Table 3.4: Max and min treadmill transmission ratios

	Motor Pulley Diameter (mm)	Transmmission Ratio
R_m max	50	2:1
R_m min	25.4	3.93:1

In systems that require absolute precision in track velocity, the belt system has caveats. Both the ribbed V-belt and the treadmill track belt have viscoelastic properties. The treadmill track feedback occurs at the motor and not the track, thus small errors in velocity may be present in the belt during load. See section 6.3.1 for a more detailed look at the treadmill dynamic system analysis.

Now that the range of transmissions is specified, it is possible to define a maximum speed and maximum torque condition for a motor. Table 3.5 outlines these two conditions. Equations (3.8) and (3.9) are used to define the motor torque and velocity specifications.

$$\tau_m = \tau_r / R \tag{3.8}$$

$$\omega_m = \omega_r * R \tag{3.9}$$

Table 3.5: Range of motor specifications

	Transmission Ratio	Motor Torq RMS / Peak	Motor Speed
Max Speed Condition	2:1	5.7 Nm / 8.5 Nm	49 rad/s = 468 RPM
Max Torque Condition	3.93:1	2.9 Nm / 4.3 Nm	96 rad/s = 917 RPM

The next step is to find a motor that can operate within the ranges listed in table 3.5. Most motor charts use RPM as a measure, thus it is a nice unit to use when specifying motor velocity.

Motor Selection

The sole F80 motors were certainly powerful enough to run Skywalker-γs tracks, however, their minimum speed was 0.5 mph on the Sole treadmill. It was never tested but, in general, brushed motors have a problem when operating at low speeds. This is due to friction and relatively coarse commutation. To use this motor for track speeds below 0.2 mph, the transmission ratio would need to be increased. However, this would mean decreasing diameter motor pulley below feasible dimensions or using another front roller, both of which were unattractive options.

Brushless Servomotors can operate at low speeds due to their precise field direction and high resolution feedback. Skywalker-γ's treadmill tracks were therefore actuated using the Kollmorgen AKM43E servomotors originally used to actuate Skywalker-α's sagittal plane motion. These motors fit the requirements to drive the treadmills. Their small size was also seen as an advantage. Figure 3-7 shows the motor curve for the AKM43E using the P-003006 Kollmorgen motor driver.

The AKM43E motor can far exceed the speed specification but the transmission ratio must be chosen carefully to support the required torque. Therefore, a transmission was designed near the maximum torque condition. A motor pinion was custom designed to mate to the AKM43E output shaft. The minimum outer diameter (D_m) for the motor pinion was specified by the manufacturer at 1. The transmission ratio was experimentally observed at 3.72 because the pitch circles of pulley system also includes half of the belt thickness that lies outside of the pulley OD (δ). This is not to be confused with the thickness of the belt. Because Skywalker uses ribbed v-belts,

72
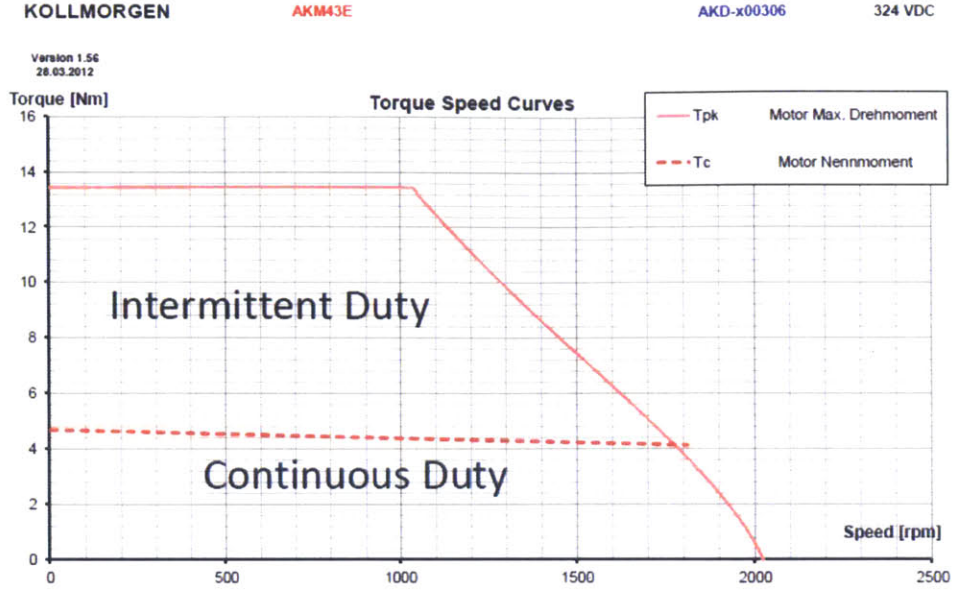
Figure 3-7: Kollmorgen AKM43E servomotor with the AKD-P00306 motor driver

the groves that protrude into the pulley do not add to the pitch circle. The pulley increases the diameter of the pulleys by 4mm and thus the calculation becomes:

$$R_{actual} = (D_r + \delta)/(D_m + \delta) \tag{3.10}$$

It is then possible to determine the motor to track transmission ratio (R_{mt}) by equation (3.11) , where r is the radius of the front roller. Ultimately, the value of R_{mt} was validated experimentally to be 102 radians per meter. Theoretical torque estimates were taken from figure 3-7 and equation (3.12) was used to estimate output linear force capabilities (f_t) of the treadmill track. The efficiency (η_b) is estimated at 0.98 for both the treadmill track and the transmission belt. δ_{tread} is the treadmill belt thickness.

$$R_{mt} = (R_{actual})/(r + \delta_{tread}) \tag{3.11}$$

$$f_t = \tau_m * R_{mt} * \eta_b^2 \tag{3.12}$$

With the 3.72:1 transmission ratio, the Skywalker treadmill belts are theoretically

73

capable of supporting the following parameters as seen in table 3.6.

Table 3.6: Skywalker treadmill theoretical performance

Performance Metric	Theoretical Performance
Continuous RMS torque at roller	16.4 Nm
Peak torque at roller	50.0 Nm
Peak speed at roller	51 rad/s
Peak torque at roller	50.0 Nm
Peak speed of the treadmill track	4.14 mph
Peak motor torque	13.4Nm at 9A
RMS motor torque	4.7 Nm at 3A
Peak force of the treadmill track	1312N
RMS force of the treadmill track	460N
R_{mt}	102 rad/m

Other Belt Drive Design Considerations

In all belt drives, there needs to be a method for tensioning the belt while still being able to assemble the whole system. In some applications, belt system designs incorporate mechanical tensioners that either use weight or a spring to apply tension. In other systems, such as treadmills, tensioning the belt requires some sort of mechanical advantage, usually via a screw. Figure 3-6 shows the belt / motor interaction point on Skywalker. In order to apply tension, the motor is fixed to its mounting plate that surrounds its output shaft. It is then slid into the main front beam and is loosely attached to the upper two holes (highlighted in blue in figure 3-8). The belt is placed into the correct groves and then the assembler can raise the rear of the motor in order to assemble the lower two mounting holes. In doing so, tension is created in the belt. Slots were cut into the mounting plate so that the motor height could be adjusted, thus applying the correct amount of tension on the belt, which was determined to be approximately 35-40 lbs at installation of a new belt. That tension settled to 30 lbs after a few months of use as the belt stretched out. The tension was tested with a HMC belt tension gauge[6]. The level of tension was acceptable for continuous running of the AKM43E motor bearings which are rated to run with up to 112 lbs of radial load.

---

[6] Additional information at www.hmc-international.com
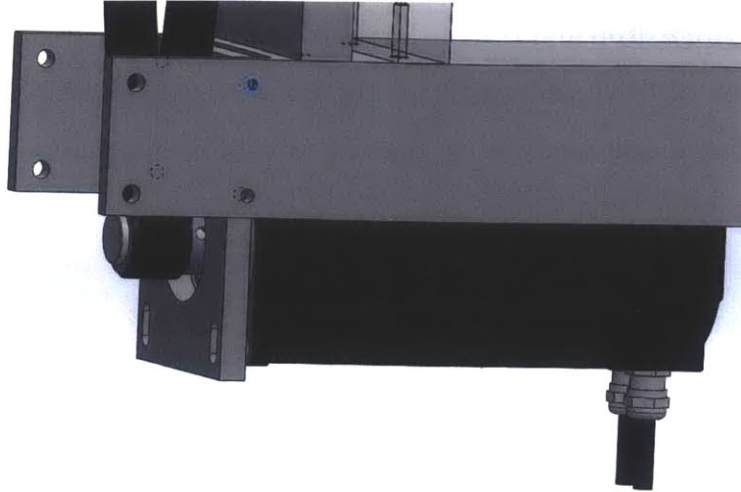
Figure 3-8: Method of tensioning the drive belt

3.2.3   Sagittal Plane Actuation

Section 2.1.3 outlines the determination of the hinged track design as a method of dropping the track underneath the subjects foot. In this section, we explore the development of the drive used to create the sagittal plane drop.

The sagittal plane drop selected parameters suggested a drop greater than 5.2 inches under the foot and drop time of 0.4 seconds. These parameters were determined by investigating the time and kinematics of the human swing phase of walking. At 2mph, there is approximately 1 stride per second. The average human gait cycle is characterized by 60% in stance and 40% in swing. For this reason, the sagittal plane drop was designed to support a 6 inch drop in 400 ms. The hinged track length is 60 inches with the subject standing 30 inches from the front axis and thus the track drop angle needs to be $-11.3°$ in order to reach the 6 inch under foot distance. The mass of the system necessitates significant power to accomplish these specifications.

Drive Specifications

In order to determine the proper drive for the sagittal plane motion of the Skywalker, a series of simulations were developed. The first simulation, as seen in figure 3-10, was developed to understand the general specifications at the track's rotational axis

necessary to create a drop and rise of the track within 0.4 seconds. Because the rising motion will need to drive the weight of the track as well as accelerate the mass of the track, the simulation was run to view the level of torque and power necessary for the rising operation within 0.2 seconds. These estimates were done prior to the final track design, so it was necessary to estimate the track inertia. Initial estimates of the mass of the treadmill system were developed by weighing the Sole F80 treadmill track and the Skywalker-α's track and scaling these numbers by the size of the Skywalker-γ track. This number was then compared to CAD models of potential track structures to estimate the Skywalker -γ's track weight. The track was estimated to weigh 70 pounds for this simulation. The track length (L) was specified to be 60 inches, and thus the rotational inertia was estimated as a rod using equation (3.13). Table 3.7 shows the simulation parameters.

$$J = 1/3mL^2 \tag{3.13}$$

A simple differential equation was used as shown in equation (3.14) to define the simulation.

$$\frac{d^2\theta}{dt^2} = \frac{\tau}{J} - \frac{mgLcos(\theta)}{2J} \tag{3.14}$$

From here, the following system of equations was simulated using the ODE23 solver in Matlab :

$$\frac{d}{dt}\begin{bmatrix} \theta \\ \dot\theta \end{bmatrix} = \begin{bmatrix} 0 & 1 \\ \frac{-mgLcos(\theta)}{2J} & 0 \end{bmatrix}\begin{bmatrix} \theta \\ \dot\theta \end{bmatrix} + \begin{bmatrix} 0 \\ \frac{\tau}{J} \end{bmatrix} \tag{3.15}$$

As depicted by figure 3-9, the torque (τ) was applied in the clockwise direction to accelerate the track upward from θ_l to θ_h and an equal τ was applied to the track in the counterclockwise direction to decelerate the track. The simulation was run iteratively, each time tweaking the Torque value and the time of torque direction change until the correct position trajectory was reached by the track. This simulation output resulted in a first order approximation of the torque, speed and power required by the sagittal
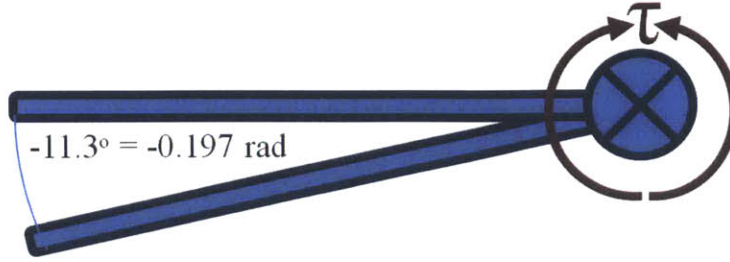
Figure 3-9: Sagittal Plane Simulation diagram

plane drive as seen in table 3.7.

Table 3.7: Sagittal Plane Specification Simulation Parameters

Parameter	Value
Track mass (m)	31.8 kg
Track length (L)	1.52 m
Moment of inertia (J)	24.5 kgm^2
Low angle (θ_l)	-0.197 radians
High angle (θ_h)	0 radians
Track torque (τ)	575 Nm
Max rotational velocity	1.95 rad/s
Max Power	1,120 W

Transmission Design

Section 2.1.3 shows the different options considered as a transmission. A single linear cam was ultimately used. Figure 3-11 shows the components of Skywalker-γ's transmission. The motor (A) is directly attached to a helical pinion gear. The pinion gear (B) drives a helical rack gear (C) which is fastened to a linear cam (D). The linear cam is supported by a linear bearing system (E). The treadmill track (F) is rigidly attached to a cam follower assembly (G) which rides inside of the nonlinear cam path of the linear cam (D). The transmission ratio of the Skywalker-γ's transmission is the product of the linear ratio of the rack and pinion (R_l) and the linear motion of the cam to the rotational motion of the track (R_t). This is shown in the block diagram in figure 3-12.

(R_l) is calculated by equation (3.16) where r_{pinion} is the pitch radius of the pinion gear and (R_t) is calculated by equation (3.17) where δx_l is the change in cam travel
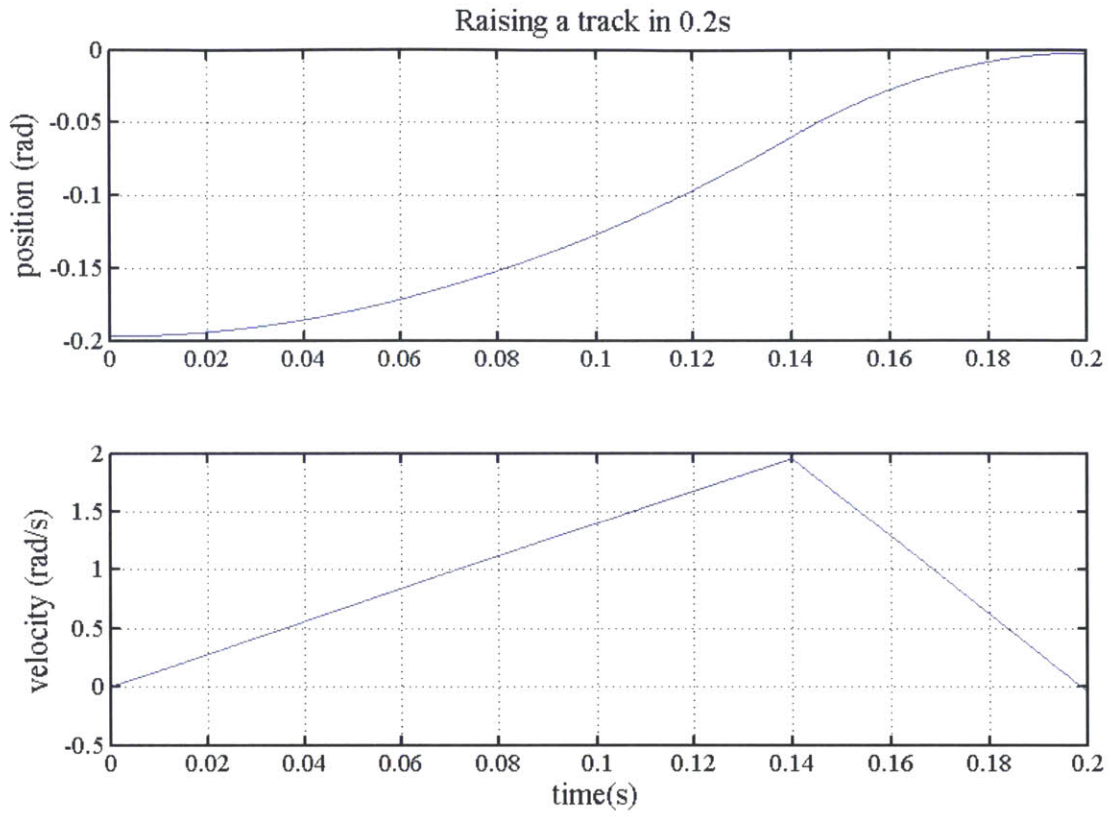
Figure 3-10: Simulation to determine sagittal plane specifications
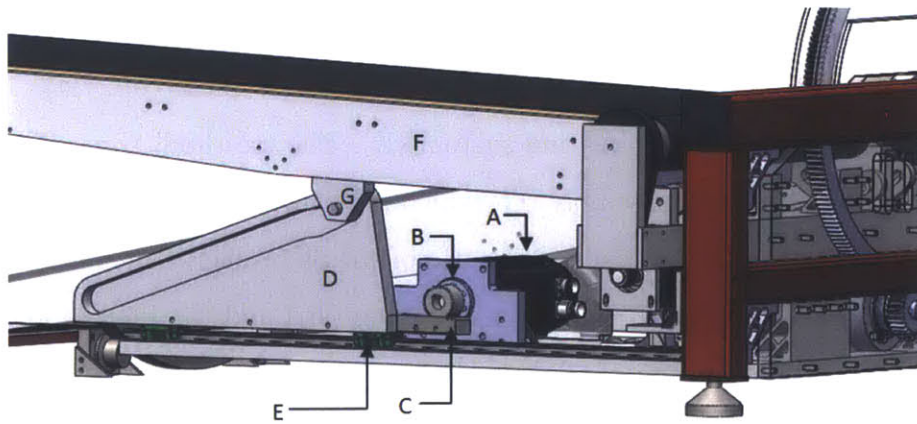
Figure 3-11: Sagittal plane drive components
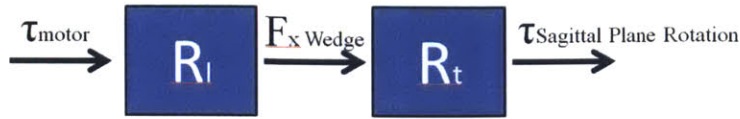
Figure 3-12: Block diagram of the sagittal plane transmission ratios

and $\delta\theta_t$ is the change in track angle . The simplest method for calculating δx_l and $\delta\theta_t$ is to use measure the CAD model at different sagittal plane angles.

$$R_l = 1/r_{pinion} \qquad (3.16)$$

$$R_t = \delta x_l/\delta\theta_t \qquad (3.17)$$

The transmission ratio of Skywalker-γ (R_s) then becomes:

$$R_s = R_l R_t \qquad (3.18)$$

Table 3.7 shows the estimated required torque and speed necessary to move Skywalker-γs track in the appropriate fashion. From Kollmorgens motor catalog[7], it is easy to see that the level of continuous torque producible by most of the motors is two orders of magnitude lower than the required torque but speed is much faster. Thus, the design activity is to explore the maximum transmission ratio possible using the mechanical architecture shown in figure 3-11.

The slope of the campath is the main driver of R_t and because the height of the cam travel is fixed by the required 6" drop of the track, the slope is limited by the length of the linear cam (the lower the slope, the greater the R_t). There is a limitation on the length of the linear cam because the base plate that supports the linear cam must be shorter than the track to allow the track end to lower to 1 off of the ground. The pinion gear pitch diameter was chosen to be at the smallest manufacturing limit to maximize R_l.

Figure 3-13 shows Skywalkers linear cam. The cam path is split into three regions.

---

[7]Available at www.kollmorgen.com
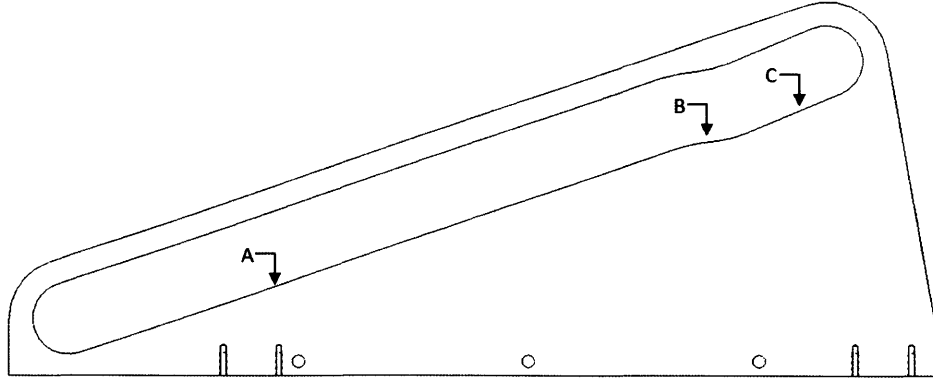
Figure 3-13: Skywalker-γ's sagittal plane campath

Region A was designed to perform the main action of dropping the track. Region B is the resting position of the tracks in the horizontal position. It is designed to minimize the torque reflected to the motor when a subject is standing on the Skywalker tracks while still providing smooth motion. Region C is designed to raise the subjects leg at the toe off position to be able to inject positive vertical motion into a patients gait before dropping. This region needs to have an increased slope in order to fit within the length requirement of the linear cam as mentioned above. The three regions are connected with fillets that ensure the cam follower will never get restricted by the transitions in the cam path. The cam path is designed to be 0.55mm larger than cam follower throughout operation. The three gear ratios are not constant due to the geometry of the linear cam path and the rotational track; however at each point in the cam path, changes in R are at most 0.5% different than those mentioned in table 3.8 so we will assume them to be constant for future calculation.

Table 3.8: Sagittal Plane

Parameter	Value
Pinion gear radius (r_{pinion})	0.0212 m
Linear transmission ratio (R_l)	47.1
Track transmission ratio of section A (R_{ta})	1.84
Skywalker motor to track rotation transmission ratio A (R_{sa})	86.7
Track transmission ratio of section B (R_{tb})	4.38
Skywalker motor to track rotation transmission ratio B (R_{sb})	206
Track transmission ratio of section C (R_{tc})	1.13
Skywalker motor to track rotation transmission ratio C (R_{sc})	53.2

80

Motor Selection

As mentioned in section 3.2.1, all motors used in the design of Skywalker-γ are from the AKM series of brushless servomotors from Kollmorgen. These motors are capable of operating at high torques for intermittent periods as seen in figure 3-14. Selecting a motor for the sagittal plane requires consideration of the motor size such that it fits into the Skywalker-γ's design, the radial load capacity to be able to withstand the amount of force generated during operation and finally and most importantly, the speed and torque characteristics required to complete the sagittal plane tasks. From the Kollmorgen catalog, it was determined that AKM53H motor would meet all of the qualifications for the motor. A simulation was developed to confirm the assumptions. The AKM53H motor curve with the AKD-P00606 motor driver is shown in figure 3-14 and key values can be found in table 3.9. The published torque constant (k_m) is 1.75 N*M/ Amp and holds until the AKM53H reaches 13.2 amps. Above 13.2 amps, k_m will begin to decrease, thus torque can only be estimated up to 23.1 Nm . The AKD-P00606 motor driver that the Skywalker uses for the Sagittal plane motion has a maximum current output of 18 Amps and a continuous rating of 6amps, which slightly limits the listed torque values. Table 3.9 shows the Skywalker-γ's operating condition changes from the AKM motor specifications sheet based on the available electrical power.

Table 3.9: Sagittal Plane motor published ratings vs. operating conditions

Parameter	AKM53H Published Motor Ratings	Skywalker Operating Conditions
Peak Torque (τ_p)	30.0 Nm	27.7 Nm
Continuous Torque (τ_c)	10.5 Nm	10.1 Nm
Peak Current (i_p)	19.8 Amps	18 Amps
Continuous Current (i_c)	6.6 Amps	6 Amps
Peak Speed (ω_p)	1970 RPM	2000 RPM
Bus Voltage (V_b)	320 VDC	324 VDC

Figure 3-15 shows the results of the full Skywalker-γ sagittal plane motion simulation considering all of the real components used in Skywalker-γ. The system of equations used in this simulation (equation (3.19)) is slightly different than the first simulation as this simulation is translated to the motor. Masses are based on the
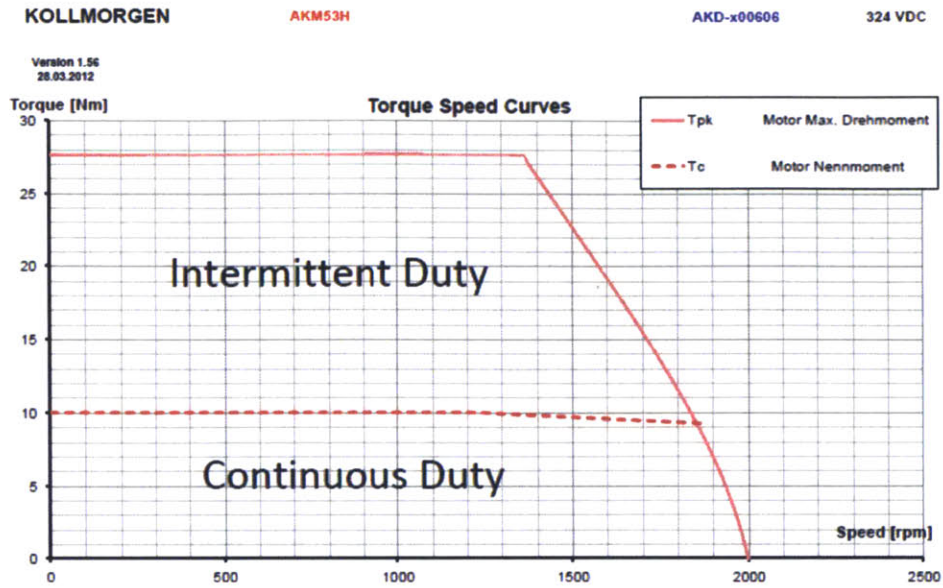
Figure 3-14: Sagittal Plane motor, the Kollmorgen AKM53H

actual components and all masses and forces are reflected to the motor through their respective transmission ratio. The inertia of the system was much higher than simply the track itself in this design[8]. The linear cam adds considerable inertia to the system and the motor and pinion gear also contribute. The linear components were reflected by equation (3.20) and the rotational components were reflected to the motor through equation (3.21). All reflected inertias were added together to calculate the total inertia J_{mtot} as seen in equation (3.22). Table 3.10 shows the breakdown of masses and their value when reflected to the motor. The purpose of the simulation is not to generate a perfect motion profile, rather to confirm that the motor can produce the desired motion with a reasonable safety factor. The torque profile chosen for this simulation is shown as the piecewise function defined in equation (3.23).

$$\frac{d}{dt}\begin{bmatrix} \theta_m \\ \dot{\theta}_m \end{bmatrix} = \begin{bmatrix} 0 & 1 \\ \frac{-mgr_{cm}cos(\theta_m/R_{sa})}{J_{mtot}R_{sa}} & 0 \end{bmatrix}\begin{bmatrix} \theta_m \\ \dot{\theta}_m \end{bmatrix} + \begin{bmatrix} 0 \\ \frac{\tau_m}{J_{mtot}} \end{bmatrix} \tag{3.19}$$

---

[8]The actual systems inertia came to 2.13x the initial estimate used to generate specifications for the motor. The use of the intermittent zone torques allowed the Skywalker to operate with a reasonably sized motor

$$J_{lm} = m_l/(R_l)^2 \qquad (3.20)$$

$$J_{tm} = J_t/(R_{sa})^2 \qquad (3.21)$$

$$J_{mtot} = J_m + J_{lm} + J_{tm} \qquad (3.22)$$

$$\tau_m(t) = \begin{cases} -20.5Nm & \text{if } t < 0.03s, \\ 0Nm & \text{if } 0.03s <= t < 0.146s \\ 23Nm & \text{if } 0.146s <= t < 0.231s \\ 2.09Nm & \text{if } 0.231 <= t < 0.306 \\ -7Nm & \text{if } 0.306 <= t < 0.4s \end{cases} \qquad (3.23)$$

Table 3.10: Sagittal plane simulation parameters with final components

Parameter	Value
Track mass (m)	25.5 kg
Track center of mass from rotational axis (r_{cm})	0.725 m
Track length (L)	1.52 m
Rotational Inertia of Skywalker track (J_t)	23.2 kgm^2
Track inertia reflected to motor (J_{tm})	0.00309 kgm^2
Limear mass of cam, rack, linear bearings (m_l)	5.95 kg^2
Linear mass reflected to motor (J_{lm})	0.00268 kgm^2
Inertia of motor, brake, coupler, pinion gear (J_m)	0.00121 kgm^2
Total inertia seen by motor (J_{mtot})	0.00694 kgm^2

Brushless motors are capable of operating at the intermittant torque levels but only for a short period of time. Kollmorgen recommends that the RMS torque value of the motors is kept below the continuous torque level of the motor. The continuous duty torque level (τ_c) of the AKM53H motor is fixed at 10.05 Nm for all speeds that are reached in the simulation (as seen in figure 3-14), thus it is necessary to calculate to the total torque RMS during operation. During walking, the motors will be enabled the entire time with the mechanical brakes released so that movements of the track can be smooth and respond quickly. Thus when the track is not dropping, it will be required to withstand the amount of torque the subject is applying to the track as
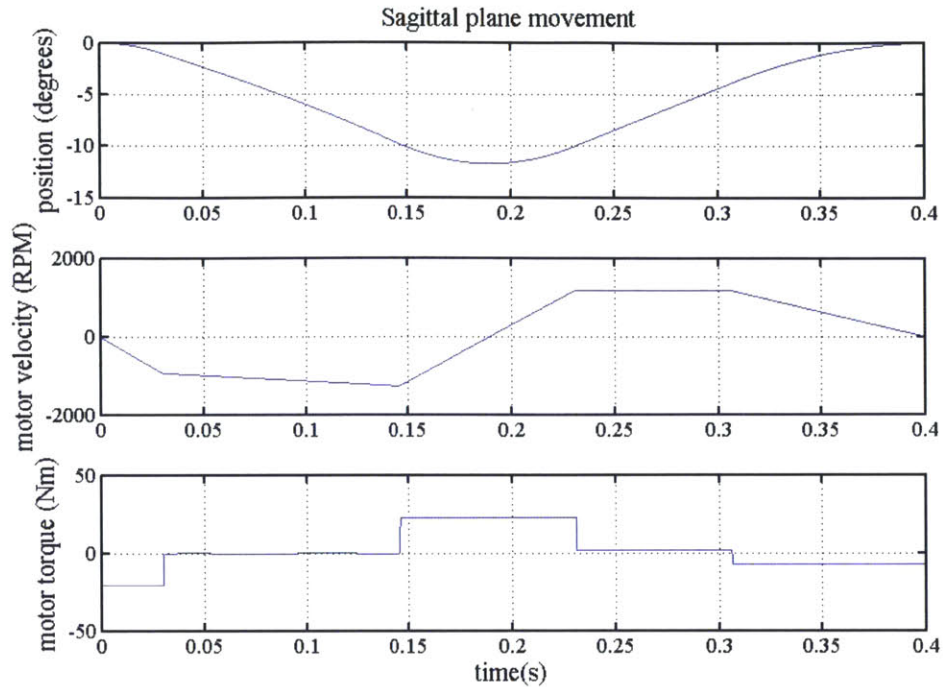
Figure 3-15: Full Skywalker-γ motion simulation

well as the weight of the track itself. Most operating conditions will include a body weight support system for the subject but as a worst case scenario for the motors, this simulation assumes a 300lb person standing in the center of one track during the remaining 0.6 seconds of the walking cycle. The body weight will create a moment of 1017 Nm of torque on the track which will add to the 181 Nm from the weight of the track to create a moment of 1198 Nm. At the horizontal position the transmission ratio (R_{sb}) is 206 and thus the motor will need to support 5.8Nm at the motor. Figure 3-16 shows the torque profile of the full Skywalker rhythmic walking training program with a 300 pound patient. The RMS torque value for the simulation is 9.09Nm which leaves 10.6% more capacity in the motor during operation. This is below the desired 25% factor of safety originally desired, however, during most use case scenarios, the patient will not be walking at a standard 2mph and thus the drop times can be slower and the motor will have more time to rest between drops. Additionally, as mentioned, a BWSS will be used to offset some of the patients weight.

84
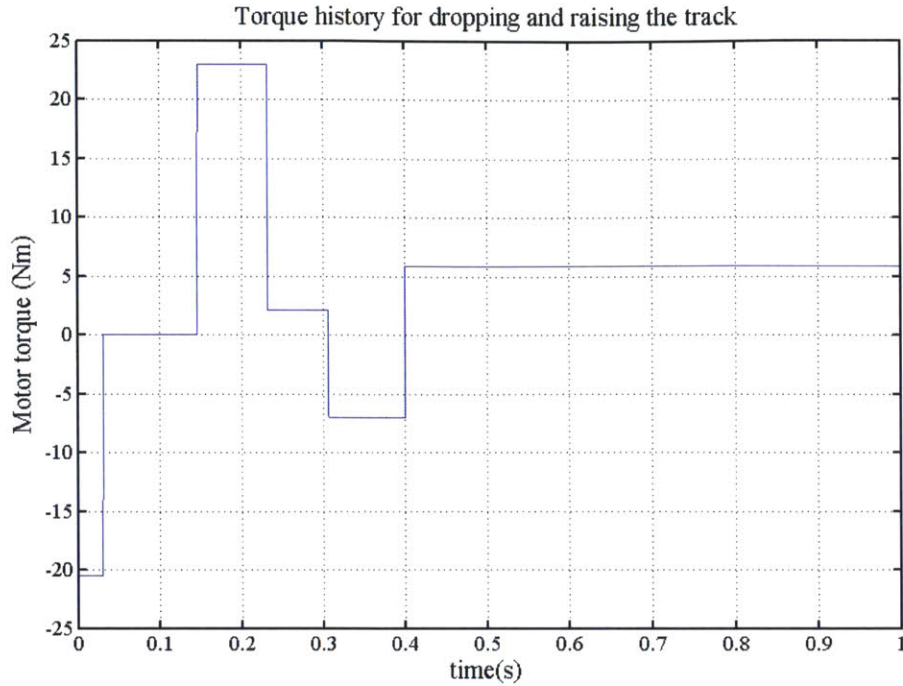
Figure 3-16: Skywalker training cycle torque profile

Efficiencies were not considered in the drive train simulation. The rack and pinion[9] gears are hardened helical gears made for efficiencies greater than 98%. The linear bearings[10] and cam follower[11] also have fairly low friction. While these efficiencies may increase the necessary torque while the track is moving, they will also decrease the projected load to the motor when a persons weight is on the track in the horizontal position. For this reason, the efficiencies were not modeled.

3.2.4 Frontal Plane Actuation

Specifications

The frontal plane rotation drive in Skywalker-γ must be able to support all body weight that will generate frontal plane torques on the system and must be able to move between -6 and 6 degrees at a speed that may invoke human balance mechanisms.

---

[9]Atlanta drives Module 2 gears www.atlantadrives.com
[10]Schneeberger BM S 15 system, www.schneeberger.com
[11]Ultra quiet cam followers from Mcmaster-carr www.mcmaster.com, item number 7803k17
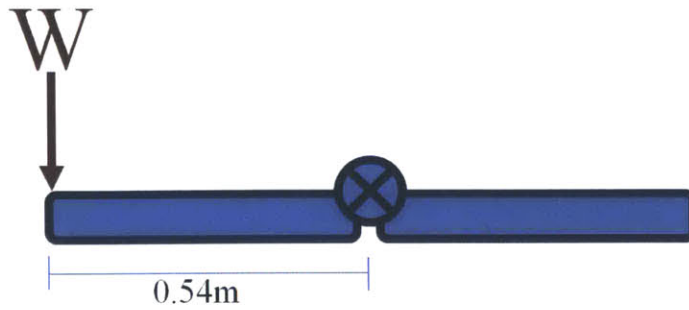
Figure 3-17: Frontal plane torques induced by body weight

Training may include two people on a single side of Skywalker-γ at one time, a therapist and a patient. In the worst case scenario, both people will be standing on the edge of the track, generating torque in the frontal plane as seen in figure 3-17. The weight of patient and therapist could be up to 500 pounds and the maximum radius from the center of rotation is 54cm, which creates a moment of 1200Nm around the axis of rotation.

In an effort to affect a patient's balance, two simulations were run to understand the torque required to tilt the whole frontal plane assembly (shown in figure 3-18). The first simulation was run to move the assembly to 6 degrees of rotation in 0.25 seconds, a perturbation that seems fairly violent and the second simulation, an easier, more sustainable perturbation rotating the track in 0.5 seconds. The results of these simulation are shown in figures 3-19(a) and 3-19(b). The parameters of the simulations are shown in table 3.11. In these simulations, no external forces were considered because their onset and specifics are difficult to predict. The simulations only considered the moment of inertia of the rotational track assembly and a person standing on the track. The frontal plane assembly inertia was measured by the CAD model and the estimation of a 6ft, 200 pound person was determined as a uniform rod as seen in figure 3-20 using equation (3.13). The simulation can be fully defined by the system of equations seen in equation (3.24). The torque profile applied to the simulation was a constant value of τ for one half of the simulation and τ for the second half. Table 3.11 lists the design specifications of torque, speed and power for both cases. Notice that in order to make this movement twice as quickly requires
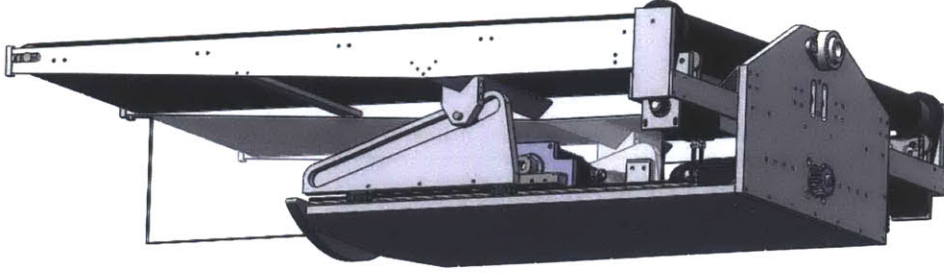
Figure 3-18: Frontal rotation assembly

8x more power and 4x more torque, a simple result of Newtons second law and the second order nature of kinematics.

$$\frac{d}{dt}\begin{bmatrix}\phi \\ \dot{\phi}\end{bmatrix} = \begin{bmatrix} 0 & 1 \\ 0 & 0 \end{bmatrix}\begin{bmatrix}\phi \\ \dot{\phi}\end{bmatrix} + \begin{bmatrix} 0 \\ \frac{\tau}{J_{ftot}} \end{bmatrix} \tag{3.24}$$

Table 3.11: Frontal plane simulation parameters and design specifications

Parameter	Value
Max torque of static body weight (τ_{bw})	1200 Nm
Frontal plane assembly inertia (J_{fp})	27.9 kgm^2
Inertia of a subject as a rod (J_p)	101 kgm^2
Total frontal plane inertia (J_{ftot})	128.9 kgm^2
Reversing torque of the fast simulation (τ_f)	860 Nm
Max speed of the fast simulation (ω_f)	0.834 rad/s
Max power required for the fast simulation (P_f)	717 W
Reversing torque of the slow simulation (τ_s)	215 Nm
Max speed of the slow simulation (ω_s)	0.417 rad/s
Max power required for the slow simulation (P_s)	89.7 W

Frontal Plane Transmission Design

Similar to the sagittal plane motion, the frontal plane motion will require very high torques to support both the static condition seen in figure 3-17 and the dynamic cases seen in figures 3-19(a) and 3-19(b) and thus a high transmission ratio needed to be designed once again. The static loading torque (τ_{bw}) must be constrained by a mechanical brake on the AKM motor. The power required for the movements resulted in the examinations of two classes of Kollmorgen motors, the AKM4 and the AKM5. The AKM4 brake can hold 5.3Nm of torque and the AKM5 brake is capable
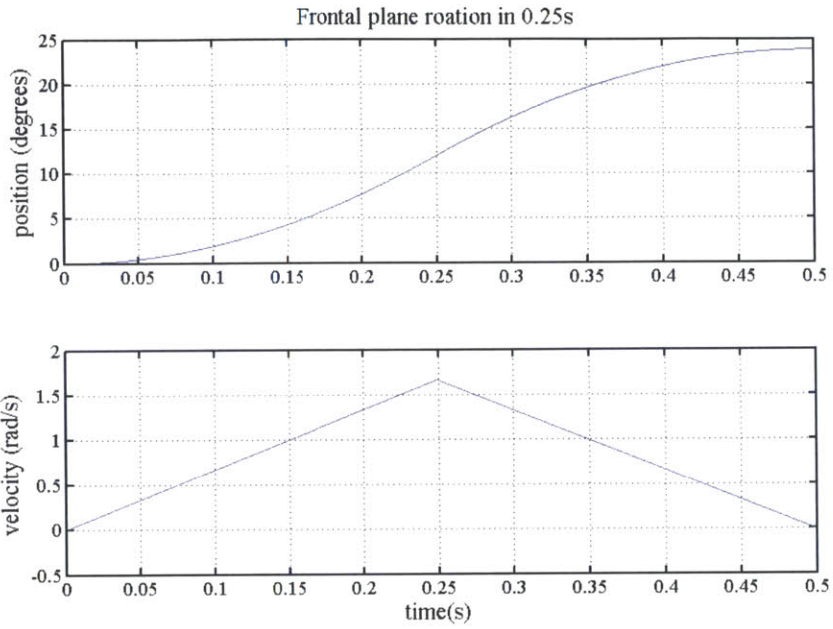
(a) Fast Perturbation
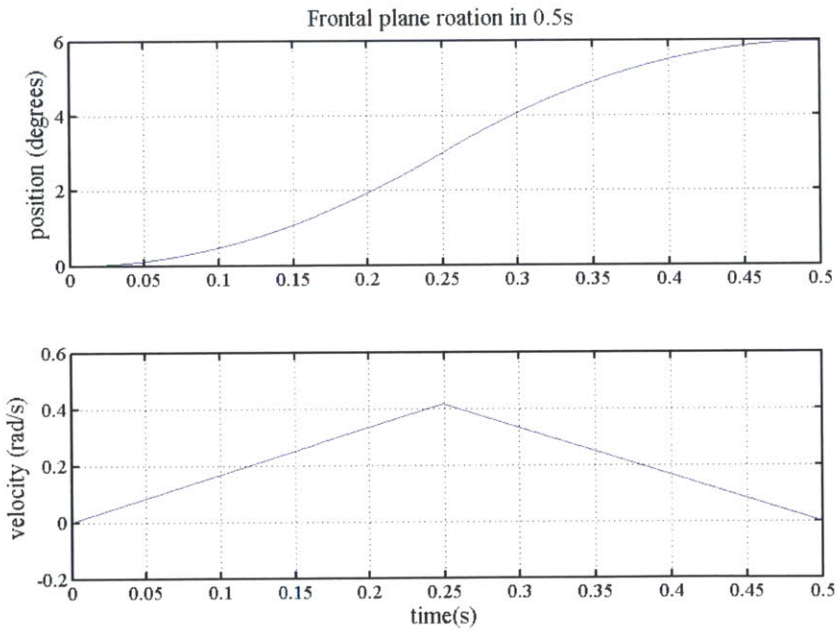
(b) Slow Perturbation

Figure 3-19: Frontal plane simulation to obtain specifications
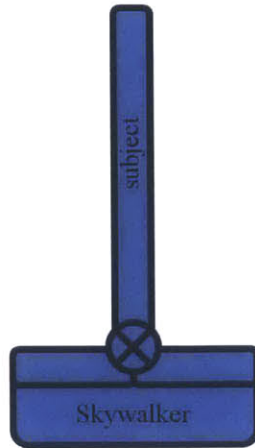
Figure 3-20: Frontal plane inertia schematic

of holding 14.5 Nm of torque. In order to support τ_{bw}, the transmission ratio of the frontal plane rotation transmission for the AKM4 and AKM5 motors would need to be greater than 227 and 83 respectively.

Many methods of transmission were considered including belts and cable systems which all presented attractive low or zero backlash properties, however, the high ratios precluded a simple pulley system and thus gears were settled upon despite their backlash properties. The chosen method of transmission for the frontal rotation assembly is shown in figures 3-21(a) and 3-21(b). The motor (A) is attached to a gearbox (B). A pinion gear (C) is pressed onto the output shaft of the gearbox (B) and mates with the ring gear (D) which is securely fastened to the frame (E). In order to support the rotation of the assembly, the rack gear needs to be curved with the same center as the rotation of the frontal rotation assembly. A partial circular gear is not a standard item at any of the gear companies contacted and thus a full ring gear was purchased. Instead of cutting the gear, for aesthetic purposes, the gear was used in the machine. It is fixed to the frame, thus the mass and weight of the gear is not a concern for the operation of the machine.

The gearbox[12] was chosen to have a 10:1 transmission ratio because it was the maximum ratio producible by a single stage of gears in the series of gearboxes chosen.

---

[12]XTRUE XT120 Planetary Gearhead from Micron - designed to mate with the standard Kollmorgen

| (a) Rear view of the frontal drive | (b) Front view of the frontal drive |
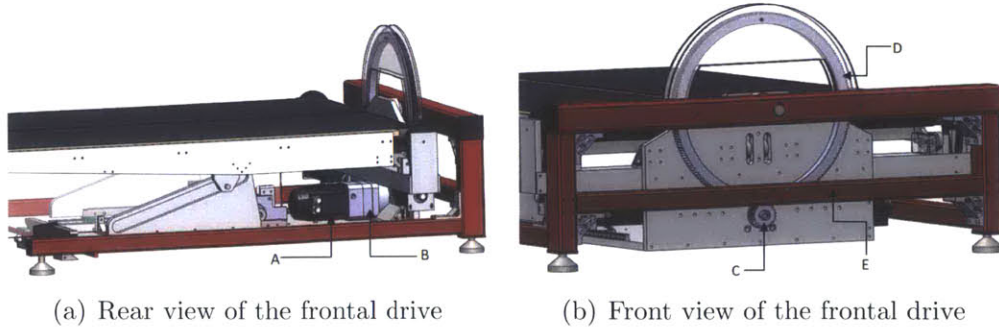
Figure 3-21: Frontal plane drive components

A two stage gear box could have been used to increase that ratio to 100:1, however, length was a limiting factor in the frontal rotation drive design of Skywalker-γ as seen in figure 3-22. Additionally, the efficiency of a two stage gearbox drops to 88% from the 93% efficiency of a single stage gearbox. The ring gear and pinion were chosen to maximize the transmission ratio using standard components. The ring gear[13] has a 500mm pitch diameter (D_r) which was necessary to mate with the position of the Skywalker gearbox output shaft. The pinion gear[14] was chosen to have the smallest pitch diameter (D_p) possible to mate to the gearbox output shaft. The gear ratio from the pinion to rotational motion of the frontal plane assembly (R_g) was calculated using equation (3.25). The gear ratios of the frontal plane transmission are shown in table 3.13.

$$R_g = D_r/D_p + 1 \tag{3.25}$$

Table 3.12: Frontal plane transmissions

Parameter	Value
Ring gear pitch diameter (D_r)	500 mm
Pinion gear pitch diameter (D_p)	62.5 mm
Transmission ratio, pinion gear to frontal rotation (R_g)	9
Transmission ratio, motor to gear box output (R_{gb})	10
Transmission ratio, motor to frontal rotation (R_f)	90

---

[13]Quality Transmissions Components part SSR2.5-200 module 2.5
[14]Quality Transmission Components part MSGB2.5-25 module 2.5
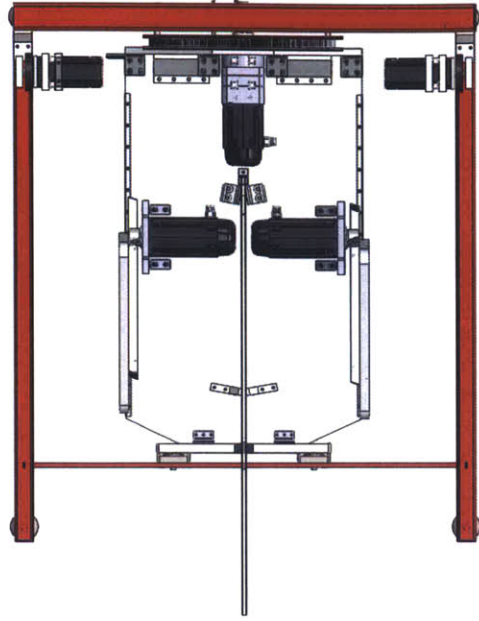
Figure 3-22: Top view of Skywalker's motors

Frontal Plane Motor Selection

The frontal plane transmission ratio (R_f) exceeds the specifications of the AKM5 series motor brake but is not large enough for the AKM4 series of motors as mentioned above. For this reason, a motor within the AKM5 series of motors was chosen, namely the AKM51E (motor curve seen in figure 3-25). This motor has a short length which allowed it to fit nicely into the Skywalker assembly (seen in figure 3-22) but also has the torque and power necessary to perform the two types of perturbations shown above. The motor was simulated to power the fast perturbations, shown in figure 3-23. In order for the torque RMS to stay under the continuous duty (T_c) line, a perturbation which drives the track to 6 degrees and back to zero requires at least 3 seconds between perturbation onsets (the torque profile is seen in figure 3-24 and has a torque RMS value of 4.49 Nm). The AKM51E can easily support continuous 0.5s perturbations with the 90:1 transmission ratio. The system of equations used for this simulation can be seen in equation (3.26). Efficiencies were modeled because they were well understood and significant. Table 3.13 shows the important values of this system.

91

$$\frac{d}{dt}\begin{bmatrix} \phi \\ \dot{\phi} \end{bmatrix} = \begin{bmatrix} 0 & 1 \\ 0 & 0 \end{bmatrix}\begin{bmatrix} \phi \\ \dot{\phi} \end{bmatrix} + \begin{bmatrix} 0 \\ \frac{\tau_m \eta_f}{J_{ftot}} \end{bmatrix} \tag{3.26}$$

Table 3.13: Frontal plane motor simulation parameters

Parameter	Value
AKM 51E continuous torque rating at 640 RPM (τ_c)	4.54 Nm
AKM51E Peak Torque (τ_p)	11.6 Nm
Motor, gearbox, pinion, brake inertia (J_m)	0.000757 kgm^2
Reflected frontal rotation assembly and subject inertia (J_{fm})	0.0159 kgm^2
Total inertia seen by the motor (J)	0.0167 kgm^2
Reversing motor torque in simulation (τ_m)	11.03 Nm
Minimum time between perturbations (t_{min})	3 s
Efficiency of the pinion, ring gear (η_g)	.98
Efficiency of the gear box(η_{gb})	.93
Efficiency of the frontal rotation assembly (η_f)	.911

3.3   Risks and Countermeasures

A step defined by the FRDPARRC method[84], the assessment of risks and counter-measures is essential to a robust mechanical design. In this section, we will explore the largest risks for Skywalker as well as the measures taken to mitigate them.

3.3.1   Personal injury

Skywalker's motors are extremely powerful and capable of dangerous forces. Safety was the primary concern in the design of Skywalker, in both the electronics (section 4.1.4) and the mechanical design (section 3.1). The body weight support provides safety by being able to support the patient in the case of a machine failure or a fall. The sagittal plane travel is limited mechanically by the linear cam path. This acts to house the mechanical motion between the two desired maximum angles, ensuring that the track can never enter a dangerous angle to the patient. Frontal plane rotation is halted at 6 degrees by the front beam which will contact the main frame and more protection is added by the base plate which will contact the floor at about 6.5 degrees. In addition to the hard mechanical stops, software limit switches are configured inside each motor driver to disable the drives if the motor angles were to

f
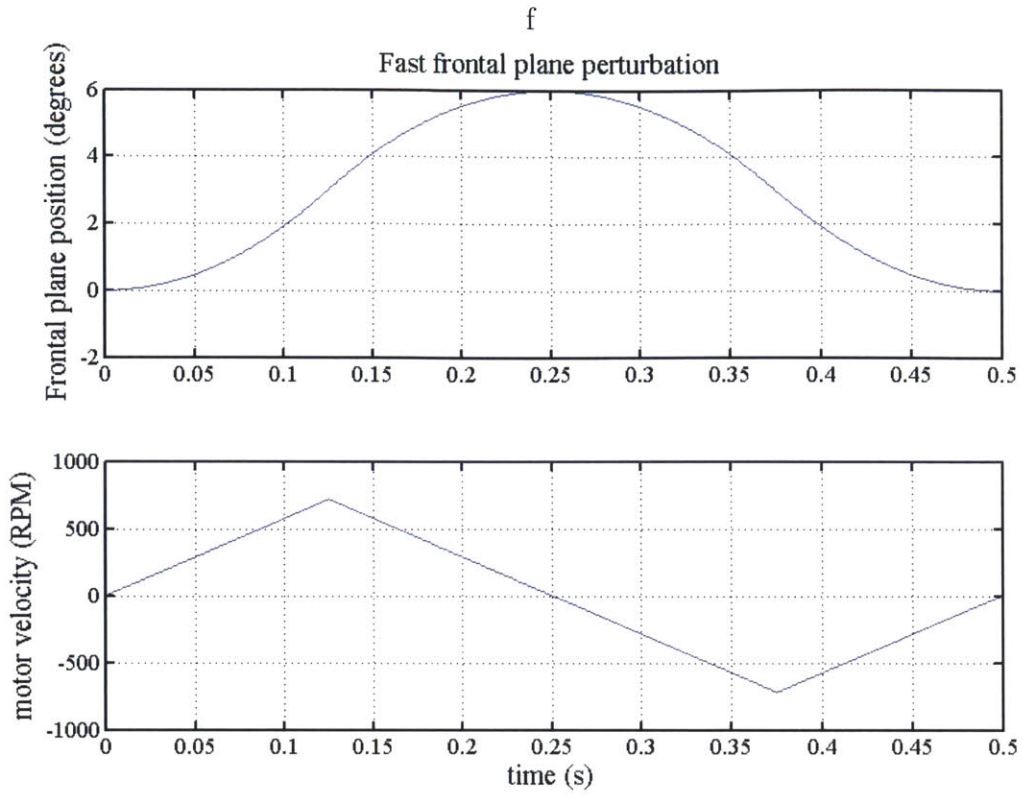
Figure 3-23: Frontal motor simulation
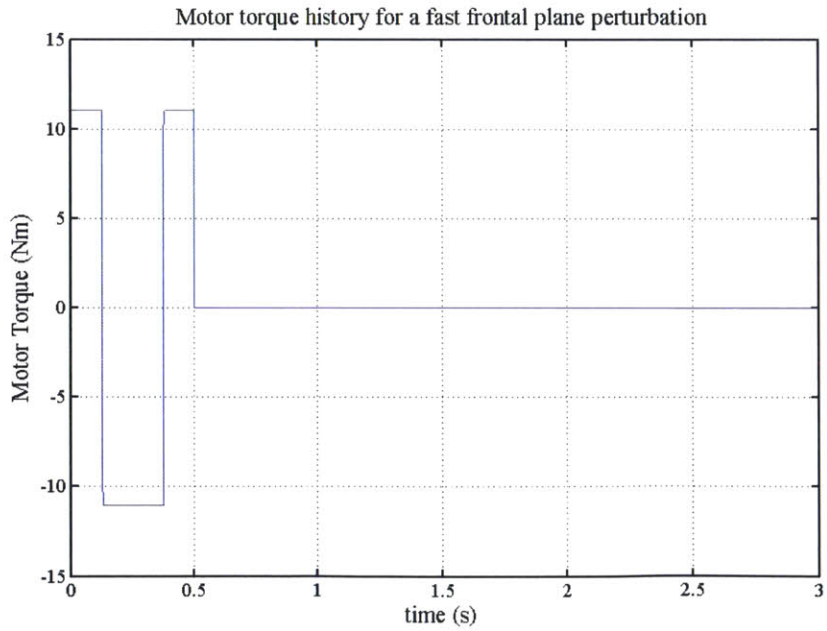
Figure 3-24: Frontal motor torque history

93
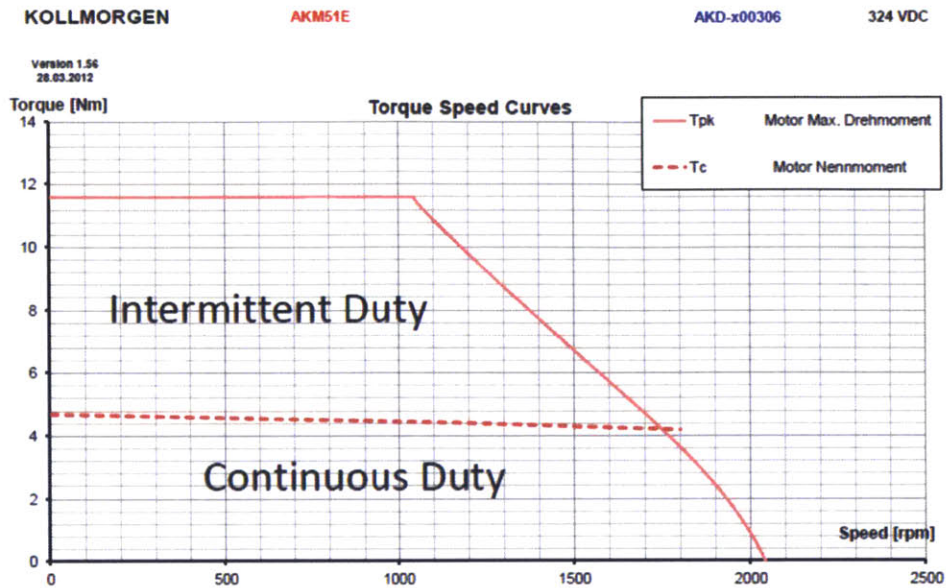
Figure 3-25: AKM51E motor curve

exceed those permitted by normal operation. Because the treadmill tracks motion is continuous, no precautions were taken to limit the motion of these tracks. This could present a dangerous condition if the track motors go unstable, but, as long as body weight support is provided, it should not induce injury.

3.3.2   Frontal Plane Track Torsion

The Skywalker track, supported only by the front offset bearings and the cam (see section 3.1.3) is susceptible to torsion caused by a subjects foot stepping on the inner edge, as depicted by figure 3-26. The offset bearings in the front of the track restrict this moment to a degree, however, there are three factors that lead to sizable deflections on the rear inside corner of the track. First, the offset bearings are designed with a small gap between the arc grooves and the outside diameter of the journal bearings. The gap was included in the design as a measure to ensure assembly and to reduce the friction in this joint. Secondly, the offset bearings themselves have non-negligible torsional deflection associated with frontal plane moments. Lastly, the track structure was designed to withstand greater moments in the sagittal plane rather than
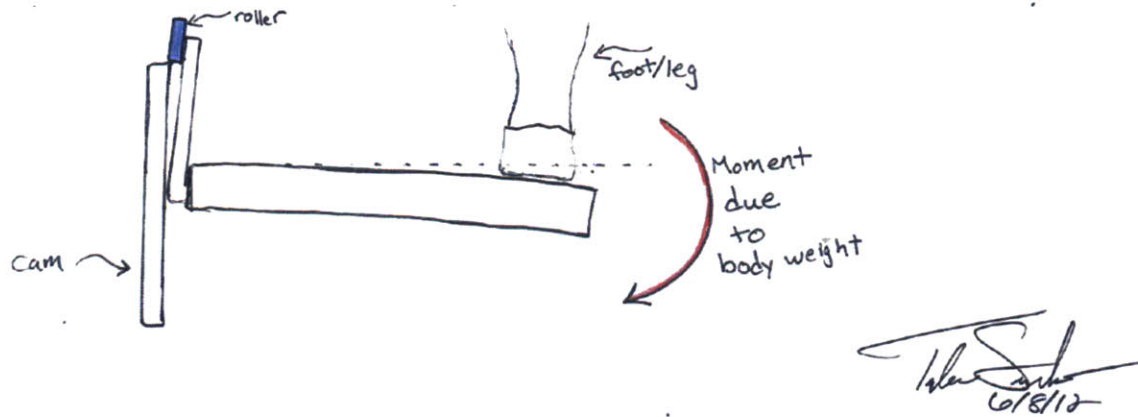
Figure 3-26: Torsional moment induced in track from offset position of foot

the frontal plane due to the larger potential moment arm in the sagittal direction. Efforts were taken to close the box of the treadmill track structure (see section 3.1.4) to maximize the second moment of area of the track in the frontal plane, however, the upper member of the box is a fairly flexible piece of plywood, which deflects under frontal plane moments. Each of these areas of compliance added together as springs in series and Abbe error propagates these small angles to the rear of the track, creating more than 1" of deflection on the rear inner point of the treadmill tracks, something that if not addressed, would most likely fatigue the wooden track to failure.

Many options were considered to combat the track torsion including a second passive linear cam, planar bearings between the two tracks, yoke bearings as a re-placement for the offset bearings, increasing the torsional stiffness by closing the box further and using a telescoping linear bearing in combination with radial bearings on the underside of the tracks; however, a two member linkage added to the underside of the track (see figure 3-27) was developed because it offers a simple design that restricts the moment near the place of foot contact during walking. This removes the need for the offset bearings and track structure to withstand the torsion created during walking. It was also fairly easy to add to the design within the free space to the inside of the cam. The linkage offers a solution with lower effective mass and lower cost than adding a second linear cam and uses parts that are more readily available and customizable than a telescoping linear bearing.

95
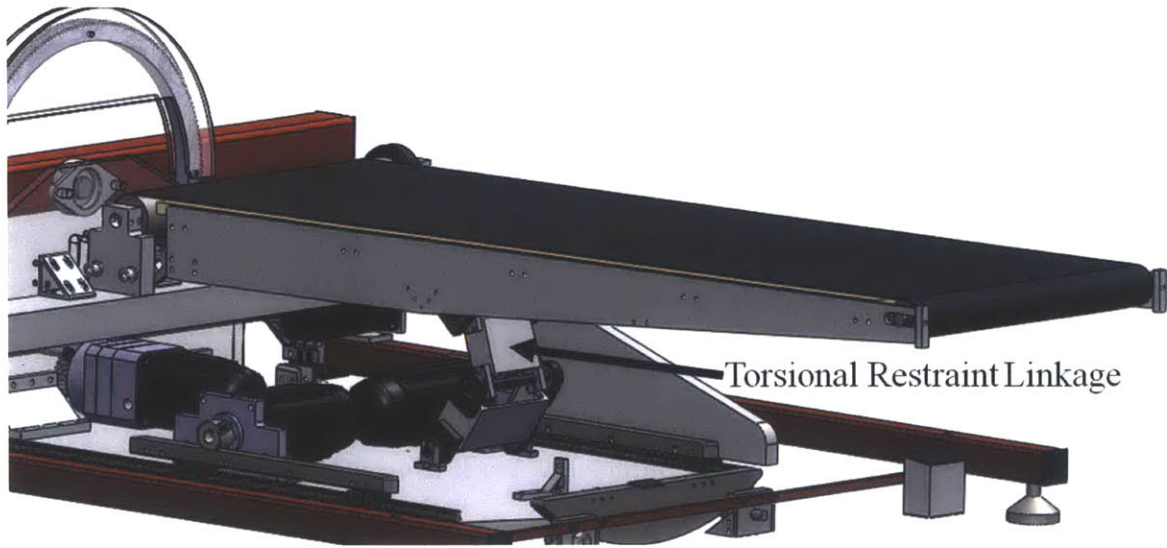
Figure 3-27: Torsional Restraint linkage: zoomed out view

Detailed Linkage Design

The design was constructed to handle the moment created by a 300 pound person walking at up to the maximum speed of the device. At 2m/s (4.47 mph), the maximum ground reaction force was shown in [85] and [86] to be about $1.42x$ the body weight of males and $1.36x$ the body weight of females. [85] shows a linear correlation between speed and ground reaction force which yields a ground reaction force at 4mph of $1.34x$ the body weight of males. Thus the linkage should support 300*1.34 lbs at a radius of .296m from the cam support for a total moment (M) of 530 Nm.

Figure 3-28 shows a zoomed in view of the linkage system. The wider the linkage, the more moment capacity the linkage system can handle. However, geometrical constraints of the rest of the Skywalker system limit the total width. To ensure structural soundness, it is necessary to consider the static load rating of the bearings, the load carrying capacity of the shaft supports, the fasteners that will be used, and finally to choose a shaft that can handle the moments created in the shaft due to the bearing and support locations. In order to do this, it is necessary to first define the forces present in the components. F_b and F_s represent the radial force taken by the bearings and the shaft supports respectively (see figure 3-29). R_b, R_s and R_m represent the distance between the bearings, shaft supports and the bearing to

96
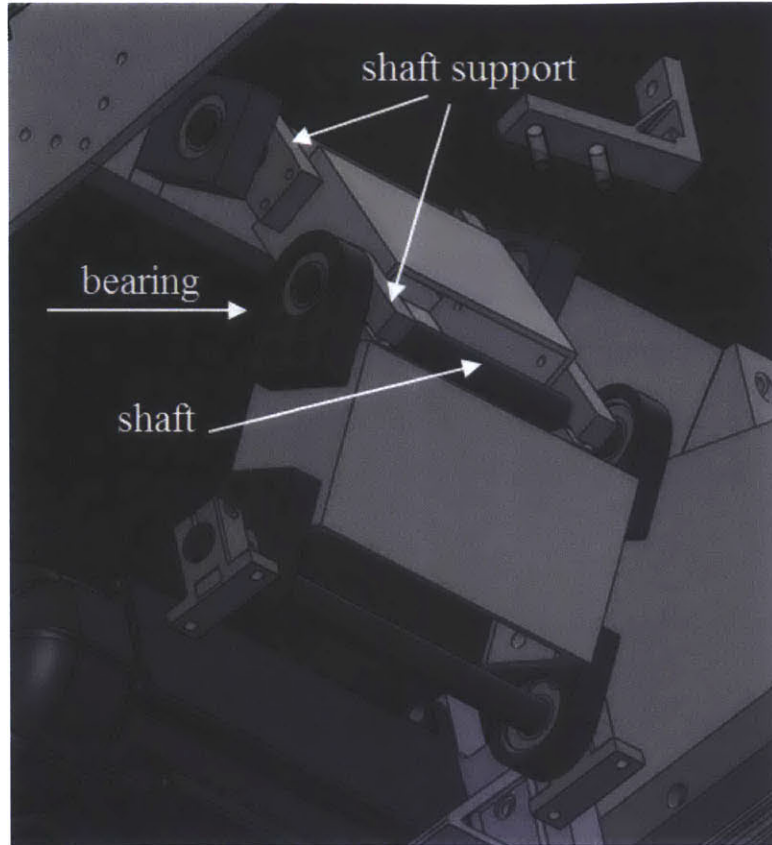
Figure 3-28: Torsional Restraint linkage: zoomed in view from underneath

support respectively. The forces and maximum moment of the shaft (M_{shaft}) are defined by equations (3.27), (3.28) and (3.29). Table 3.14 lists the values associated with this design.

$$F_b = M/R_b \tag{3.27}$$

$$F_s = M/R_s \tag{3.28}$$

$$M_{shaft} = F_b R_m \tag{3.29}$$
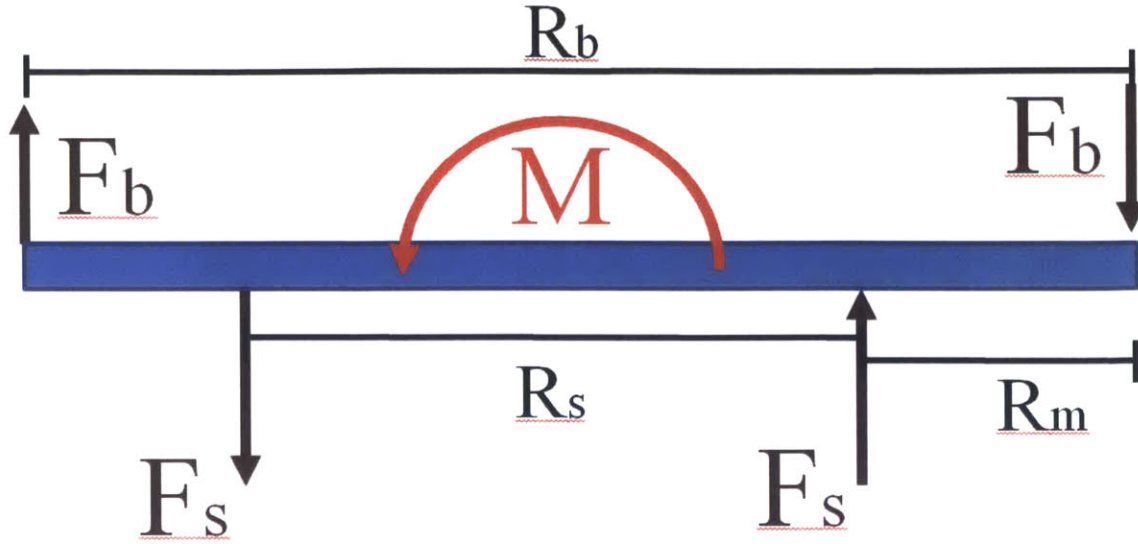
Figure 3-29: Schematic of each shaft in the torsional restraint linkage

Table 3.14: Torsional restraint linkage: parameters and values

Parameter	Value
Moment from subject's weight (M)	530 Nm
Distance between bearings (R_b)	161 mm
Distance between shaft supports (R_s)	102 mm
Radial force on the bearings (F_b)	3290 N
Force on the shaft supports (F_s)	5190 N
Distance between the bearing and shaft suport (R_m)	29.5 mm
Max moment in the shaft (M_{shaft})	97.0 Nm

Bearings

Bearings were chosen based on their load rating. The chosen bearings are offered by Misumi[15] under part number B6202zz. These bearings have a static load rating of 3,600 N and a dynamic rating of 7,750 N. Bearing ratings in static load are generally lower than the dynamic load due to the galling of material under a static load. During loading, the bearing will be static and thus under the most extreme load possible on Skywalker-γ, there will be a 1.09 factor of safety (FOS) for the inside of the bearings to resist gulling. The bearings were ordered pre-mounted in housings to reduce the amount of precision machining necessary in house.

---

[15] us.misumi-ec.com

98

von Mises (N/m^2)

229,218,528.0

210,123,920.0

191,029,328.0

171,934,736.0

152,840,144.0

133,745,544.0

114,650,952.0

95,556,352.0

76,461,760.0

57,367,172.0

38,272,576.0

19,177,980.0

83,386.2

→ Yield strength: 275,000,000.0
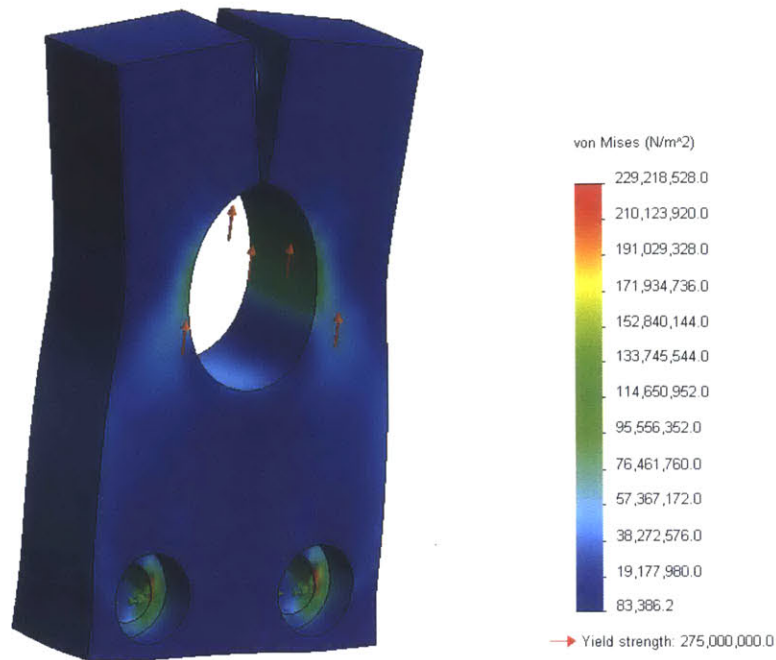
Figure 3-30: Shaft mount FEA

Shaft Supports

FEA analysis was conducted for the shaft supports as seen in figure 3-30. 5190 N was applied to the upper side of the shaft hole. The holes are constrained on the lower half of the surface. The factor of safety to yield is 1.2 with the concentration of stress existing at the counterbored surface of the supporting holes. When the shaft support is fastened to the square beam, the friction on the non-counterbored surface will aid as a constraint to relieve this point to a degree but this point will remain highly stressed.

Shaft Support fasteners

The fasteners chosen for the shaft support are also of concern. The shaft supports were stock and thus the design was limited by the holes supplied. Opening up the holes was an attractive idea but the position of the holes precludes the idea. Another idea considered was adding another fastener between the two holes, but this left less aluminum to withstand the forces so the design was unchanged. The holes are 4.5mm

Figure 3-31: Shaft mount distances

in diameter and thus M4 fasteners are used with a pitch diameter of 3.5mm. The fasteners chosen were made from high strength alloy steel with a tensile stress of 1220 MPa. Because the thickness of the shaft support, the fasteners will take both a sheer and axial loading from the bending moment. Assuming both fasteners split the load from the shaft (F_s), the force taken by each fastener (F_f) becomes $F_f = F_s/2$. The following equations were used to determine the principle stresses in the fasteners. The moment seen by the bracket is calculated as:

$$M_f = F_f t_{ss}/2 \qquad (3.30)$$

Figure 3-31 shows the thickness of the shaft support (t_{ss}) and the distance from the fastener to the end of the shaft support (R_f).

Axial force (F_a) will result due to the moment on the fastener as a lever with the fulcrum at the lower edge of the shaft support, thus the axial force on the fastener will be:

$$F_a = M_f/R_f \qquad (3.31)$$

The axial stress (σ_a) will then be:

100

$$\sigma_a = 4F_a/\pi D_f^2 \qquad (3.32)$$

Of course, we must still consider the sheer stress (τ) which will simply be:

$$\tau = 4F_f/\pi D_f^2 \qquad (3.33)$$

From Mohr's circle for plane stress, the prinicple stresses are:

$$\sigma_1, \sigma_2 = \sigma_a/2 \pm \sqrt{(\sigma_a/2)^2 + \tau^2} \qquad (3.34)$$

Table 3.15 shows the values for these fasteners. Because there was no published yield stress value for the fasteners, the factor of safety was calculated using the tensile strength (ultimate stress parameter) specified by the manufacturer. No other fasteners on the linkage were analyzed because the size of these fasteners and the innermost location of the shaft supports create the most highly stressed area in the linkage.

Table 3.15: Torsional restraint linkage: parameters for most highly stressed fasteners

Parameter	Value
Force on the fastener (F_f)	2,595 N
Thickness of the shaft support (t_{ss})	12 mm
Moment seen by the shaft support (M_f)	15.6 Nm
Distance from center of the fastener to end of shaft support (R_f)	5 mm
Axial force in the fastener (F_a)	3114 N
Pitch diameter of the fastener (D_f)	3.5 mm
Axial stress of the fastener (σ_a)	324 MPa
Sheer stress of the fastener (τ)	270 MPa
Principal stress 1 (σ_1)	476 MPa
Principal stress 2 (σ_2)	-153 MPa
Ultimate stress of the fastener steel alloy (σ_u)	1,220 MPa
Factor of safety (Ultimate) (FOS)	2.6

Shafts

The major stressing element in the shaft is the moment (M_{shaft} as defined above) that is developed between the bearing and shaft supports. Sheer loads on the shaft are orders of magnitude smaller and thus neglected in the calculation.

$$\sigma_s = M_{shaft} c / I \tag{3.35}$$

where c is the radius of the bar $(D/2)$ and I is the second moment of area. For a round shaft, I becomes:

$$I = \pi D^4 / 64 \tag{3.36}$$

In order to define the minimum shaft diameter (D_{min}), mathematical manipulations yields equation (3.37) where σ_y is the yield stress of the chosen shaft material(1045 carbon steel).

$$D_{min} > \sqrt[3]{32 M_{shaft} / \pi \sigma_y} \tag{3.37}$$

Table 3.16 shows the parameters chosen for this shaft design. The diameter of the shaft (D) must be greater than 13.5mm. Therefore a 15mm shaft was chosen. The factor of safety for yielding can then be calculated using the result from equation (3.35) and σ_y:

$$FOS_y = \sigma_y / \sigma_s \tag{3.38}$$

Table 3.16: Torsional restraint linkage: parameters for shaft design

Parameter	Value
Max moment of the shaft (M_{shaft})	97.0 Nm
Yield stress of 1045 carbon steel (σ_y)	405 MPa
Minimum shaft diameter $(D_m in)$	13.5 mm
Bending stress of a 15mm diameter shaft under load (σ_s)	292 MPa
Factor of safety (FOS)	1.38

Bearing and shaft tolerances

All bearings used were of the same type and size to make use of a single calculation and single part numbers. The bore and shaft nominal size was 15mm. The shaft has a G6 tolerance, with the range of 14.983 14.994 mm while the bearing ID was specified
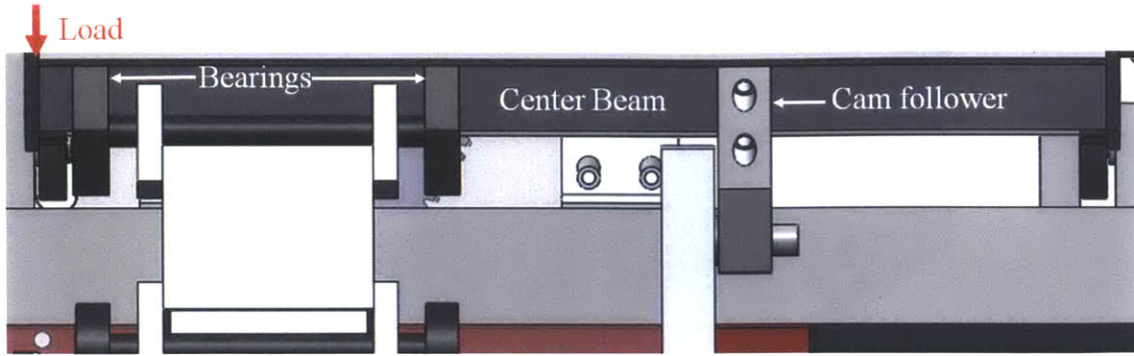
Figure 3-32: CAD: Center beam of the track assembly as seen from the rear
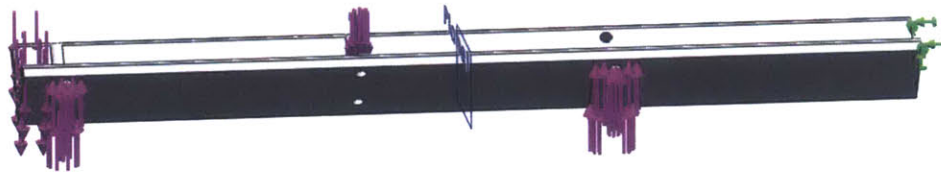
Figure 3-33: Center beam FEA loads

under the JIS B 1514 Class 0 standard to have an ID of 14.992 15.000 mm. This yields a locational transition fit which is ideal in this case because the linkages design cannot accept a gap between the hole and shaft. Interference fits seem attractive but have the potential to decrease the life of a bearing. The locational transition fits also allow fairly easy assembly without the need for a press.

Loading of the center beam

The last step was to check the strength of the middle track beam (figure 3-32) for soundness with the new forces and holes. An FEA was run as shown in figure 3-33 and figure 3-34. Of concern were the areas around both bearing mounts. Load values are consistent with table 3.14. A 1.88 factor of safety was calculated at the circle of material on which the inner-most mounted bearing fasteners are located.

This concludes the design of the torsional restraint linkage. The two weakest points on the linkage are the interface of the fasteners on the shaft mounts and the bearings, each with a factor of safety below 1.25 for the most extreme condition of a 300 pound person walking at 4 mph. Under more normal conditions of a 180 pound

von Mises (N/m^2)
145,759,280.0
133,626,024.0
121,492,776.0
109,359,528.0
97,226,280.0
85,093,032.0
72,959,784.0
60,826,532.0
48,693,284.0
36,560,036.0
24,426,788.0
12,293,538.0
160,289.2
→ Yield strength: 275,000,000.0
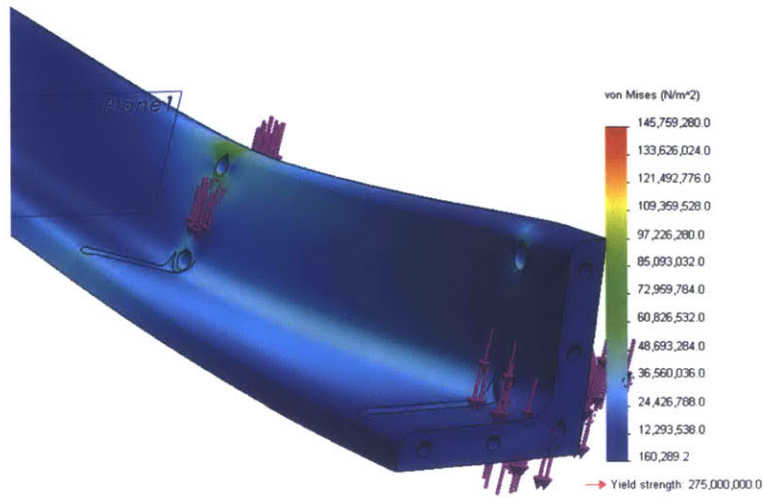
Figure 3-34: Center beam FEA loads

person walking at 2 mph, the factor of safety for these areas of concern moves above 2.

Chapter 4

Electronics

4.1 Power Electronics

Power Electronics Design involves the manipulation of electricity for high power use. This contrasts to electronic signal design in that it often deals with higher currents and thus safety is more of a concern, all components become larger and electromagnetic interference derived from the device becomes more noticeable. In our application, power electronics design refers to the conditioning of the wall AC power to produce controllable movement of the Skywalker robotic system.

4.1.1 Motor Drivers

Motor drivers are devices that send the appropriate amount of electrical power into a motor to produce a desired mechanical output whether that output is speed or torque. The term motor driver is a general term. In its simplest form, a motor driver may be a simple H-bridge device that opens and closes channels controlled by a pulse width modulated signal to control speed in a brushed DC motor. This operation can be built into small integrated circuits and for low power motors (9 Watts), they can be purchased for less than $2.50.[1] At their peak, motor drivers are a large integrated

---

[1] The Sanyo LB1836M Motor Driver IC sells for $2.49 from Pololu Robotics & electronics in the quantity of 100

motion control system that can power motors in excess of 60,000 Watts.[2] They may include a power supply, processing power to command current into brushless dc motor coils or even built-in firmware to program control algorithms and act as a full motion control suite.

4.1.2   Skywalker's Motor Drivers

Skywalker uses 5 brushless servomotors as electromechanical transducers to create the desired mechanical motion. As shown in Figure 4-1, inside each of these motors is three stator coils with a permanent magnet rotor. The motor creates a magnetic field in the direction specified by the superposition of the three stators magnetic fields and the rotor responds accordingly. In order to control the stators, Skywalker uses independent integrated Kollmorgen AKD motor drivers for each motor. The AKD drivers have circuitry that will send the proper amount of current to each one of the coils to generate the desired amount of torque in the motor. The control of the current in each stator coil is smooth and precise. The AKD drives are advertised as being AC servo drives, meaning that each one of the coils produces a continuous sinusoidal current profile to generate torque rather than a trapezoidal current profile as was the standard when DC brushless motors first came into existence. While it is important to understand what the drive is doing, as an engineer, we can simply rely on the drive to produce the correct amount of current in each coil without the need to think any further. To interact with the drive, the engineer needs to simply think of the Driver as a black box which accepts motion commands and outputs the desired mechanical behavior.

Drive Power Supply

Before the drive can send accurate power to each of the coils, power must be converted from AC power into DC power. Inside of each of the drives, there exists a switching power supply that generates and stores a bit of DC power. In a commercial product,

---

[2]The Kollmorgen AKD-09607 is rated to supply 64,000 Watts of continuous output power
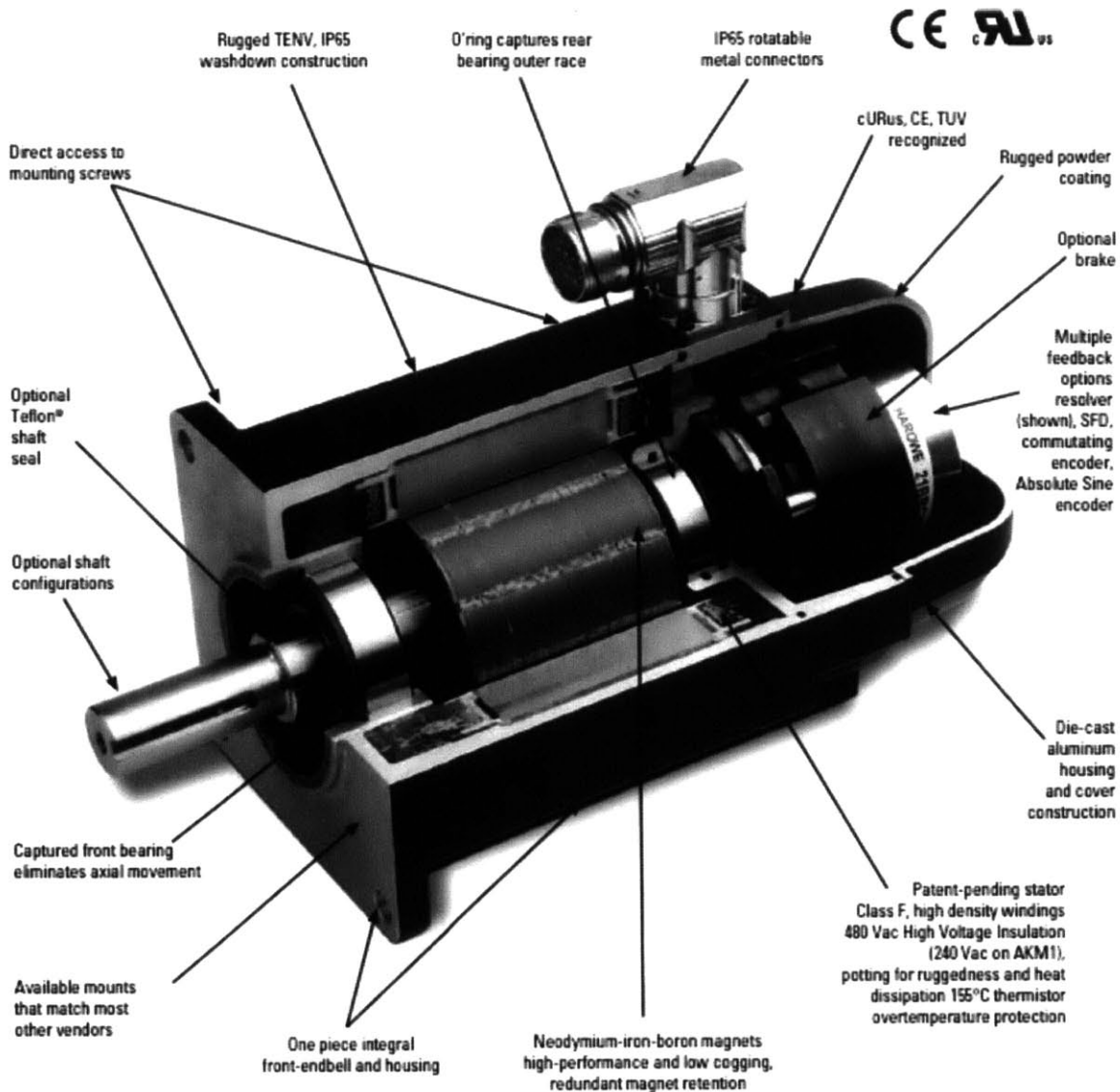
Figure 4-1: Section view of a Kollmorgen AKM motor from the 2013 Kollmorgen AKM Servomotor Selection Guide

a designer may wish to consider the option of using a single power supply to create the DC power required to run each of the motors but for the brevity of this prototype design, Skywalker makes use of the built in power supplies in the AKD drives, feeding each drive with conditioned AC power from the wall socket.

4.1.3   Design of Skywalker's Power Electronics

While the motor drives provide a great deal of functionality that the system needs to run, in order to operate a full system, there must be other supporting devices of the power electronics system. Figure 4-2 shows a full schematic of Skywalkers power electronics system designed for Skywalker.

Power Distribution

Starting from the lower left side of Figure 4-2, wall outlet power comes into the system. The black, white and green traces represent the hot, neutral and ground wires respectively. Power enters the ground fault circuit interrupter (GFCI, see section 4.1.4) and then the main power switch. Next, power travels into a 1:1 isolation transformer (see section 4.1.5) before going into the main enclosure of the control box represented by the light gray rectangle. Once inside of the box, power travels into the surge protector which will protect all the equipment from an external power spike. Power is then delivered to three power buses, which deliver power to the rest of the system. 5 independent two pole circuit breakers distribute the AC power to each Kollmorgen AKD drive (shown in the orange rectangle) which allows for certain drives to be shut off while others run. Each breaker is rated at 20Amps, adding an additional level of over-current protection. It was important to use two pole circuit breakers (Hot and Neutral) rather than just a single pole hot line breaker because neutral was not a flat 0V signal. Power from the transformer at MIT came into the wall socket in the following fashion: hot-ground = 136VAC, neutral-ground = 117VAC. Hot and neutral are at nearly opposite phases, combining to form hot-neutral voltage of 226VAC. This 240 Volt" power scheme is fairly common in the

United States so just cutting off the hot line may not completely remove power from the drive and may create an imbalance from capacitive coupling to the ground line.

24 Volt DC

The buses also directly power a 24 Volt direct current power supply which can be seen at the bottom right of figure 4-2. This supply is necessary for the firmware logic power within the drives and provides two levels of safety, a direct electrical power control and an enable function. In the absence of a 24 Volt signal to the Safety Torque Off (STO) pin on an AKD drive, the power stage of the drive is disabled, disallowing power to be sent to the motors. Likewise, without 24 Volts being sent to the enable pin, the connected motor will not be able to run. Thus, an emergency switch is connected at the output of the 24 Volt supply. When the switch is depressed, it maintains an open circuit between the 24 Volt supply and both safety pins of the drives. The STO and the Enable pins on the AKD drives are pulled down to ground in the absence of input voltage, causing all of the motors to deactivate once the switch is pressed. The fan is connected after the switch as an audible signal to the operator that 24 Volt power is absent from the drive.

Communication

Each of the drives has its own motor power cable (shown in orange) and motor feedback cable (shown in purple). The drives are capable of integrated feedback control and take higher level control commands from a control suite. The control suite sends both digital and analog signals to each of the drivers to create motion. Digital signals can be used to initiate various functions in the drives, such as to begin a homing procedure or other motion profile stored in the firmware of the drivers. Analog signals can be sent to the drive as a reference signal which, depending on how the drive is programed, can correspond to position, velocity or torque. The control suite can receive emulated quadrature encoder data from each drive as digital inputs. The AKD drives can be set up to emulate the encoders at any resolution from 1 line per rev to the motors individual encoder resolution limit. The control suite can also
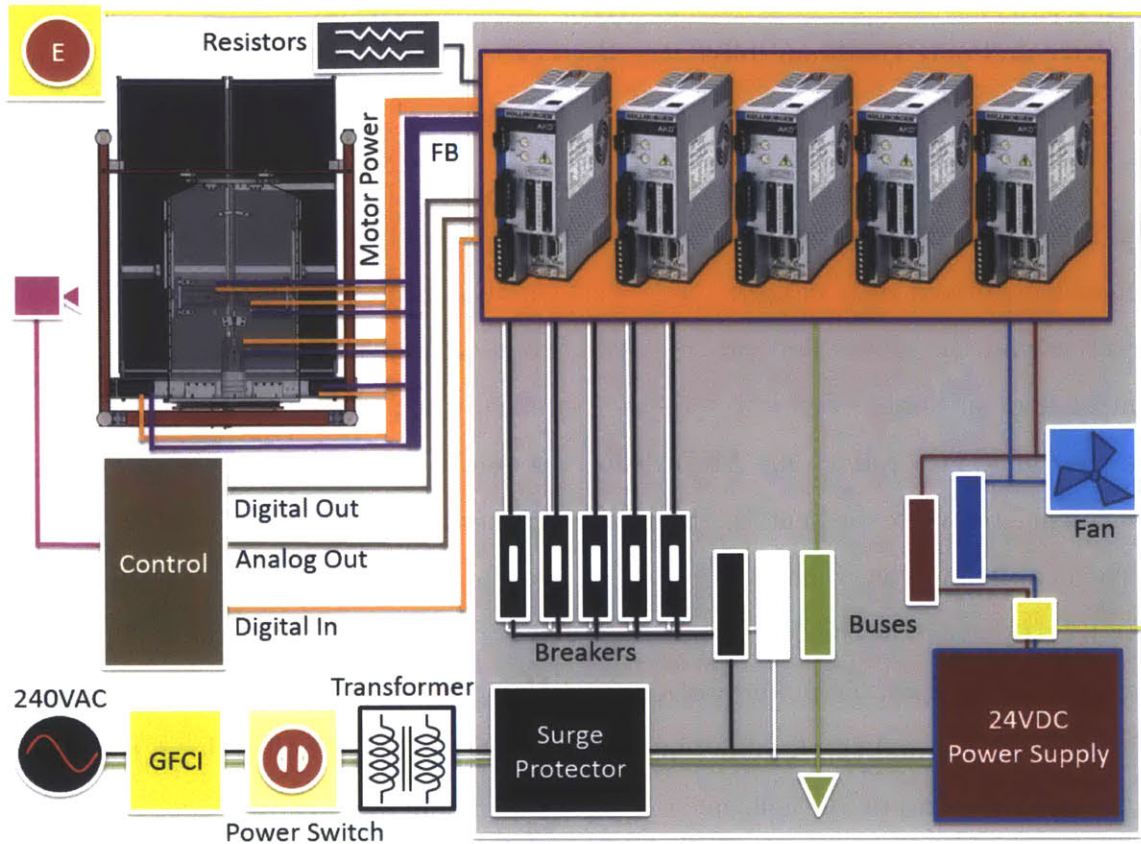
Figure 4-2: Full Skywalker Power Electronics Schematic

gain feedback from other sensors such as a video camera, shown in magenta, EMG or accelerometers via analog input or specialized input cards.

4.1.4 Safety

There are many levels of safety in the power electronics of Skywalker II. The emergency button can be depressed to cut all operation of power to the motors. Additionally, all of the drivers have software limits to set the limits of position, current, voltage and speed of the motor. If exceeded, the drivers will cease operation and report a code corresponding to the error.

To protect people from possible shock, a ground fault circuit interrupter (GFCI) was implemented into the design of the power electronics. The GFCI[3] will trip the

---

[3]TRC 26000 016-3 GFCI http://www.trci.net

electrical circuit if the line current differs from the neutral current, a condition that will occur in the case of electricity flowing through a person during an electric shock. GFCIs typically trip with a 5mA difference between L and N, however, based on our tests, the GFCI was tripping above 2.6mA of AC current in the ground line. The tripping will occur in less than 25ms.

To further prevent the possibility of electric shock, close attention was paid to proper grounding of the main electrical box chassis and lid, the isolation transformer chassis, the motor drivers and all other peripheries inside of the box. The locations inside of the main box where all the drivers and ground buses are attached were sanded to be free of paint in order to make a direct electrical connection between these items and the grounded box.

As an added measure of electrical safety, an isolation transformer was used before electricity was delivered to the main box. The isolation transformer removes a direct connection between the main box and the wall power which breaks a common mode current loop which is described further in the next subsection. This improves the safety in the case of a person touching an exposed L or N line with one hand and a ground line with the other.

4.1.5   Isolation Transformers

When running more than 3 Kollmorgen servo drives, the GFCI tripped due to an excess of ground current measureable at 0.8mA per servo plus 0.2mA for the power supply. Including an isolation transformer after the GFCI fixed the problem. Incoming power often times has a common mode current path between Line (L in figure 4-3) and Ground (G in figure 4-3) as well as between Neutral and ground, caused primarily by capacitance (C_{com}) between the power lines. Our motor drivers are all outfitted with switching power supplies and because $i = C\frac{dV}{dt}$, the switching operation created current through the stray capacitance shown in figure 4-3 as C_g. This current that flowed created a continuous conductive loop between both the Line - ground path and the Neutral - ground path. In an attempt to decrease C_g, all connection points between the motor drivers and the electrical box were sanded and cleaned.
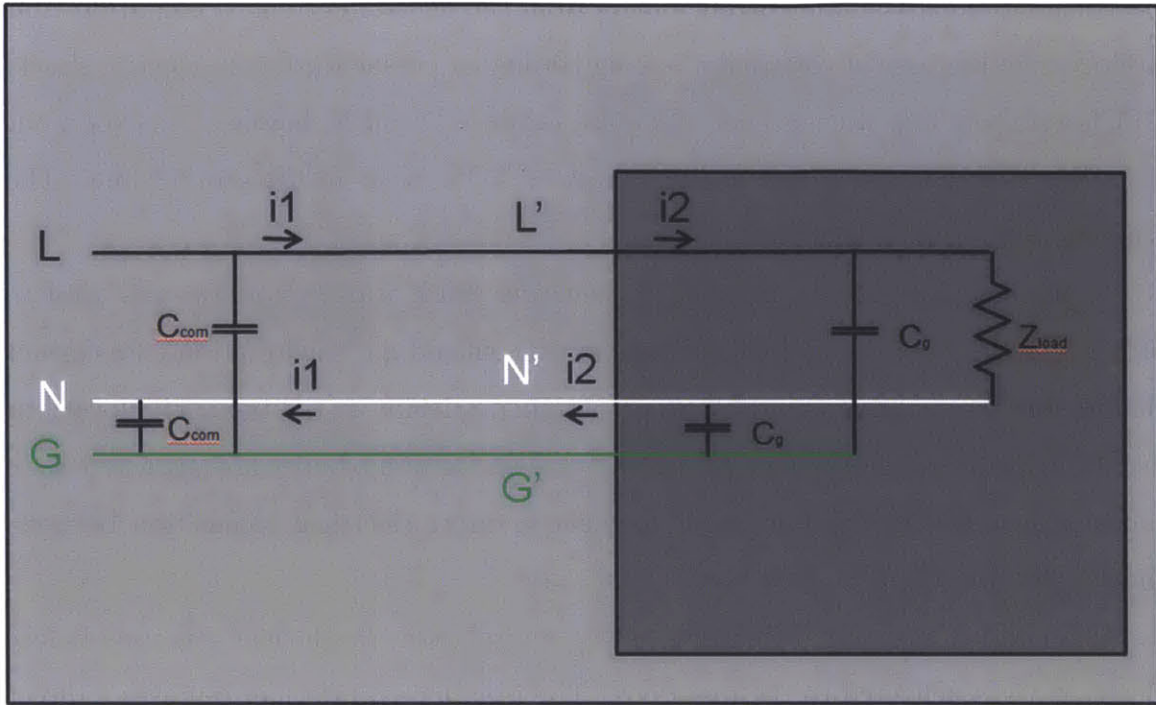
Figure 4-3: Power circuit without isolation transformer

This decreased the ground current marginally but not enough to stop the GFCI from tripping.

To fix the problem, a 1:1 transformer was added to the system as shown in figure 4-4. The transformer creates a second L and N that are coupled to L and N via the magnetic field of the coils, however, the transformer breaks the conductive path between the primary circuit and the secondary circuit. Therefore, the continuous conductive loops between Line-Ground and Neutral-Ground are broken such that no current can flow in these paths anymore.

Placing a GFCI before this isolation circuit still provides safety in case of an electric shock because if a person were to become part of the circuit, the energy is still leaving the system through conduction through the body. It is for this reason that a GFCI is still necessary while using the isolation transformer.
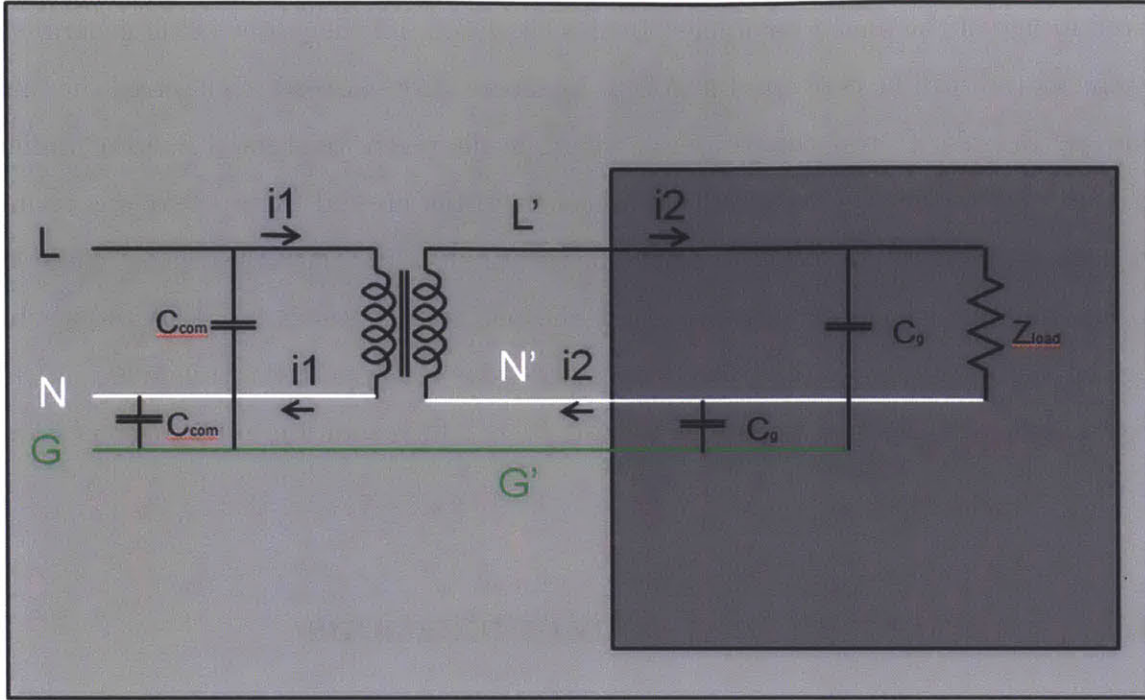
Figure 4-4: Power circuit with an isolation transformer

4.1.6 Regen Resistors

When operating the Sagittal plane drive at high accelerations, specifically decelerations, the driver was faulting and allowing the treadmill to slam to the ground. Upon inspection, it was deduced that the cause was the regeneration of mechanical power during deceleration into electrical power which was boosting the bus voltage on the drive to an unsafe level. To protect the electronics, the AKD driver is outfitted with overvoltage protection. Under normal circumstances the bus voltage is held to 320 VDC. The overvoltage protection will disengage the driver from the motor when the bus reaches 420VDC. The motor is then able to freewheel to rest or in our case, it is allowed to slam to the floor.

To address this problem, 500 Watt 33 ohm power resistors were wired into the Sagittal plane drives. The resistance of 33 ohms was recommended by Kollmorgen and the power of 500 Watts was determined with a factor of safety by estimating the RMS kinetic energy over time dissipated during deceleration. The firmware internal to the drive can be programmed such that during deceleration, the resistor will be

wired in line of the motor terminals. In this condition, all the power being generated by the motors will be converted into heat by the resistors instead of charging the bus voltage. In order to test the results of wiring in the regen resistors, a motion profile that ultimately sent the treadmill freewheeling to the ground (figure 4-5) was rerun with the resistors in place (figure 4-6). The results show that the resistors are capable of handling the generated power to keep the bus voltage under the 420V limit. In further testing (section 6.2.3), the drivers were able to support the treadmills in the most harsh step response conditions making them a final solution to the regeneration problem.

4.2 Fabrication and communications

4.2.1 Electronics Implementation

The implementation of the power electronics follows the schematic very closely. The component layout is shown in figure 4-7. All cables and drivers are color coded to match with each motor for easier troubleshooting. The full view of the whole power electronics system is shown in figure 4-8. The isolation transformer is kept outside of the electronics box because it weighs 75 pounds and is very large. Figure 4-9 shows the method for strain relief on all of the cables. Notice that D-sub connectors require an adapter for strain relief while cables with flying leads can use standard cord grips.

4.2.2 Methods of Communication

The AKD drivers are capable of communicating through several ports which can be found in the Kollmorgen AKD User Guide[4]. Programming the drives is done over an ethernet connection using the Kollmorgen AKD Workbench software. Within this environment, it is possible to configure controllers, motion profiles, feedback options and to setup the input ports that will be used for control. Skywalker uses digital signals to initiate motion profiles programmed into the drivers for both the

---

[4]User guide at: www.kollmorgen.com
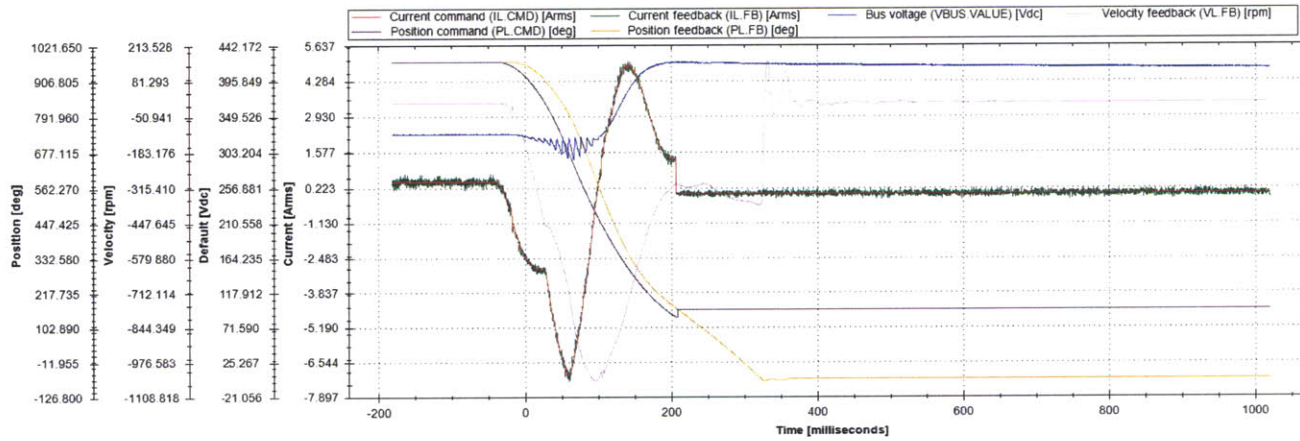
Figure 4-5: Failed drop without regen resistors, bus voltage in blue
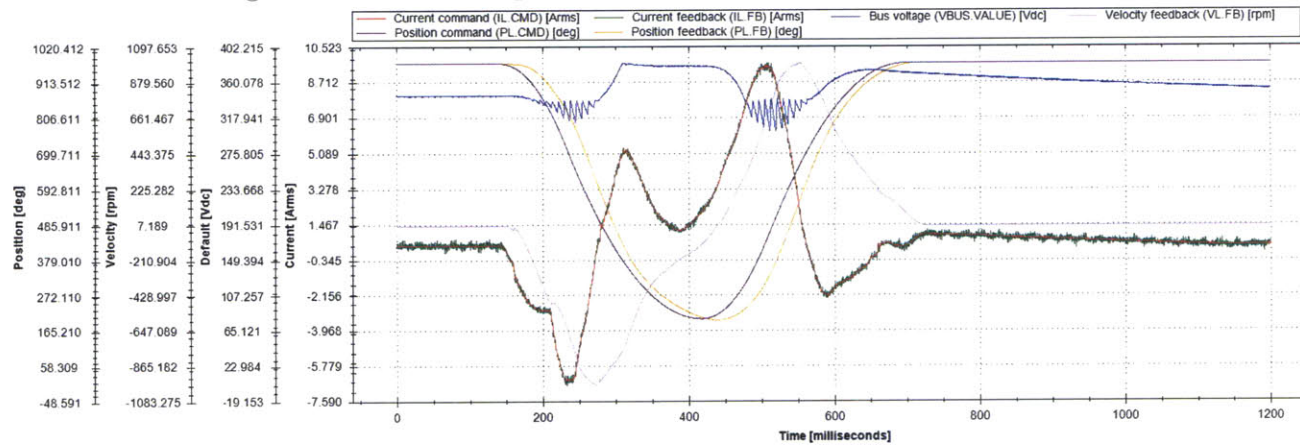
Figure 4-6: Successful drop with regen resistors, bus voltage in blue
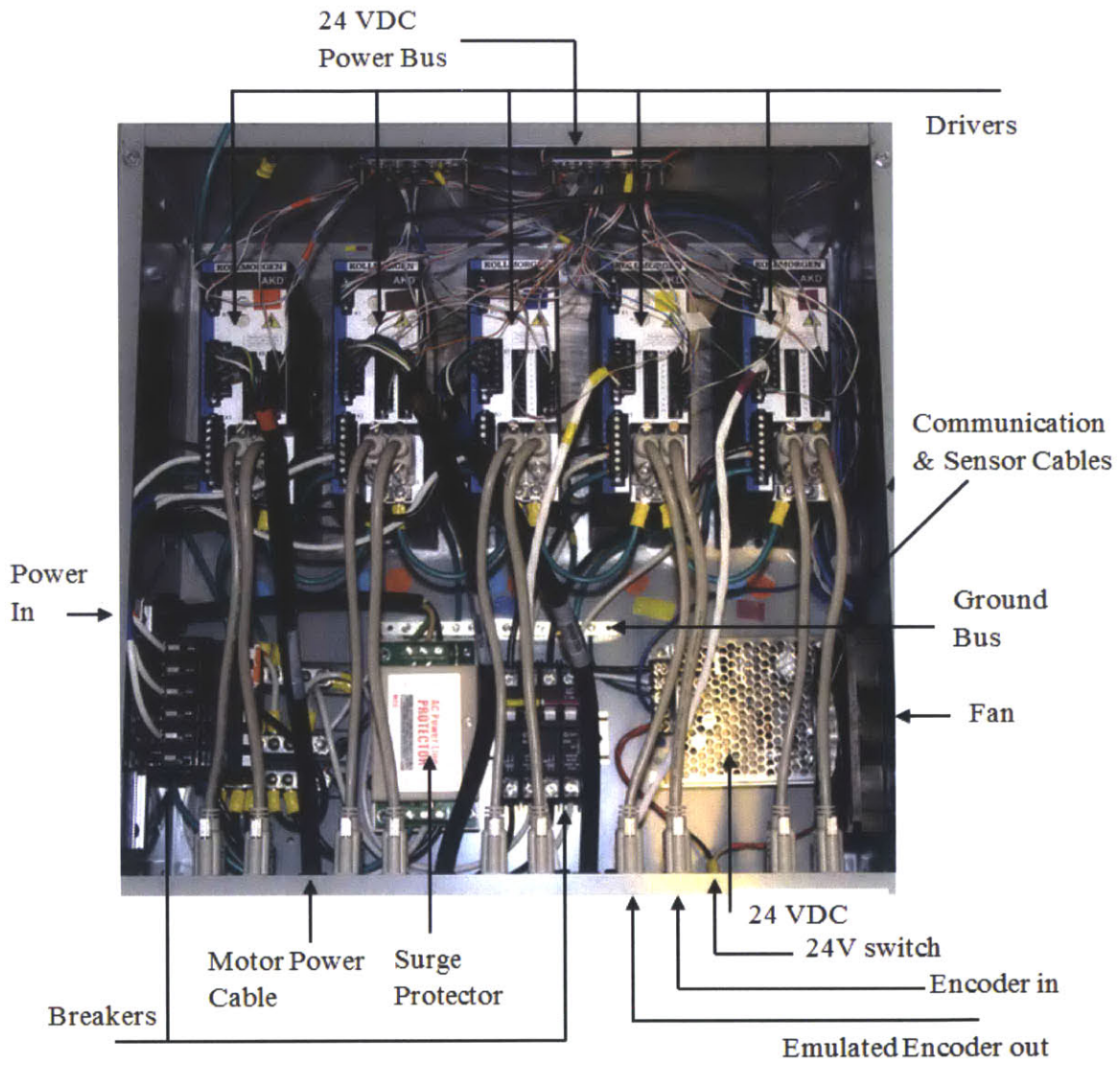
Figure 4-7: Electrical box components

Main Power
Switch

Isolation
transformer

226 VAC

GFCI

Power In
To Box

Passive
Vent

24VDC
Emergency
Switch
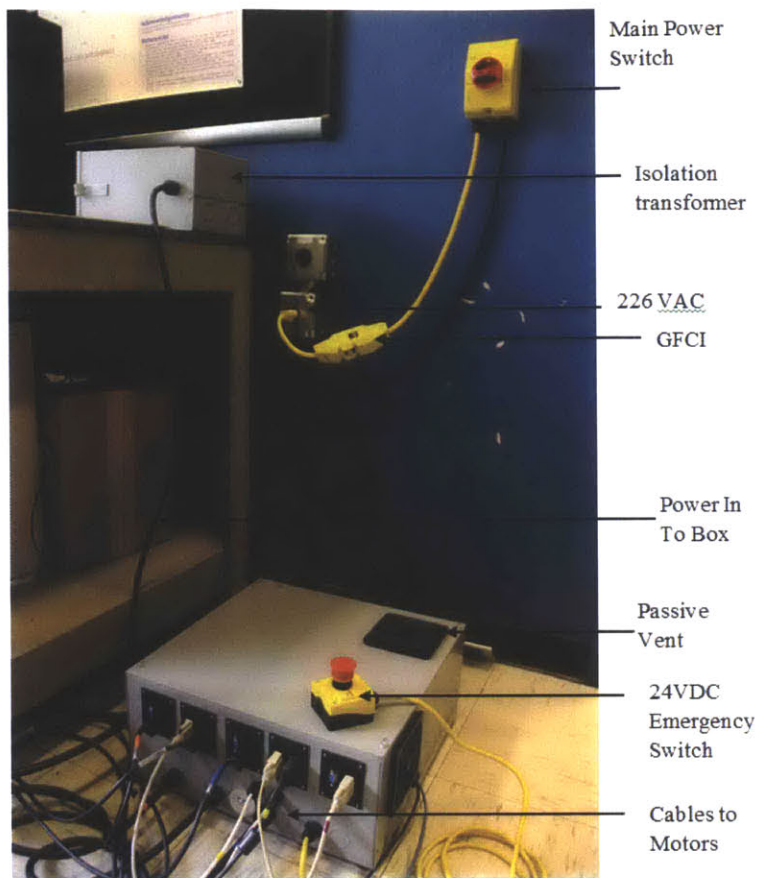
Cables to
Motors

Figure 4-8: Full view of the Skywalker II power electronics
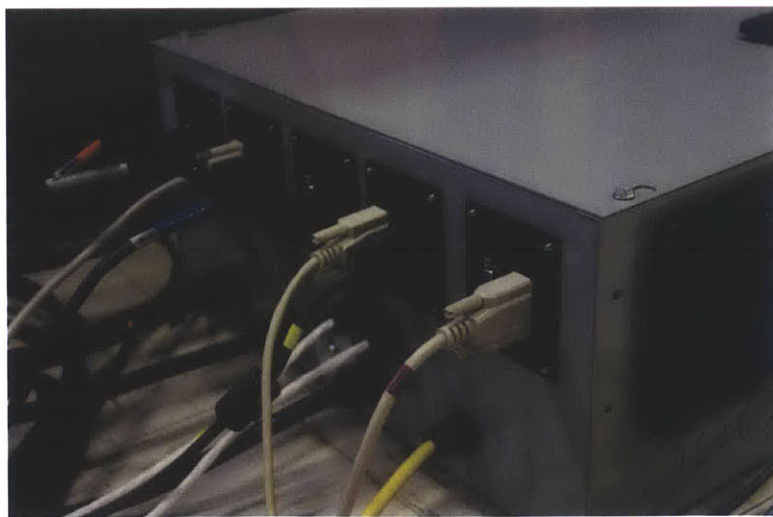
Figure 4-9: Motor cable strain relief

sagittal plane and frontal plane drives. The treadmill operates using analog input voltage commands that are scaled to represent either a torque command or a velocity command depending on what mode Skywalker is operating under. More detail on how Skywalker is set up in different operation paradigms can be found in section 6.1.2.

Feedback transducers are integrated into each of the motors. The treadmill motors use 5000 line incremental encoders. The other three motors use a Kollmorgen SFD (Smart Feedback device) which is based on a resolver. These signals come into the driver boxes through 15 pin d-sub connectors, which also carry information such as motor temperature. The drivers are programmable to send an emulated encoder signal then to a control suite such as our National Instruments PXI control suite.

Chapter 5

Vision System

The vision system developed for Skywalker tracks infrared emitting diodes attached to a subject's legs in order to autonomously determine the machine's behavior and to simultaneously record the subject's kinematics.

5.1 Hardware

The hardware required for a vision system are a camera and a computer with an appropriate interface to capture images.

5.1.1 Computer and interface

The Skywalker control system includes a standard host computer (used to write code) and a National Instruments PXIe-8135 controller (real time computer)[1]. The National Instruments PXI environment is a modular system that allows easy integration with an assortment of input/output cards. For vision, we are using the PXIe-1435 image acquisition card which accepts Camera Link Cables (very high speed cables for fast transmission of high resolution images).

---

[1]National Instruments Corporation, Austin, TX www.ni.com

Figure 5-1: Skywalker camera locations

5.1.2 Cameras

Two Basler[2] acA2000-340kc cameras (figure 5-2) are used on the Skywalker system, located on either side of the subject (as seen in figure 5-1) to record sagittal plane kinematics of the hip and knee on each leg. The maximum frame rate supported by the camera is $340\, frames/second$ at a maximum resolution of $2046x1086\, pixels(2.22MP)$. This is a very high rate of data, accomplish-able only by the camera link interface which includes 15 LVDS pairs (15 signal wires). Spectral Analysis for this camera is shown in figure 5-3. The important quality we're looking for in the spectral analysis is sensitivity in the infrared region. Many commercially available cameras employ an infrared cut filter (most SLR cameras, webcams, etc.), which blocks infrared light.

---

[2]Basler AG, Ahrensburg, Schleswig-Holstein, Germany, http://www.baslerweb.com/en
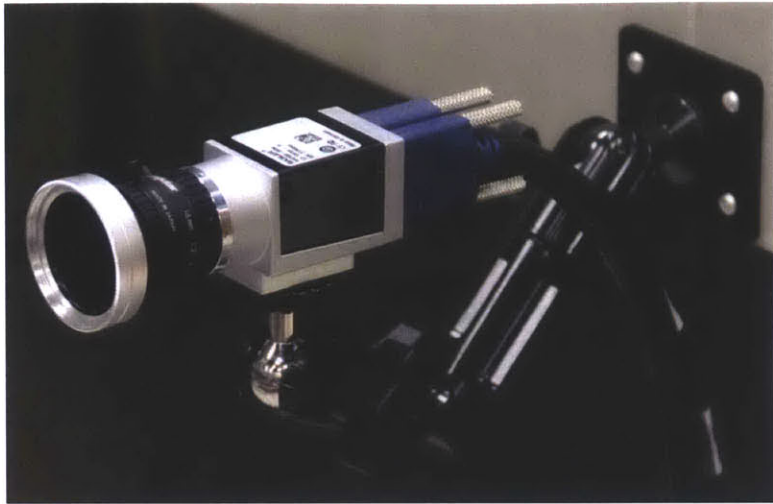
Figure 5-2: Basler camera used on the Skywalker
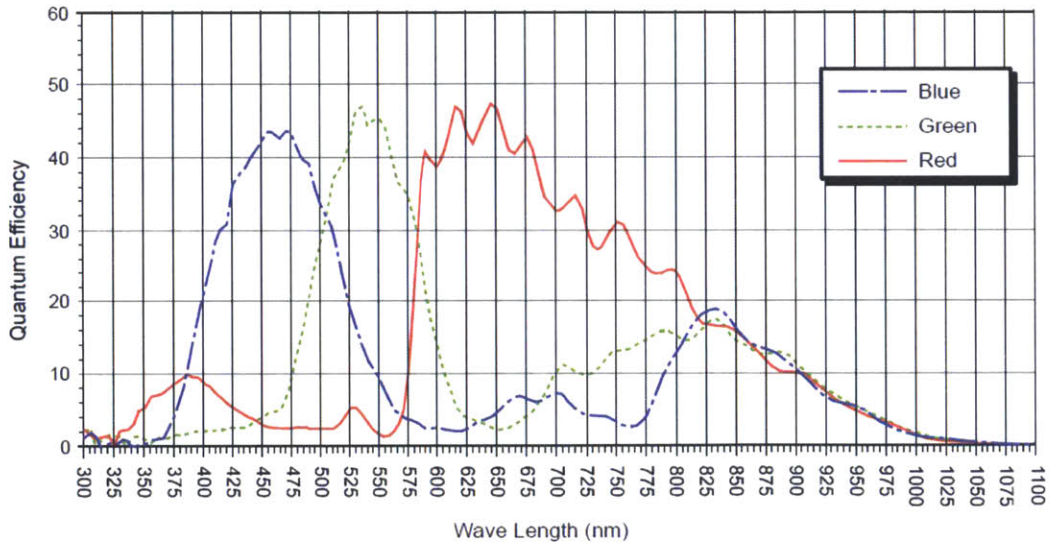
Figure 5-3: Basler acA2000-340kc spectral analysis

Standard camera view   **With 720nm filter**
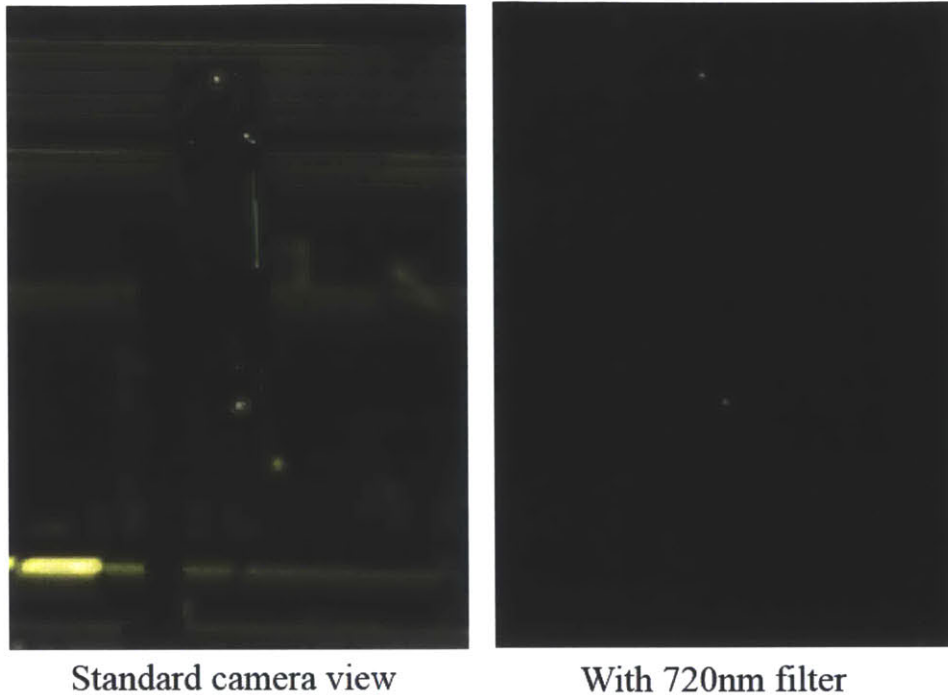
Figure 5-4: Image from the Basler camera before and after installing the 720nm transmitting filter, from [4]

5.1.3 Infrared Marker System

Motion tracking can be done by looking for certain colors or brightness but the advantage of using infrared markers is that infrared sources are only available at low intensities in natural environments, thus there's less risk of confusing a certain color or bright reflectance. Our cameras are outfitted with a infrared transmitting filter (figure 5-2) which removes all visible light and passes waves above 720nm. As an example, figure 5-4 shows the effect of looking at an environment of 850nm emitting diodes through our 720nm transmitting filter. Notice that all of the background is gone, leaving only two white dots, a much easier image to analyze for our software.

The infrared marker system, developed by Krithika Swaminathan, can be seen in figures 5-6(a) and 5-7(a). It was designed to minimize the time that it takes to don the marker system and to minimize power. A green light illuminates when the infrared markers are powered on. In previous renditions, the infrared markers, which are barely visible to the naked eye, were often left in the on position overnight which

Figure 5-5: Raw camera image of the marker system during a training session

drained the battery. Each system runs on a single 9 volt battery which illuminates all four IR markers and the green LED. The two IR markers on the thigh are used to estimate the angle of the hip and the two markers on the shin are used in conjunction with the hip angle to estimate the knee angle. Figure 5-5 is an example image of the camera observing a subject's gait via the infrared markers.

5.2   Software

As shown in figure 2-1, the machine operates in three distinct modes. In the rhythmic and balance modes, the vision system is set up to estimate the heel position of each leg by tracking the hip and knee angles as seen in figure 5-6. In the discrete mode, the vision system estimates the heel position solely based on the two lower markers. The advantage of the rhythmic method is that it bases the estimation of heel position on the thigh (L_t) and shin (L_s) lengths of the subject measured once before the study began. It was acceptable for deciphering the position of toe off (to actuate the sagittal plane drop). The discrete program (described in detail in section 7.1.2) relies on more precise heel measurements and so we estimate it based on the position of the lower markers (figure 5-7) which negates the effect of hip translation (not observed in the rhythmic estimation) in the sagittal plane during training. The marker location (L_m)

123

(a) Picture of study participant during rhythmic training

(b) Marker numbers, lengths and angle definitions
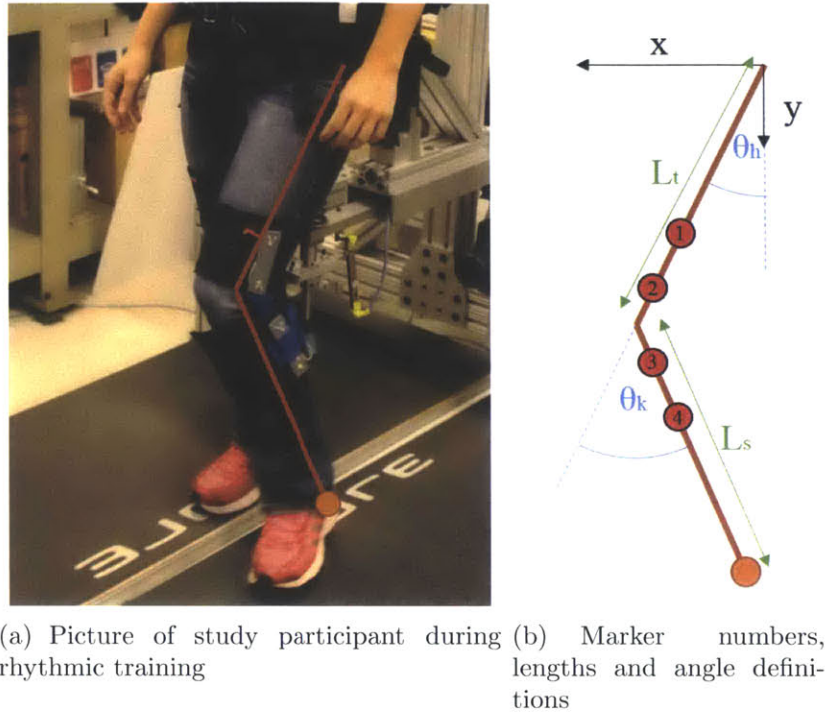
Figure 5-6: Rhythmic method of vision

must be measured each time the subject is fitted with the IR markers.

5.2.1 Vision Loop

Image acquisition and processing occurs in a single timed loop at 100Hz. Figure 5-8 depicts the vision loop. An image is grabbed from the camera, it is then converted to a binary image via a brightness threshold (assigning 1 to light spots and 0 to dark spots). Once the image is mapped into binary, partical analysis is conducted to measure the position of each infrared marker $(x_n, y_n | n = 1 \ldots 4)$. Finally, appropriate trigonometric math is applied to the location of the four markers to estimate the position of the heel by the methods described below.

5.2.2 Angle offset programs

It is difficult to accurately align the infrared emitters with the bones of the thigh and the shin. To account for the error (and to record the initial position of sensor 3 for the discrete case), angle offset programs were run prior to running the main Skywalker

124
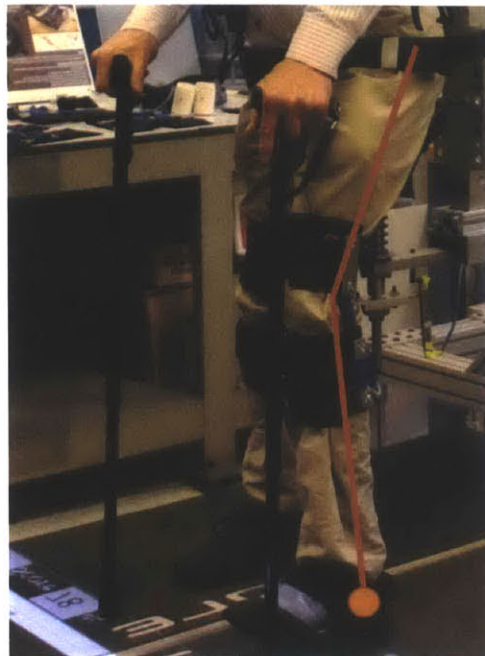
(a) Picture of study participant during discrete training
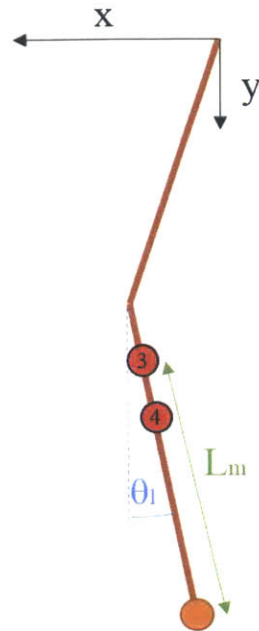
(b) Marker numbers, lengths and angle definitions

Figure 5-7: Discrete method of vision
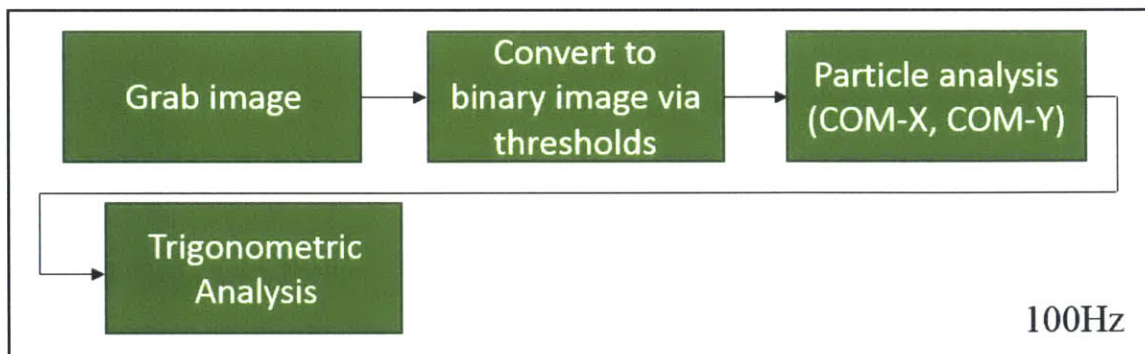
Figure 5-8: Vision loop

programs.

Rhythmic and balance offset program

Subjects were asked to stand straight with their feet directly underneath the hips. Equations (5.1) and (5.2) were used to compute the angle errors of the hip (θ_{hi}) and shin angle with respect to the vertical (θ_{1i}) so that we can offset this error during Skywalker training and data analysis. The rhythmic offset angle loop can be seen in figure 5-9.

$$\theta_{hi} = tan^{-1}\left(\frac{x_2 - x_1}{y_2 - y_1}\right) \tag{5.1}$$

$$\theta_{1i} = tan^{-1}\left(\frac{x_4 - x_3}{y_4 - y_3}\right) \tag{5.2}$$

Discrete offset program

Because we ask participants to point their heel at targets, it is necessary to get a zero position of the heel before running the experiment. For this step, a target is displayed on the track 30mm head of the body (so that subjects can see it). Once the subject moves his heel to the target, the angle offsets and the x-pixel location of marker 3 (x_{3i}) are recorded. Code for the discrete offset program is shown in figure 5-10.

5.2.3   Measuring angles during training

Rhythmic and balance mode

As previously stated, the rhythmic and balance mode estimates the heel position based on the measured hip and knee angles. The hip angle (θ_h) is calculated as seen in equation (5.3). The knee angle (θ_k as defined in figure 5-6(b)) is relative to the axis of the thigh, which is a measure of pure knee bend, calculated by equation (5.4). Finally, x_r, the x-position (position of the heel along the fore-aft axis of the treadmill) is calculated in real time via equation (5.5), where L_t is the length of the
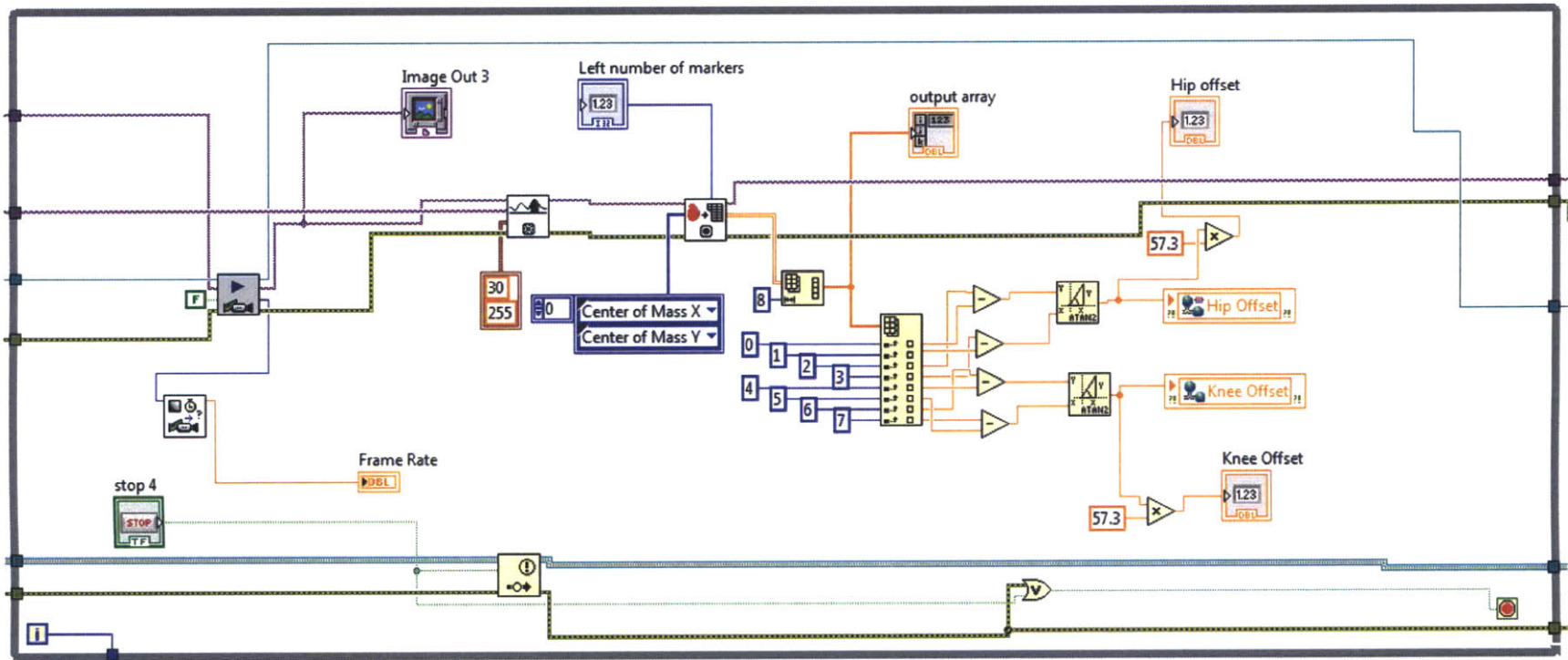
Figure 5-9: Rhythmic angle offset program
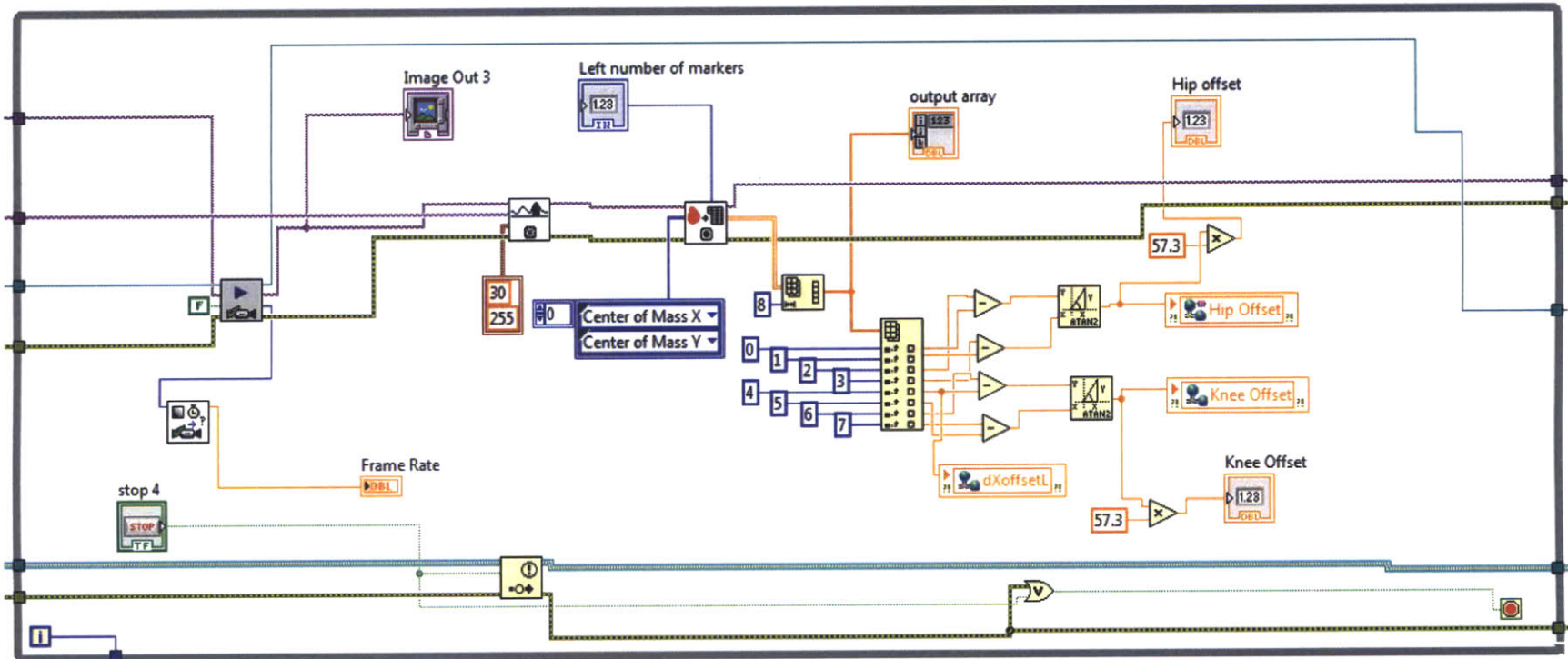
Figure 5-10: Discrete angle offset program

thigh measured from the hip joint to knee joint and L_s is the length of the shin measured from the knee joint to the lateral malleolus. Notice here the origin and coordinate system defined at the top of figure 5-6(b). Code for the rhythmic vision loop is shown in figure 5-11.

$$\theta_h = tan^{-1}(\frac{x_2 - x_1}{y_2 - y_1}) - \theta_{hi} \tag{5.3}$$

$$\theta_k = \theta_h - (tan^{-1}(\frac{x_4 - x_3}{y_4 - y_3}) - \theta_{1i}) \tag{5.4}$$

$$x_r = L_t sin(\theta_h) + L_s sin(\theta_h - \theta_k) \tag{5.5}$$

Discrete Mode

The discrete program utilizes only the lower two markers as seen in figure 5-7(b). Here we calculate the x-position (x_d) as seen in equation (5.6), where L_m is the distance from marker 3 to the lateral malleolus, x_3 is the x-position of infrared marker 3, k is the real world conversion factor (0.4mm/pixel - not shown here), and 30 mm are added to the position to account for the zero position being taken 30mm ahead of zero as mentioned above. The shin angle (θ_1) is calculated via equation (5.7). Notice in figure 5-12, that we still record both hip and knee angles during discrete training.

All Labview algorithms shown negate the final x-values. This is because Labview partical analysis sets a coordinate system at the top left corner of the picture. For simplicity in this chapter, the coordinate system for the equations presented is shown in figure 5-7(b), positive x in the direction of a forward step.

$$x_d = k(x_3 - x_{3i}) + L_m sin(\theta_1 - \theta_{1i}) + 30 \tag{5.6}$$

$$\theta_1 = tan^{-1}(\frac{x_4 - x_3}{y_4 - y_3}) \tag{5.7}$$

129
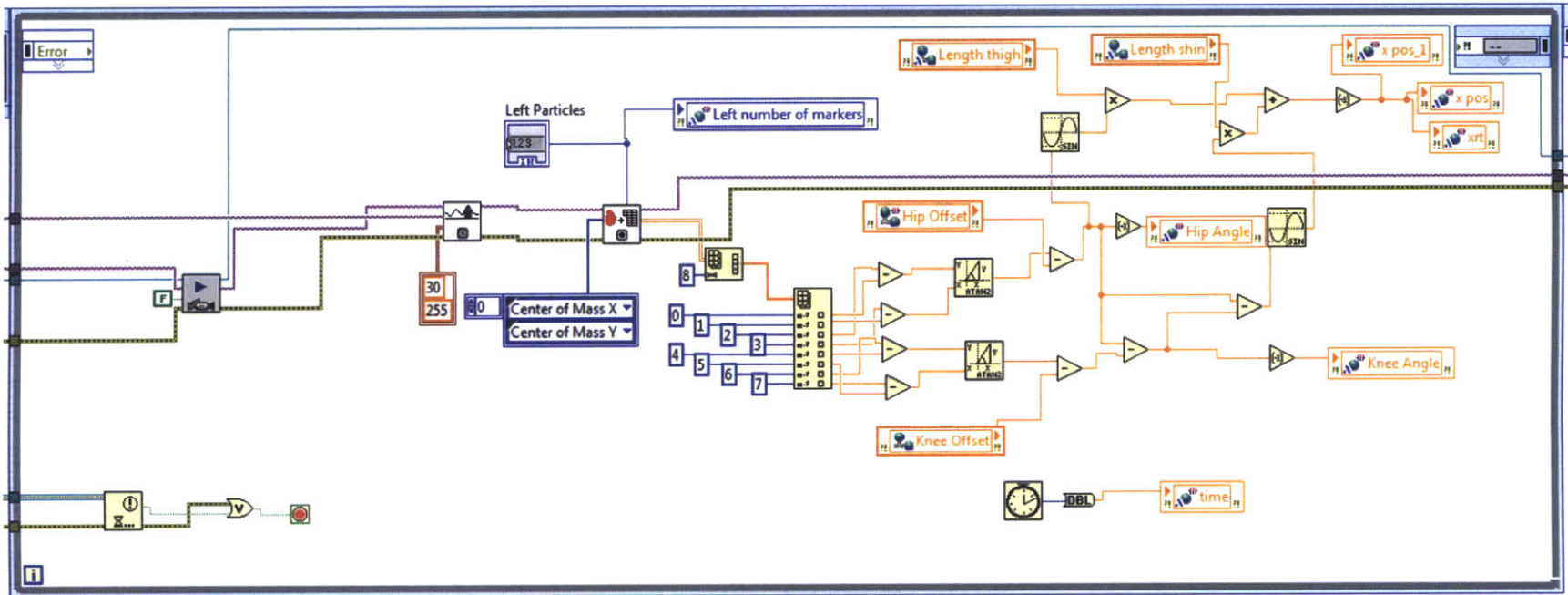
Figure 5-11: Rhythmic real-time vision tracking algorithm
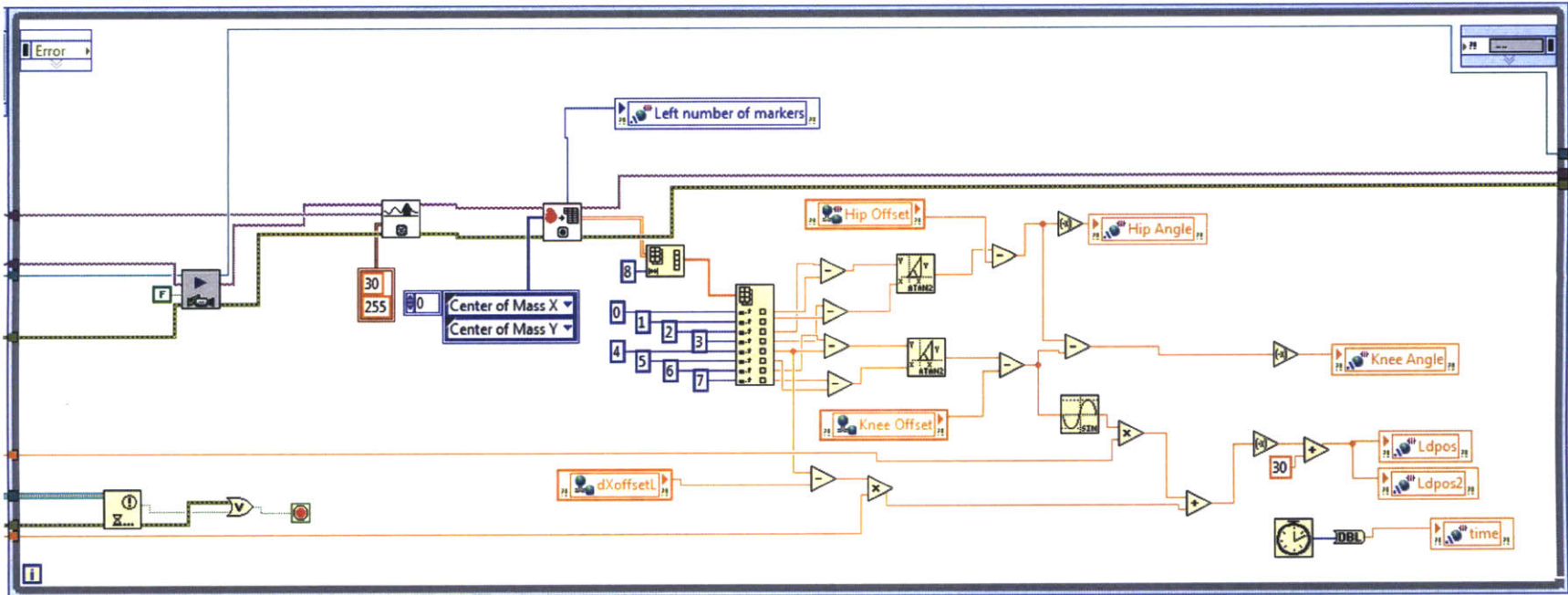
Figure 5-12: Discrete real-time vision tracking algorithm
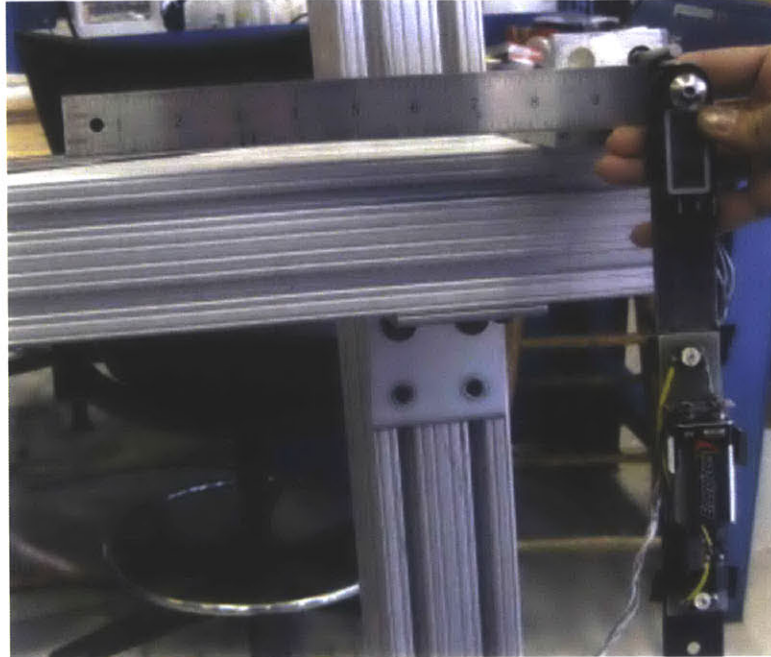
Figure 5-13: Digital Protractor used for angle accuracy measurements

5.3 Characterization

To determine the maximum loop rate of the vision loop, the non-specified (run as fast as possible) loop completion time was recorded. Over 300 ms of recorded loops, the mean loop time was 7.35ms with a standard deviation of 1.43ms. Because we wanted the loop to be mostly repeatable but also to run as fast as possible, a loop time of 10ms was chosen. The system proved that it was capable of sustaining the 100Hz rate through all of our programs.

To test the accuracy of measured angles, a digital protractor[3] with a published accuracy of $\pm 0.2 degrees$ was mounted at the position of the subjects legs in front of the camera (figure 5-13). The protractor was moved from -80 to 80 degrees and 100 measurements at each position were taken by the vision system. Figure 5-14 shows the angles measured by the cameras, most of which stay within the accuracy band of the digital protractor. Thus, our vision system's accuracy is $\pm 0.3 degrees$.

---

[3]igaging digital protractor 35-408 http://www.igaging.com/
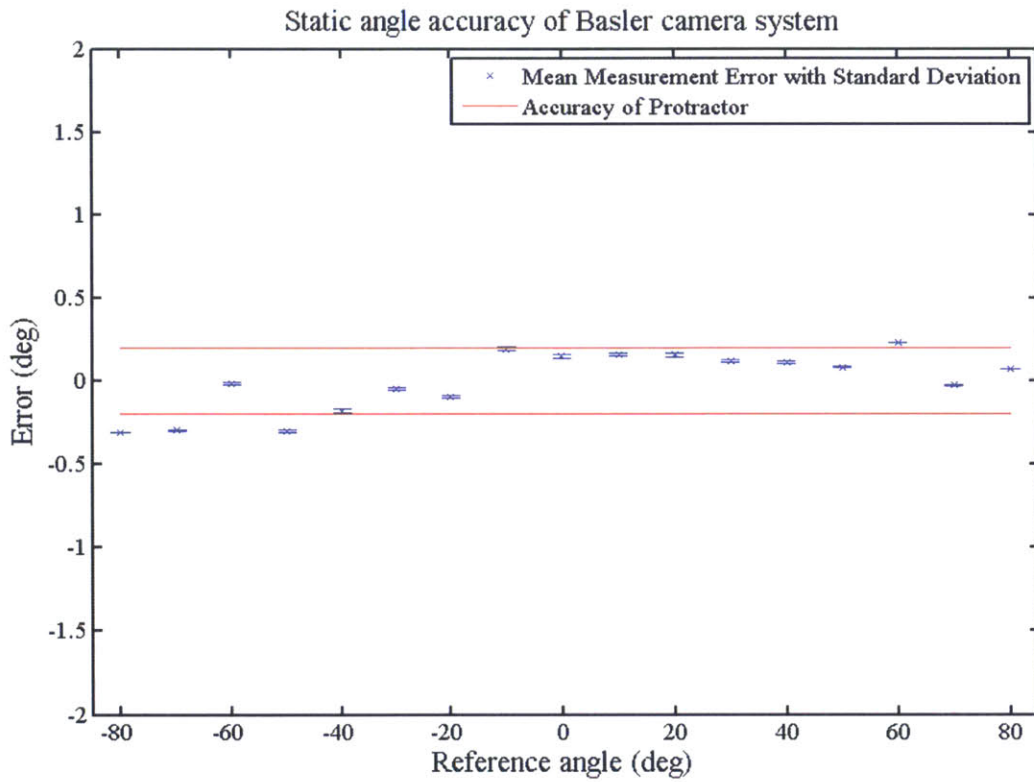
Figure 5-14: Angular accuracy of the vision system

Chapter 6

Controls and Characterization

Skywalker-γ has 5 independent active degrees of freedom (as shown in section 3.1) which can be broken into 3 unique drives because the system is symmetric across the center sagittal plane. This chapter provides more detailed dynamic models of each drive system and highlights the design of each feedback control system.

In characterizing Skywalker-γ, care was taken to follow the steps taken by previously designed rehabilitation robots to properly characterize the system[52, 53, 42, 50, 60, 87, 54, 55]. While literature varies surrounding the introduction of a new rehabilitation robot, a typical path for characterizing a system can be defined by the following steps.

1. Define the technical capabilities of the machine

2. Compare EMG and relevant kinematic profiles between healthy subjects with and without the machine

3. Conduct a feasibility study with patients using the new hardware

Figure 7-10 shows the kinematic differences of walking on Skywalker with and without the body weight support system. Chapter 7 details an initial feasibility study conducted with 3 impaired individuals and this chapter focuses on the the technical characterization of the MIT-Skywalker-γ to fully understand the hardware. Specifically, we observe the capability of track drops, the speed and bandwidth of the
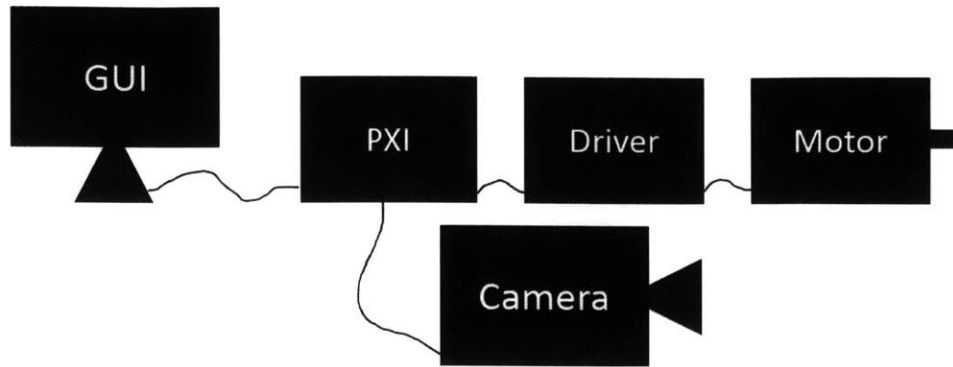
Figure 6-1: High Level Controls System Architecture

treadmill tracks, and the ability of the machine to create frontal plane perturbations that disturb balance.

6.1 High Level System Controls

6.1.1 Control System Architecture

The full control system is shown in figure 6-1. The high level controls are programed in Labview[1] via the graphical user interface. The controls are then sent to the National Instruments real-time PXI control module, a modular device that can easily add functionality via a large assortment of input/output cards. The PXI module will receive and issue real-time analog and digital commands to the Kollmorgen AKD motor driver[2]. The driver will receive an appropriate signal and shape that signal into a current to provide torque to the motor. The motors are outfitted with either Smart Feedback Devices (SFD), a proprietary method of feedback from Kollmorgen which is based on a resolver or 5000 line incremental encoders (in the case of the treadmill motors). The feedback device will send information about motor position and velocity to the Driver.

Integrated motion controls can be set up within the motor driver using the Kollmorgen AKD workbench, a graphical user interface that acts as a compiler for the

---

[1]National Instuments, Austin, TX - www.ni.com
[2]Kollmorgen, Danaher Business Systems, Radford, VA - www.Kollmorgen.com

136

firmware inside of the AKD motor driver. There is also the option of using the driver as a current controlled amplifier while handling the controls within an external device, in our case the National Instruments PXI box. The drivers are capable of being programmed to output the position of the motor, operating in an emulated encoder mode. This information is sent to a PXI card which incorporates a counter to obtain position information. The PXI box will then close the feedback loop and output an analog voltage output corresponding to the current command to the drivers.

Two high speed cameras are used for feedback on the positions of the upper thigh and shin of the subject on the treadmill track to estimate the phase of gait. The vision data is processed by the PXI system to output the position of the foot on the track for use in generating control outputs.

Integrated Motor Controls

Integrated Controls inside of the Kollmorgen motor drivers offer a single solution for motion control, which allows novices the ability to work with motion control. It also scales up with customizable filters and controllers for those with a more acute controls understanding. Specifically, the Kollmorgen motion controllers can be set up in one of four ways:

1. **PST, Automatic Tuning** There is the PST (performance servo tuner) which supplies noise to the system, defines the system and then applies gains and filters to define a system with 0.6 or 0.7 damping ratio. As a side note, in all three of the different types of drives used in Skywalker, I was unable to get the PST to work properly. In the sagittal and frontal plane drives, the backlash in the gears made the system unidentifiable by applying noise. The treadmill track has resonances at somewhere near 100 Hz and thus noise in this range made the drive sing considerably, to the extent it was highly disturbing to surrounding labs and thus it was stopped before completing the sweep.

2. **Bode Plot, Manual Tuning** Similar to the PST, the system can manually be run through a sinusoidal sweep to generate a bode plot. This function is fairly

powerful and allows the controls designer to then shape the loop with internal controls manually. The advantage of this method is the freedom to define the excitation frequencies which allows the user to avoid the high frequency resonances that became pronounced in the PST. This method was used to define the frequency characteristics of the treadmill drive.

3. **Sliding Tuner, Automatic Tuning** There is a sliding tuner that can be used to make the system stiffer or softer (essentially scaling the bandwidth). The drive will then define PI gains that will create the desired drive feeling. Kollmorgen recommends observing the machines operation and if a faster response is needed, the tuner should be moved higher. Alternatively, if the motor begins resonating, the tuner should be moved lower. This is the crudest way to define controls but could work in some applications, specifically those without multiple resonances.

4. **Inertia Approximation, Automatic Tuning** The final method of sytem tuning is to input the inertia projected onto the motor from which the drive software will determine initial gains. Based on the performance, the controls designer can then modify these controllers as needed to get better performance. A step response can be used to validate the understanding of the loop dynamics and improve the system performance. This method was used with both the frontal plane and the sagittal plane controls.

The full controller loop defined by the Kollmorgan AKD drivers is shown in figure 6-2. A motion profile is given to the position loop as a series of positions in time. This profile can be internally defined by a trapezoidal profile or a customized set of points given to the driver or can be specified by an external analog voltage input. The output of the position loop is the input to the velocity loop. Finally, the output of the velocity loop is the input to the current loop.

Position Loop

The parameters for controlling the position of the motor.

Velocity-Feed Forward Gain

d/dt

Velocity Profile

Position Command

Max Position Error

Integral Gain

Proportional Gain

Velocity Command

Position Feedback

(a) Position Loop

Velocity Loop

The parameters for controlling the velocity of the motor.

Acceleration Feed Forward

d/dt

Velocity Profile

Ramp Limiter

Velocity Clamp

Friction Compensation

SIGN

Viscous Damping Compensation

Observer Bandwidth

Velocity Command

AR 1

AR 2

PI Controller

Current Command

Observer Mode Control

Observer

Current Command

AR 4

AR 3

Velocity Feedback

Unfiltered Velocity Feedback

10Hz Lowpass

Filtered Velocity Feedback

(b) Velocity Loop

Current Loop

Parameters for controlling the torque/force of the motor. Usually no changes are needed with correct motor data.

Coulomb Friction Comp.

Velocity Command

Current Command

Limiter

PI Controller

Voltage Command

Current Offset

Current Feedback
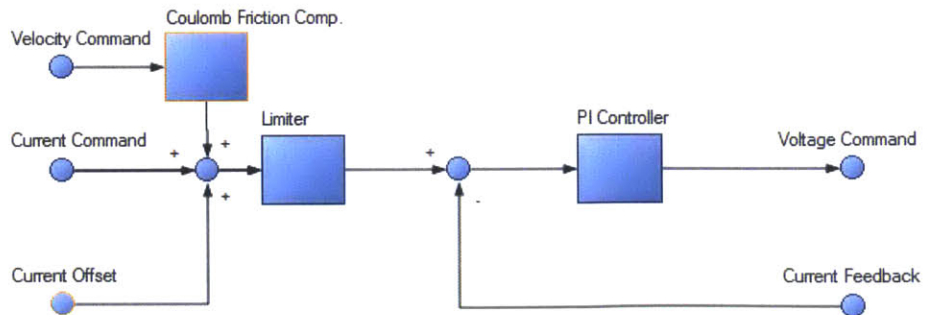
(c) Current Loop

Figure 6-2: Kollmorgen Integrated Control Loops

Custom Motor Controls

While the integrated controls offer the ability to create motion faster, it is often difficult to understand the low level functions of the drives. I will give three examples run into during this thesis:

1. When using the automated homing functions inside of the motor driver, it requires setting up very specific parameters, which the user may not understand. In our case, I used a homing mode that looks for mechanical stops, upon finding the stops, it will reverse direction. However, as I found out, if the current limit is set too low for the stops, it will not be able to complete the full drop of the sagittal plane. The result was that the full homing motion could not be performed with the set torque. When the homing timed out, the current limit was set back to the maximum of the motors which created a huge surge of torque and pushed the track back to horizontal in a very fast manner which was not only scary but dangerous. This is an example of a conceptual bug in the plug and play controls system that can have potentially dangerous consequences.

2. It is difficult to discern technical concepts such as delays within the control loop because the internals are hidden from the designer. We know that delays in control systems both compromise stability and increase the oscillatory nature of systems.

3. Using the integrated bode plot function was somewhat unclear. Even when switching to position mode, the plant bode plot would always result in a current in velocity out which took time to understand. In this case, I found myself having to reverse engineer the system to understand what was happening. It is still unclear if the bode pot shows current-in or torque-in. My model agrees with torque-in but is that an error in my model? These are the types of uncertainty associated with integrated functions. It is important to note that Kollmorgen outsources its support to the salesmen that sell the machines who are versed in the basics of motion control but do not fully understand the in-depth engineering to aid in issues such as these.

Writing custom controls is not completely transparent because were still using the drivers as a current controlled amplifier, which in itself is a closed loop control system. However, it is generally assumed that electronic dynamics are far faster than mechanical dynamics so it is usually a safe assumption to ignore these.

The advantage of custom controls is the ability to write a controller that is well understood by the designer and capable of being started from scratch. The downside of custom controllers is that it will take far more time upfront to write custom controllers and will require fast hardware. Skywalker-γ will use a custom position controller for the treadmill tracks during the discrete training paradigm. This is because the analog input to the motor drivers and from the PXI box is -10 to 10V. In implementing fine control of the tracks, we will run out of position points because the drivers are sensitive to millivolts not microvolts meaning that we can only command a maximum of 20,000 points if the resolution is perfect for millivolts which was not observed to be the case in tests. In fact, the voltage read in by the drivers was observed to have an error of approximately 0.8% of the PXI voltage out. If this is the case, the resolution drops by a factor of 10 so we can command 2,000 position points. Using custom controls inside of the PXI box allows an infinite number of position points for the motor so we never have to worry about the position of the track reaching a limit. We simply output an analog signal between -10 and 10V that corresponds to current.

6.1.2   Drive Controls of the Different Training Paradigms

In designing Skywalker-γ, it was important to be able to quickly switch between training paradigms in order for a patient to be able to use each mode within the same therapy session. For this reason, care was taken to carefully consider the methods by which each drive would interact with the PXI box. The sagittal plane and frontal plane drives are only used in one mode in which motion profiles (MPs) are defined within the AKD motor drivers but the treadmill drive needs to switch between velocity mode and current mode for the rhythmic and discrete training paradigms respectively. Details about the training paradigms themselves can be found in section 7.1. Table 6.1 shows a summary of the methods of closed loop motor control in each training

Table 6.1: Summary of control modes for each training paradigm

		Paradigm		
		Rhythmic	Discrete	Balance
Treadmill	Controls	Driver Integrated	Custom Labview	Driver Integrated
	Type	Analog/Velocity	Analog/Current	Analog/Mode
Sagittal Plane	Controls	Driver Integrated	N/A	Driver Integrated
	Type	Digital/MP	N/A	Digital/MP
Frontal Plane	Controls	N/A	N/A	Driver Integrated
	Type	N/A	N/A	Digital/MP

paradigm. In this table the type refers to the actual voltage signal type reaching the motor driver from the PXI control box. In the case of analog voltages, they can be programmed in the drive to correspond to velocity, position or current. The balance paradigm can be used to augment both the discrete and rhythmic training paradigms and thus the type of treadmill control will vary depending on the mode selected. Digital voltage types will correspond to saved MPs within the firmware of the drive.

6.2 Sagittal Plane Technical Characterization and Controls

The sagittal plane motion was designed primarily to accomplish the Skywalker rhythmic training paradigm (ie. to drop during swing phase) but can also be used for practice walking at a ascending or descending slope or for perturbations. This thesis focuses on training, and thus characterization of the sagittal plane focuses on unloaded drops.

6.2.1 Sagittal Plane Modeling

The sagittal plane drive can be modeled as shown in figure 6-3. This lumped parameter model reflects the inertias of the treadmill track including the torsional restraint linkage into a single rotational inertia (J). Section 3.2.3 explores a similar model that
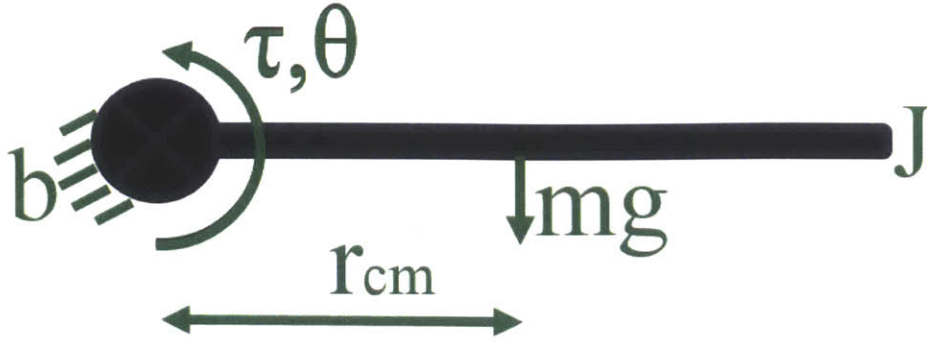
Figure 6-3: Sagittal plane model for control

was used to determine a proper drive during design. The current model is developed to aid in the development of a controller. A linear representation of the system allows us to use the many simplistic linear control methods including bode plots, step responses and root locus visualization tools.

The equation of motion for this simple system is shown below:

$$J\ddot{\theta} + b\dot{\theta} + mgr\cos(\theta) = \tau \tag{6.1}$$

Linearizing this equation about $\theta = 0$ yields the equation:

$$J\ddot{\theta} + b\dot{\theta} = (\tau - mgr) \tag{6.2}$$

Equation (6.2) is linear, however, because of the constant mgr term, it fails the homogeneity requirement of a linear system. The *mgr* term can be thought of as a torque input to the system which will add to the input torque when torque is in the negative direction and subtract from the net torque in the positive direction. This is one of the nonlinearities within the system. The final homogeneous linear model to be used for control is shown in equation (6.3).

$$J\ddot{\theta} + b\dot{\theta} = \tau \tag{6.3}$$

Finally, we can take the Laplace Transform of equation (6.3) to arrive at the transfer function:

143
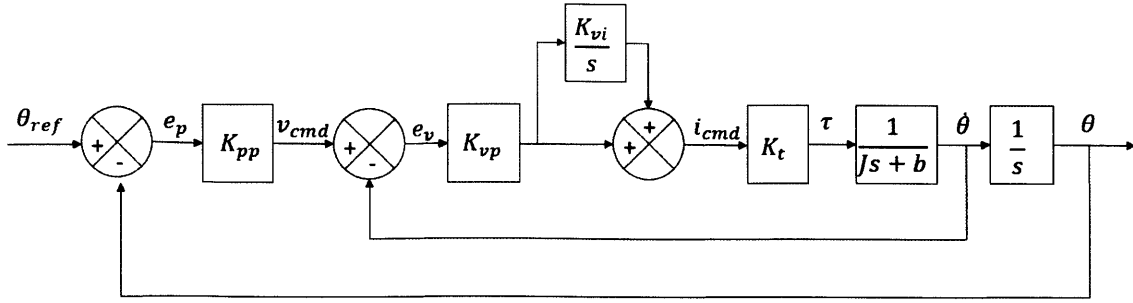
Figure 6-4: Sagittal plane closed loop control

$$\frac{\theta(s)}{\tau(s)} = \frac{1}{s(Js + b)} \tag{6.4}$$

Other nonlinearities not modeled in this mechanical system include the backlash between the motor pinion gear and the linear rack and the backlash between the cam follower and the linear cam. It is important to note that the cam path on the linear cams is nonlinear with a significantly higher transmission ratio in the horizontal position. Additionally, the sagittal plane angle introduces another source of nonlinear behavior considering the torque generated by the weight and the angle between cam path and the track.

6.2.2 Sagittal Plane Controls

The PST was very rough on the sagittal plane and due to backlash in the gears, could not accurately measure the sagittal plane drives. In order to get a starting place for control, the reflected inertia seen in table 6.2 was entered into the AKD Workbench software. The software then defined appropriate gains. The linearized control loop that was generated can be seen in figure 6-4. The current loop is defined as simply K_t because is not modifiable and assumed to be much faster than the mechanics of the system.

This type of control is known as full state feedback, implementing a velocity loop inside of the position loop. The closed loop transfer function of the inner loop is:

144

$$\frac{\dot{\theta}}{v_{cmd}} = \frac{K_{vp}K_t(s + K_{vi})}{Js^2 + (b + K_{vp}K_t)s + (K_{vp}K_tK_{vi})} \tag{6.5}$$

To utilize a bode plot for stability and transient behavior prediction, the return ratio (R.R.) is developed below:

$$R.R. = \frac{\dot{\theta}}{v_{cmd}} \frac{K_{pp}}{s} \tag{6.6}$$

Table 6.2 shows the parameters used within this model. The inertia (J) was calculated from the Skywalker β calculations from section 3.2.3 while adding on the reflected inertia due to the Skywalkerγ linkage. Motor damping (b_m) is published and the system damping (b) was determined with a course estimation of the remaining friction elements taken through the transmission ratio associated with that damping. The torque constant (K_t) is published and the remaining gains were determined by the AKD drive based on the reflected inertia of the system.

Table 6.2: Sagittal plane control simulation parameter values

Parameter	Value
Skywalkerγ reflected motor inertia (J)	0.007 kgm^2
Published motor damping (b_m)	0.00052 Nm/(rad/s)
System reflected motor damping (b)	0.001 Nm/(rad/s)
Torque constant (K_t)	1.75 Nm/Amp
Position loop proportional gain (k_{pp})	50
Velocity loop proportional gain(k_{vp})	0.164
Velocity loop integral gain (k_{vi})	1

Using these parameters with the return ratio specified by equation (6.6), we end up with return ratio poles at 0, -1 and -40 with a zero at -1 radians per second. The corresponding bode plot and simulated step response is shown in figure 6-5. From the bode plot, we can observe a bandwidth (magnitude crossing -3dB) at 47 radians per second with a phase margin of 47 degrees. These theoretical values will correspond to a system natural frequency (ω_n) of 7.5 Hz with a damping ratio of approximately 0.47, which is ultimately shown in figure 6-5(b).

It is important to note that the control gains from table 6.2 are a starting point set up by the software of the Kollmorgen AKD Workbench and by no means optimal.

Bode Diagram
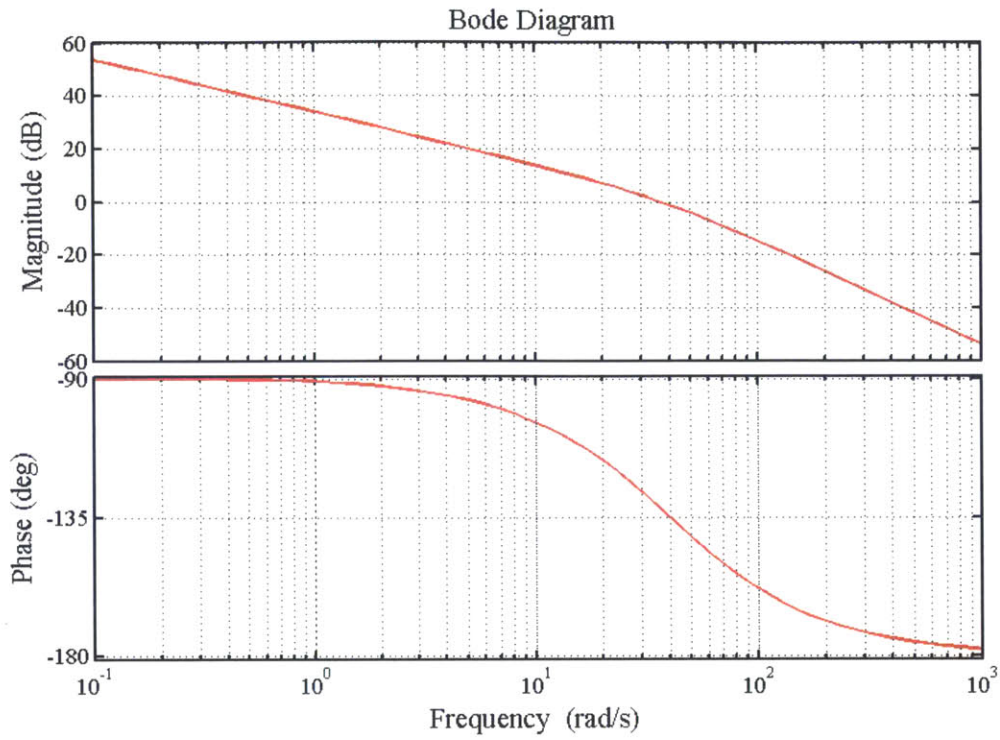
(a) Original control return ratio bode plot
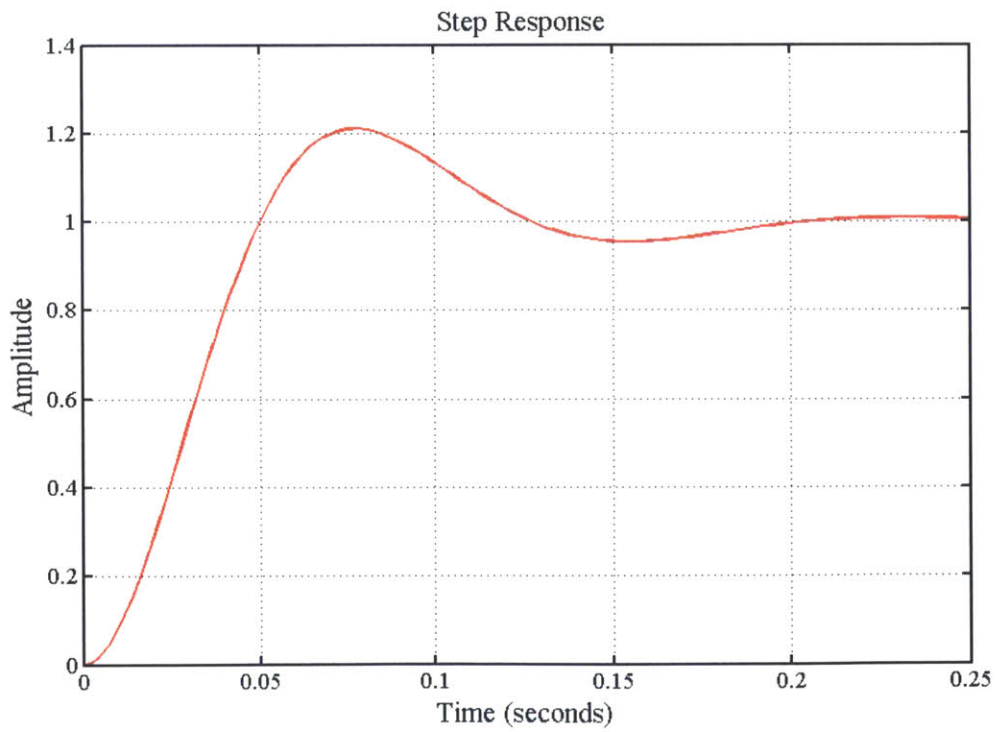
Step Response

(b) Original control closed loop step response

Figure 6-5: Sagittal Plane, initial control analysis

146
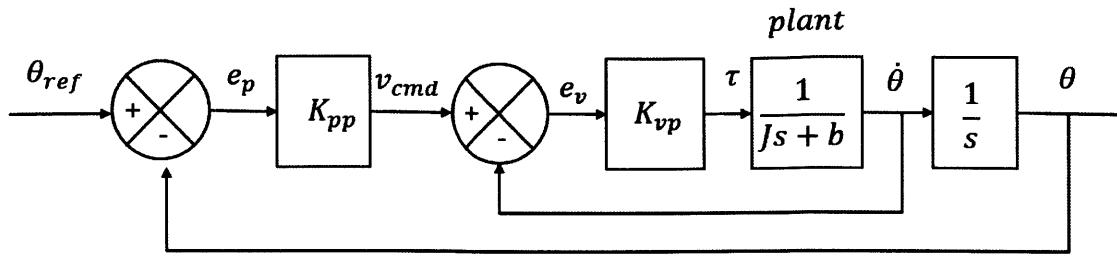
Figure 6-6: Simple full state feedback sagittal plane control loop

The integrator term, K_{vi} in the velocity loop does little for the response of the system, making it respond a little bit faster but with a lower damping ratio, leading to a more oscillatory system, especially at higher integrator gains. To improve the response of the system, we can take advantage of the pole placement nature of full state feedback by placing the second pole further negative. To illustrate this point, consider a simpler control loop as shown in figure 6-6. In this loop, the integrator term (K_{vi}) in the velocity loop and the torque constant (which can simply be considered as part of K_{vp}) are removed. The closed velocity inner loop will now be:

$$\frac{\dot{\theta}}{v_{cmd}} = \frac{K_{vp}}{Js + (b + K_{vp})} \qquad (6.7)$$

The return ratio of the position outer loop will become:

$$R.R. = \frac{\dot{\theta}}{v_{cmd}} \frac{K_{pp}}{s} \qquad (6.8)$$

Thus, increasing the value of K_{vp} sends one of the two poles in the position loop further negative. This action will make the system response more damped because the phase margin will increase. The further the pole is pushed left, the greater K_{pp} can be made while keeping the system optimally damped. Of course, this is at the expense of control effort and for large accelerations of the track, the system will run out of torque capacity. Theoretical responses are shown in figure 6-7 for various values of K_{vp}, holding all other values constant as shown in table 6.2, except K_{vi} which is now set to zero corresponding to the control loop in figure 6-6.

147
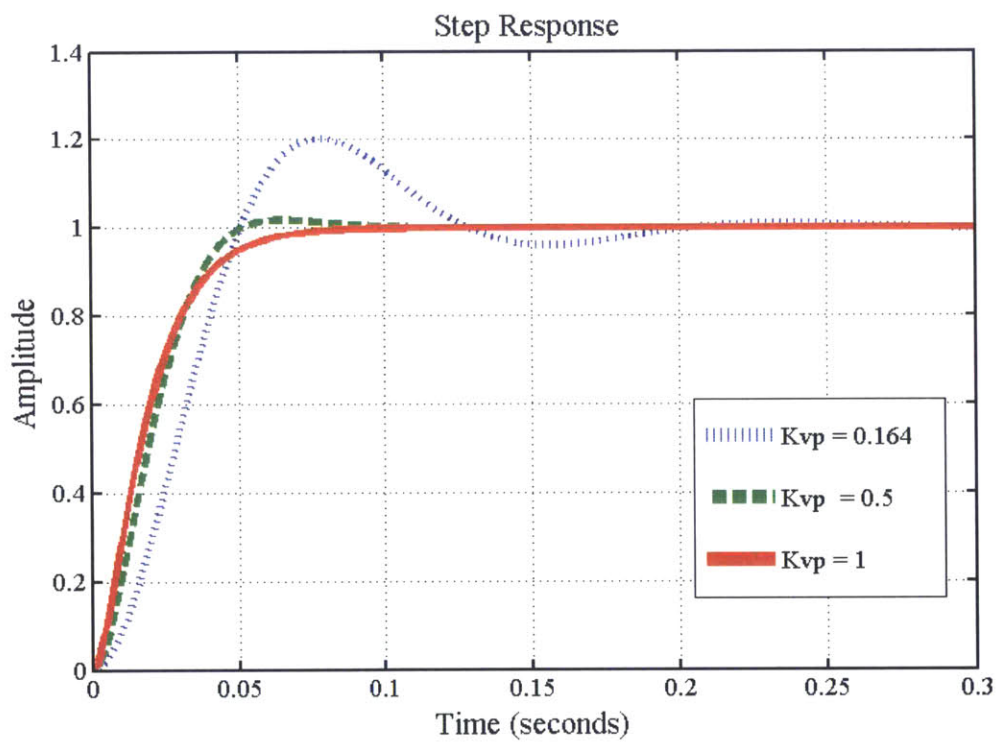
Figure 6-7: Step responses with variable K_{vp}

To test the controls and to define the bandwidth and damping ratio, a step response of the Skywalker-γ hardware was observed in order to compare it to the linear model. Figure 6-8 shows the behavior of the the system for a small drop step response (200° motor angle corresponds to 2.3° drop of the track). Notice that the Kollmorgen drivers do not allow infinite acceleration, thus the motion profile resembles a ramp rather than a step. In order to compare this response to the model, the model was run using the "'ltisim"' function in Matlab[3] to test the theoretical response to the same input. The red line in figure 6-8 corresponds to the input command, the black to the actual response of the Skywalker hardware, the blue to the theoretical response to that input, and the green line shows a theoretical step response of the model. The peak time of the actual plot is 10ms slower than that of the actual model, with the same general response, showing a close resemblance between actual and simulated response. It should be noted that a 20% increase in the theoretical mass and damping within the model makes the response match closer.

The homogeneity property of LTI systems tells us that as we scale the input, the output will scale to the same degree. To test the level of Skywalker's conformance to this property, another step response was run, this time, lifting the track from 400° to 800° as referenced to the motor or a range of about 4.6° as referenced to the track angle. Figure 6-9 shows the response to this motion profile. The peak time of the actual system is 15 ms behind that of the theoretical model this time, showing small signs of nonlinearities in the model.

There are several properties of the actual sagittal plane drive that violate the requirements of a linear time invariant system, for example, the backlash in the gears, the operating condition in the vertical plane and friction. Additionally, at higher torque values, the torque constant (K_t) becomes nonlinear ie. it takes more incremental current (δi) to produce an incremental torque($\delta \tau$). This happens at 13.2 Amps according to Kollmorgen[4]. The current plot when performing the step response in figure 6-9 is shown in figure 6-10. Notice that when performing the lifting step

---

[3]MathWorks www.mathworks.com

[4]Kollmorgen AKM selection guide
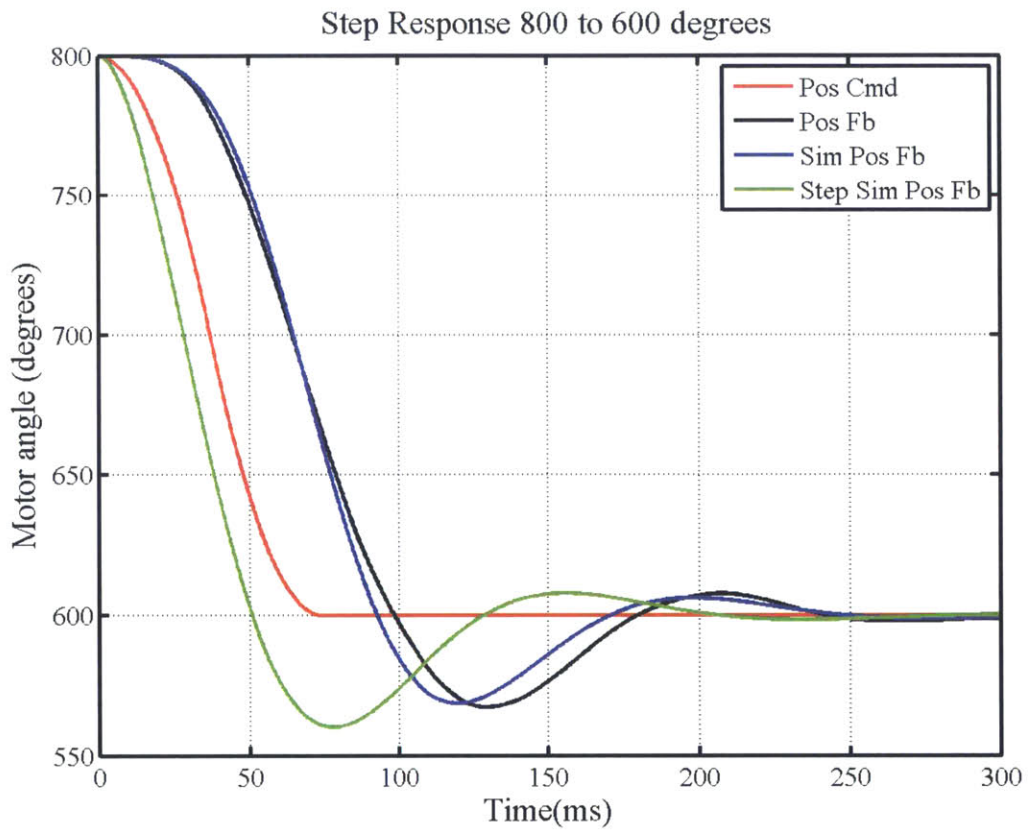
Figure 6-8: Sagittal Plane Step Response: 200 motor degree drop
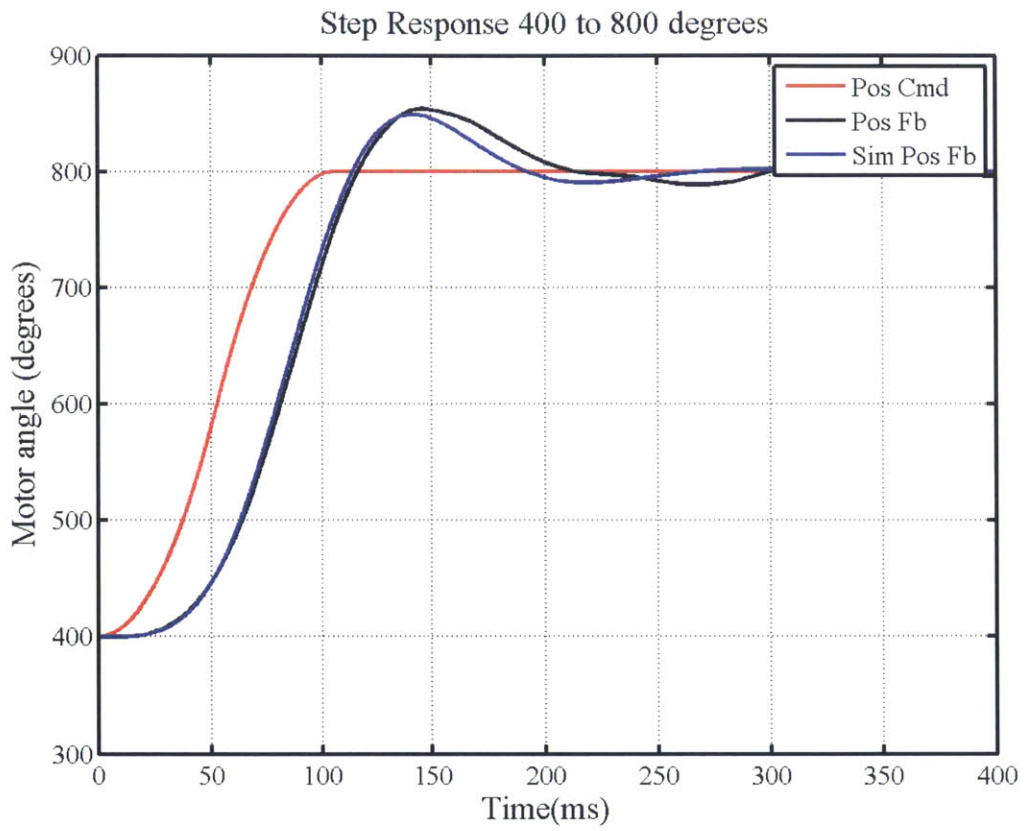
Figure 6-9: Sagittal Plane Step Response: 400 motor degree lift

Step Response Current 400 to 800 degrees

13.2 A

Time(ms)
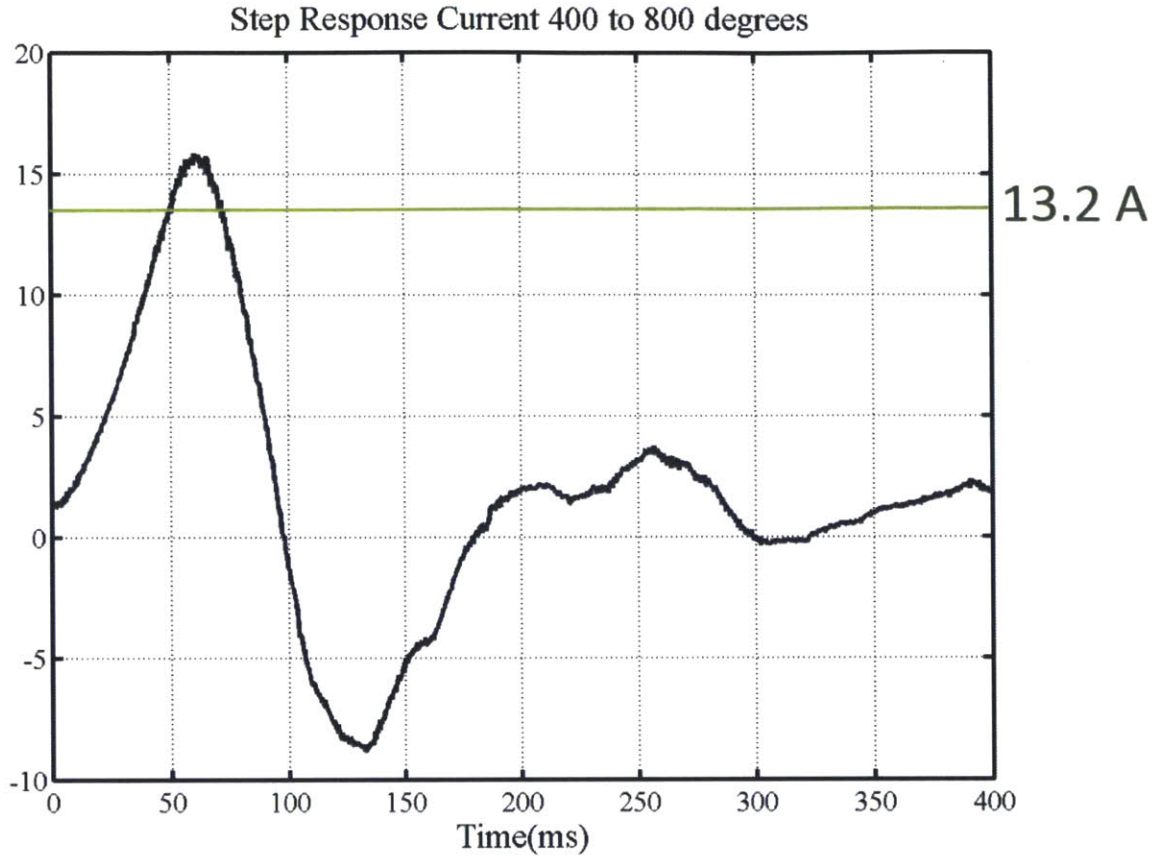
Figure 6-10: Sagittal plane step response current: 400 motor degree lift

response, we spend 20 ms or so in the nonlinear range. Some combination of these nonlinearities is likely the cause of the increased peak time.

6.2.3 Sagittal Plane Characterization

The primary purpose of Skywalker is to encourage gait rehabilitation for stroke patients. In doing so, it is important to know the "'track drop"'capabilities of the machine, ie. how fast and how far the track may drop. Once known, it is important to know what drop profiles will feel comfortable to a patient. The step responses above, while very fast, were very intense, resulting in high acceleration that would be felt by the subject. Finally, in previous Newman Lab robots such as the Anklebot, force could be estimated precisely using the motor current. This capability was tested briefly, showing the effect of loading the track at various locations. This section will

be broken down into four smaller sections: range of motion, technical system response characteristics, practical drop profiles and current / force estimation.

Range of motion

The cam-path is capable of dropping the track to $-11.6°$, however, the Skywalker-γ will rest on hard stops at $-11°$. It is important to know the low position in order for the tracks to come down for a person to mount as well as to know how deep to drop during training. When homing the tracks, we use a magnetic reed switch on the rack gear that finds a zero position corresponding to a track position of about $-10.3°$. Reed switches will recognize the magnetic field at a fairly wide range, therefore, we want it to catch one of the ends of travel to know we hit the same boundary of the magnetic field each time. The Skywalker will then move to a motor position of $920°$ which corresponds to the horizontal position of the tracks. In order to command the Skywalker to move to the resting low position, we can encode the motor to drop to position $-63°$ which corresponds to a track position of $-11°$. The upward position is limited only by the cam which has a $2.5°$ gain in angle over the horizontal. In summary, table 6.3 shows the obtainable range of motion for the sagittal plane drive.

Table 6.3: Sagittal plane range of motion

	High Angle	Horizontal Position	Low Angle
Track Angle	$2.5°$	$0°$	$-11°$
Motor Angle	unknown	$920°$	$-63°$

Technical system response characteristics

Step responses and bode plots permit understanding of the capabilities of hardware, telling us the bandwidth (ie. the natural frequency of a step response - the fastest frequency the system can follow), the phase margin (ie. the damping ratio - the characteristic oscillatory behavior) and how close a linear model corresponds to the actual hardware. This information lets us know how fast we can perturb a subject when mounted on the device, something that may be useful in future studies if Skywalker is used to deduce the mechanical impedance of the body during walking. It could

also be used for studies that we are not considering at the moment. For immediate use, this information allows us to know the limit of how fast we can move the tracks for use with the rhythmic paradigm.

To determine the the damping ratio (ζ) of the sagittal plane system, we will use equation (6.9), a common equation that can be found in any controls textbook (where $\%OS$ is the percent overshoot).

$$\zeta = \frac{-ln(\%OS/100)}{\sqrt{\pi^2 + ln^2(\%OS/100)}} \tag{6.9}$$

Figure 6-8 shows the step response of both the simulation and the actual skywalker tracks. Notice that equation (6.9) corresponds only to a true step response, not one of the profile that the actual system was given. However, we can see from figure 6-8 that the simulation has approximately the same overshoot as the real system with the given input. Because of this, we can make the statement that the real system has approximately the same $\%OS$ of the simulation. In the true simulated step response, the $\%OS_{Simulation} \approx 20\%$, which corresponds to a damping ratio of $\zeta_{simulation} \approx 0.46$ and thus $\zeta_{real} \approx 0.46$. We can now estimate the natural frequency of the system using equation (6.10).

$$\omega_n = \frac{\pi}{T_p\sqrt{1 - \zeta^2}} \tag{6.10}$$

Again, equation (6.10) corresponds only to a true step response. We can use it to estimate the simulation step response natural frequency which comes to $\omega_{n,step} = 48rad/s$. In order to find the real system's ω_n, we can estimate the peak time that the real system would have ($T_{p,real}$) to a true step input as equation (6.11) because the real system's peak occurred 10ms behind that of the simulated system to the same input.

$$T_{p,real} = T_{p,Step} + 10ms \tag{6.11}$$

We can then use equation (6.10) with $T_{p,real}$ to estimate a real system natural

154

frequency of $\omega_{n,real} \approx 42 rad/s \approx 6.7 Hz$.

Using the same method, we can then estimate the damping ratio and natural frequency of the raising step response seen in figure 6-10. Notice this time that the real system has slightly higher overshoot, ($\%OS_{Real} \approx 1.1 * \%OS_{Real}$). We can then use equation (6.9) to conclude that in this situation, $\zeta_{real} \approx 0.43$. To find the natural freqency of this response, we use the same approximation as before, this time with a 15 ms delay on the peak time:

$$T_{p,real} = T_{p,Step} + 15ms \tag{6.12}$$

This leads us to estimate a peak natural frequency of $\omega_{n,real} \approx 39 rad/s \approx 6.2 Hz$ for this case. Table 6.4 shows the summary of this section. It can be noted that the natural frequency decreases a bit with the higher amplitude step response in the upward direction. It can be reasoned that the natural frequency of the system will decrease further if the step response was done on the full length of travel for the drive but it will not be tested because of how violent these drops are to the hardware. Slow motion video shows the system nearly jumping off of the floor during the upward step response.

Table 6.4: Sagittal plane damping coefficient and natural frequency

	Damping Ratio (ζ)	Natural Frequency (ω_n)
Simulation	0.46	$48 rad/s \approx 7.6 Hz$
800° to 600° Step	0.46	$42 rad/s \approx 6.7 Hz$
400° to 800° Step	0.43	$39 rad/s \approx 6.2 Hz$

6.3 Treadmill Technical Characterization and Controls

The Skywalker treadmills must be able to be controlled with respect to both position and velocity to support the discrete and the rhythmic training paradigms. Much like the other two drive axes, a position loop was closed around a velocity loop, however, in this situation, the velocity is closed within the Kollmorgen AKD motor driver while

<div align="center">(a) Velocity Control   (b) Position Control</div>
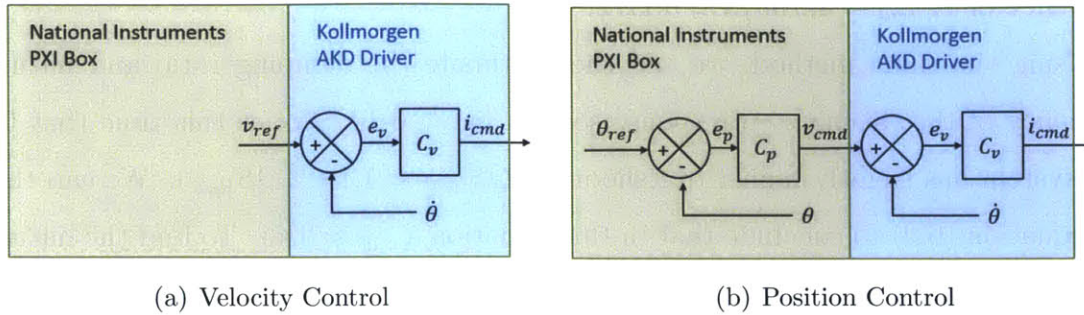
Figure 6-11: High level treadmill control schemes

the position loop is closed within the National Instruments PXI box. In doing so, a Labview Virtual Instrument (VI) running within the PXI box outputs a velocity command in the form of an analog voltage to be read in by the AKD motor driver. The Labview VI can be switched between velocity and position modes. In velocity mode, the VI ignores the position feedback and simply outputs a velocity command (figure 6-11(a)). In position mode, the VI will compare the position command to the position feedback from the motor encoder in order to generate an error which will be scaled as the velocity command to the inner velocity loop (figure 6-11(b)).

The ultimate goal in the design of the most aggressive treadmill controls was a bandwidth above that achievable by a human in the position loop (above about 4 Hz) with zero overshoot in a realistic motion profile such that the controls move fast without oscillation. This would be a condition for perturbation. For the discrete paradigm, it is more advantageous to have a lower bandwidth for the soft feel.

6.3.1 Treadmill Modeling

The treadmill mechanical drive differs from the other two drives on the Skywalker because it employs a belt drive rather than gears. The advantage of the belt drive is that it relies on friction for transmission, thereby eliminating backlash. The disadvantage of the belt drive is that it introduces a fairly low resonant frequency between the motor and the front roller due to the viscoelastic properties of the transmission belt. Therefore, in order to determine a representative 4th order model, a dynamic system analysis (DSA) tool within the AKD motor drivers was used to generate a

bode plot of both the right and the left plants (figures 6-12(a) and 6-12(b)). The bode plot shows a resonance beginning to develop for the treadmill at around 500 rad/s, something that is audibly observable and potentially destructive, thus the bode plot data collection was stopped here.

Analytical models were developed in an attempt to match the bode plot of the plants. Figure 6-13(b) shows a full linearized schematic of the treadmill drive assuming the subjects' foot to be a mass. The desired output of the full system is of course the coordinate of the mass, however, in order to reduce the model's order that describes the dynamics of interest for control, the schematic in figure 6-13(c) was built. This schematic lumps the friction and mass of the treadmill belt and the rear roller into a single mass and damper at the front roller (J_2, b_r), assuming the treadmill tape to have zero compliance and its transfer function from current-in to rotational velocity-out can be seen in equation (6.13) (R is the transmission ratio of the drive, θ_1 refers to the angle of the motor and θ_2 refers to the angle of the lumped front roller in the model). In doing so, we reduce the order of the model from 8th to 4th order considering only the compliance in the drive belt. As seen in figure 6-12, this model is capable of describing the resonance that begins to build at 500 rad/s quite nicely, however it can not reproduce the low frequency rising slope nor the pole pair at around 30 rad/s.

$$\frac{\dot{\theta}_1(s)}{i_m(s)} = \frac{k_t[J_2 s^2 + (R^2 b + b_r)s + R^2 k]}{[J_1 J_2 s^3 + (J_1 b R^2 + J_1 b_r + J_2 b_m + J_2 b)s^2 + (J_1 k R^2 + b b_m R^2 + b_m b_r + b b_r + J_2 k)s + (b_m k R^2 + k b_r)]}$$
(6.13)

Equation (6.14) shows the transfer function of the rotational velocity of the lumped front roller, which, by our model is the transfer function of the treadmill track to the input torque, our true concern, however feedback in the drive is limited to the motor encoder, so for controls purposes, we will consider θ_1.

$$\frac{\dot{\theta}_2(s)}{i_m(s)} = \frac{k_t[R(bs + k)]}{[J_1 J_2 s^3 + (J_1 b R^2 + J_1 b_r + J_2 b_m + J_2 b)s^2 + (J_1 k R^2 + b b_m R^2 + b_m b_r + b b_r + J_2 k)s + (b_m k R^2 + k b_r)]}$$
(6.14)

In order to account for the apparent pole pair at approximately 30 rad/s and the

(a) Right track

(b) Left track
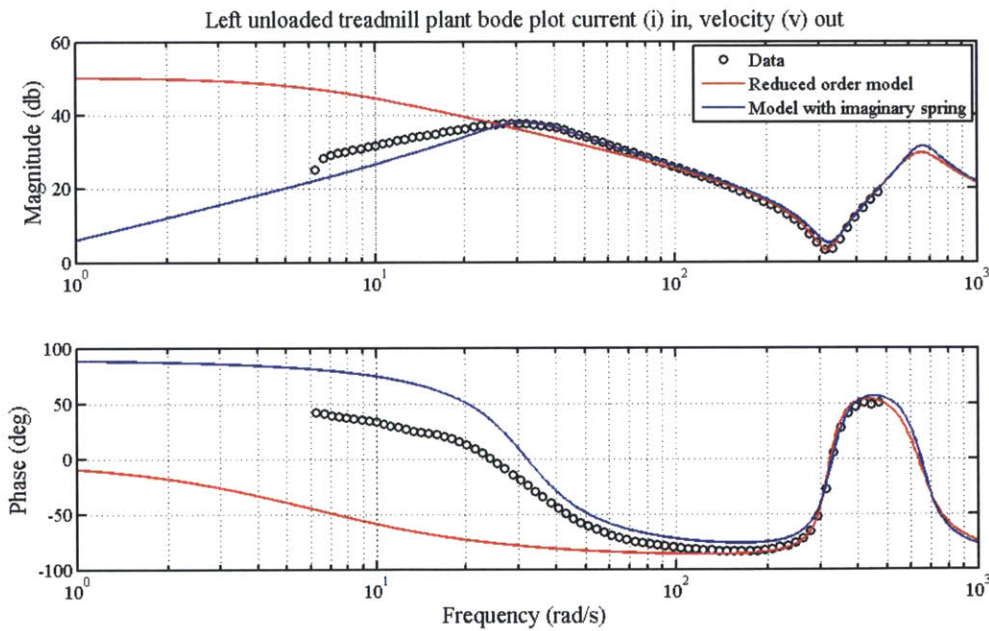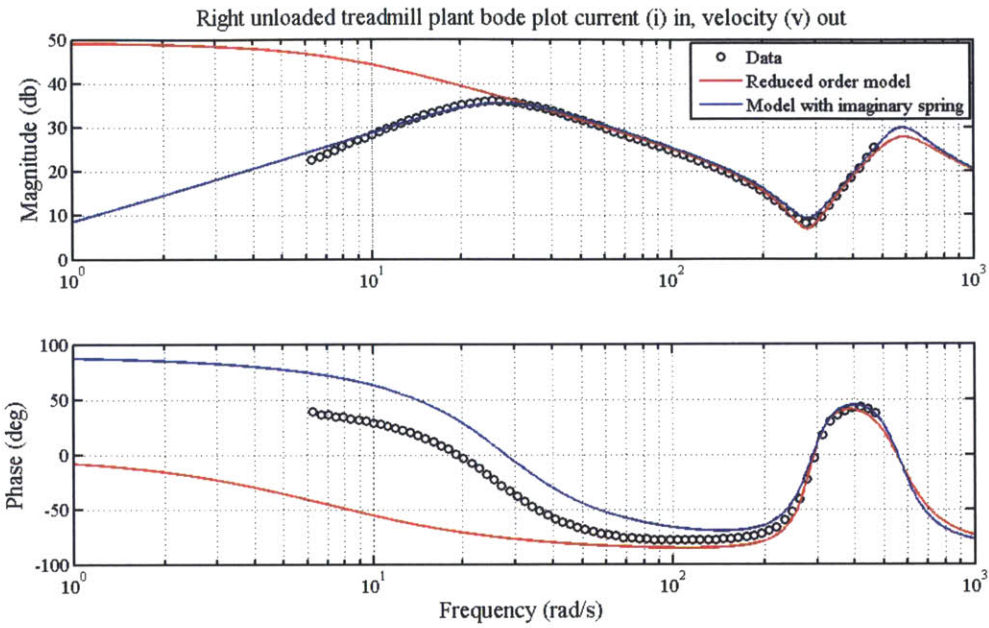
Figure 6-12: Bode plots of the treadmill track plants
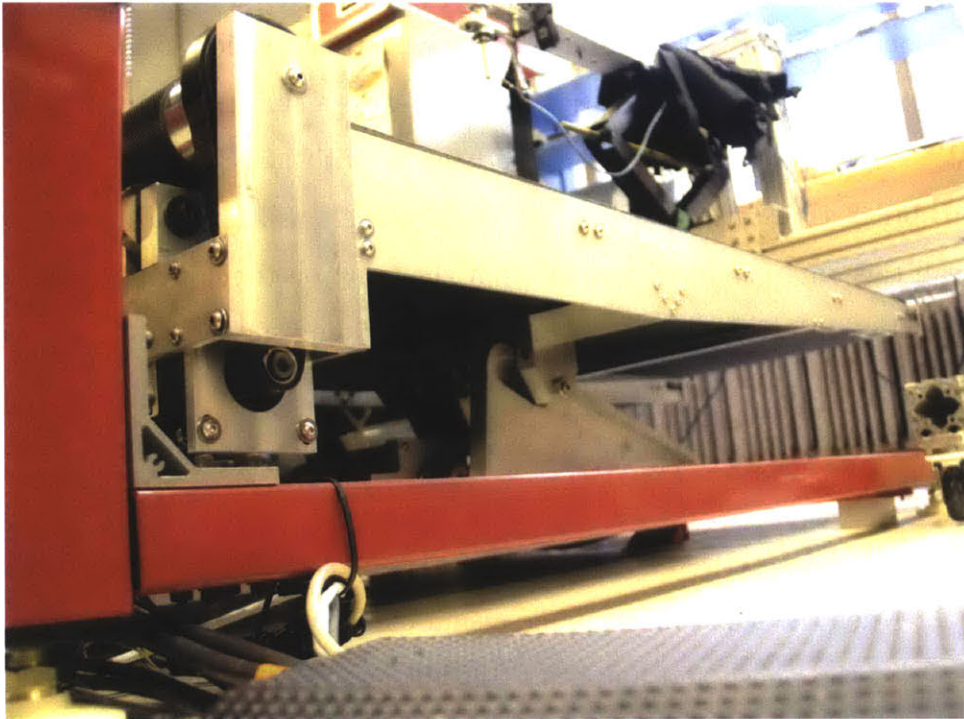
(a) Treadmill drive
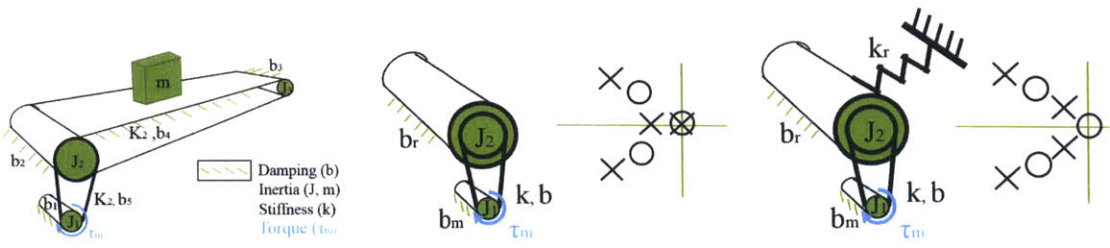
(b) Full model of treadmill drive

(c) Reduced order linearized treadmill model

(d) Reduced order linearized model with imaginary spring

Figure 6-13: Treadmill Drive Modeling

rising slope at low frequencies, we must consider what creates such a phenomenon. An initial rising bode plot slope indicates a zero gain at DC, in other words, in our transfer function when torque is steadily applied, the velocity of the system will be zero. Mechanically, this occurs when system is coupled to ground by a spring. The constant torque term will be equaled by the spring force and thus held in equilibrium with no velocity. Figure 6-13(d) shows the schematic by which to match the model and equation (6.15) shows the transfer function with a spring to ground on the load roller. We know this cannot be the case because with a DC current of magnitude enough to break the static friction, the treadmill belt will be continuously moving. Thus, I call this an "imaginary spring" that shows up on the bode plot due to static friction (or stiction) of the treadmill track on the sliding surface.

$$\frac{\dot{\theta}_1(s)}{i_m(s)} = \frac{k_t s[J_2 s^2 + (R^2 b + b_r)s + (R^2 k + k_r)]}{[J_1 J_2 s^4 + (J_1(bR^2 + b_r) + J_2(b_m + b))s^3 + (J_1(kR^2 + k_r) + b_m(bR^2 + b_r) + bb_r + J_2k)s^2 + (b_m(kR^2 + k_r) + kb_r + k_r b)s + kk_r]}$$
(6.15)

Stiction, as characterized in figure 6-14(a), refers to the extra friction at zero velocity[5]. When the DSA was running, a sinusoidal current profile was injected into the motor and the phase and amplitude output was read by the encoder. In order for the track to move, it first had to break through the stiction. This leads to a lower amplitude. The DSA was limited to a low frequency of 1Hz in the AKD driver software and thus all we could see was an increasing slope.

Stiction, at the microscopic level, will behave like a stiffness as seen in figure 6-14(b), as the small imperfections (asperities) in each of the sliding surfaces, catch on each other and deflect with their own stiffness before yielding. Therefore, the type of model in 6-13(d) seems like an appropriate model describing the behavior in the lower frequencies of the DSA. We can see in figure 6-12 that the magnitude of the bode plot of this model more closely resembles that observed from the actual track during the DSA testing. However, there is still sizable differences in the phase. This is consistent with other more in-depth studies that show an amplitude dependent resonance as a result of friction[88]. Mechanical reasoning tells us that the spring is an artifact due to the nonlinear static friction and was discarded in the development

160

(a) Nonlinear friction model   (b) Diagram of sliding surfaces
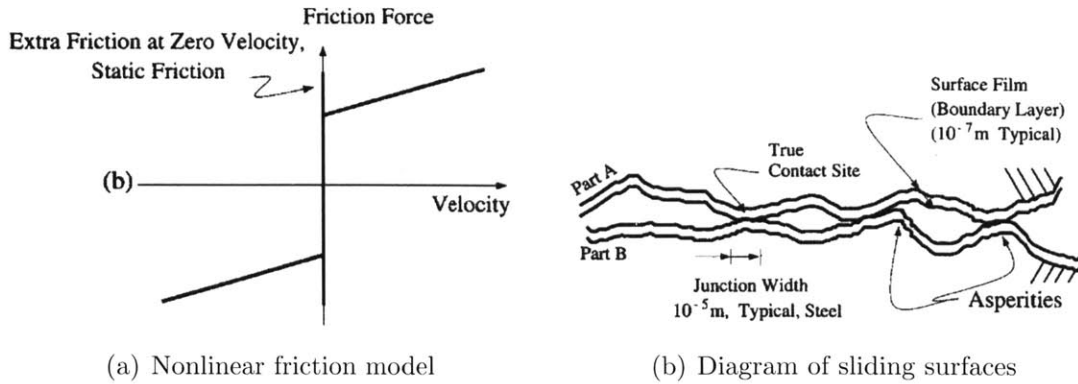
Figure 6-14: Friction considerations taken from [5]

of the controls.

Determination of model parameters

The plant has 9 total variables to match. The motor inertia (J_1), damping (b_m) and constant (k_t) are published by Kollmorgen, the motor manufacturer. The belt transmission ratio (R) was determined experimentally as seen in section 3.2.2. Varying the load inertia (J_2) alters the bode plot magnitude, and thus can be honed by matching the model to the bode data (figure 6-12). The transmission belt stiffness (k) and damping (b) are determined next by matching the zero pair as well as considering the upward slope in the magnitude plot after the zero pair. Finally, the load damping (b_r) is determined observing the velocity step responses seen in figure 6-19. Tables 6.5 through 6.10 show the model parameters used to create the bode plots in figure 6-12. For the system controls, the reduced order model parameters will be used.

When measuring the dynamics of the system with a subject standing on a single track, it is assumed that all parameters will remain constant with the exception of the load inertia (J_2) and the load damping (b_r). To match the loaded data, the model assumes the same parameters as table 6.5 and table 6.6 with the modifications shown in table 6.10. Figures 6-15(a) and 6-15(b) were used to match the parameters. A 6'0" tall 190 lb. subject stood on one foot on the track being tested while holding on to the back of the body weight support for balance during testing. The poles and zeros for the three usable reduced order models are shown in table 6.11 .

161
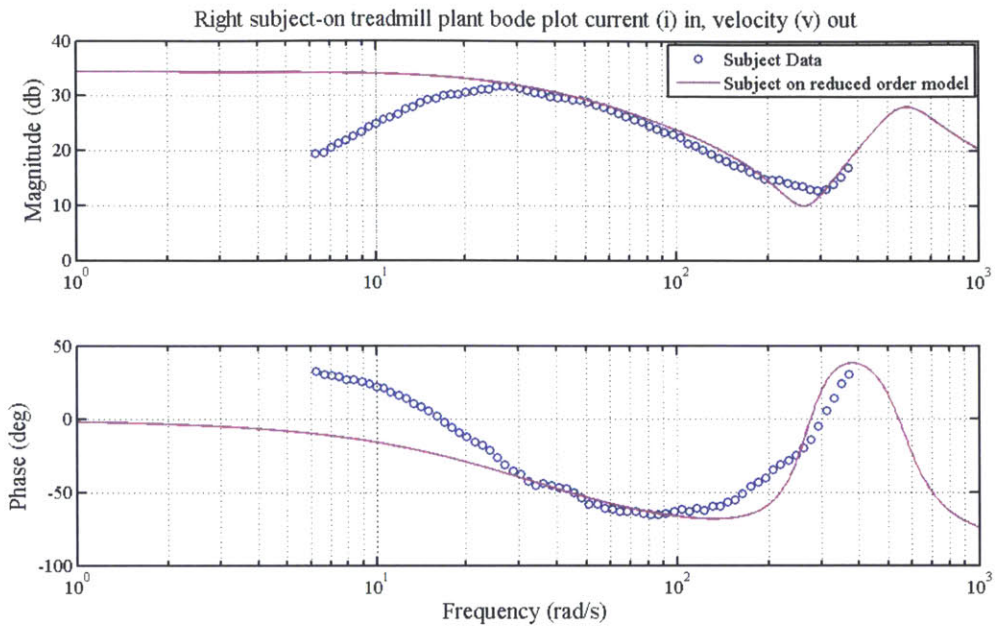
(a) Loaded bode
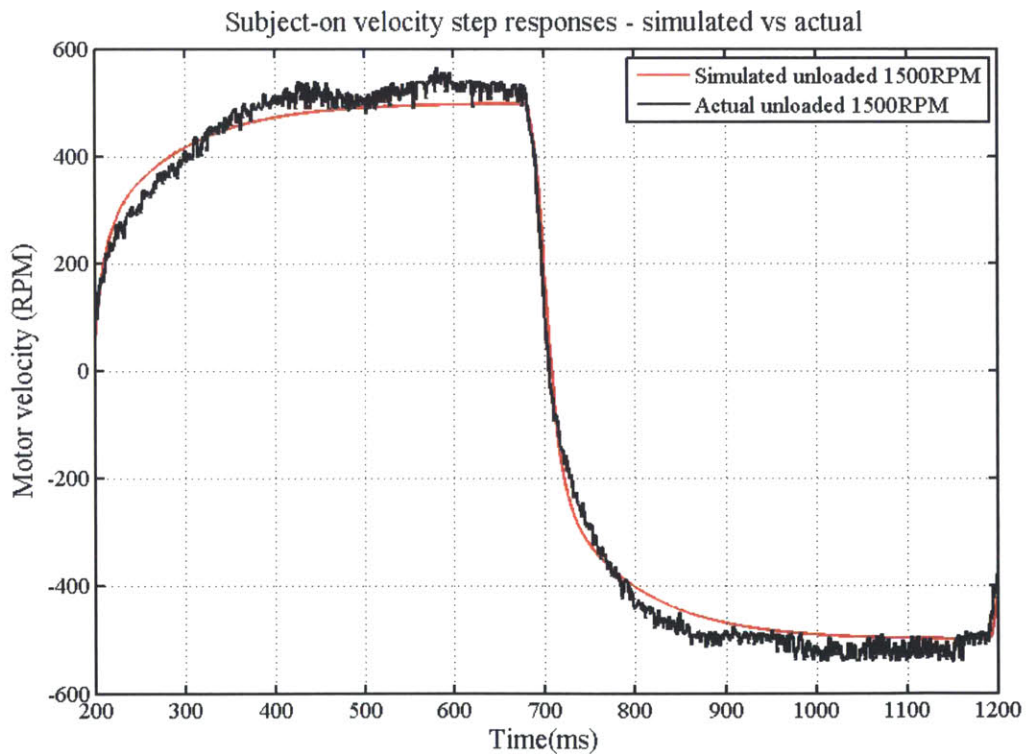
(b) Loaded velocity step response

Figure 6-15: Right track plots with a subject standing on the track

Table 6.5: Fixed treadmill model parameters across all models

Parameter	Value
Motor inertia (J_1)	$2.1e^{-4}\ kgm^2$
Motor damping (b_m)	$1.62e^{-4}\ Nm/(rad/s)$
Transmission ratio (R)	3.72
Motor constant (k_t)	$1.72\ Nm/ARMS$
Load inertia (J_2)	$90e^{-4}\ kgm^2$

Table 6.6: Right track reduced order model parameters

Parameter	Value
Load damping (b_r)	$0.08\ Nm/(rad/s)$
Transmission Belt stiffness (k)	$52\ Nm/rad$
Transmission Belt damping (b)	$0.04\ Nm/(rad/s)$
Stiffness to ground (k_r)	$0\ Nm/rad$

Table 6.7: Right track imaginary spring model parameters

Parameter	Value
Load damping (b_r)	$0.4\ Nm/(rad/s)$
Transmission Belt stiffness (k)	$52\ Nm/rad$
Transmission Belt damping (b)	$0.03\ Nm/(rad/s)$
Stiffness to ground (k_r)	$9\ Nm/rad$

Table 6.8: Left track reduced order model parameters

Parameter	Value
Load damping (b_r)	$0.07\ Nm/(rad/s)$
Transmission Belt stiffness (k)	$66\ Nm/rad$
Transmission Belt damping (b)	$0.032\ Nm/(rad/s)$
Stiffness to ground (k_r)	$0\ Nm/rad$

Table 6.9: Left track imaginary spring model parameters

Parameter	Value
Load damping (b_r)	$0.3\ Nm/(rad/s)$
Transmission Belt stiffness (k)	$68\ Nm/rad$
Transmission Belt damping (b)	$0.025\ Nm/(rad/s)$
Stiffness to ground (k_r)	$12\ Nm/rad$

Table 6.10: Treadmill subject-on model parameter modifications

Parameter	Value
Load inertia (J_2)	$100e^{-4}\ kgm^2$
Load damping (b_r)	$0.45\ Nm/(rad/s)$

6.3.2 Treadmill Controls

As shown in figure 6-11, the controls for the treadmill track must be able to function in both position and velocity mode and do so by closing a velocity loop inside of a

Table 6.11: Treadmill poles and zeros

	Poles	Zeros
Right Track Unloaded	$-127 \pm 558i, -6.91$	$-35.2 \pm 281i$
Left Track Unloaded	$-102 \pm 636i, -6.07$	$-28.5 \pm 317i$
Right Track subject-on	$-128 \pm 550i, -35.1$	$-50.2 \pm 264i$

position loop. Thus a controller for the velocity loop must work for the velocity loop but also must be approriate for accepting commands from the position loop. Design was done in a two step process. First, the velocity loop was developed, then before being implemented, the position control was overlayed to determine proper operation. The simulated controls were compared to the feedback from the motor encoders to double check the control loop and to verify the modeling done in section 6.3.1.

Figure 6-16 shows the complete control scheme used for both position and velocity control. During velocity control, the outside loop is replaced by a velocity command as seen in figure 6-11. Table 6.12 lists the gains used and tables 6.13 and 6.14 show the bandwidths and phase margins. The low pass filter frequency was chosen to be high enough such that the associated phase did not effect the return ratio, but low enough that it canceled out the system's audible noise. Additionally, the low pass filter decreases the magnitude of the resonance slightly. The integrator in the velocity loop is necessary to remove steady state error in the velocity loop and the proportional gains were picked to make sure that the resonance did not cause problems while trying to maximize the bandwidth of the system. The return ratio bode plots of both loops are shown in figure 6-17. Notice that, even though the poles and zeros are slightly different between the left and right track models, the bandwidth and phase margin remain fairly consistent when using the same control gains. This is desirable because we want to be able to move both tracks in unison.

Figure 6-18 shows the return ratios for the subject-on condition. Notice that when a subject is loading the track, the bandwidth decreases in both the position and velocity loops. The phase margin in the velocity loop increases while in the position loop it decreases slightly.

To confirm the controls, velocity pseudo-step responses were run for the unloaded

164
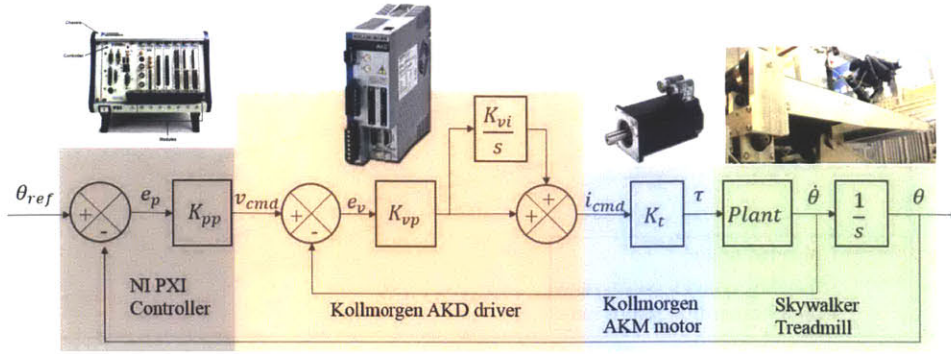
Figure 6-16: Full treadmill control scheme

Table 6.12: Control loop gains

Parameter	Value
Position loop proportional gain (k_{pp})	25
Velocity loop proportional gain (k_{vp})	0.032
Velocity loop integral gain(k_{vi})	5π
low pass filter frequency (p)	250π rad/s

Table 6.13: Treadmill velocity loop return ratio bandwidth and phase margin

Parameter	Value
Right track unloaded return ratio bandwidth	$85.0\ rad/s$
Right track unloaded return ratio phase margin	$78.0°$
Left track unloaded return ratio bandwidth	$85.3\ rad/s$
Left track unloaded return ratio phase margin	$77.3°$
Right track subject-on return ratio bandwidth	$72.5\ rad/s$
Right track subject-on return ratio phase margin	$106°$

Table 6.14: Treadmill position loop return ratio bandwidth and phase margin

Parameter	Value
Right track unloaded return ratio bandwidth	$35.4\ rad/s$
Right track unloaded return ratio phase margin	$68.6°$
Left track unloaded return ratio bandwidth	$35.7\ rad/s$
Left track unloaded return ratio phase margin	$68.4°$
Right track subject-on return ratio bandwidth	$25.9\ rad/s$
Right track subject-on return ratio phase margin	$67.5°$

right track (figure 6-19(a)), the unloaded left track (figure 6-19(b)) as well as the loaded right track (figure 6-15(b)). As can be seen in all of these responses, the control model and the feedback from the motor match nicely, confirming both our models and controls for the velocity loop.

To confirm the position loop, step responses were recorded in a similar fashion,
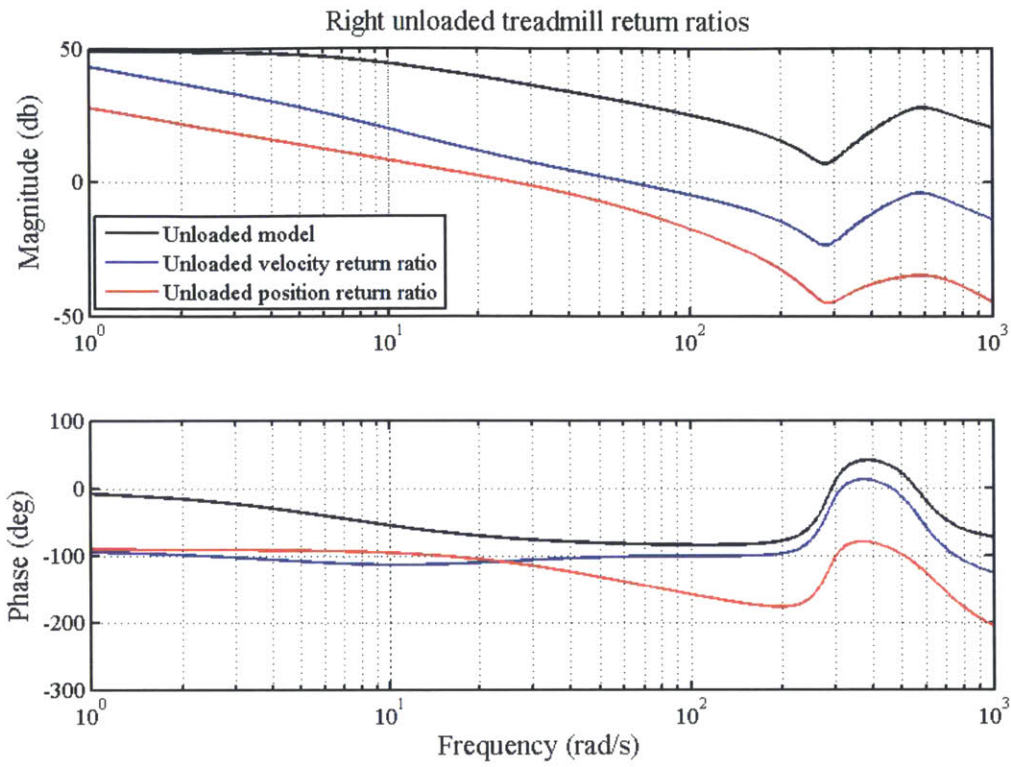
(a) Right track
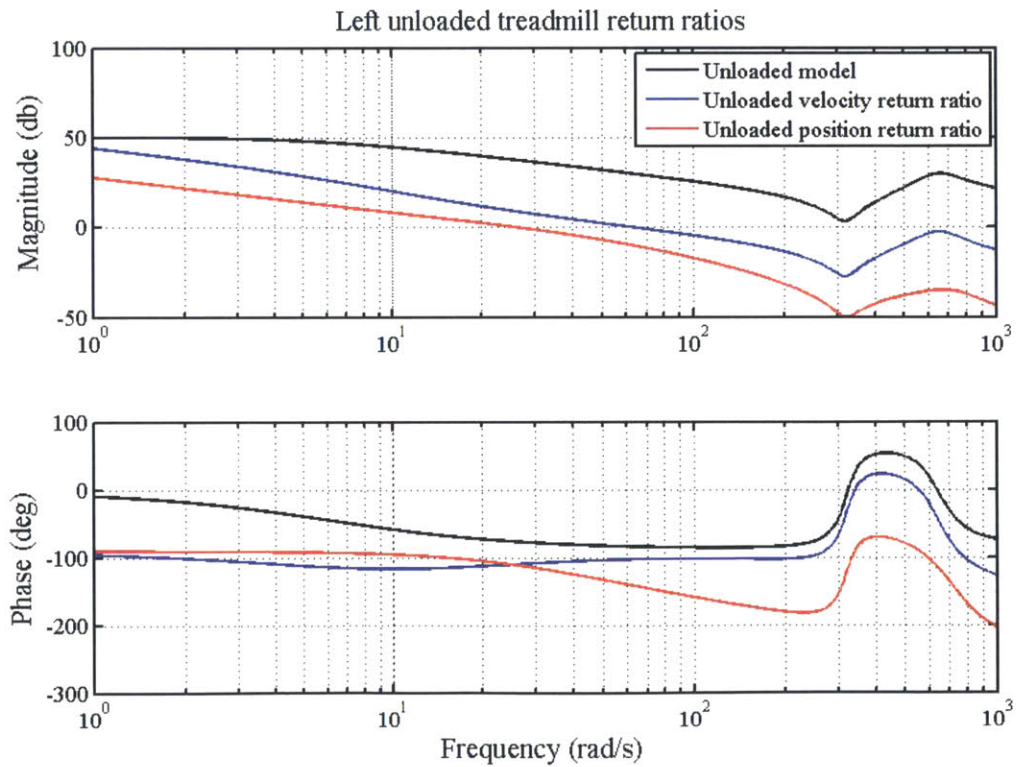
(b) Left track

Figure 6-17: Treadmill control return ratios
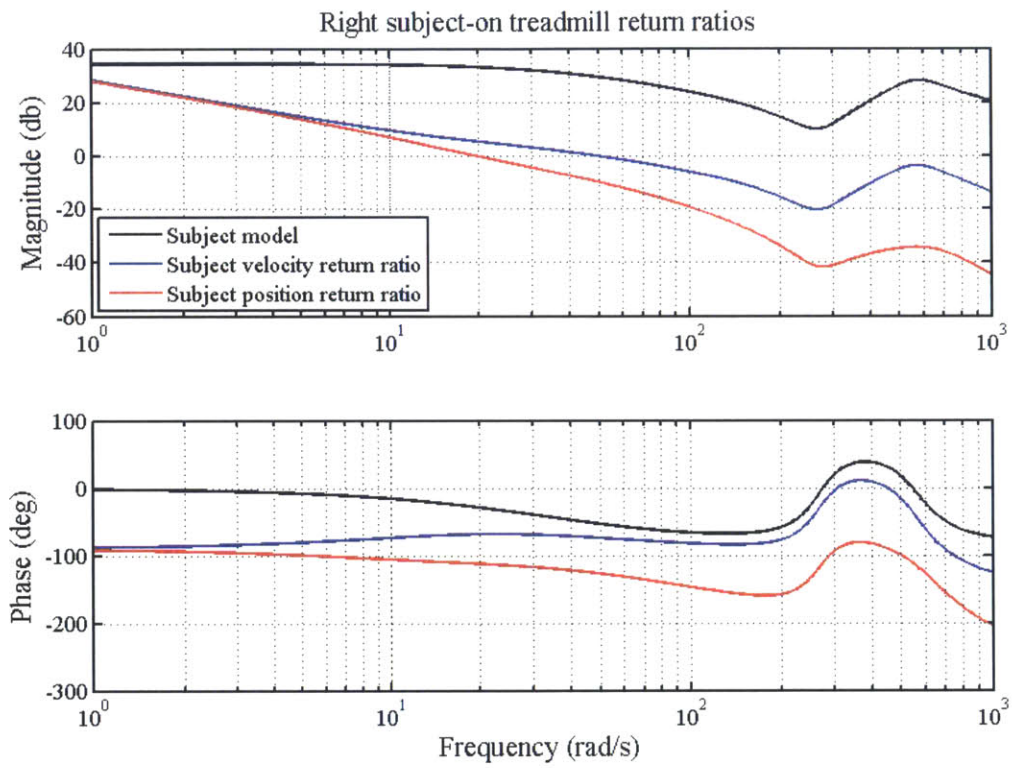
Figure 6-18: Subject-on return ratios
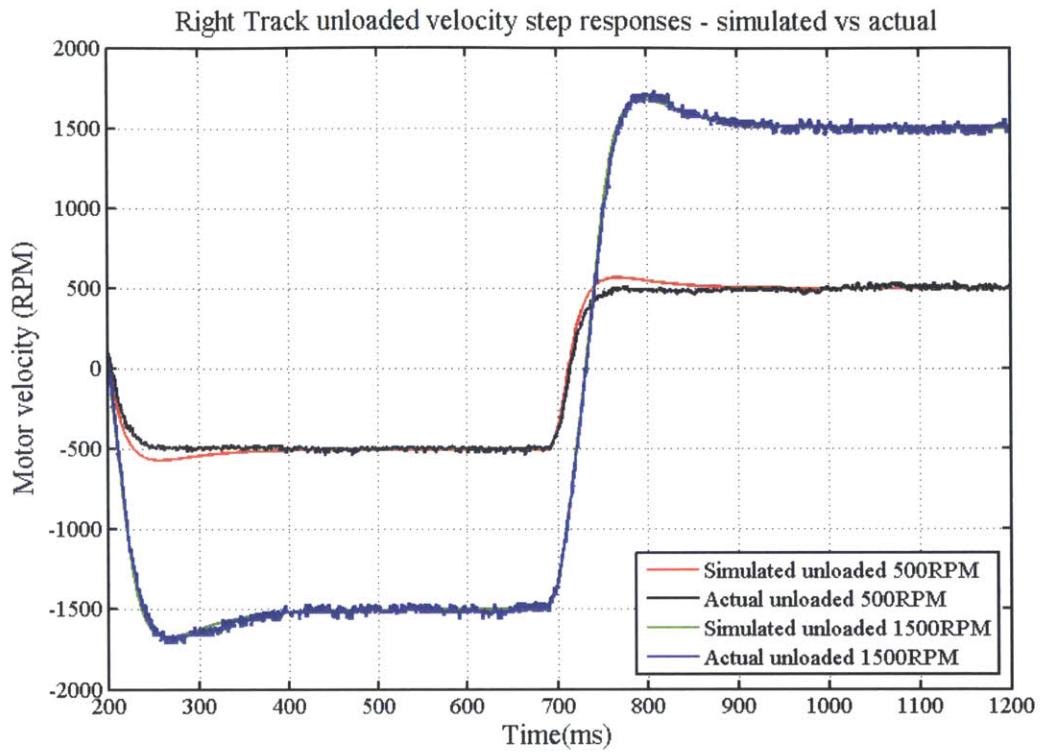
(a) Right track
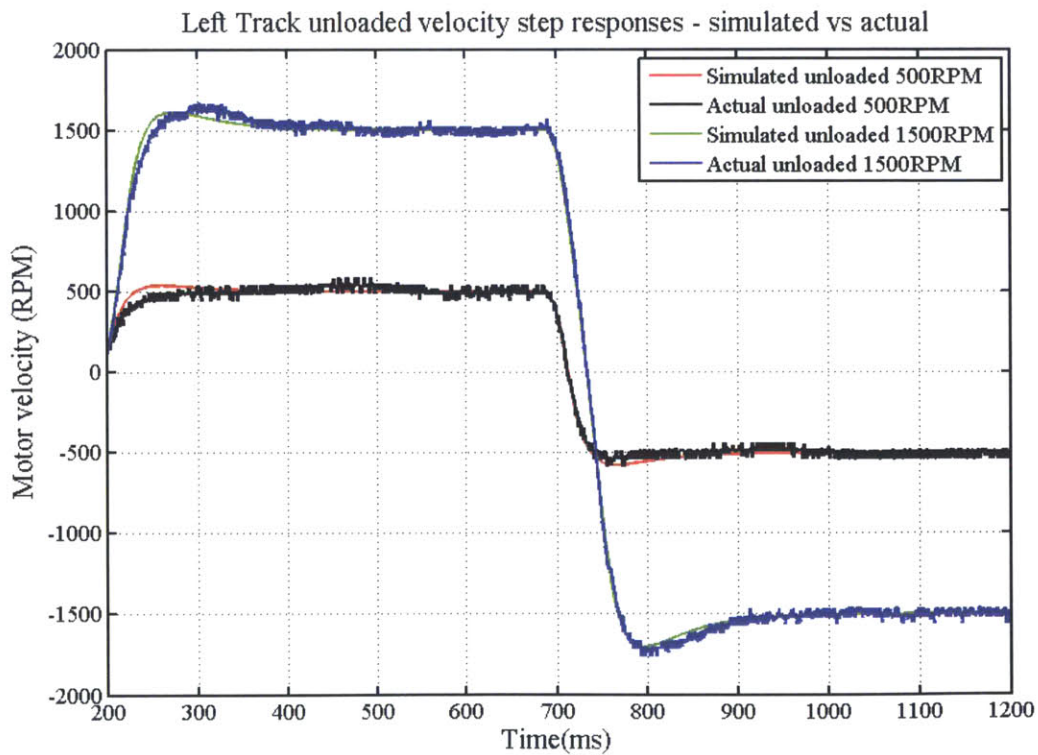
(b) Left track

Figure 6-19: Velocity step responses of the left and right track with the final controls

168

however, the exact motion profile can not be simulated this time because, the position loop is receiving a pure step command, which is later filtered within the AKD motor driver's acceleration and velocity limits. An acceleration limit of 1 million rpm/s (black trace in figure 6-20) was used such that the acceleration limit did not significantly alter the motion trajectory. A velocity limit of $185rad/s$ is in place by the control scheme that limits the maximum speed of the treadmill track to $4mph$. The limit effect is smaller on small amplitude step responses as seen in figure 6-20(a) but becomes more pronounced for step responses of longer length (see figure 6-20(c)). The blue profiles marked in figure 6-20 show how the profile is affected by lowering the acceleration limit to $50,000RPM/s$ ($5235rad/s^2$ or about $51m/s^2$ in track coordinates), which still very high acceleration.

Figure 6-20(b) shows a zoomed in view of the settling profile of both the high acceleration limit and the low. The difference in these plots is that friction compensation torque was applied in the black trace. Friction compensation torque is applied in the following manner as written in Kollmorgen's AKD user guide : "the velocity command derivative sign is multiplied by the friction compensation value to be injected to the current command". With this setting on, any noise in the analog input signal is amplified, resulting in high frequency ringing when settling, observable audibly and tactically as a vibration. From my experience, friction compensation should only be used with zero noise reference signal such as those generated internally by the AKD drives. The blue plot removes the friction compensation scaling factor and produces a smooth settling trace. A small steady state error without friction compensation results as small deviations in the position error are not enough to break stiction but the error amplitude is so low that it is of no consequence for our application.

6.3.3 Treadmill Technical Characterization

Operating torque

The current from the velocity step profiles seen in figures 6-15 and 6-19 are shown in figure 6-21. When loaded, the current in steady state with the subject on the track

169
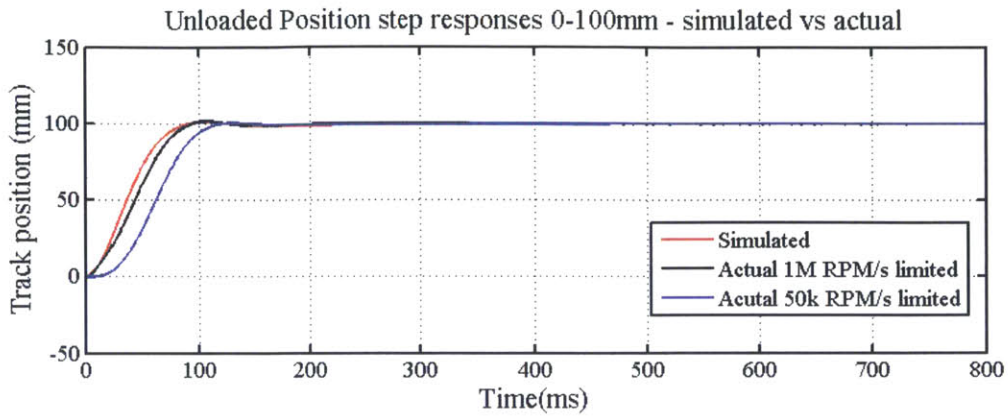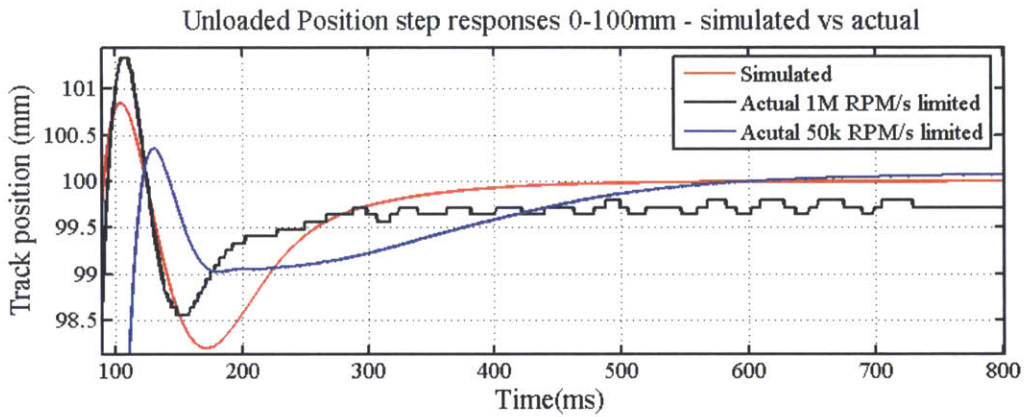
(a) 0-100mm steps

(b) 0-100mm steps zoomed
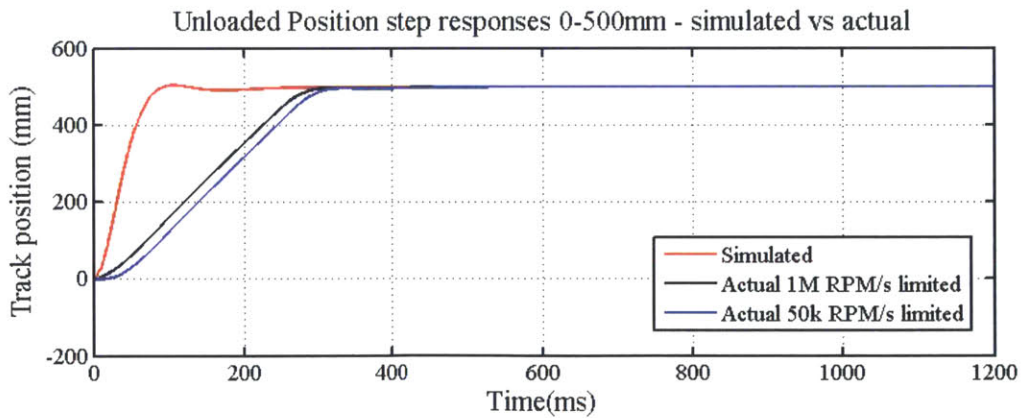
(c) 0-500mm steps

Figure 6-20: Treadmill position steps

170
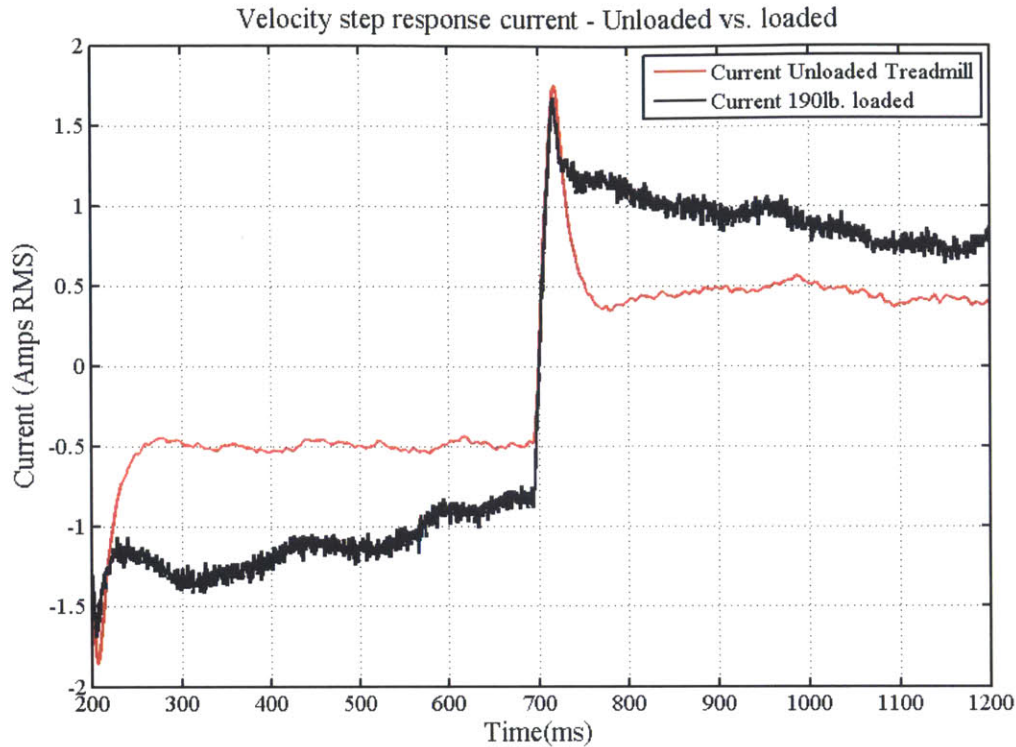
Figure 6-21: Current plot for treadmill velocity steps

is nearly double than when the system is unloaded. The torque constant (K_t) for the treadmill motors (Kollmorgen AKM43E) is $1.72 \ Nm/ARMS$. During these profiles, the peak torque is approximately $3 \ Nm$ with a constant operating torque under load at 500RPM of $1.4 \ Nm$ if we estimate that the steady state current is $0.8 \ ARMS$. 500RPM at the motor corresponds to 1.15 mph at the track which is in the range of what we would expect when Skywalker is working with a patient.

The AKM43E has a continuous torque rating of $4.70 \ Nm$ with a peak torque of $13.4 \ Nm$ as seen in figure 3-7. At 1.15 mph track speed, the system has 5.9 times the torque capacity while staying under the continuous rating.

Soft controls

The step responses seen in figure 6-20 are excellent for disturbing balance. While standing on the track, the feeling is similar to slipping on ice. This control scheme is strong enough to elicit startle reflexes and without the body weight support, can be

171
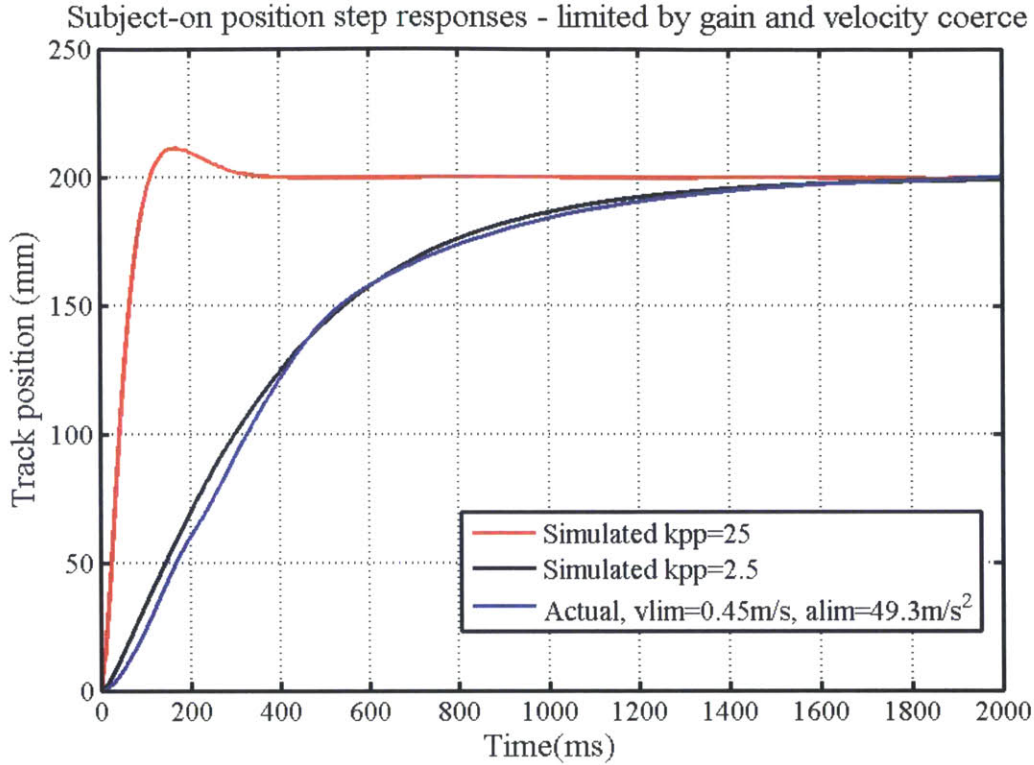
Figure 6-22: Subject-on soft control position step responses

dangerous.

For the discrete paradigm, the system must feel a bit "softer", ie. it should respond with lower accelerations and should be speed limited. During the feasibility study described in section 7.1.2, K_{pp} was changed from 25 to 2.5 which lowers the crossover frequency of the return ratio, making the system response slower. Figure 6-22 shows the simulated step response with a subject on the track using a $K_{pp} = 25$ (red) and $K_{pp} = 2.5$ (black). The blue trace is actual loaded position data when a 50,000 RPM/s motor acceleration limit ($49.3m/s^2$ treadmill limitation) is in place within the AKD driver and a 1mph ($0.45m/s$) treadmill speed limit is implemented within the Labview position control program. The blue plot was run with a 190 lb. subject. The gain was experimentally chosen by dialing down K_{pp} until the profile felt comfortable for our study participants.

172

6.4 Frontal Plane Technical Characterization and Controls

The frontal plane rotation drive was designed to be able to disrupt balance with the goal of providing a safe environment for patients to practice balance. The Skywalker system relies on the body weight support system for safety while the frontal plane drive provides different lateral angles and perturbations for patients to practice.

6.4.1 Frontal Plane Modeling

As shown in figure 6-23(a), Skywalkerγ's frontal plane axis of rotation is coincident with the walking surface on the frontal rotation assembly (figure 3-18). Figure 6-23(b) shows a graphical model of the unloaded system. The center of mass is located below the axis of rotation and thus the system acts as a pendulum. The action of the pendulum sets an equilibrium point for the system when the torque due to the pendulum equals the torque due to the springs (figure 6-23(c)) For small angles, the torque due to the pendulum can be linearized to be a constant stiffness term. To show it in a simpler context, figure 6-23(d) shows the system represented by a mass between two preloaded springs, whose rates add as springs in parallel(eq.(6.16)). At the equilibrium point, or about 5°, the preload forces from each spring will cancel each other and thus the linear stiffness model will hold.

$$k = k_{spr} + k_{pend} \tag{6.16}$$

Thus the model becomes a simple second order mass-spring-damper system seen in equation (6.17), where θ_o is about 5 degrees from the horizontal. All terms are reflected to the motor through the transmission ratio (R_f) of the frontal gear set as seen in equation (6.25).

$$\frac{\theta(s)}{\tau_m(s)} = \frac{1}{Js^2 + bs + k} \tag{6.17}$$

173

Center of Mass

Frontal Plane hinge
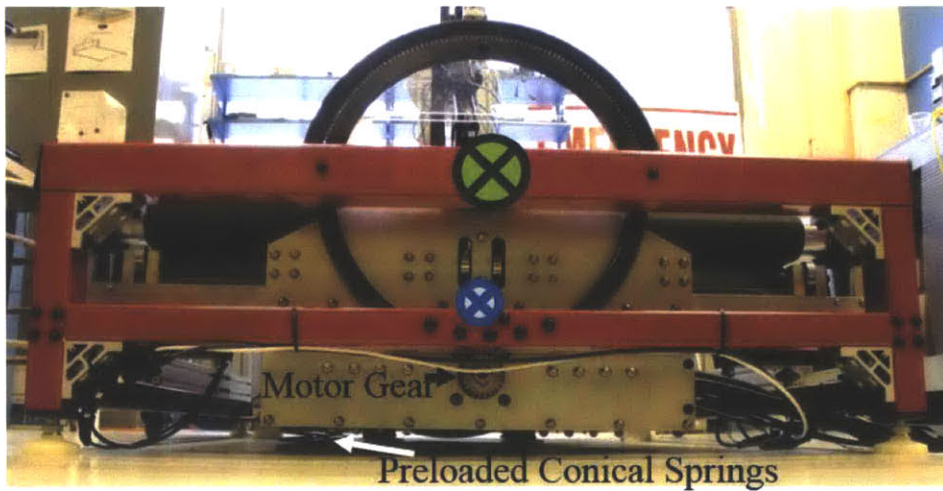
(a) Front view of Skywalkerγ
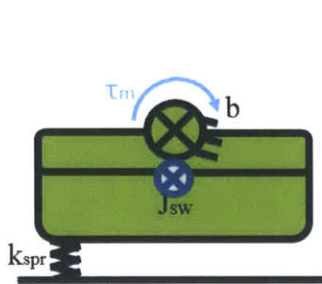
(b) Model at horizontal posi-
tion
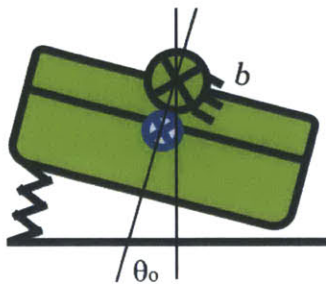
(c) Model at equilibrium posi-
tion
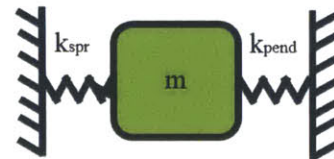
(d) Preloaded spring model

Figure 6-23: Frontal rotation assembly model

Determination of model parameters

The model parameters can be seen in table 6.15. The inertia of the frontal plane assembly was determined using the solid model generated in Solidworks[5]. This was reflected similar to equation (6.25) and added to the mass of the motor and gear train to estimate the total system inertia (J). Damping (b) was estimated by tripling the published motor damping coefficient which is 0.000315Nm/(rad/s) seeing as the damping coefficient was not given for the gear box but it is likely higher than that of the motor[6].

In order to estimate the rotational stiffness due to the spring (k_s), a simple approximation was used. The conical springs[7] have a published spring rate (k_{pub}) with a free length (l_f). At the horizontal position, the distance between the ground and the underside of the base plate (h_i) was measured with digital calipers. The compressed length (δ_l)at the horizontal position was determined by equation (6.18). Figure 6-24 shows a diagram for these parameters.

$$\delta_l = l_f - h_i \tag{6.18}$$

The force of a single spring becomes simply:

$$F_s = K_{pub}\delta_l \tag{6.19}$$

The effective torque due the four springs used in the frontal plane assembly (τ_s) becomes:

$$\tau_s = 4F_s(w/2) \tag{6.20}$$

If we assume that the bottom of the spring is able to slide in the x-plane without friction (ie. we care only about the y-component of displacement), the angle at which the spring is at its free length (θ_{osl}) can be found via equation (6.21) after

---

[5]Dassault Systmes SolidWorks Corp, Waltham, Massachusetts, www.solidworks.com

[6]Gear box: Micron XT120-10, Danaher co., Washington, D.C., www.thomsonlinear.com

[7]Part no. CX-52, Reid Supply, Muskegon, MI, www.reidsupply.com
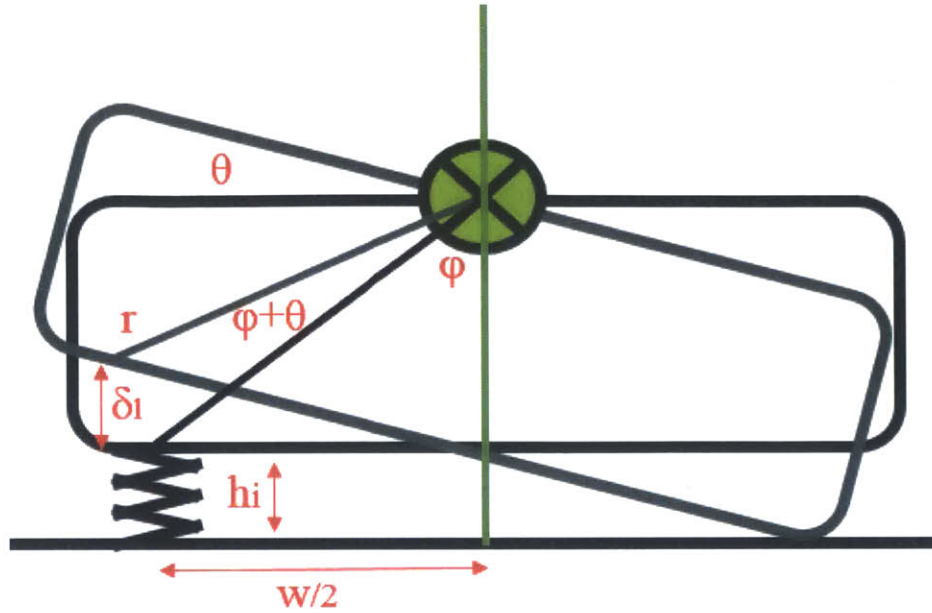
Configuration at Horizontal
Configuration at angle

Figure 6-24: Angle schematic

some geometric manipulation where r is the radius of the spring end's center to the rotation axis.

$$\theta_{osl} = \phi - cos^{-1}(\frac{\delta_l}{r} + cos(\phi)) \qquad (6.21)$$

If we assume the both ends of the spring to be fixed, the angle (θ_{of}) can be estimated by a simple arc equation:

$$\theta_{of} = \frac{\delta_l}{r} \qquad (6.22)$$

The actual situation is likely in the middle of both of these estimations, and thus for the spring rate, we will use θ_{os} as the average of θ_{osl} and θ_{of}.

Thus the spring rate due to the conical springs on the load side of the gear train becomes:

$$k_{spr-out} = \tau_s/\theta_{os} \qquad (6.23)$$

176

In order to estimate the total stiffness, as shown in equation (6.16), we then have to calculate $k_{pend-out}$, which can be estimated simply in equation (6.24) where m is the mass of the frontal plane assembly and r_{cm} is the radius of the center of mass from the axis of rotation. This equation makes use of the assumption that $sin(\theta) = \theta$ for small angles.

$$k_{pend-out} = mgr_{cm} \tag{6.24}$$

Reflecting the mass and stiffness into the motor is done by simply dividing by the transmission ratio (R_f) squared. For example:

$$k_{pend} = k_{pend-out}/R_f^2 \tag{6.25}$$

Once both stiffnesses are reflected through the transmission ratio, they are added together as shown in equation (6.16) to arrive at the stiffness as seen by the motor (k).

Table 6.15: Frontal plane model parameters

Parameter	Value
Motor side inertia (J)	$0.0042\ kgm^2$
Motor side damping (b)	$0.001\ Nm/(rad/s)$
Published spring stiffness (K_{pub})	$4240\ N/m$
Free length (l_f)	$74.6\ mm$
Initial height (h_i)	$36.5\ mm$
Compressed length (δ_l)	$38.1\ mm$
Individual spring force (F_s)	$162\ N$
Spring width radius $(w/2)$	$310\ mm$
Torque at $\theta = 0°$ (τ_s)	$200\ Nm$
Spring to axis radius (r)	$469\ mm$
Equilibrium θ - sliding assump (θ_{osl})	$7.6°$
Equilibrium θ - fixed assump (θ_{of})	$4.7°$
Equilibrium θ of the spring (θ_{os})	$6.2°$
load side spring stiffness $(k_{spr-out})$	$1848\ Nm/rad$
frontal assembly mass (m)	$172\ kg$
center of mass radius (r_{cm})	$175\ mm$
load side pendulum stiffness $(k_{pend-out})$	$295\ Nm/rad$
Frontal plane transmission ratio (R_f)	90
motor side total stiffness (k)	$0.265\ Nm/rad$

6.4.2 Frontal Plane Controls

For the sake of experimentation with the AKD control options, the slider tuning was used to define an initial control loop. This is done by selecting a bandwidth. This led to an unstable system initially, but by lowering the slider and the gains, it was acceptable for a slow command. This initial control scheme included a PI controller in the position loop and a P controller for the inner velocity loop. The gains chosen by the slider can be seen in table 6.16. A simulation using our model (shown in equation (6.17)) with this initial controller is shown in figure 6-27(a) for a step input.

A final controller was developed via the loop shaping technique (figure 6-25). The basic control loop is similar to the default controller but also makes use of a low pass filter at 300 Hz to reject audible noise. Without this filter, the gains chosen excite some higher frequencies that are an annoyance. To fix the original loop, the integral term was divided by 10, pushing a zero closer to the origin and the velocity loop gain was increased by an order of magnitude to push one of the system poles further negative, in essence, shaping the loop to have a higher bandwidth with increased phase margin for increased stability. The gains for this controller can be seen in table 6.16.

Table 6.16: Frontal plane control gains

Parameter	Value
Initial k_{pp}	30
Initial k_{pi}	6.28
Initial k_{vp}	0.04
Final k_{pp}	30
Final k_{pi}	0.628
Final k_{vp}	0.5
Motor Constant (k_t)	1.72

The inner loop transfer function is shown in (6.26). Notice that increasing K_{vp} will increase the damping ratio of the natural response of the velocity loop, which will take care of any oscillation from the high stiffness of the system.

$$\frac{\dot{\theta}}{v_{cmd}} = \frac{K_{vp}K_t s}{(Js^2 + bs + k)(s/600\pi + 1) + k_{vp}k_t s} \tag{6.26}$$

178
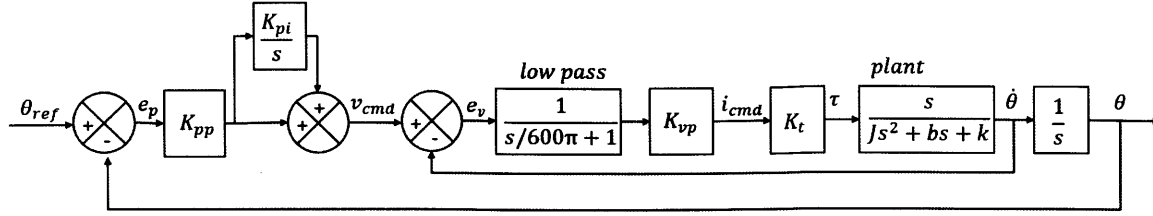
Figure 6-25: Frontal plane closed loop control

The return ratio of the position outer loop will then become:

$$R.R. = \frac{\dot{\theta}}{v_{cmd}} \frac{K_{pp}(s + k_{pi})}{s^2} \tag{6.27}$$

The poles of the return ratio are at 0, 0, -0.287, -234 and -1650. The zeros are located at 0 and -0.628. The bode plot of the return ratio can be seen in figure 6-26(a) and the step response of the closed loop system can be seen in figure 6-26(b). This controller yields a theoretical bandwidth of 42 radians per second or a natural frequency (ω_n) of 6.7 Hertz and a phase margin of 78 or a damping ratio (ζ) of 0.78.

In order to test the simulated model, the model was simulated with the same position command given to the actual hardware system. The simulation was run from 450° motor coordinates to zero because 450° motor coordinates corresponds to 5° Skywalker coordinates, which is the system's equilibrium point. Figure 6-27(a) shows a series of step or "pseudo" step responses. The drives define a maximum acceleration and thus profiles are not simple step responses. The red line shows the position command given to the controller. The black line shows the position feedback directly from the feedback device on the motor and the blue line shows the simulation position. The hardware response is remarkably similar to the simulation, validating the control and system model. The green line shows a theoretical step response of the frontal plane if given a true step response and the pink line shows the theoretical step response from the original controller that was discarded.

Figure 6-27(b) shows the current feedback from the motor, the velocity command (simply a location within the control loop), the velocity feedback and the position feedback. As can be seen in all of the velocity feedback and current feedback plots,
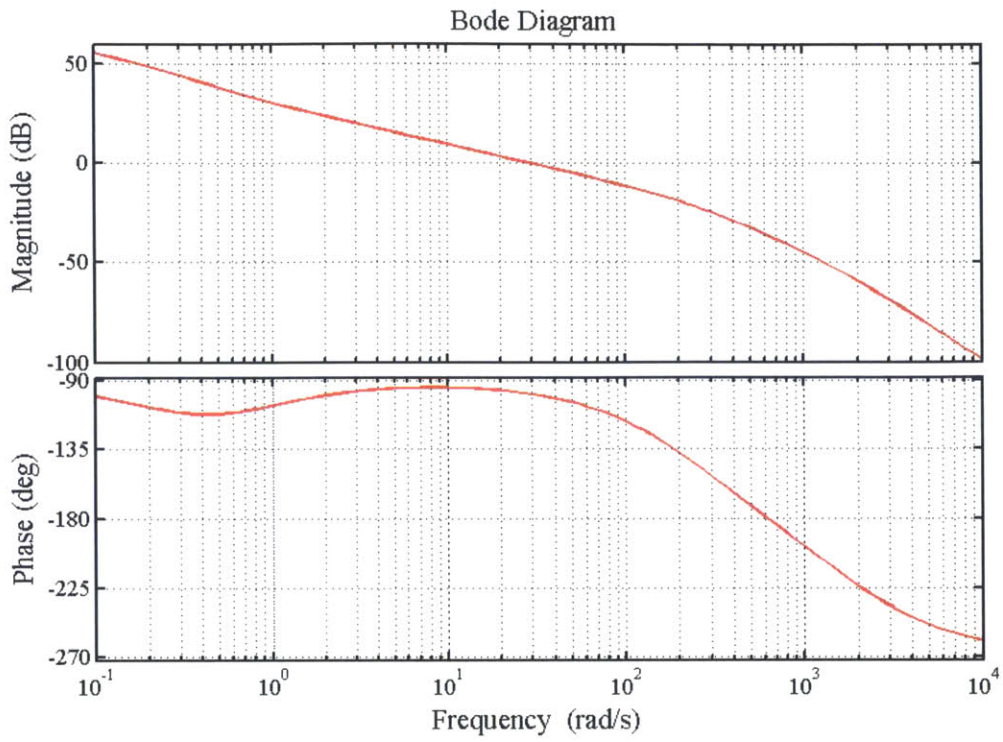
(a) Frontal plane return ratio bode plot
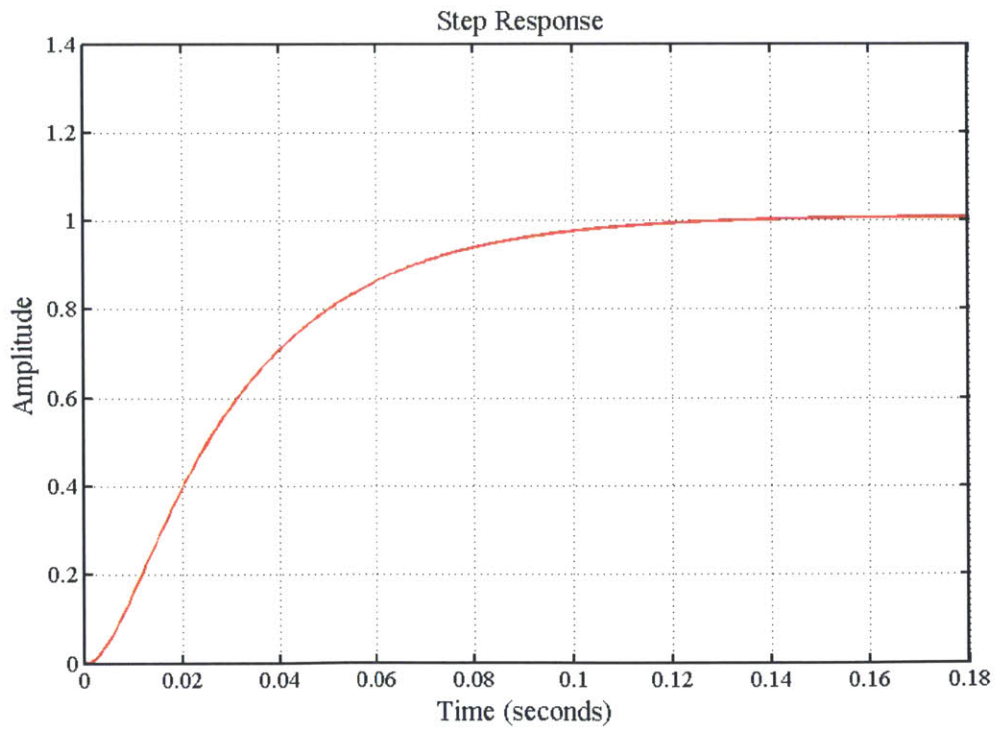
(b) Frontal Plane closed loop step response

Figure 6-26: Frontal plane control analysis

there is a non-linearity that occurs at about 4.8° Skywalker angle. Watching the physical system, this looks as though the motor gear is slipping between ring gear teeth, however, at this point, current spikes and velocity lags the velocity command. Therefore, it seems that the system may be cocking a bit in yaw, causing the frontal plane gears to bind. The motor responds by sending a pulse of torque to rectify the situation and the motion profiles are unscathed with respect to the simulated model which tells me that the non-linearity is not too harsh.

6.4.3 Frontal Plane Technical Characterization

The controls section of the frontal plane motion was done without a subject on the track because it closely resembles a linear time invariant system. However, the frontal plane motion of the system will always be loaded by an unpredictable subject during operation. When designing the drive (section 3.2.4), the most extreme system inertia was considered, assuming a 6'0" tall, 200 lb. subject as a rigid rod fixed to the tracks. As can be seen in figures 3-23 and 3-24, this assumption limits the $0 - 6 - 0°$ perturbation time to be greater than 0.5 seconds using maximum motor torque during both acceleration and deceleration. In reality, the human body more closely resembles a double inverted pendulum coupled to the track with springs and dampers (figure 6-28).

Instead of modeling the inverted pendulum system in an attempt to match the dynamics, we observed the variations in the motion parameters of the loaded and unloaded situations. A fast perturbation, capable of significantly affecting balance was run from $0 - 5 - 0°$ Skywalker degrees with a large subject (6', 190 lbs), a small person (5'4" 130 lbs) and with the system unloaded to compare the motion profile, current and velocity feedback. The subjects' height and mass were used to calculate the rod inertia assuming the subject was fixed to the track ($J = 1/3ml^2$) for comparison purposes. The body inertias were approximately $96kgm^2$ and $50kgm^2$ respectively. Figure 6-29 shows that the addition of a subject only increases the current marginally (current RMS values seen in table 6.17). The motion profile was identical in all cases and the velocity feedback showed only very small changes. This

181
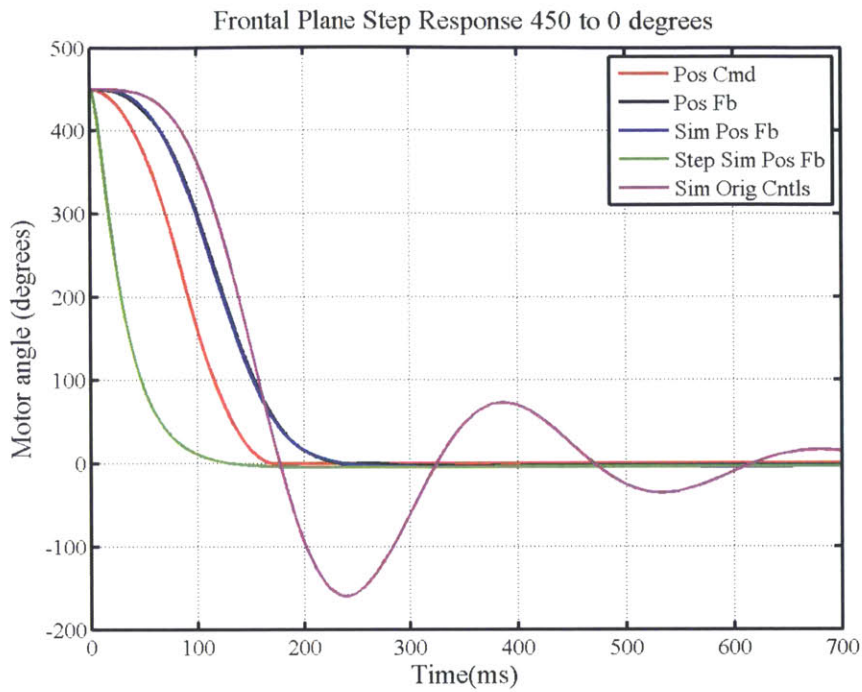
(a) Frontal plane step responses 5°
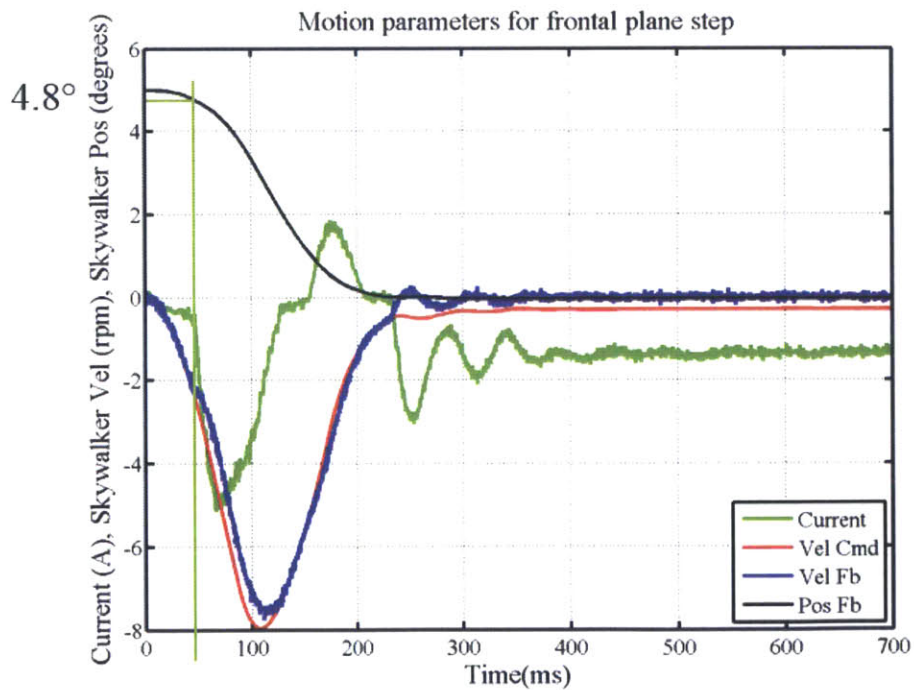
(b) Frontal plane step response current, velocity and position

Figure 6-27: Frontal plane step response characteristics
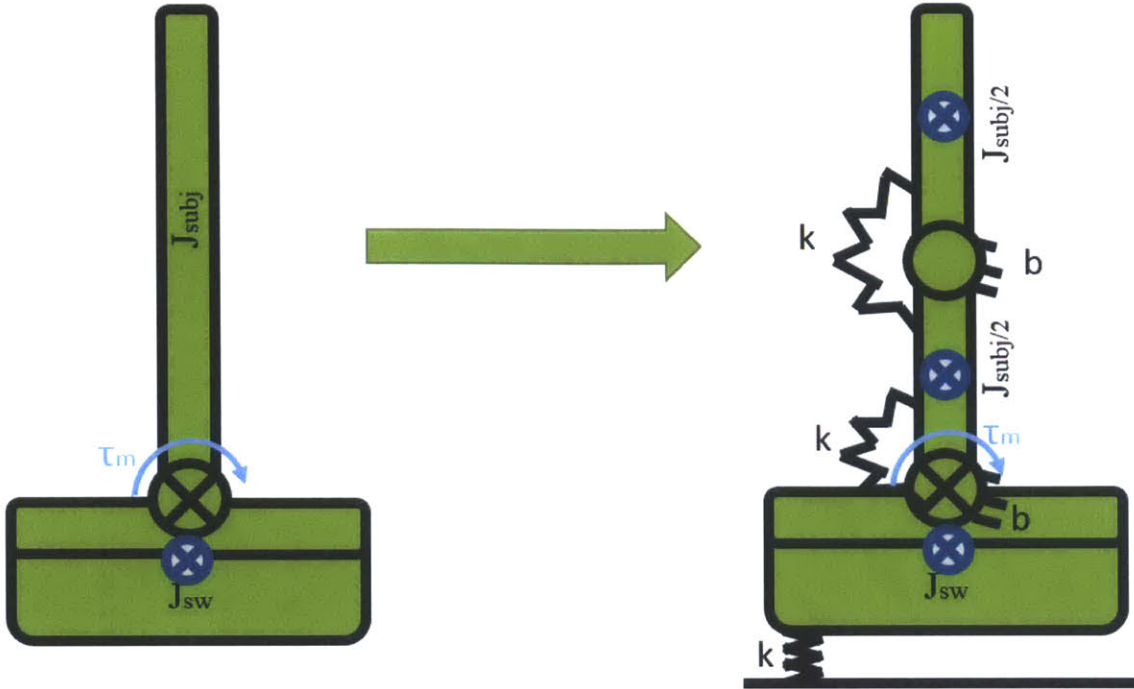
Figure 6-28: Frontal plane closed loop control

motion profile was saved as the starting point for the standard perturbation to be used with subjects in an effort to disturb balance.

Table 6.17: Frontal plane RMS current for the $0 - 5 - 0°$ in figure 6-29

	RMS current (A)
96 kgm^2 large subject	1.59
50 kgm^2 small subject	1.69
Unloaded	1.41

Acceleration and velocity limits

The AKD servomotor drivers set an initial acceleration limit based on the motor being used. For the frontal plane drive, the driver set an acceleration of 10,000 RPM/s as the acceleration limit and the profile seen in figure 6-29 was run with a velocity limit of 500 RPM. The acceleration limit acts to create a softer movement profile but also limits the system's performance. Releasing the velocity limit, yields a max velocity of approximately 700 RPM, which also decreases the time of perturbation (see figure 6-30). Notice, that the current now peaks around 5 Amps. Releasing the acceleration

183
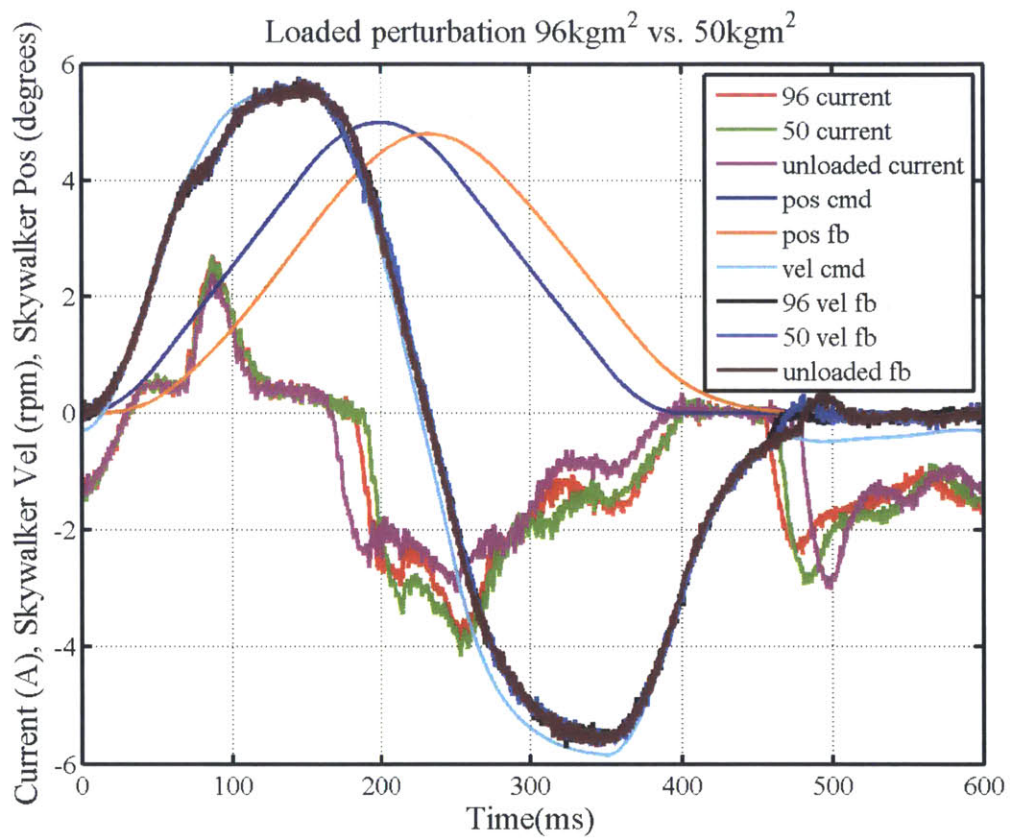
Figure 6-29: Frontal plane closed loop control
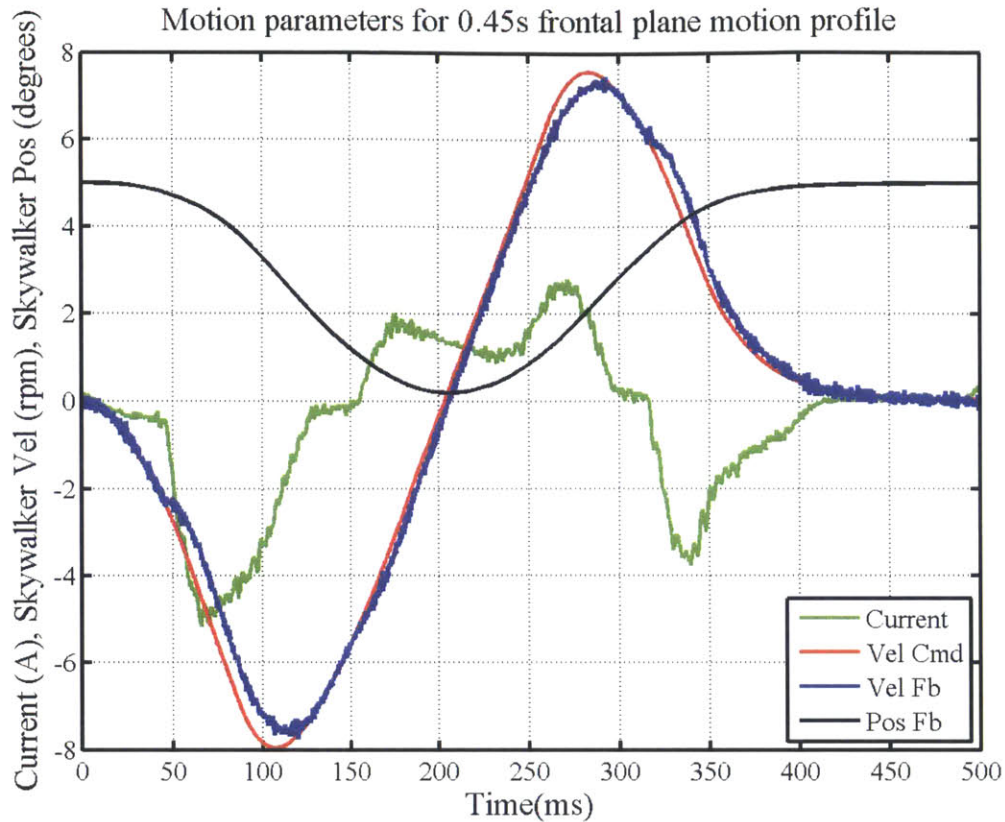
Figure 6-30: Frontal plane $5 - 0 - 5°$ profile without velocity limit

limit will allow for faster profiles limited only by the torque capacity of the motors.

Frontal plane torque capacity

The Kollmorgen AKM51E motor used in the frontal plane drive has a continuous current rating of 2.56 ARMS. The current to torque relationship (K_t) is linear up to 5.5 Amps and it is capable of reaching up to 8.2 Amps at peak. The RMS current of the motor during operation must be kept below that of the continuous current rating. All motion profiles run in this section are well below that limit. Above 5.5 Amps, the current - torque relationship will become nonlinear and thus for faster perturbations, it is likely that the achievable bandwidth of the system will decrease due to current saturation.

It is also worth noting that the frontal plane drive is in constant pre-load by the conical springs. When not enabled, the electromechanical brake, capable of a holding

torque of 14.5 Nm at the motor, restrains the frontal plane rotation through the gear reduction of 90:1. The preload due to the springs is calculated to be approximately 200 Nm from the published spring constant and thus the motor is holding approximately 2.2 Nm of constant torque. Observing the enabled motor current to be 1.2 Amps at the horizontal position and using the published motor constant of 1.72 Nm/Amp, the torque at the motor can be estimated to be 2.06 Nm via equation (6.28). This loosely confirms both the spring rates and the motor constant.

$$\tau_m = K_t i_m \tag{6.28}$$

Range of motion

The range of motion of the frontal plane is 6.0° when rotating away from the pre-load springs, limited by the interference between the front support beam and the steel frame. In the direction of the pre-load springs, the the maximum reachable angle is 2.8° limited by the solid height of the springs.

Chapter 7

Feasibility Study

The first-ever patient study was conducted on the Skywalker system with persons with gait impairments due to cerebral palsy and stroke. The primary purpose of the study was to evaluate the feasibility and safety of the Skywalker system when working with persons with disabilities. A secondary focus of the study was to observe the effects of training with system. The training programs, including the algorithms and machine kinematics are described in section 7.1. The study itself will be represented as case studies, following each of our very unique participants in section 7.2. One of the greatest features of the Skywalker-γ system is its versatility which was made evident by our ability to tailor the training to each of our unique participants, a characteristic that stands out in comparison with all rehabilitation robots available commercially.

7.1   Rehabilitation Training Programs

The study made use of three classes of rehabilitation training programs (Rhythmic, Discrete, and Balance). The rationale for developing these three programs can be found in chapter 2. This section explores the intricacies of each program. For details on the setup and running procedures for each training program, see appendix A.

Before and after each training program, a diagnostic program observed the participant's gait. The purpose of the diagnostic program was to record the kinematics of the participant at the comfortable walking velocity (determined on the first day
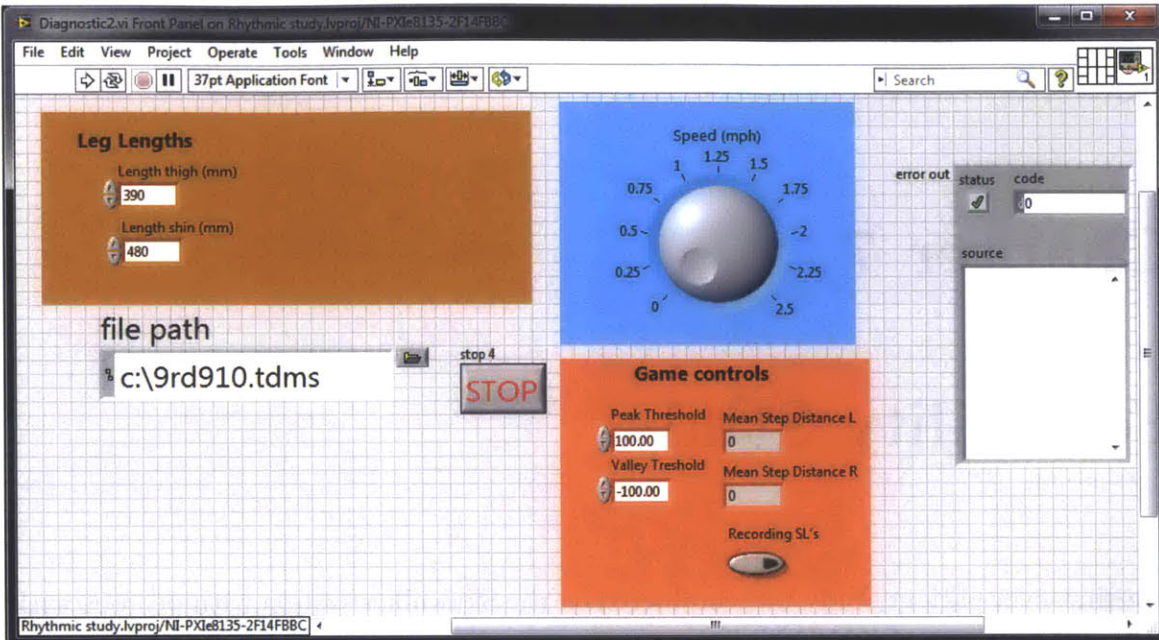
Figure 7-1: Diagnostic Program Graphical User Interface

of the trial). The graphical user interface (GUI) for the diagnostic program, seen in figure 7-1, displays the average step length of each leg so that the operator could immediately assess symmetry and the overall step lengths before and after training.

7.1.1 Rhythmic Training Program

The rhythmic training paradigm used by the Skywalker-γ was originally conceptualized by Caitlyn Bosecker and Hermano Igo Krebs using the alpha prototype version of the Skywalker[73]. Figure 7-2 depicts the basic structure of this paradigm. The first phase is a heel strike on a moving treadmill. The treadmill then moves the foot to the toe off position. When the participant initiates a forward movement, the track will drop, allowing gravity to assist the swing phase of gait in a pendular fashion. This training method relies on a split belt treadmill and can be done on one or both sides of the body depending on the impairment of the patient. The work was furthered by Panagiotis Artemiadis[89], who first introduced a machine vision system as a way to determine the gait phase. Various tests were done with the alpha prototype including a demonstration of a passive mannequin ambulating via the rhythmic paradigm

| 1) Heel Strike | 2) Toe Off | 3) Gravity Assisted Swing |
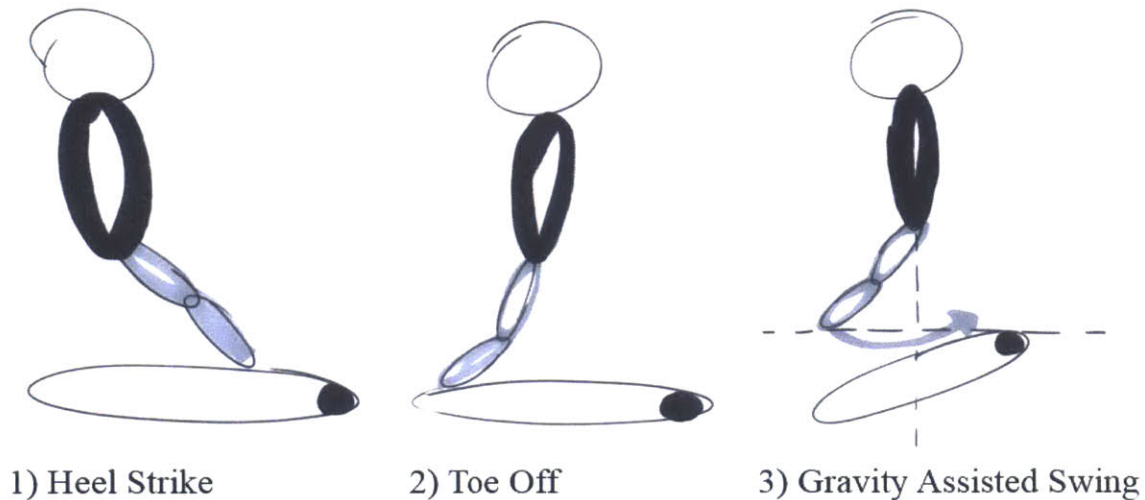
Figure 7-2: Depiction of the Skywalker Rhythmic Training Paradigm

and an early study of healthy subjects walking on the device. The alpha prototype provided a bed to test the rhythmic paradigm but was not fit for further research. Hardware limitations (lack of power in both the treadmill motor and the sagittal plane actuators) necessitated the development of new hardware which became the Skywalker-γ.

The Rhythmic Program developed with the Skywalker-γ differs in multiple ways. It makes use of its independent treadmill track motors to smoothly set both treadmill speeds, sometimes to the same speed and other times at different speeds to alter gait asymmetries. The linear cam system grants us to programmatically define the track drop profiles, adding versatility in the hands of the operator depending on the patient's impairment level. The final major difference of the rhythmic program is the addition of an interactive game that allows patients to view and consciously alter their step length and gait symmetry.

Drops

As shown in Chapter 7, the Sagittal plane drops are capable of being made up to 6 inches under-foot (11.6°), though in our trial we did not need to drop to that extent. For this trial, three drop depths (figure 7-3) were programmed via the AKD Workbench application with parameters shown in table 7.1. Notice that the speed of
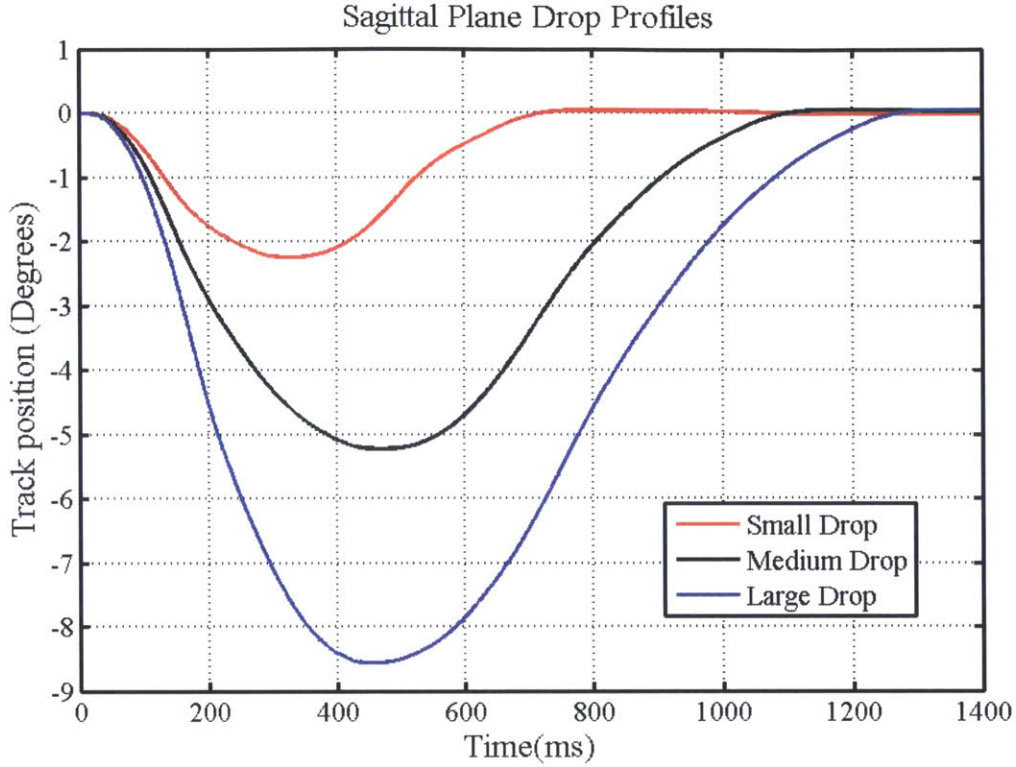
Figure 7-3: Feasibility Study Rhythmic Drop Profiles: in system coordinates. Plots are generated from the data collected from the sagittal plane motor encoders divided by 90 to estimate the angular position of the track. See 3.8 for more details on the transmission ratio.

these drops is far below the capabilities of the machine as defined in chapter 7. This is because at high accelerations and decelerations, the machine's movements appear violent, making a booming sound and can make the Skywalker system jump from the floor.

Table 7.1: Drop profile parameters (Trapezoidal profile)

	motor pos[deg]	motor vel[rpm]	motor accel[rpm/s]	motor decel[rpm/s]
Small Drop Down	−200	950	2000	1000
Up	0	950	1000	500
Medium Drop Down	−470	950	3000	1000
Up	0	950	1000	500
Large Drop Down	−770	950	4000	2000
Up	0	950	1000	500

190

Software Algorithm

The algorithm used for the rhythmic drops is shown in figure 7-4. The purpose of this algorithm is to locate the time in which the patient initiates swing phase and to quickly send a signal to the motor drivers to initiate a drop. The chosen method for doing so is to locate a minimum in the estimated heel position (assumed toe-off position). A valley finder algorithm (1) was written as a sub vi (Labview-speak for a user defined function) that looks for valleys below an entered threshold (9) in an array built from estimated heel positions (2). Additional features were built into the algorithm for operator control and safety. An enable toggle switch (3) must be in the true position for drop signals to be sent and the four infrared emitters representing the subject's legs must be correctly identified (4) to prevent errant drops due to a failure in the IR emitters or if the patient's position exceeds the camera's field of view. Figure 7-5 shows an early plot of the drops while monitoring the state of each of the inputs to the AND gate (Fig. 7-4 (6)).

Notice, as marked by (1) in figure 7-5, that the valley finder algorithm incorrectly identifies a valley in an area of xpos where there appears to be no valley. This would cause a second drop in this case. A time check was implemented (marked as (5) in figure 7-4). This time check ensures a certain amount of time to exist between each drop. This solves the problem of double drops but cannot fix an errant drop during mid or late stance. The valley finder (fig. 7-4 (1)) smooths data using a linear interpolation of w data points and uses the results to determine the location of the valley. Increasing w creates a smoother dataset but also introduces a delay in finding the valleys. It was experimentally determined that increasing w from 3 to 10 data points prevented faulty drops and also solved a problem that occurred infrequently of missing drops. Missing drops became a dangerous situation because patients begin to rely on the drops to walk. If a drop missed, the patient would trip and fall. Of course, the trade-off was a delay in the onset of the drop which increased from and average time of $23ms$ to $68ms$ after the raw heel position valley. This delay is shown in figure 7-6. The change was imperceptible to healthy subjects prior to the study.

191
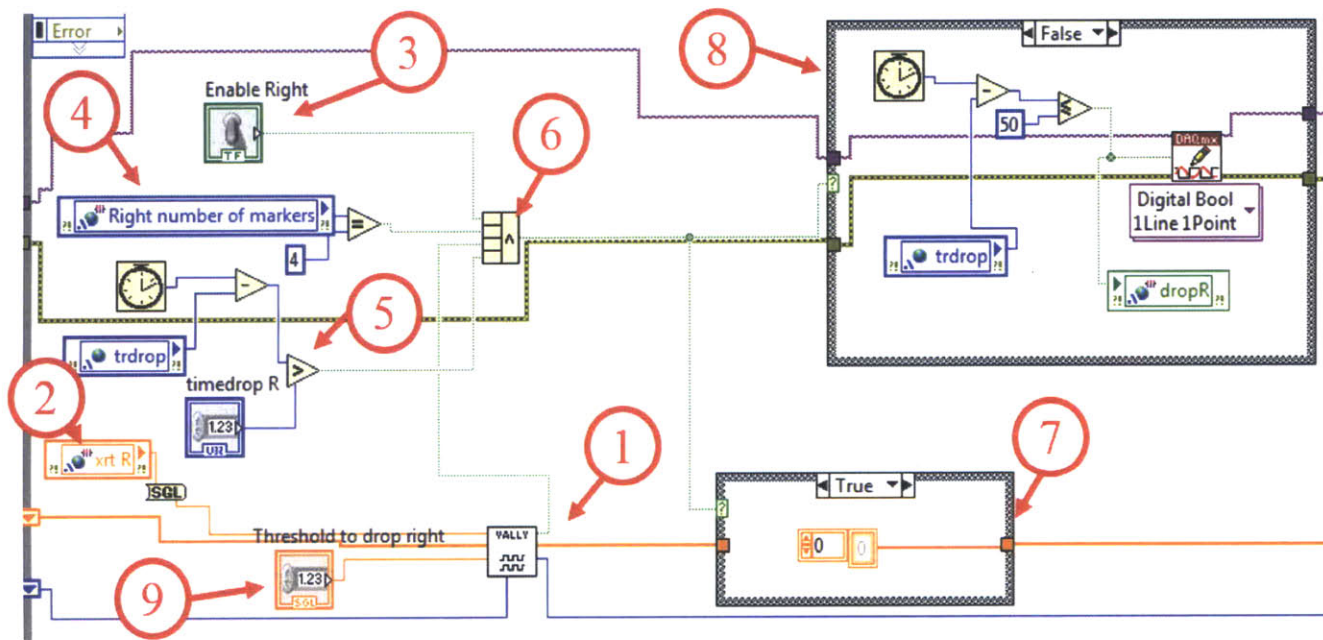
Figure 7-4: Algorithm: Track Drops
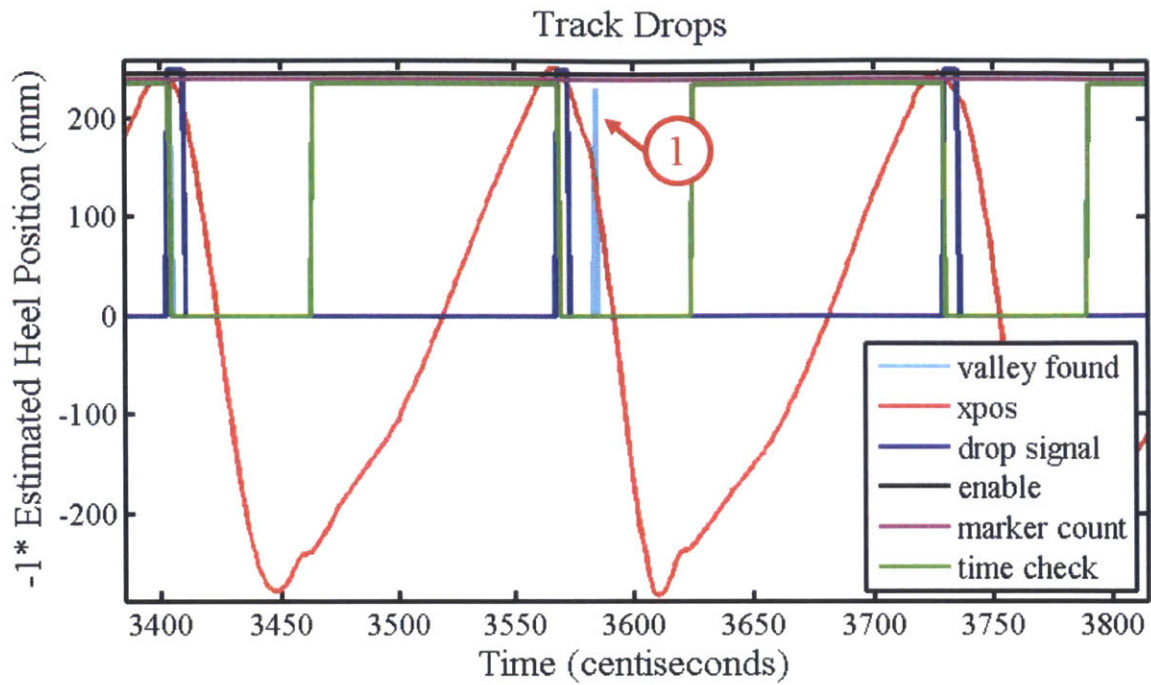
Figure 7-5: Drop Boolean Check
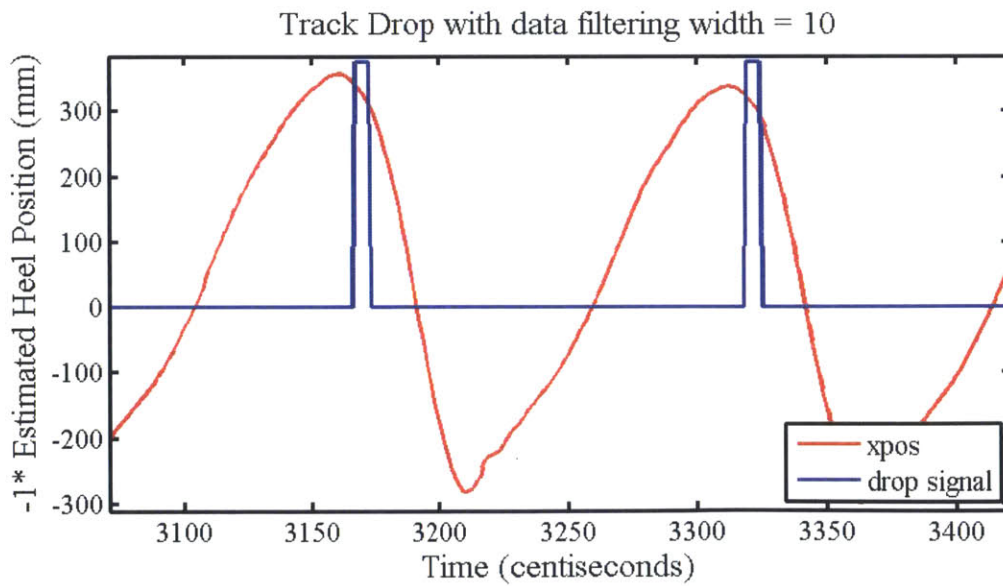
Figure 7-6: Final Drop Digital Output

Once the AND gate (figure 7-4 (6) receives all 4 true signals, it writes a digital line high, which is connected to a digital input channel of the AKD motor driver to initiate one of the chosen drop profiles (figure 7-3). The case structure (8) constrains the high signal time to 50 ms. Another case structure (7) resets the array being analyzed by the valley finder sub vi. This eases the computational load on each loop. The digital drop loop in figure 7-4 runs at 100Hz. The full rhythmic program consists of two of these loops (right and left track), an analog loop that writes the track speed, a logging loop, two vision processing loops, one emergency stop loop that monitors a physical stop button and one loop that runs the rhythmic game described below, all running in parallel.

GUI

Figure 7-7 shows the GUI used for the rhythmic program. Drops are enabled via the Enable Left / Enable Right toggle switches (a). On the front panel, the operator can select the threshold that the participant's heel must exceed to initiate a drop (b), the drop depth (c) and the delay time between each drop (d). The robot operator controls the speed via the virtual knob (e). For the split speed variety of the rhythmic program (described below), the knob (f) is used to increase the speed of one track and while decreasing the speed of the other track as determined by the initial symmetry observed in the diagnostic program.

Interactive game

Figure 7-8 represents the interactive game seen by the patient. The black bars represent the respective position of each foot. They grow as the foot moves forward and are reset when the participant makes their next step with that leg. The dotted line is the step length during the diagnostic program and the solid line is the average step lengths of all steps within that training session. The goal of participants is to equalize the two step lengths.

194
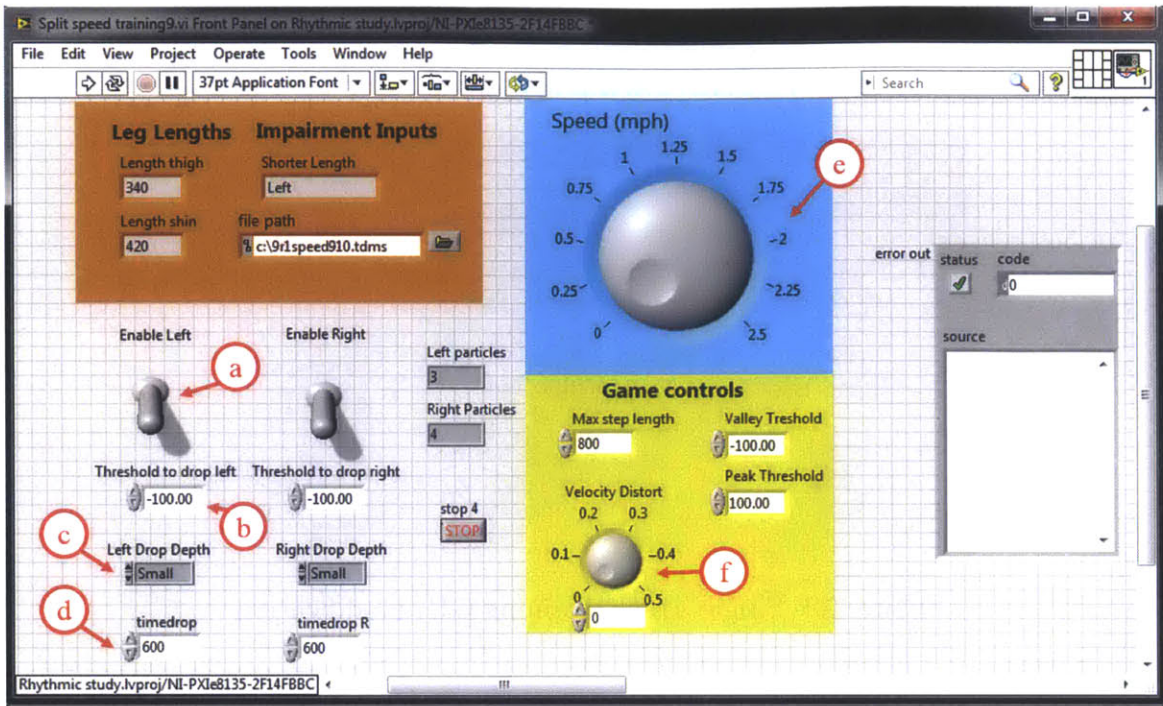
Figure 7-7: GUI: Rhythmic Split Speed Program
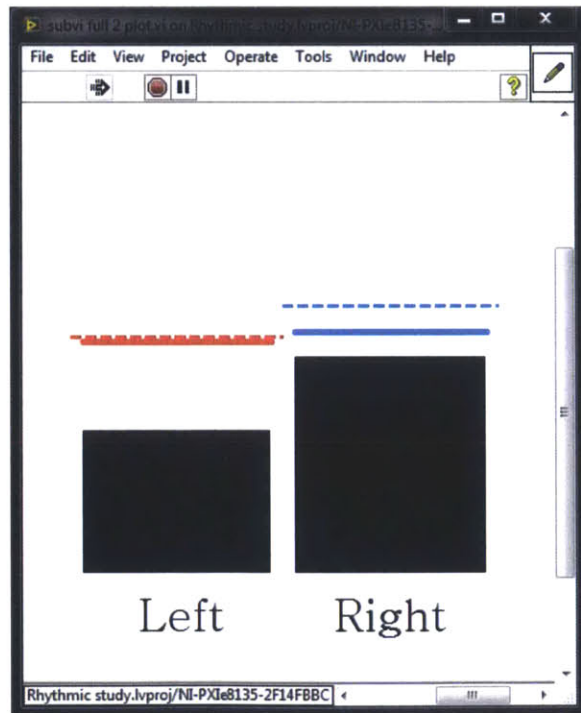
Figure 7-8: Interactive Rhythmic Game

Rhythmic program variations

Three independent variations of the rhythmic program were used with patients.
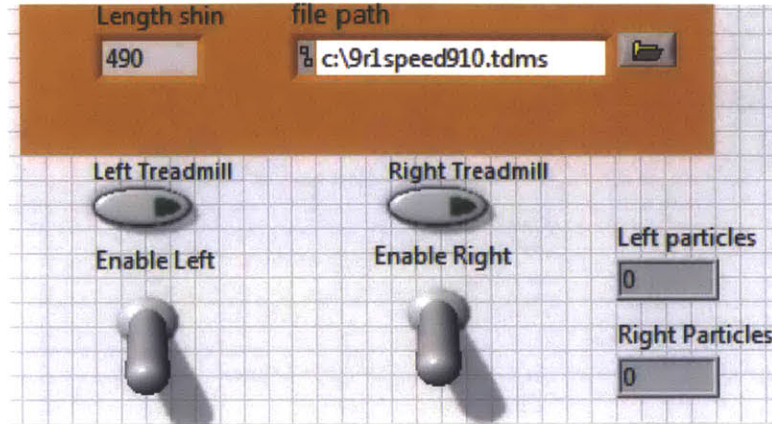
Figure 7-9: Single Track Training GUI modification

Speed Distortion This program used a nominal speed as defined by knob (e) in figure 7-7. A second knob (f) in figure 7-7 was used to distort the speed of each track by a percentage. For example, if knob B reads 1mph and knob B reads 0.07, one track will be set to 1.07mph and the other to 0.93mph. The faster track would correspond to the side of the participant which had a longer step length in the initial diagnostic program to augment the asymmetry in a way loosely resembling Reisman et al.[7][90] (More on this in section 8.3.1). This program could be run with or without the visual game shown in figure 7-8.

Visual Distortion This program relied on the visual game shown in figure 7-8. In this program, knob (f) represented the distortion to the height of the bars again by a percentage. For example, if the distortion was turned up to 0.07, one bar would appear 7% higher and the other would appear 7% lower. This program could be altered to augment or decrease the step length asymmetry.

Single Track Training This embodiment of the rhythmic program was developed specifically for participant 2 (the most impaired participant) who was having trouble with the rhythmic program. In this variation of the rhythmic program, one treadmill is stopped while the other is allowed to move at a desired speed,

allowing the patient to practice full steps on leg at a time. Drops and the operation of each treadmill are independently enabled via the GUI modification shown in figure 7-9.

Sagittal Plane Kinematics comparison using drops and BWS

To test the transparency of the sagittal plane drops and the body weight support, a test was conducted with a healthy subject (6'0" male). This was his first time walking with rhythmic drops. The test was done with and without the body weight support using the small drop profile shown in figure 7-3. The average body weight support over the BWS trail was 50% (during the feasibility study, BWS % never exceeded 30%). His kinematics from the Skywalker were compared to a speed matched trial on a standard treadmill. Data from 15 cycles of walking was cut and analyzed with the ensemble method described in figure 7-21. Figure 7-10 shows the kinematic results from the tests. The small rhythmic drops, used here did not have a large effect on the kinematics, showing a slightly decreased knee angle but nearly identical hip angles. Without the body weight support, the swing phase initiates later in the gait cycle. With the body weight support, swing phase began earlier. Notice that the body weight support limits the hip angle. It is unclear if this is a consequence of the bicycle seat design or if it is specific to the high level of BWS used here. The x-y trajectory in figure 7-10(c) is estimated based on the hip and knee angles as the position of the heel with reference to the hip joint.

7.1.2 Discrete Training Program

The discrete training program is the first of its kind, attempting to target the submovement primitive by facilitating patient-guided movements with defined start and stop points. An overhead projector (figure 7-11(a) (1)) is setup to display an interactive game, issuing targets (figure 7-11(b) (1)) randomized in side and length. The patient is allowed as much time as needed to initiate a movement and the target is held until the movement is completed. Whether or not the target is successfully hit
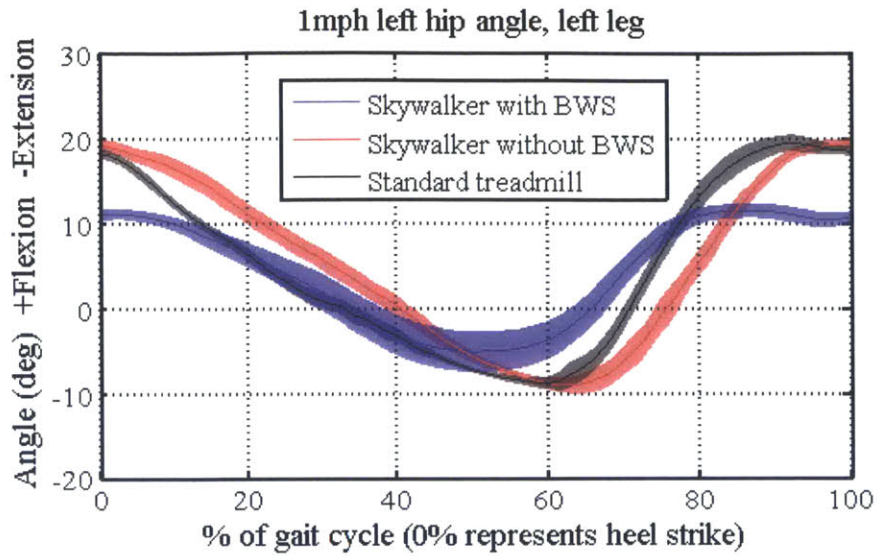
(a) Hip Angles
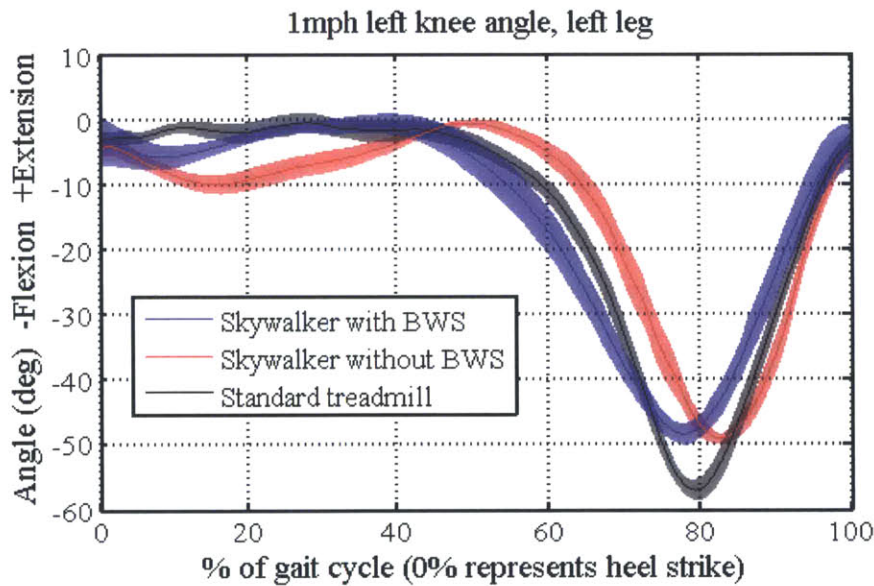
(b) Knee Angles
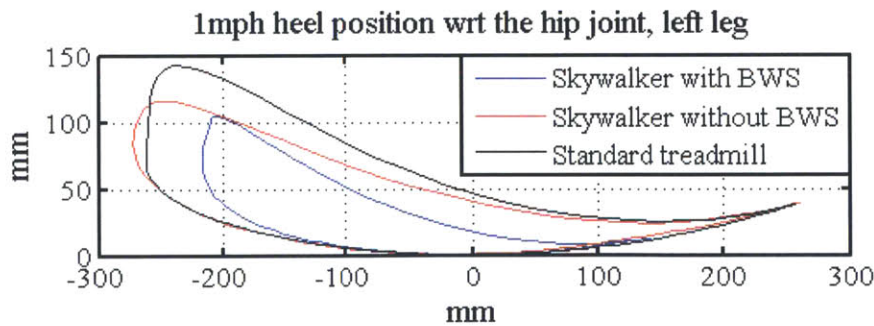
(c) Heel trajectory with respect to the hip

Figure 7-10: Sagittal plane kinematics of a healthy subject on Skywalker and a standard treadmill

(a) Overhead Projector Setup   (b) Discrete Game
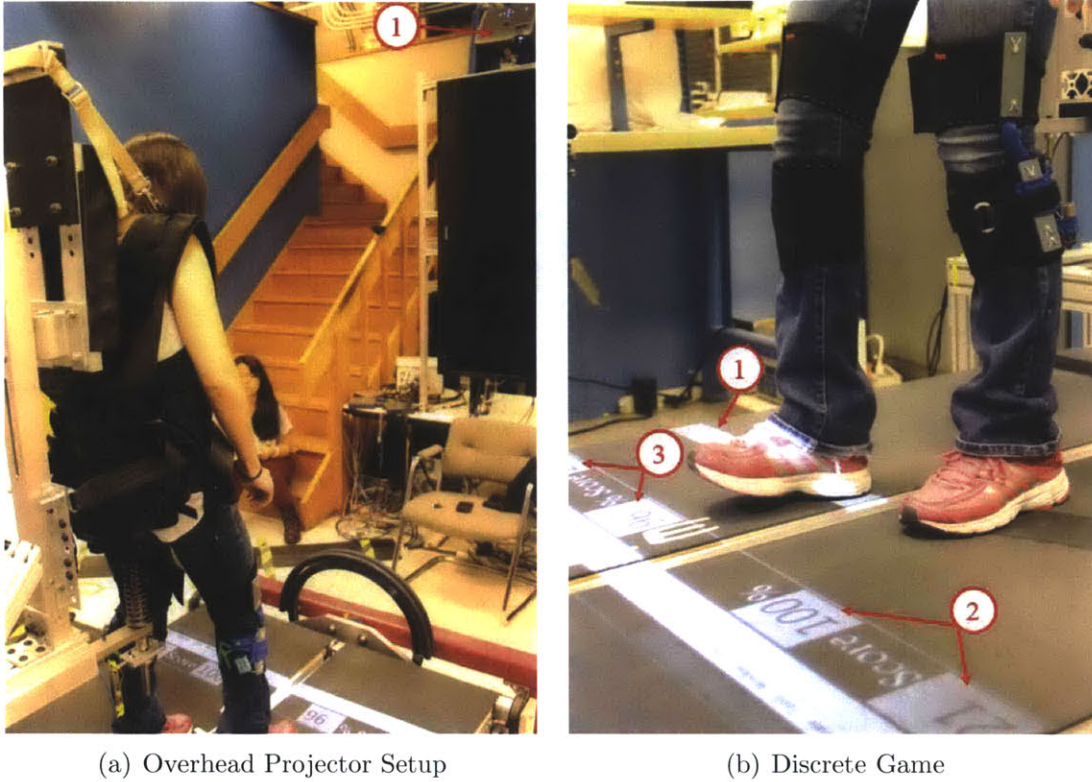
Figure 7-11: Discrete Program Interactive Game and Setup

by the patient's heel, the ipsilateral treadmill is moved to reposition the heel underneath the body. A score is displayed on the front of each treadmill corresponding to the number of targets successfully hit and the percentage of successful motions per side (figure 7-11(b) (2,3)).

Software Algorithm

Figure 7-12 show the full and broken down sequence structure that defines the discrete game. In sequence structures, each frame must be completed before moving to the next frame. The first frame defines the target locations. Separate random number generators (figure 7-12(b) (1)), which output a pseudo-random number from 0-1, are called to define a random target side and target location. The top generator output is compared with 0.5 to create a boolean command that defines the side. The lower generator's output (r) is manipulated by equation (7.1) (marked by (2) in figure 7-12(b)) to define the target's pixel location to the projected image (x_{pix}). q is a
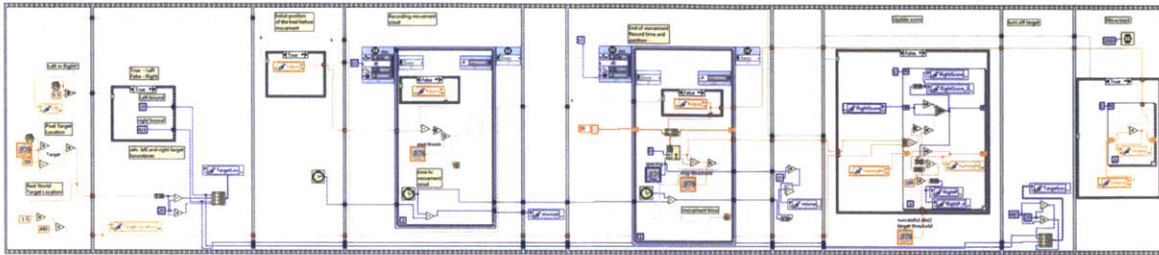
(a) Full Discrete Sequence Structure
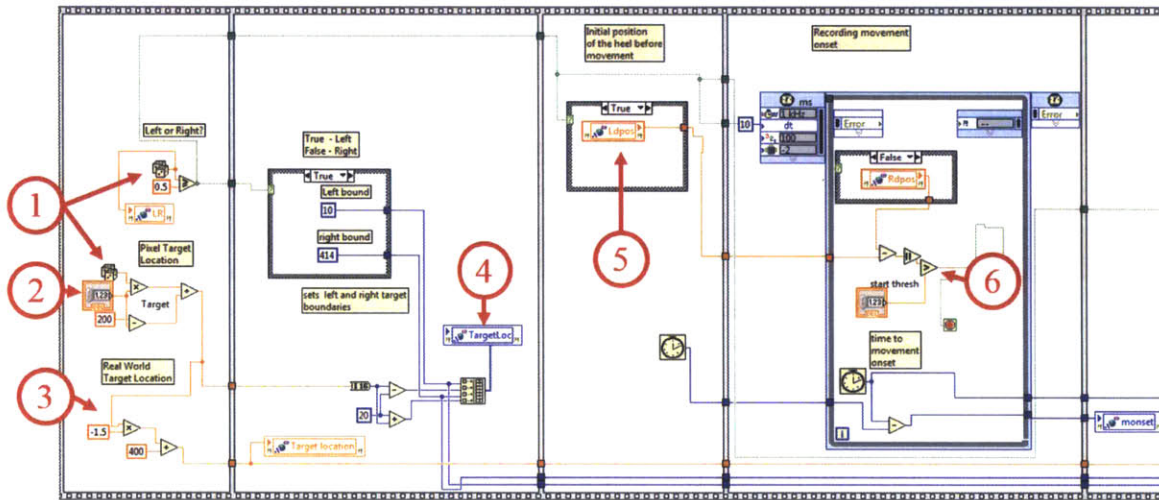
(b) Left Piece of the sequence structure
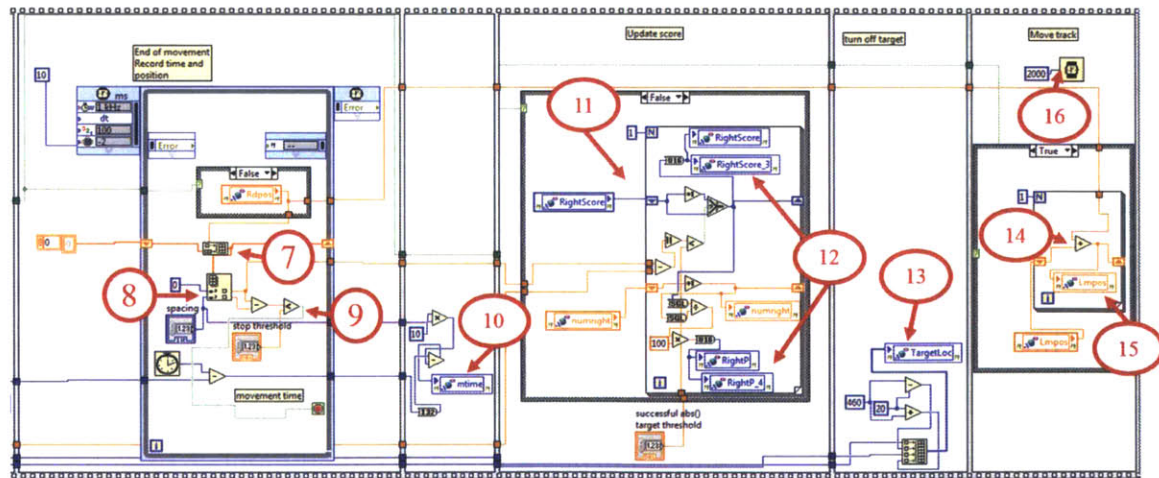
(c) Right Piece of the sequence structure

Figure 7-12: Discrete Algorithm

constant, controllable on the GUI (figure 7-14 (a)) that changes the upper limit of the target.

$$x_{pix} = r * q + 200 - q \qquad (7.1)$$

This is transformed to real world coordinates (x_{rw}) by equation (7.2) (marked by (3) in figure 7-12(b))to convert the pixel vertical axis to the treadmill x-axis in mm (defined as a line from treadmill back to front with the participant's original heel position at the origin).

$$x_{rw} = x_{pix} * (-1.5) + 400 \qquad (7.2)$$

Pixel target locations, defined by the first frame, are written to a shared variable ((4) in figure 7-12(b)) which is shared with the game control loop (not shown here). The next frame (5) identifies the starting location of the heel before a movement by reading from a shared variable that was written in the vision loop. The current position as defined by the vision loop is compared to the initial position (6) and a boolean is issued to conclude this frame when the difference in position reaches a threshold (controlled in GUI - figure 7-14 (b)). This frame also records the movement onset time and writes it to a shared variable in the next frame.

The end of a movement is recorded in the following manner. An array is built ((7) in figure 7-12(c)) of positions defined by the vision loop. The array is indexed (8) to compare (9) the current heel position to the heel position at a previous array position defined by the GUI (figure 7-14 (c)). If the two positions are within a certain length (controllable on the GUI (figure 7-14 (d))), a boolean is sent to stop the current frame. The movement time is recorded in the next frame (10).

The frame marked as (11) compares the location of the heel when the movement was stopped to the target position (x_{rw}) set by (3) in figure 7-12(b) and assigns a point if the distance is less than a threshold (controlled in the GUI - figure 7-14 (e)). This frame also calculates the percentage of targets successfully hit per side and writes the scores to shared variables (12) that are read and displayed by the game loop (not

201
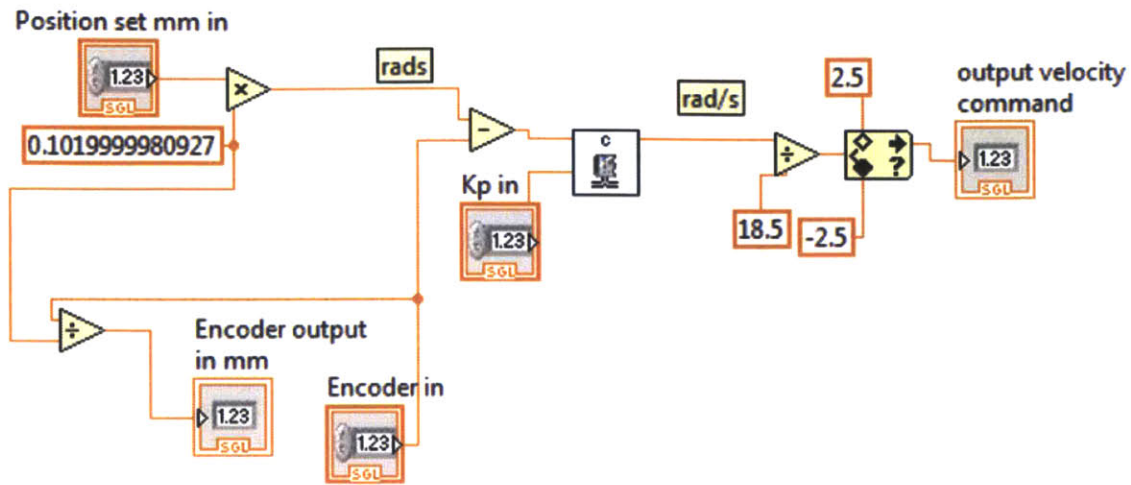
Figure 7-13: Labview position controller

shown). The next frame sets the target distance outside of the visible screen via a shared variable (13), effectively making the target disappear.

Finally, in the last frame, the distance observed when the movement ended is added to the current position position reference (14) and written to a shared variable (15) which is read by the track position controller (figure 7-13) and compared with the absolute position of the motor encoders to generate the motion of the treadmill underfoot.

A while loop is wrapped around this sequence structure such that, as soon as a treadmill movement is completed and 2 seconds have elapsed (16), a new target is generated and the full sequence structure begins again.

Track Controller Gains and movements

The high level control scheme is shown in figure 6-16. The k_{pp} gain was set at 2.5, with velocity and acceleration limited, yielding the position profile seen in figure 6-22. The full Labview implementation of the controller is shown in figure 7-13.
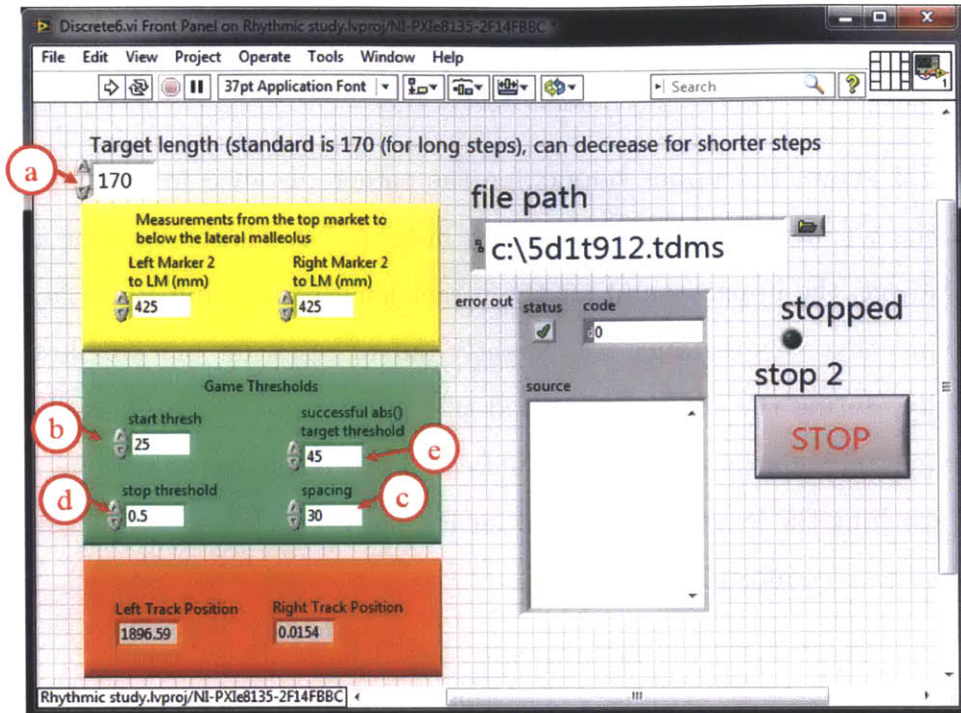
Figure 7-14: GUI: Discrete Program

Table 7.2: Discrete program setting per patient

	T. Length (a)	Starth Thresh (b)	Spacing (c)	Stop Thresh (d)	T. Thresh (e)
Healthy	170	$25mm$	$30points$	$0.5mm$	$45mm$
P1	90	$25mm$	$35points$	$0.5mm$	$45mm$
P2	70	$35mm$	$50points$	$1mm$	$50mm$
P3	90	$35mm$	$30points$	$0.5mm$	$45mm$

GUI and game parameters

Substituting for x_{pix} in (7.2) from (7.1) yields (7.3). Notice that q in this equation makes reference to the target length (seen as (a) in figure 7-14) and r is a random number between 0 and 1.

$$x_{rw} = (-1.5) * (r * q + 200 - q) + 400 \qquad (7.3)$$

Targets are displayed in front of the patient at a distance referenced from the initial heel position directly under the body. No matter what is used for q, the lower bound ($r = 1$) for the targets will be 100mm. The upper bound will be achieved when $r = 0$ in which case equation (7.3) becomes:

$$x_{rw} = 100 + 1.5c \qquad (7.4)$$

Table 7.3 shows the upper bound for the target distance for each participant based on the q (Target Length) values seen in table 7.2. Notice that for a 5'8" tall healthy subject, the upper bound for the target length was comfortable at 355 mm. It was found that this distance was slightly out of reach for our smallest patient. Additionally, during the study we learned that shorter steps were more difficult for each of our study participants, which increased the challenge of training. P2 had difficulty reaching the length determined for P1 and P3, so his max target length was scaled down to a comfortable level.

Table 7.3: Discrete program target length upper bound

	Upper bound
Healthy	$355mm$
P1	$235mm$
P2	$205mm$
P3	$235mm$

The movement distance that signaled the onset of movement (column (b) in table 7.2) was increased to 35mm for P2 because his movements were not smooth. Increasing the threshold solved a problem of disappearing targets that were caused by the algorithm assigning the start of the movement prematurely. For P2, we also increased the spacing and stop threshold for the stopped position to ensure he stopped his movement before the track began to move. The successful target threshold was also increased for him to increase the percentage of targets hit. To ensure the patient did not get frustrated with the game, the percentage was kept above 80%. The successful target threshold is the width of the band, centered at the target location (x_{rw}), in which the patient will score a point.

7.1.3   Balance Training Program

The balance program is based on frontal plane perturbations that simulate waves (rocking 2.5° in one direction, moving to 2.5° in the other before moving back to 0°).
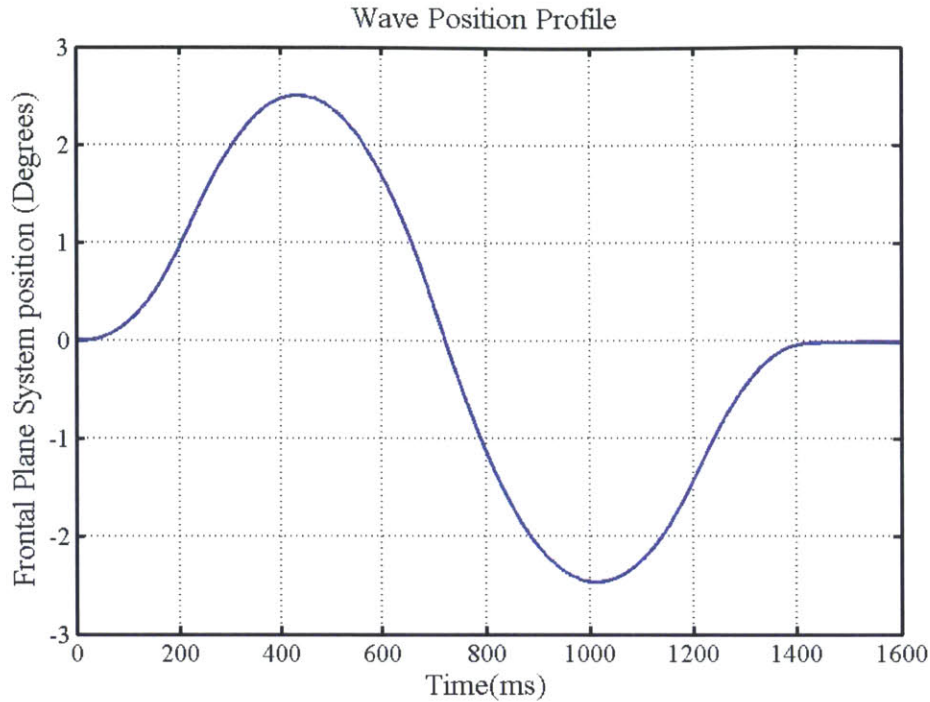
Figure 7-15: Frontal plane wave profile recorded from the frontal plane motors and scaled by the frontal plane transmission ratio

The waves can be enabled independently of treadmill speed and sagittal plane drops defined in section 7.1.1 and their timing is defined by six discrete levels of the game described below. For this initial feasibility study, the wave profiles were fixed for the whole study.

Waves

The left and right waves are mirror images of each other. The frontal plane profile for the waves was designed to be gentile with just enough acceleration and speed to disrupt a healthy person's balance when walking at 1mph. Figure 7-15 shows the system's profile in frontal plane and table 7.4 shows the profile parameters as programmed in the Kollmorgen AKD motor drivers.

Table 7.4: Wave profile parameters (Trapezoidal profile)

	motor pos[deg]	motor vel[rpm]	motor accel[rpm/s]	motor decel[rpm/s]
Left	225	250	900	900
Right	−225	250	900	900
Center	0	250	900	900

Software Algorithm

The software algorithm adds to the rhythmic program defined in section 7.1.1. As can be seen in figure 7-17, the controls for speed and sagittal plane drop are the same as for the rhythmic program. The balance program adds the ability to call the waves.

The algorithm begins with a level selection (a) in figure 7-17 and (1) in figure 7-16 which defines the level of the wave game. Increasing the level, increases the difficulty of the balance game. Each level has independent code. Figure 7-16 shows the code for level 6. (2) in figure 7-16 represents the direction that the wave will initially drop. This variable is updated each time a drop occurs. The code marked (3) shows the algorithm that defines the random start time for each wave. A millisecond timer compares the current time to the time of the last drop. If this number exceeds a randomly generated threshold defined by (4), a true boolean is sent to the case structure (5) which writes a true signal to a shared variable (6) that is read by a digital output loop and sent to the motors to begin the motion task of the waves. Level 6 of the game is unique because it also distorts the warning lights. A random number generator (7) with a uniform distribution compares to 0.8. If the output is false, the warning light occurs on the correct side, otherwise it sends the warning signal to the opposite side of the game such that 80% of the time, the warning light is on the side that will drop first. 20% of the time, the game displays misinformation to the participant to further increase the difficulty of anticipating the movement of the machine. The warning light illuminates 500ms prior to the wave being called (8).

The game levels determine three parameters of the waves: the time between adjacent waves, the behavior of the warning lights and the direction of the waves. The time between drops refers to the time between the onset of movement. Two warning lights are displayed on the main game screen as seen in figure 7-18 (4). Their purpose

206
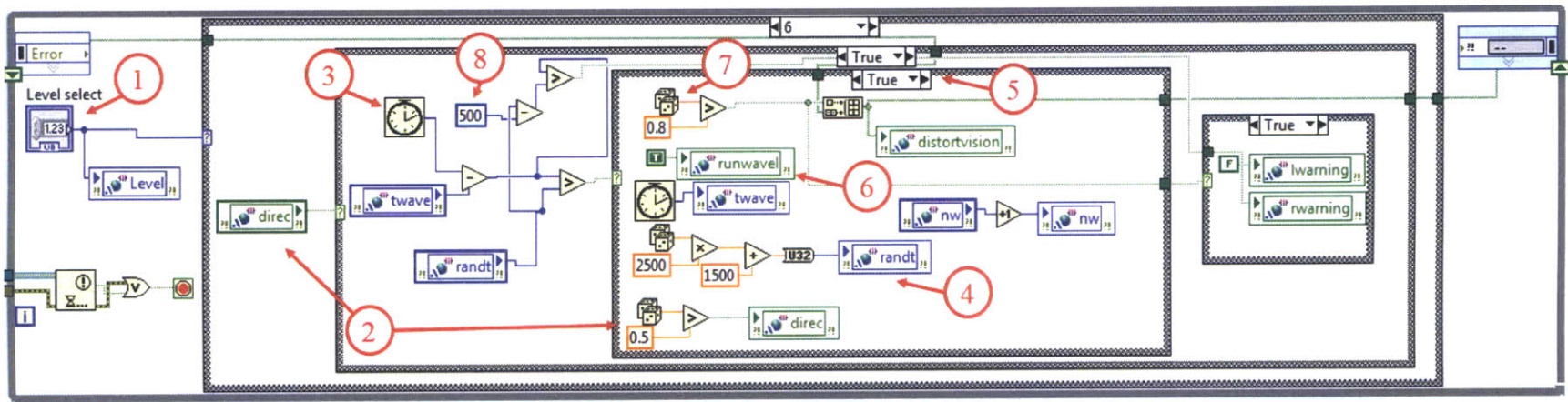
Figure 7-16: Balance Loop

Table 7.5: Balance game level chart

Level	Time between waves	Warning lights	Direction
1	No drops	N/A	N/A
2	8s	Yes	One
3	2-6s	Yes	One
4	2-6s	Yes	Both
5	2-4.5s	No	Both
6	1.5-4s	80% correct	Both

is to alert the participant when the drops are about to occur. If a light illuminates on the right side, for example, the wave will first descend on the right side and vice versa. Levels 2,3 and 4 set the lights to illuminate 500ms before wave movement onset. Level 5 disables the lights and as mentioned above, during level 6, the lights work but occasionally signal the incorrect direction. The initial direction of the wave is also varied by selecting different levels. Level 2 and 3 of the game allow drops to only occur in a single direction (the left side falls first). All higher levels randomly assign a starting direction of the waves to add difficulty to the program. Table 7.5 summarizes the 6 levels of the balance game.

GUI

The GUI is shown in figure 7-17. It provides a simple way to choose which functions are enabled with each patient. The level select (a) controls the frontal plane waves, (b) controls the speed of the treadmill tracks and (c) independently enables each sagittal plane to drop in the rhythmic fashion described in section 7.1.1.

Game

The balance game is the least interactive of all three training modes because the movements and timing are generated by the software, however the number of waves ((2) in figure 7-18) are representative of the level of the game selected by the patient. The game also displays the level(1) and the speed of the track (3). The surfing beaver is attached to the horizontal blue line (5) and rotates with the wave. His position is controlled by the frontal plane motor encoder. The warning light will be illuminated
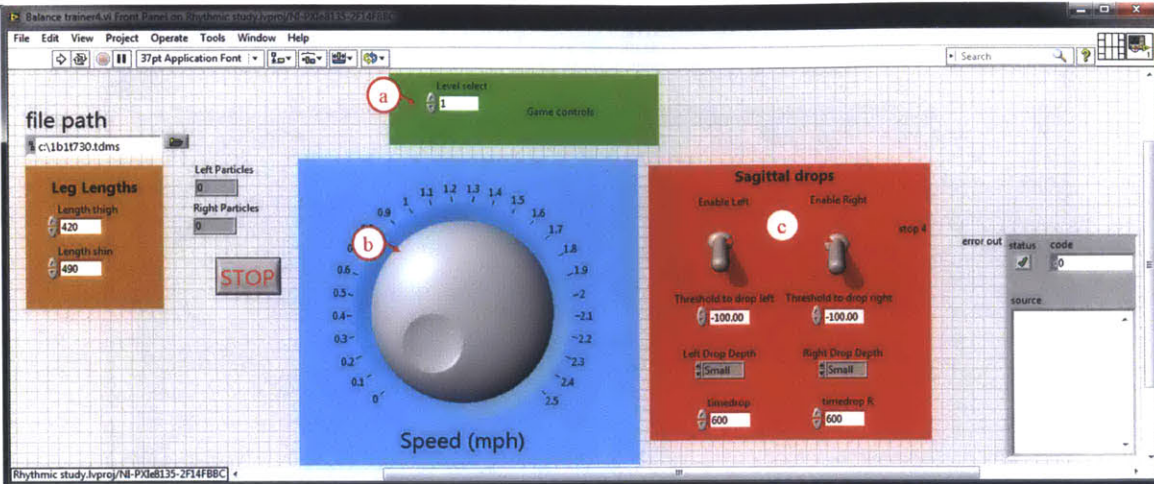
Figure 7-17: Balance GUI

on the side that the blue line will touch first during a movement.

7.2 Case Study Structure

Three adult individuals joined this study. Two were diagnosed with cerebral palsy and the other sustained a stroke approximately 5.5 years prior to the study. All participants gave their informed consent prior to participating and the Committee on the Use of Humans as Experimental Subjects (COUHES) at MIT approved the study (see appendix G). Participants who customarily wore an ankle-foot orthosis were allowed to wear it during robotic training but were asked to remove the device during electromiography of the tibialis anterior and soleus during the evaluations prior to and after training. Other devices such as canes or functional electrical stimulation devices for the tibialis anterior were excluded from training and evaluation when possible. Detailed study conditions for each participant can be found in the following pages.

7.2.1 Participant 1 (P1)

P1 is a 24 year old female with spastic triplegia cerebral palsy. Her height and weight are 5'1" and 101 pounds respectively. Her comfortable overground walking speed before the trial was 1.99 mph. She uses no devices for normal day-to-day walking. Her
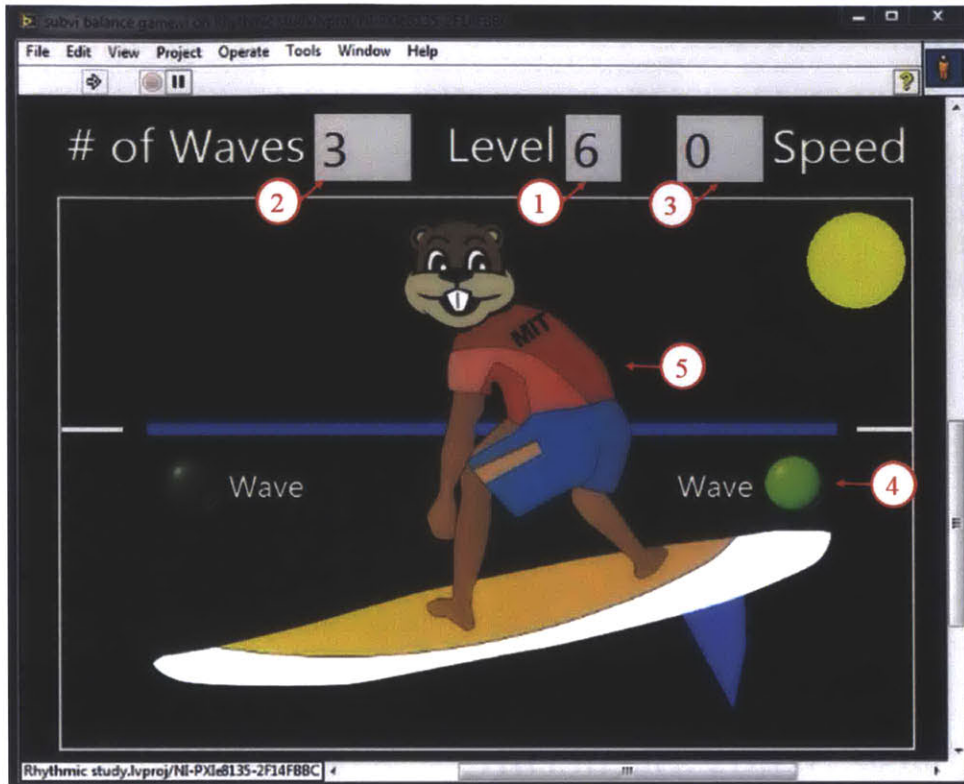
Figure 7-18: Balance Game

gait has noticeable scissoring. Initially, she had a problem with foot scuffing during swing phase on both feet, but she mentioned that it occurred more frequently on the right foot, especially when she becomes fatigued or during cold weather situations. Of the three participants, P1 is the least impaired.

Training Sessions

P1 trained for 16 sessions on the Skywalker-γ system over a period of 1 month, averaging 4 sessions per week. These were broken down into 9 rhythmic sessions (broken down into 1 introductory program, 3 speed trainings and 5 symmetry trainings, discussed at length in section 8.3.1), 4 discrete sessions and 3 balance sessions. It took two sessions for P1 to get comfortable with the body-weight support. Mounting and dismounting was easy and quick. Donning and adjusting the BWS took seconds.

7.2.2 Participant 2 (P2)

P2 is a 56 year old male diagnosed with spastic diplegia cerebral palsy at birth. Of the three participants, P2 is the most impaired. His height and weight are 5'10" and 145 pounds respectively. His comfortable overground walking speed before the trial was 1.12 mph. He uses bilateral ankle foot orthoses and a cane in each hand, which results in a pronounced forward lean (24° from the vertical). During training and in all evaluations except the treadmill kinematic and EMG study, he was allowed to wear the AFOs. The first two weeks of rhythmic training were done with the canes. The next two were done without canes, but used the new handrails made specifically for P2 (figure 2.2.5). All discrete training programs were run with the canes, though precautions were made to guarantee that the cane did not cross the line between the Infrared Emitting Diodes and the cameras. This happened on initial trials due to tassels that were attached to the handles of the canes, which caused the vision loop to misinterpret the position of the heel. The first and second week of balance training were done with the canes in hand. As the system ran through waves, the participant was encouraged to lift the canes off the ground and to stand erect. The third and fourth session, P2 was able to release his canes to the robot operator as he worked on riding the waves.

Training Sessions

P2 trained for 12 sessions on the Skywalker-γ system over a period of 1 month, averaging 3 sessions per week. These were broken down into 4 rhythmic sessions, 4 discrete sessions and 4 balance sessions, each being trained once per week. It should be noted that it took two weeks for P2 to get comfortable and trust the body weight support system of the machine. The rhythmic sessions were aimed at getting P2 to stand more upright while focusing on getting more heel clearance. The final rhythmic session was done with the single track program mentioned in section 7.1.1 to work on individual legs before bringing them together. Doing this seemed advantageous for P2 as this was the only session that overall speed was able to be increased reliably

above 0.25 mph. Because of the more severe level of impairment of P2, no symmetry programs were attempted.

Mounting and dismounting were challenging and while robot operators and P2 got more used to it, the process was never easy. Donning the BWS was fairly easy, though more difficult than with P1 because flexibility was more limited in P2. The body weight support was uncomfortable the first session and P2 complained of chaffing but this never occurred again in the study.

7.2.3   Participant 3 (P3)

P3 is a 58 year old female who suffered a stroke roughly 5.5 years before the study began which resulted in left side hemiparesis. The ankle is completely paralyzed, though manual muscle tests showed a decreased but existing amount of strength in the knee and hip in both extension and flexion. Her initial walking speed was 1.19 mph. She uses a functional electrical stimulation (FES) device for the left tibialis anterior and a single cane in her right hand. The FES device was excluded for all training and evaluations. The cane was allowed only for overground walking evaluations but was never used during training or for kinematic studies on the treadmill. Her left arm was also severely impaired. The hand was normally clenched and the shoulder was subluxed, which often led to pain.

Training Sessions

P3 trained for 12 sessions on the Skywalker-γ system over a period of 1 month, averaging 3 sessions per week. These were broken down into 4 rhythmic sessions (2 introductory and 2 symmetry-based routines), 4 discrete sessions and 4 balance sessions, each being trained once per week. It took one week for P3 to get acclimated to the machine. Mounting and dismounting was fairly easy, though it necessitated care and operator support getting on and off the machine. Donning the BWS was fairly easy as her flexibility was good, often taking less than a minute to done the BWS and adjust it to the proper height.

7.3 Clinical Evaluations

The following subsections are presented as a case study and outline both the clinical changes and qualitative observations by the participants. Further clinical details can be found in Appendix E.

As a baseline Hornby et al. [49] showed an average of a 16% increase in comfortable walking speed, a 14% increase in maximum walking, an increase of 1 point on the Berg balance scale and a 16 meter increase in the 6 minute walk test for chronic stroke patients after 12 training sessions with the Lokomat and greater improvements with therapist-aided rehabilitation. However, there are no robotic locomotion rehabilitation studies that test adults with cerebral palsy. Because of our mixed patient population, mixed training protocol (3 different training paradigms) and low sample size, it is inappropriate to compare this study to Hornby or others. It should also be noted that P3 (our only stroke patient) participated in multiple robotic rehabilitation programs prior to our study, which typically excludes a patient from a study because that a portion of the obtainable gains have potentially already been realized prior to the new rehabilitation program.

Clinical Measures

Because the study includes only 3 patients, 1 a stroke survivor and 2 adults born with cerebral palsy, we have chosen to use the same clinical tests for all 3 patients. The evaluation time was designed to be 2 hours in total. Table 7.6 details the target population for which each test is commonly used, as well as the test purpose and an estimated completion time. The Borg Scale and continuous heart-rate recording were used to assess the level of effort during the 6 minute walk test. Participant 1 was asked to select a comfortable treadmill walking speed both before and after the study. P2 and P3 were not asked to do so because they were less comfortable on a standard treadmill.

The joint range of motion, manual muscle Test, and the Fugl-Meyer lower extremity scale are clinical scales that rely on a therapists judgment to score qualitatively.

213

Table 7.6: Clinical Evaluation Measures

Used for:	Evaluation	Test purpose	Span (min)
CP	Joint Range of Motion	Passive and active ROM	10
CP	Manual Muscle Test	Level of strength	10
CP	Tardieu scale	Spasticity	10
Stroke	Fugl-Meyer Lower Extremity	Motor and sensory impairment	20
Stroke	Berg Balance Scale	Balance	20
Both	Foot kinematics and EMG	Biomechanics evaluation	30
Both	10 m walk test	Max / comfortable speed	10
Both	6 minute walk test w/ HR	Endurance	10
Stroke	Stroke Impact Scale	Daily Life Questionnaire	At home

The Fugl-Meyer lower extremity scale was never done in full by the therapist, omitting certain measures due to the lack of equipment, so we report only the scores from the measures tested. The full Fugl-Meyer lower extremity scale comprises 86 possible points.

In tables 7.7, 7.8 and 7.9, the normal comparison column was created in the following ways: Published literature of the 6 minute walk test shows the average distance walked in 6 minutes to be 631m for healthy participants aged 50 to 85 years [91]. Age and gender matched overground comfortable and maximum speeds can be found in [92]. Healthy self-selected treadmill speed is reported as the average of three healthy subjects (aged 19-30) walking on a standard treadmill in our lab. All other normal comparison values assume a perfect score on the remaining clinical scales as tested for this study.

7.3.1 Participant 1 Evaluation

Table 7.7 highlights P1's clinical evaluation. A more detailed evaluation summary is shown in Appendix E. P1 exhibited the greatest changes in all of the over-ground walking tests, increasing her 6 minute walk test by 67 meters (The minimal clinically important difference is 54-80 meters [93]), her comfortable walking speed by 31% and her maximum over-ground speed by 10%. She selected a 23% higher walking speed on the treadmill and was able to balance on one foot for greater than 10 seconds which increased her Berg Balance score by one point. A V3 Tardieu measurement

initially showed spasticity in right hip flexion and knee extension. Afterward, the hip flexion spasticity was found but the knee extension spasticity could not be induced as it was prior to the training. The partial Fugl-Meyer was reported to be 5 points higher due to increased passive hip flexion, ankle plantarflexion and increased scoring on proprioception movements. The stroke impact scale (SIS) increased substantially. Questions that were scored more than one point higher on the final SIS included walking without losing balance, the ability to climb several flights of stairs, carry heavy objects (bag of groceries), open a jar, tie a shoe lace and to participate in sports and outings.

Qualitative Observations

P1 reported a large change in foot scuffing and a noticeable increase in speed and stamina of everyday walking. Prior to the study, she estimated that she scuffed her foot (usually the right foot) on the ground 1-2 times within a 5 minute period of walking, causing her to stumble. After the study, she reported that she may do it once per half hour. She observed herself consciously thinking about tripping during everyday walking prior to the study. After training with the Skywalker, she no longer had to consciously alter her gait to avoid stumbles. She could walk for longer periods of time with her friends and family without needing to sit for a rest and they also noticed an increase in her speed while walking together. After the study she noted that she lost 3 pounds during the training period.

7.3.2   Participant 2 Evaluation

Table 7.8 highlights P2's clinical evaluation. The most significant change for P2 was the increase in the Berg balance scale. The Berg balance scale is comprised of 14 individual assessments, which together assign a balance score for the patient. A score between 0-20 indicates a high fall risk, 21-40 represents a medium fall risk and 41-56 represents a low fall risk. P2 increased his score dramatically from 10 to 37, scoring a perfect 4 in some of the categories that he previously scored a 0 in the initial

Table 7.7: Participant 1 Clinical Evaluation Summary

	Initial	Final	Change	% Gain	Normal
6 minute Walk test (m)	478	546	68	14	631
Borg Scale (/20)	15	18	3	20	N/A
Avg. HR during 6mwt (bpm)	145	157	12	8	N/A
10m walk test, comfortable (mph)	1.99	2.61	0.62	31	3.14
10m walk test, fast (mph)	3.36	3.69	0.33	10	5.53
Treadmill selected speed (mph)	1.3	1.6	0.3	23	2.6
Berg Balance scale	54	55	1	2	56
Tardieu Scale (Spasticity Observe)	N/A	N/A	no RK spas	N/A	N/A
Manual Muscle tests	46	48	2	4	50
Partial Fugl-Meyer	55	60	5	9	72
Passive ROM	731	796	65	9	760
Stroke Impact Scale	313	364	51	16	395

evaluation (see table E.4 in appendix E). He gained the ability to stand without the use of his hands, to stand unsupported for a full 2 minutes, to stand with his eyes closed and he was able to turn 360 degrees by himself, all of which he could not do at the initial evaluation. He walked 9 meters further in the 6 minute walk test and increased his maximum over-ground speed by 7%. There was no change in spasticity. The passive range of motion was reported to be much higher, however, lower scores were given for the manual muscle test.

Table 7.8: Participant 2 Clinical Evaluation Summary

	Initial	Final	Change	% Gain	Normal
6 minute Walk test (m)	200	209	9	5	631
Borg Scale increase	2	2	0	0	N/A
Avg. HR during 6mwt (bpm)	126	131	5	4	N/A
10m walk test, comfortable (mph)	1.12	1.12	0	0	3.1
10m walk test, fast (mph)	1.32	1.41	0.09	7	4.63
Treadmill selected speed (mph)	N/A	N/A	N/A	N/A	N/A
Berg Balance scale	10	37	27	270	56
Tardieu Scale (Spasticity Observe)	N/A	N/A	No ch.	N/A	N/A
Manual Muscle tests	64	51	-13	-20	80
Partial Fugl-Meyer	53	53	0	0	72
Passive ROM	493	663	170	34	800
Stroke Impact Scale	311	315	4	1	395

7.3.3 Participant 3 Evaluation

Table 7.9 highlights P3's clinical evaluation. Final over-ground walking tests recorded the same or slightly lower performance than prior to the training routine. The Berg Balance scale was increased due to the ability of P3 to stand on one leg. Spasticity was originally found on the Tardieu scale at the hip, knee and ankle of the paretic (left) side but was absent at the final evaluation. The manual muscle test of the paretic leg increased by 3 points, the Fugl-meyer increased by 2 and all passive joint motions were reported to be higher after training.

Qualitative Observations

In overground walking, P3 self-reported longer, more symmetric steps. She noticed an increase in stamina, telling us that she could walk a quarter mile after training, something she could not do before training with the Skywalker. One month after the study, she reported a 10 pound weight loss since the beginning of Skywalker training.

Table 7.9: Participant 3 Clinical Evaluation Summary

	Initial	Final	Change	% Gain	Normal
6 minute Walk test (m)	213	204	-9	-4	613
Borg Scale (/20)	N/A	10	N/A	N/A	N/A
Avg. HR during 6mwt (bpm)	93	91	-2	-2	N/A
10m walk test, comfortable (mph)	0.53	0.5	-0.03	-6	3.12
10m walk test, fast (mph)	0.58	0.58	0	0	4.5
Treadmill selected speed (mph)	N/A	N/A	N/A	N/A	N/A
Berg Balance scale	52	55	3	6	56
Tardieu Scale (Spasticity Observe)	N/A	N/A	no LH,LK,LA	N/A	N/A
Manual Muscle tests	22	25	3	14	50
Partial Fugl-Meyer	38	40	2	5	72
Passive ROM	225	380	155	69	450
Stroke Impact Scale	184	195	11	6	390

7.4 Kinematic Changes

In the following subsections, the participant kinematics prior to and after training will be presented as both a composite and a case study, examining each participant's

kinematics individually. This section reports highlights of sagittal plane kinematics. Appendix C contains additional plots.

Data collection

The kinematic data was collected using a 3D Guidance trakSTAR system(Ascension Technology Corporation, Milton, VT). Participants were asked to select the fastest speed at which they felt comfortable on a standard Sole F80 Treadmill. For P1, this was 1.3mph and for P2 and P3, this was 1mph. Two tests were run per subject, one that recorded hip and knee angles of the more paretic side and another that recorded 3 dimensional position data of the toe and heel on each foot.

Data was recorded at 60Hz. The hip and knee data analyzed here was taken from the patient-selected more affected leg (right for P1, left for P2 and P3) by attaching two magnetic sensors to the thigh and shin respectively as seen in figure 7-19. Equations 7.5 and 7.6 were used to then determine hip and knee angles at each data collection time assuming a right handed coordinate system originating at the hip. In the interest of following [6], these equations represent hip flexion as positive and knee flexion as negative. The zero position was not recorded for these studies so the plots were zero'd by video inspection.

$$\theta_h = \arctan(\frac{x_2 - x_1}{y_2 - y_1}) \tag{7.5}$$

$$\theta_k = \arctan(\frac{x_4 - x_3}{y_4 - y_3}) - \theta_h \tag{7.6}$$

Much of the data analysis relies on estimating heel-strike and toe-off events. In an effort to stay consistent with the Skywalker system, which can only monitor heel position, all foot position data was based on heel positions including the toe-off event. Heel data estimated toe-off 2% before the toe data in one subject (valleys in figure 7-20).
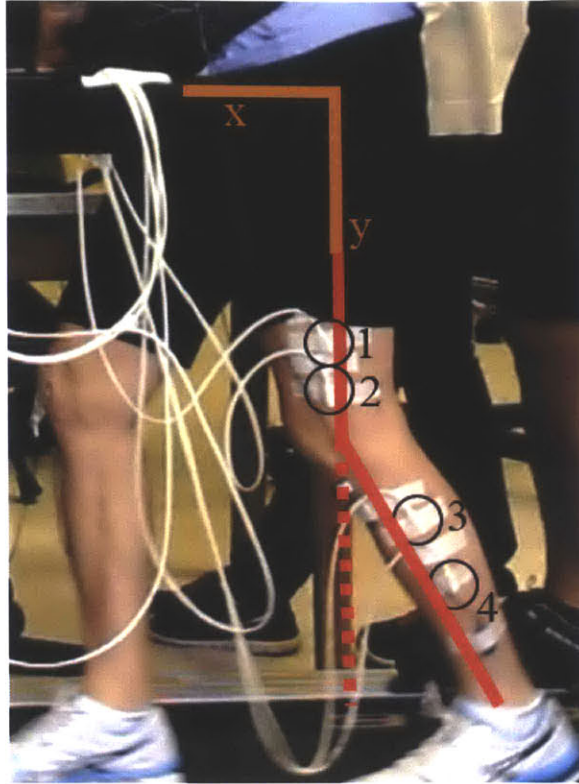
Figure 7-19: Coordinate system definition and marker definition
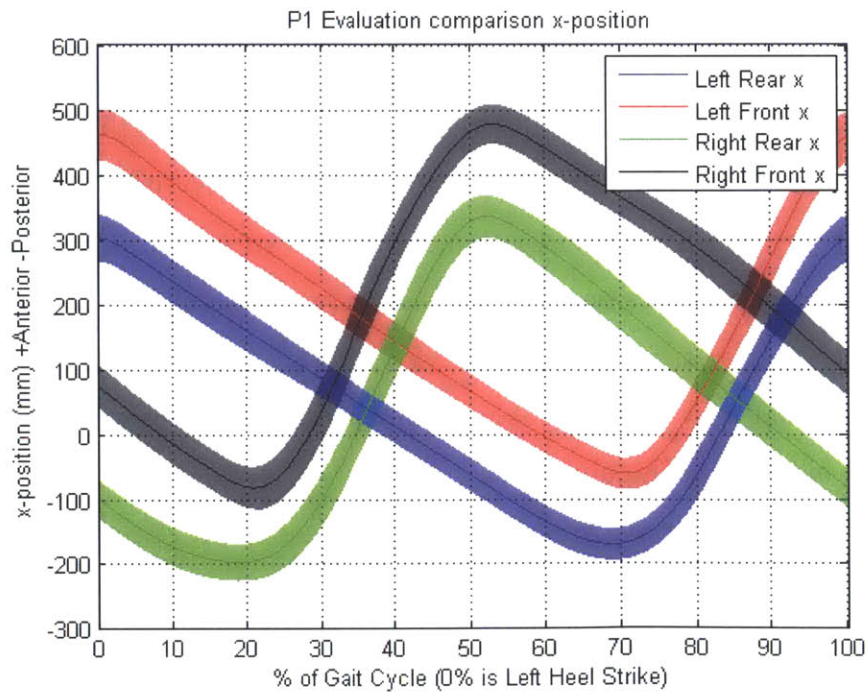
Figure 7-20: x-position heel (rear x) and toe (front x) trajectories, center line is the mean, band represents 1 standard deviation each direction, data cut at left heel strike

Statistical analysis

Statistical tests were run on key measures as can be seen in tables 7.10,7.11 and 7.12.

Data for the step length, step length asymmetry, average time per stride and joint angle ROM (15 cycles) passed the Jarque-Bera test and thus a paired t-test was used to asses statistical significance. An α of 0.05 was used to test for significance.

Standard deviation data did not pass the Jarque-Bera test and was skew in some cases (see appendix D, figure D-6), thus the two tailed sign test (which compares the medians of the samples without assuming a normal distribution) was used to assess the statistical significance.

7.4.1 Aggregate Data Analysis

Here we present the generalizable results seen across the three participants before assessing the individual cases.

Training varied significantly between participants due mainly to the level of impairment of each participant, and thus the results we saw from each patient varied. For instance, P1's initial proficiency in walking allowed us to increase the number of sessions and to experiment with different methods of step-length (SL) symmetry correction. P1 underwent 5 sessions of different SL symmetry programs to test her ability to improve her SL asymmetries (more on this in section 8.3.1). P1's kinematic evaluation was the only one to show a statistically significant decrease in step length asymmetry after training (see table 7.10). P3 underwent only 2 symmetry training sessions and we were never able to implement these programs for P2 due to the severity of his walking impairment.

Double stance asymmetry increased for P1, decreased for P2 and reversed in P3 (Initially greater left ahead of the right foot time, inverse relationship afterward). Stride length increased for P1 and P3 but decreased for P2. Double stance times followed the stride length (greater stride length, greater double stance time) because swing time (single stance time) was approximately the same before and after for all participants. The only measure that consistently changed for all participants after

the study was the x-position (fore-aft position) and paretic joint angle cycle variance of gait over 15 gait cycles.

7.4.2   Cycle variance

Studying the kinematics on a treadmill must be done carefully and it is sometimes cloudy to understand if a change is a sign of recovery. Double stance time is used in overground walking [94] but, as mentioned, we learned here that double stance time for our patients was a consequence of changing stride length on a treadmill.

Variability of stride-to-stride gait timing has been shown to be exaggerated in patients with Parkinson's and Huntington's disease in overground walking [95], however, there is no evidence that the reduction in stride-to-stride variation corresponds to gait recovery for stroke or cerebral palsy patients on a treadmill. In fact, in our study, the participant that improved gait speed by 30% (P1 table 7.10) showed an increase in the variance of stride-to-stride timing.

Treadmill assessments are convenient because they require less space and equipment than overground assessments. However, the treadmill induces a constant speed constraint on subjects, thus altering normal gait and potentially hiding changes seen in overground walking. Identifying a measure on a treadmill that corresponds to gait recovery would simplify evaluations.

As mentioned, the one consistent result we saw in our patients after training was a decrease in the x-position and paretic joint angle cycle variance. Every participant decreased their x-position cycle variance on both legs (3 of 6 measures significant) and their cycle variance on both the hip and knee joints of the most paretic leg (6 of 6 measures significant). This can be seen in the bottom four rows of tables 7.10,7.11 and 7.12. The average standard deviation never increased after training. Notice that the healthy comparison (last column on tables 7.10,7.11 and 7.12) showed substantially lower standard deviation in x-position, hip angle and knee angle.

Thus, we can propose a hypothesis for further testing. If all impaired patients started with a higher cycle variance, decreased the variance after training in the direction of a healthy variance, logic would contend that cycle variance is correlated

to walking proficiency if we make the assumption that each participant's walking proficiency improved after training.

Data processing of cycle variance

15 walking cycles are cut at heel strike (the maximum x-position) of the side being studied. Each cycle comprises roughly 80-100 data points. These points are spread out or condensed into the average number of points of the 15 gait cycles using the interp1 function in Matlab. Each cycle location now has 15 points at each gait cycle position and can be analyzed for the mean and standard deviation. Figure 7-21 shows a zoomed cartoon of this process. The mean and standard deviation of each cycle location can be plotted and compared (figure 7-20 shows the mean x-position of the foot, represented by the solid line and one standard deviation, represented by the shaded region). The mean of the 80-100 standard deviation points is shown in tables 7.10,7.11 and 7.12 and the median value is tested by the sign test to assign a p-value.

The shapes of the standard deviation over the cycle locations can be seen in appendix D. In most cases, the variance is highest during swing, especially of the contralateral side on which the data was cut. This is the reason that the data must be cut for each leg individually.

Cyclograms

Cyclograms were generated for all participants to analyze the relationship between hip and knee angle. Figure 7-22 was taken from [6] and illustrates how to read the cyclogram figure. Each participant's cyclogram will be discussed in the case study sections that follow.

7.4.3   Data Reporting

Kinematic data is reporting in the following sections. It should be noted that all parameters reported with a p-value were done by studying 15 gait cycles individually. The % of gait cycle measurements (such as % in single stance - Right, etc.) are
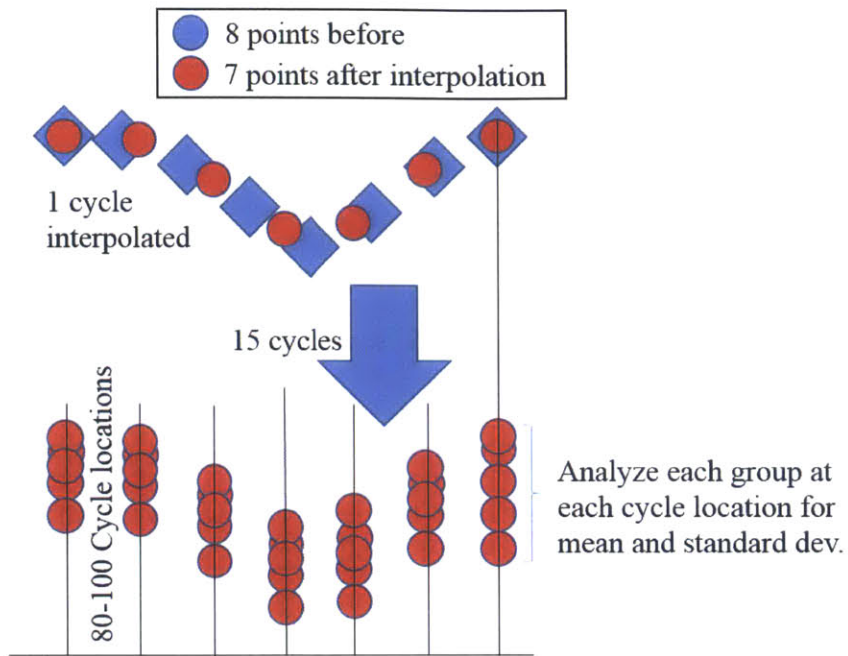
Figure 7-21: Cycle variance data processing
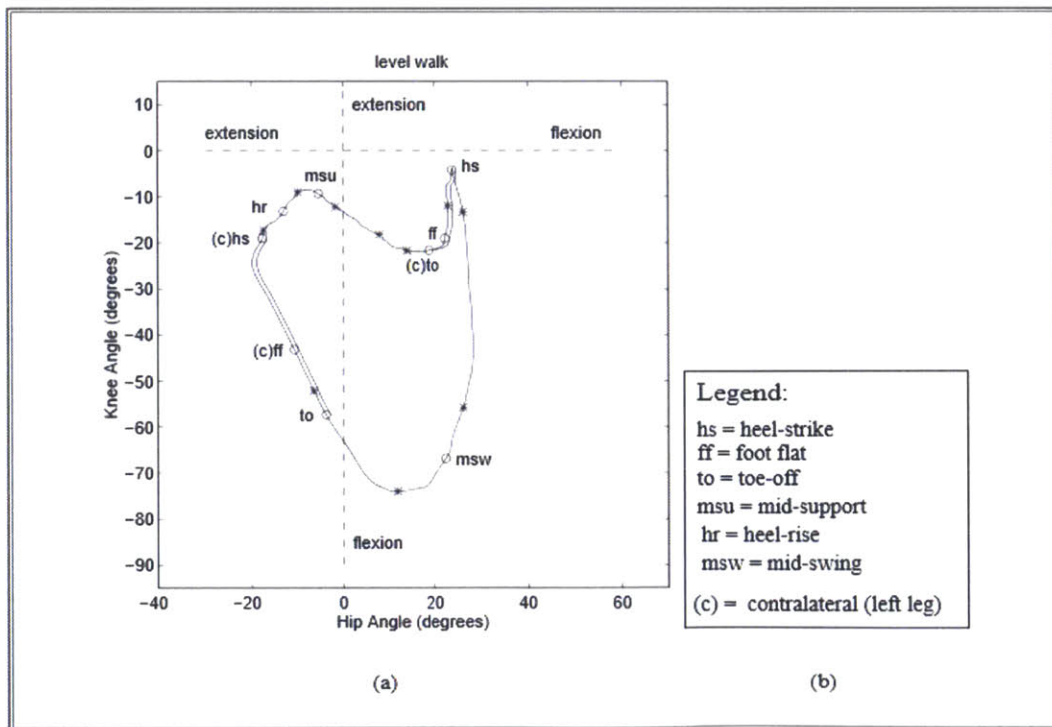
Figure 7-22: Guide on analyzing cyclograms, overground walking, taken from [6]

calculated based on the means of the ensemble method as described in figure 7-21, which precludes statistical significance testing.

7.4.4   Participant 1 Kinematic Data

Table 7.10 depicts the full summary of the sagittal plane kinematics for study participant 1. Statistically significant parameters ($p < 0.05$) include an increase in the left step length, a decreased step length asymmetry, an increased right hip range of motion (ROM) with a decreased right knee ROM. Each cycle variance (standard deviation) decreased though only the joint angles were significant via the sign test. The double stance asymmetry increased by 6%. The cyclogram (figure 7-23) shape moved closer to the healthy shape, especially on the left half, which corresponds to a greater hip angle before the onset of a more rapid knee bend.

Table 7.10: Participant 1 Kinematic parameters over 15 strides

	Initial mean	Final mean	% change	p-val	Healthy
Left SL (mm)	485.40	514.81	6	0.002	574.02
Right SL (mm)	542.19	526.44	-3	0.040	617.20
Stride Length (mm)	1027.59	1041.25	0	N/A	1191.23
Step Length Asymmetry (%)	-11	-2	-82	0.000	-7
% Total Time Double Stance (%)	36	36	1	N/A	38
% L Ahead of R Double Stance (%)	20	20	4	N/A	20
% R Ahead of L Double Stance (%)	16	16	-2	N/A	19
% Double Stance Asymmetry (%)	19	25	29	N/A	5
% in single stance - Left (%)	32	33	3	N/A	31
% in single stance - Right (%)	32	31	-3	N/A	30
Average time per cycle (s)	1.46	1.50	3	0.09	1.71
Standard deviation cycle time (s)	0.030	0.050	73	N/A	0.020
Right Hip ROM (deg)	34.93	38.28	10	0.000	28.28
Right Knee ROM (deg)	32.46	29.18	-10	0.000	55.83
Right Hip avg. std dev (deg)	1.58	1.51	-4	0.047	1.09
Right Knee avg. std dev (deg)	2.40	1.46	-39	0.000	2.23
Left x avg. std dev (mm)	27.14	23.46	-14	0.000	22.93
Right x avg. std dev (mm)	26.52	30.80	16	0.053	21.16
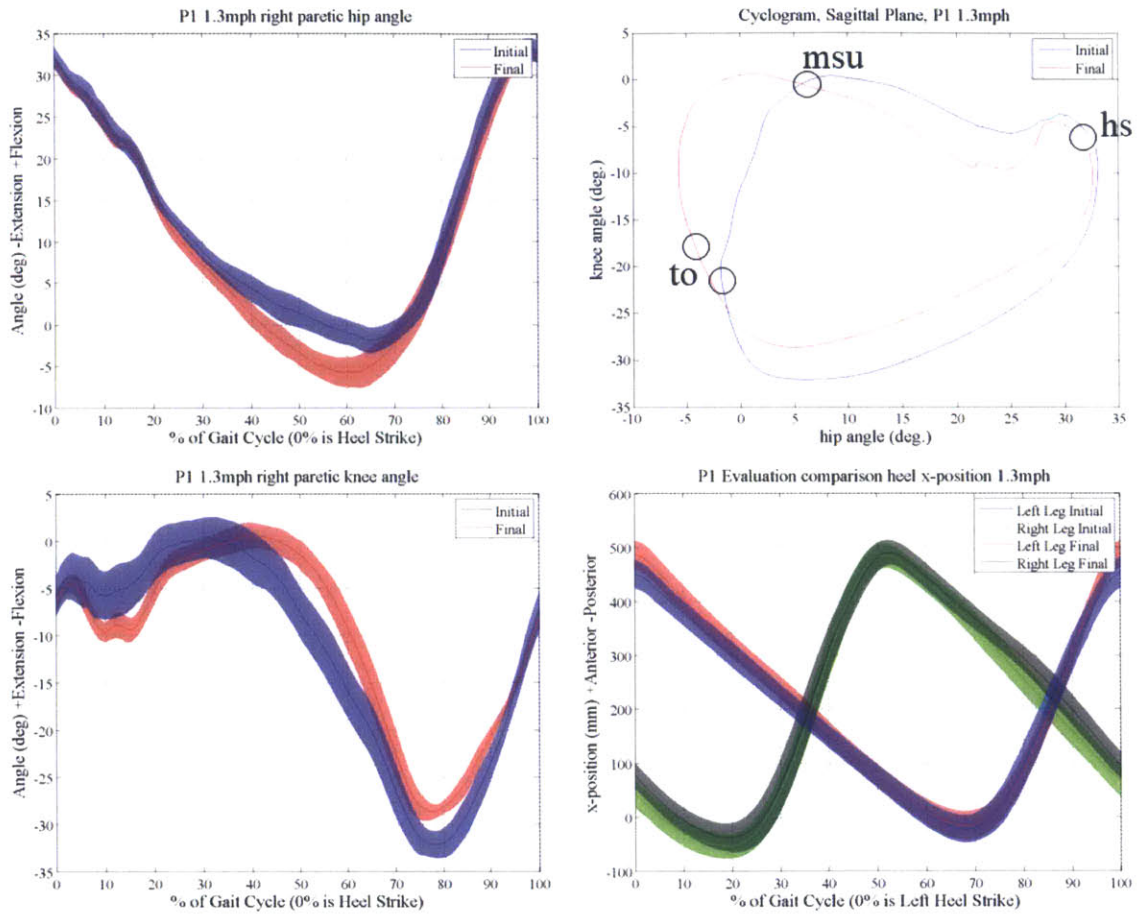
Figure 7-23: Participant 1 kinematic summary. Solid lines represent the average over 15 cycles. The shaded region represents +/- 1 standard deviation.

| Initial Evaluation | Final Evaluation |
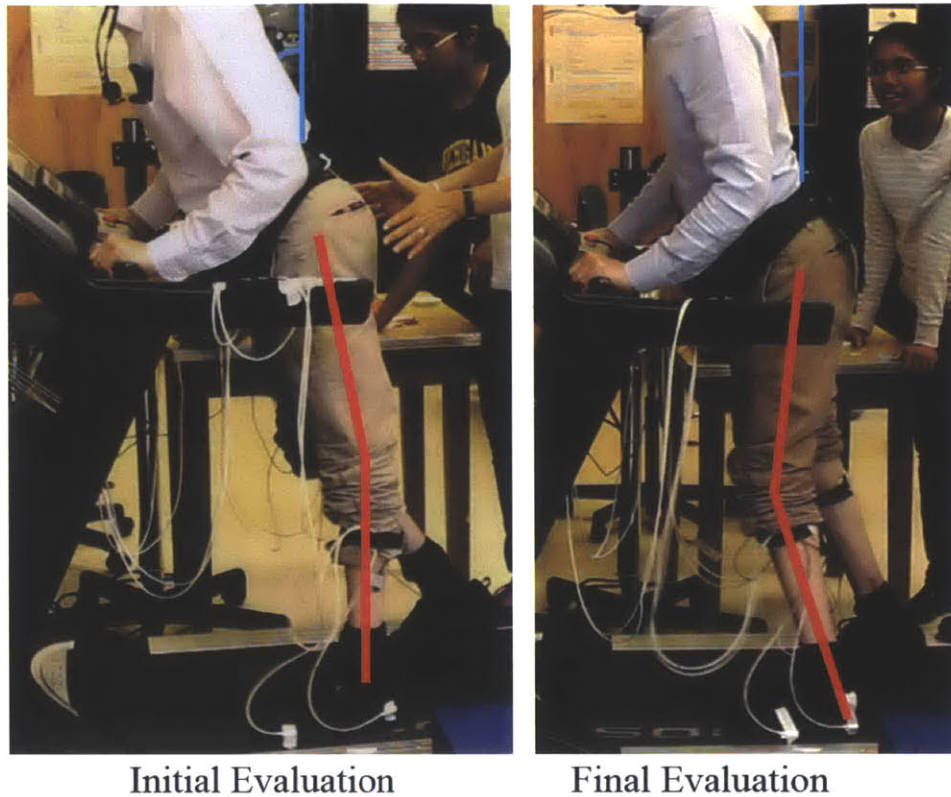
Figure 7-24: Participant 2 mid-stance in the pre-training and post-training treadmill evaluation

7.4.5 Participant 2 Kinematic Data

Table 7.11 shows the full summary of the sagittal plane kinematics for participant 2. A decrease in both left and right step length, hip angle and knee angle were statistically significant but step length asymmetry was not. From video observation (figure 7-24) P2 is leaning forward less on the final evaluation (18 degrees final vs. 24 degrees initial) and the knees no longer hyperextend in mid stance. This could be the reason for the shorter steps. The standard deviations of 3 of the four analyzed motion profiles showed significant decreases. The cyclogram appears quite abnormal (figure 7-25). Notice here that the knee is bent at heel-strike and extended on toe-off, a consequence of leaning far forward. Figure 7-26, shows P2 in left heel-strike and toe-off.

226
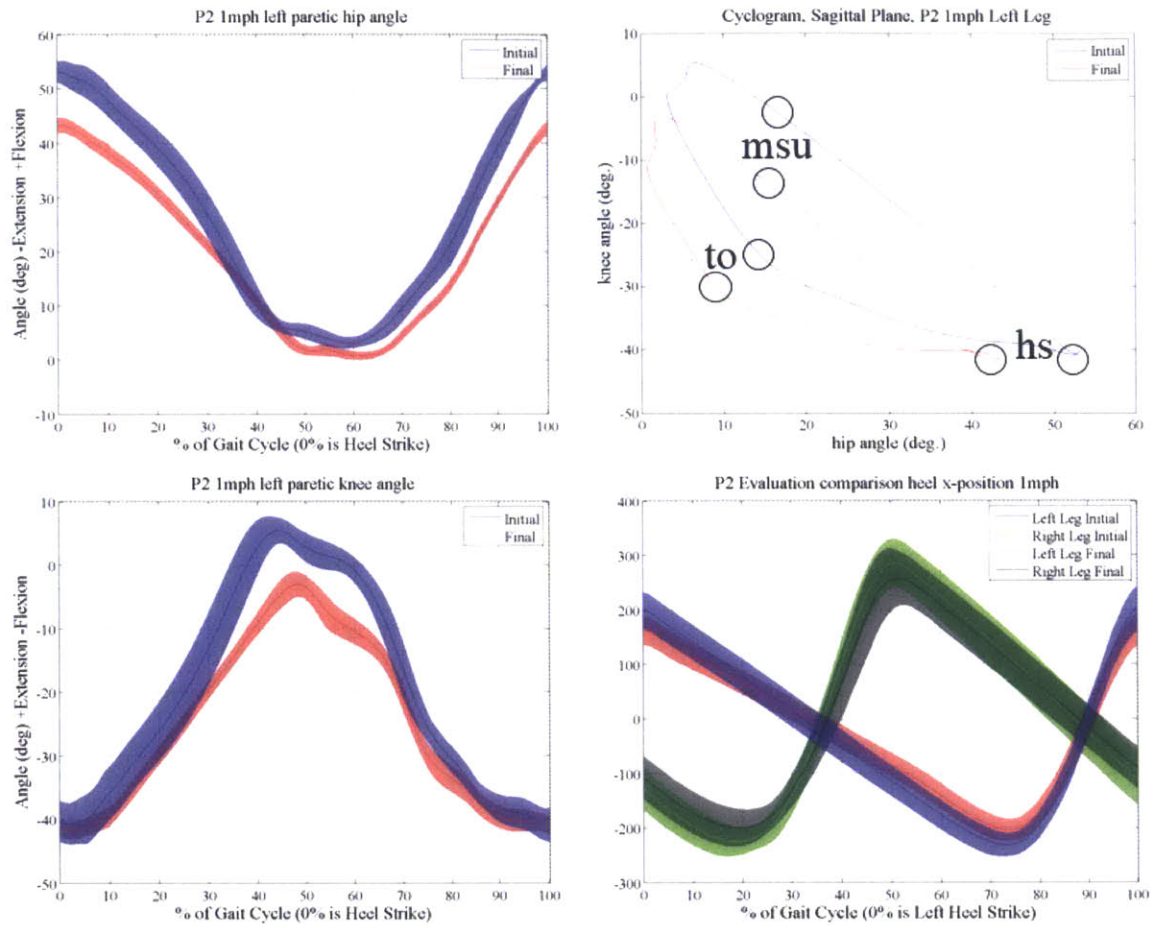
Figure 7-25: Participant 2 kinematic summary. Solid lines represent the average over 15 cycles. The shaded region represents +/- 1 standard deviation.

Left Toe-Off   Left Heel-Strike
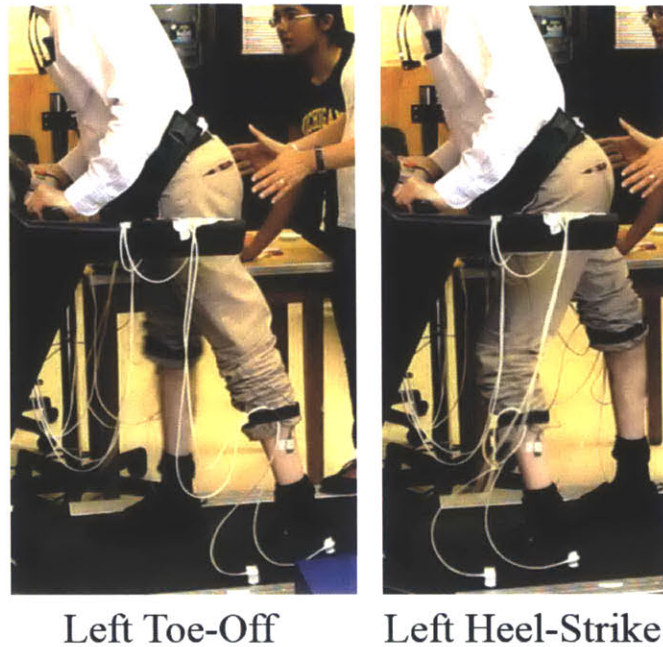
Figure 7-26: Participant 2 toe-off and heel-strike

7.4.6 Participant 3 Kinematic Data

Table 7.12 shows the full summary of the sagittal plane kinematics for participant 3. An increase in both step lengths were statistically significant over 15 strides but no changes in step length symmetry were observed. The percentage of time spent with the left leg ahead of the right in double stance decreased and the time spent with the right in front of the left increased, flipping the double stance asymmetry after training. The cycle standard deviation was significantly decreased in all four measures examined. The cyclograms unusual shape is not noticeably changed (figure 7-27) but the knee angle has become sharper, similar to what was observed with P1. The oscillatory appearance comes from a knee joint that seemed to bounce during stance. The left (paretic) knee has a low range of motion during walking (14 degrees vs. a healthy 56 degrees). If the ROM was higher, the bounce may not be as apparent.

The left x-y foot trajectory in the sagittal plane had a marked change as can be seen in figure 7-28. Notice that dramatic change at heal-strike (hs). At the initial evaluation, the rounded trajectory resulted from vaulting the foot forward during swing and hanging the foot in the air before lowering it to the treadmill. The final
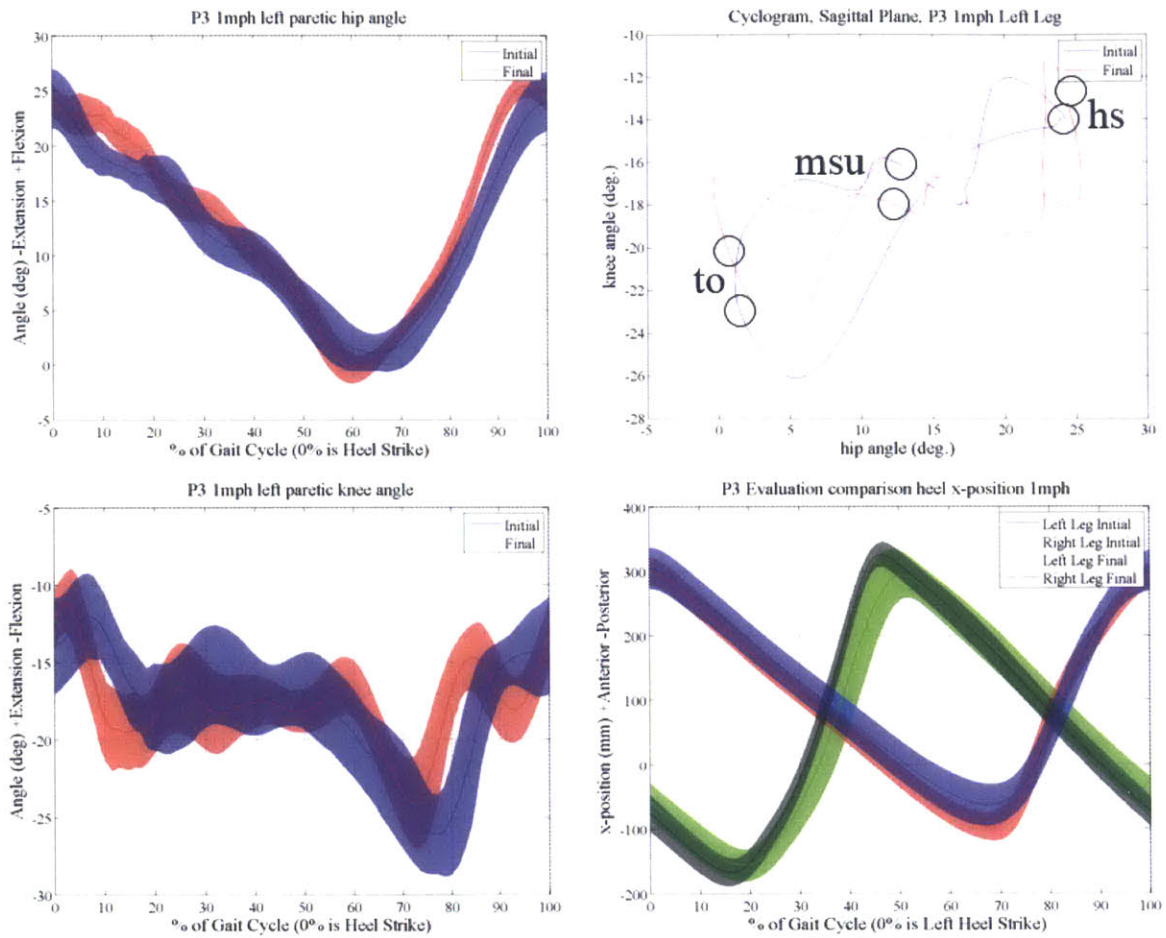
Figure 7-27: Participant 3 kinematic summary. Solid lines represent the average over 15 cycles. The shaded region represents +/- 1 standard deviation.

Table 7.11: Participant 2 Kinematic parameters over 15 strides

	Initial mean	Final mean	% change	P-val	Healthy
Left SL (mm)	456.28	388.35	-15	0.000	521.99
Right SL (mm)	547.64	461.98	-16	0.000	575.80
Stride Length (mm)	1003.92	850.33	-15	N/A	1097.80
Step Length Asymmetry (%)	-18	-17	-3	0.769	-10
% Total Time Double Stance (%)	42	44	5	N/A	43
% L Ahead of R Double Stance (%)	19	21	7	N/A	21
% R Ahead of L Double Stance (%)	22	23	3	N/A	21
% Double Stance Asymmetry (%)	-15	-11	-24	N/A	00
% in single stance - Left (%)	32	31	-3	N/A	30
% in single stance - Right (%)	27	26	-4	N/A	28
Average time per cycle (s)	1.64	1.38	-16	0.000	1.87
Standard deviation cycle time (s)	0.06	0.04	-33	N/A	0.02
Left Hip ROM (deg)	49.82	42.52	-15	0.000	28.15
Left Knee ROM (deg)	46.16	38.67	-16	0.000	56.22
Left Hip avg. std dev (deg)	2.75	1.18	-57	0.000	0.90
Left Knee avg. std dev (deg)	3.39	1.77	-48	0.000	1.70
Left x avg. std dev (mm)	29.58	24.16	-18	0.000	15.80
Right x avg. std dev (mm)	46.18	43.00	-7	0.002	14.19

evaluation showed a more healthy shape (see appendix C) in which the participant guides the foot to the treadmill. Notice also that the initial trajectory ends and begins (hs) with the heel above the surface of the treadmill. This tells us that the toe is hitting the ground first. The final evaluation shows heel strike at the ground level, meaning that the foot is striking the treadmill with the heel.

7.4.7 Healthy Kinematic Data

Figure 7-29 provides a speed comparison of a 6'0" tall, 185 pound male to show healthy kinematics. Notice that the cyclogram differs slightly from figure 7-22 due to the absence of the double dip in the knee data. This was likely due to a treadmill speed that was much slower than the healthy subject's preferred walking speed. Tables 7.10,7.11 and 7.12 show the healthy comparison data in the far right column.
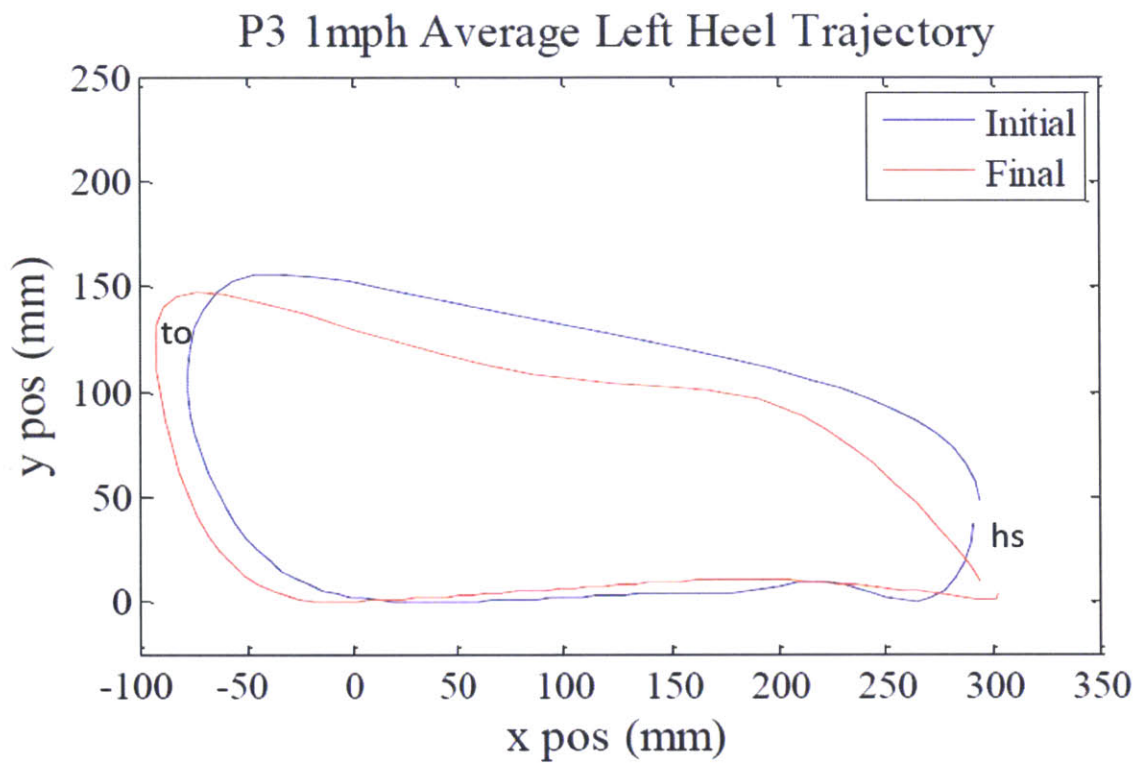
Figure 7-28: Participant 3 left heel trajectory during the treadmill evaluation before and after Skywalker training
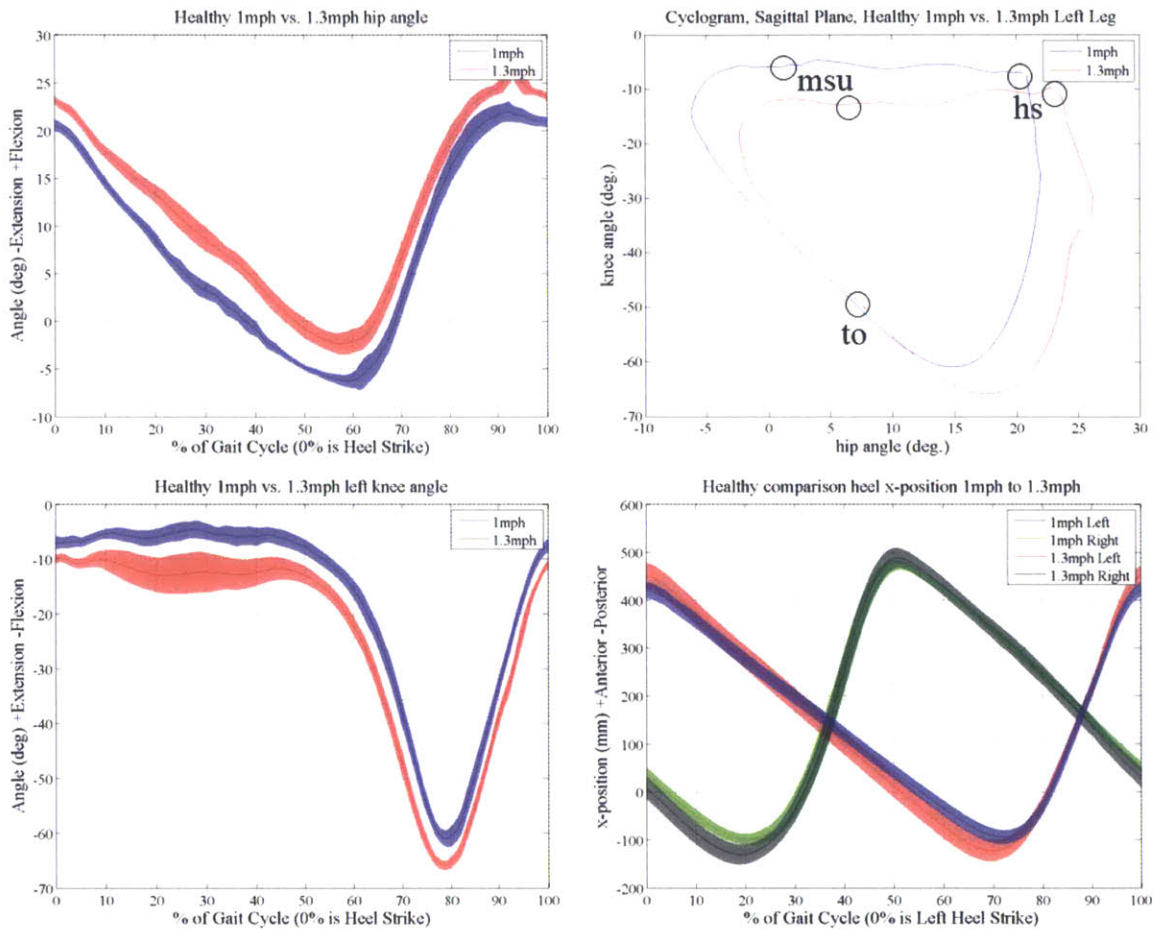
Figure 7-29: Healthy kinematic summary. Solid lines represent the average over 15 cycles. The shaded region represents +/- 1 standard deviation.

Table 7.12: Participant 3 Kinematic parameters over 15 strides

	Initial mean	Final mean	% change	P-val	Healthy
Left SL (mm)	389.82	394.64	1	0.637	521.99
Right SL (mm)	483.01	491.25	2	0.370	575.80
Stride Length (mm)	872.83	885.89	1	N/A	1097.80
Step Length Asymmetry (%)	-21	-22	2	0.855	-10
% Total Time Double Stance (%)	36	38	6	N/A	43
% L Ahead of R Double Stance (%)	20	17	-14	N/A	21
% R Ahead of L Double Stance (%)	16	21	29	N/A	21
% Double Stance Asymmetry (%)	18	-22	-222	N/A	00
% in single stance - Left (%)	31	30	-3	N/A	30
% in single stance - Right (%)	32	32	0	N/A	28
Average time per cycle (s)	1.52	1.57	3	0.123	1.87
Standard deviation cycle time (s)	0.090	0.050	-41	N/A	0.020
Left Hip ROM (deg)	23.19	25.76	11	0.593	28.150
Left Knee ROM (deg)	14.11	12.93	-8	0.028	56.220
Left Hip avg. std dev (deg)	2.21	1.50	-32	0.000	0.900
Left Knee avg. std dev (deg)	2.86	2.29	-20	0.000	1.700
Left x avg. std dev (mm)	29.18	23.66	-19	0.000	15.80
Right x avg. std dev (mm)	32.21	25.7	-20	0.000	14.19

7.5 EMG changes

During the treadmill evaluation study, we recorded electrical activity of the muscles via electromyography (EMG) signals of the soleus and the tibialis anterior (TA) of each leg. Data was recorded using surface electrodes of the Delsys Myomonitor IV EMG system at 1,000 Hz. Raw data was forward-backward (zero-phase) band-pass filtered (20-500 Hz) using a second order Butterworth filter. It was then rectified and low passed filtered with a 5Hz forward-backward 4th order Butterworth filter. Finally, the data was normalized by the maximum filtered EMG signal during the walking trial. The data was ensemble averaged based on synchronized kinematic data from the 3D Guidance trakSTAR system via a digital signal sent from the EMG system at the onset of recording. The EMG ensemble data includes 15 cycles to be consistent with the kinematic data.

7.5.1 Healthy EMG

For comparison purposes, figure 7-30 shows the normalized EMG signals of the TA and soleus of both legs. The right and left leg data are cut from the ipsilateral heel strike. All EMG plots show the mean as the solid line and the shaded region indicates one standard deviation above and below the mean.

We will study the timing of EMG onset and peaks. It is important to note that the electromechanical delay (EMD) between EMG activity and muscle force has been estimated to be between 30-100ms, meaning that the EMG signals foreshadow a muscle contraction [96].

The healthy TA activity has two peaks. The larger peak has an onset at about 10% (170ms) before toe-off and a maximum at approximately 7% (120 ms) after the toe-off position, to lift the toe during swing. The smaller peak has an onset at approximately 8% (137ms) before heel strike and a maximum at approximately 5% (85ms) after heel-strike to control the foot drop after heel-strike.

The soleus data for our healthy comparison had more variance and shows two peaks that seem to be blended, the onset beginning at heal strike and the maximums occurring at about 25% and 45-50% of the gait cycle which corresponds to 45% and 20-25% (770ms and 342-428ms) before toe-off . These signals indicate ankle propulsion. There is low soleus EMG activity during the swing phase.

7.5.2 P1 EMG

P1's TA EMG resembles the healthy comparison, with the appearance of a large peak occurring after toe-off and some activity directly after heel-strike. The small peak seems to occur later than the healthy's small peak (25% (375ms) on left final 10% (150 ms) on right final evaluation). The left TA's small peak is moving towards the healthy timing after training and the right small peak seems to have become more distinct. The onset of the large peak occurs slightly earlier on the final evaluation for both the right and left leg. Notice that the final evaluation cycle time is 40ms longer than the initial cycle time. The onset of the left TA is approximately 285 ms before
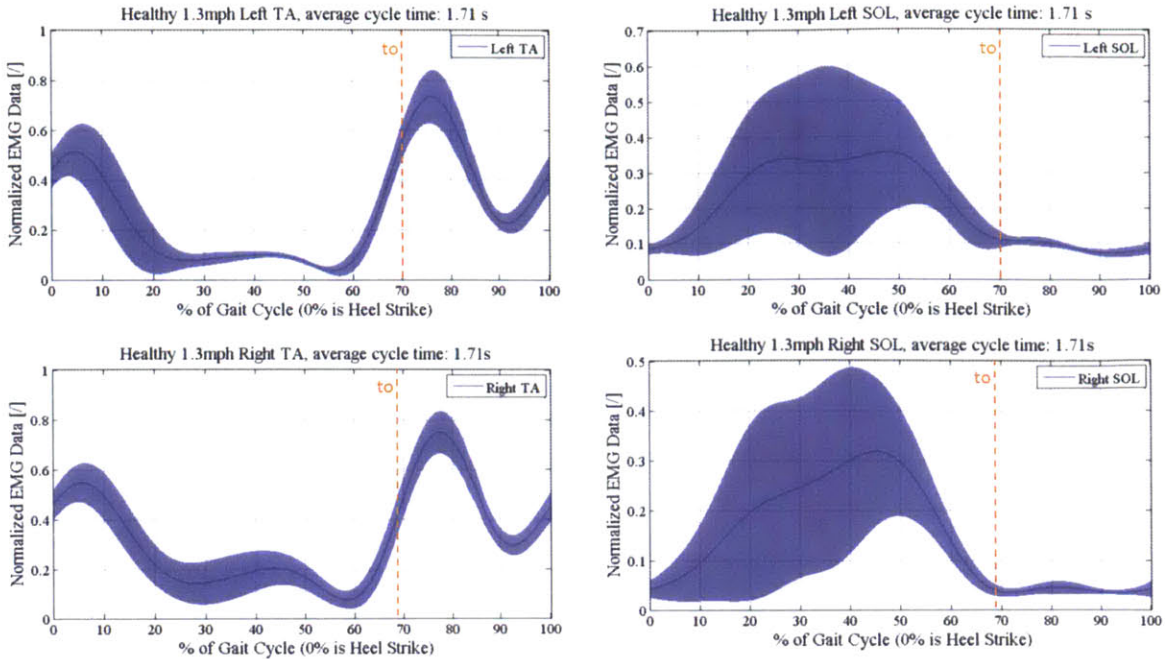
Figure 7-30: Healthy comparison EMG during treadmill walking

toe-off on the final evaluation and 262 ms before toe-off on the initial evaluation. The peak of the TA is also earlier than the final, indicating an earlier toe-up during swing. P1 mentioned that she no longer scuffed her feet, this could be the reason. The right TA has the same phenomenon. It should be mentioned that the right final toe-off is about 1% earlier than the left. Toe-off timing is indistinguishable for the left foot.

P1's soleus maintains a double peak shape as seen on the healthy comparison. The left large peak has moved to an earlier position post training. One observed difference from the healthy comparison is the onset of the soleus before heel strike, which occurs on both sides.

7.5.3 P2 EMG

P2's walking patterns were highly abnormal. On the initial evaluation, he took significantly larger steps than on the final. The initial TA activity on both sides was highest just after toe-off, similar to the healthy subject, however, this patterned changed on the final evaluation. The final TA pattern hardly resembled healthy. There was a small TA peak on the right that resembled the small peak for the healthy subject,
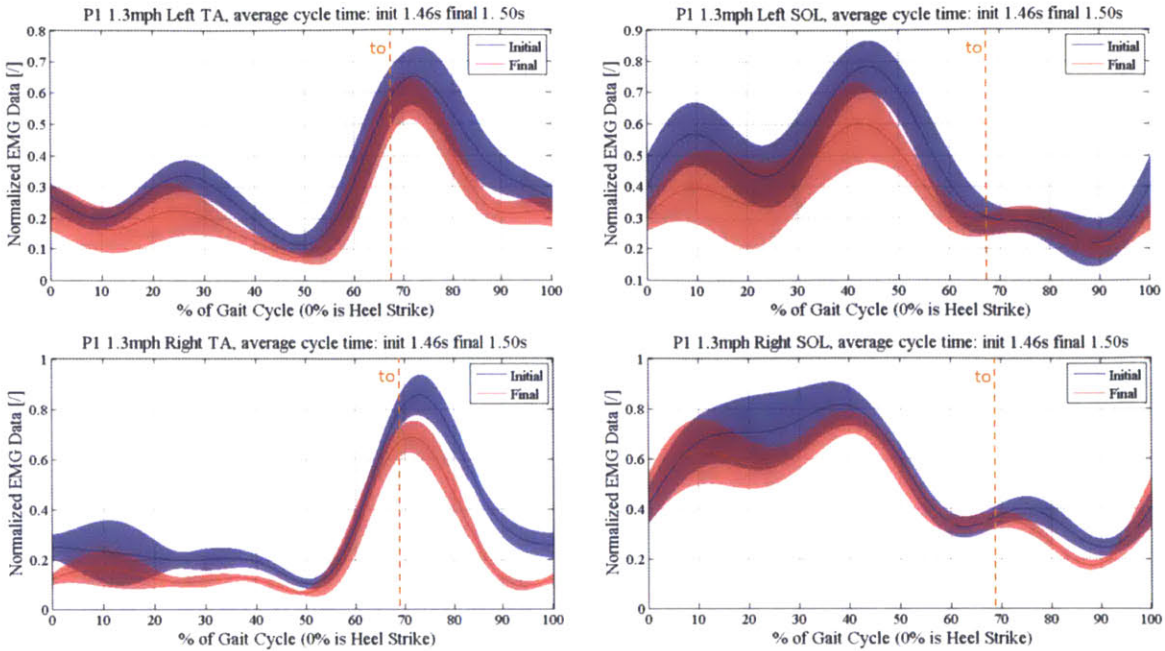
Figure 7-31: P1 EMG during treadmill walking before and after training

but the TA activity was relatively flat.

The left soleus exhibited three peaks, one of which was located in the swing phase. The right soleus seemed a bit more normal, showing peaks in the stance phase and relaxation in the swing phase. It should be mentioned that P2 trained with AFOs on the Skywalker, which likely limited the involvement of his ankle muscles during training.

7.5.4 P3 EMG

P3 was a stroke patient with left hemiparesis. On the left side, she could not consciously move her ankle and no EMG could be elicited prior to walking on the treadmill. Nevertheless, while walking, EMG signals were visible on the Delsys software. A point of interest here is that the EMG on the right (unimpaired side) differed from the healthy subject. The TA peak happened before toe-off and was much more active during the whole stance phase. During swing, the right TA was not active. The impaired TA showed a near-healthy shape prior to training, exhibiting a large peak directly following toe-off. After training, the left TA had a peak at about mid-stance

236
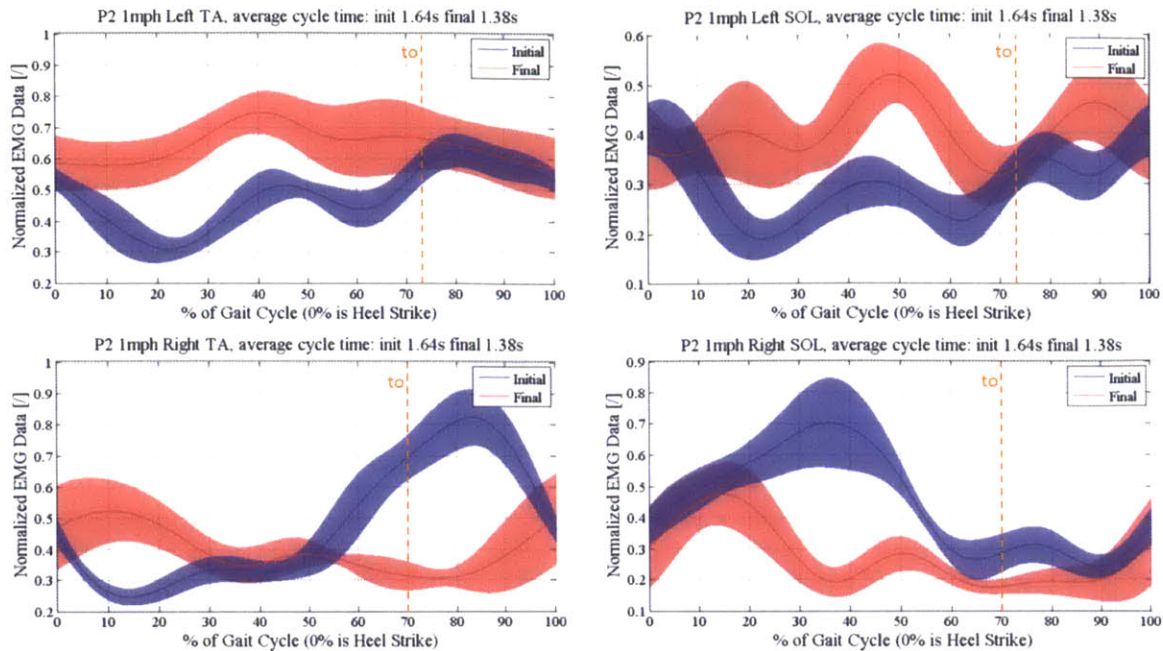
Figure 7-32: P2 EMG during treadmill walking before and after training

and was absent during swing in most cases, indicating that the participant was relying on her hip and knee.

The soleus profile on both sides showed three peaks. On the left side, the highest peak moved towards a more normal location, closer to toe-off on the final evaluation. The peak on the right side is closer to toe-off than the healthy comparison, indicating maximum muscle contraction very near the point at which the toe comes off the ground.

The differing muscle patterns between the non-paretic side and the healthy comparison likely indicate compensatory movements due to the impairment on the left side of the body.
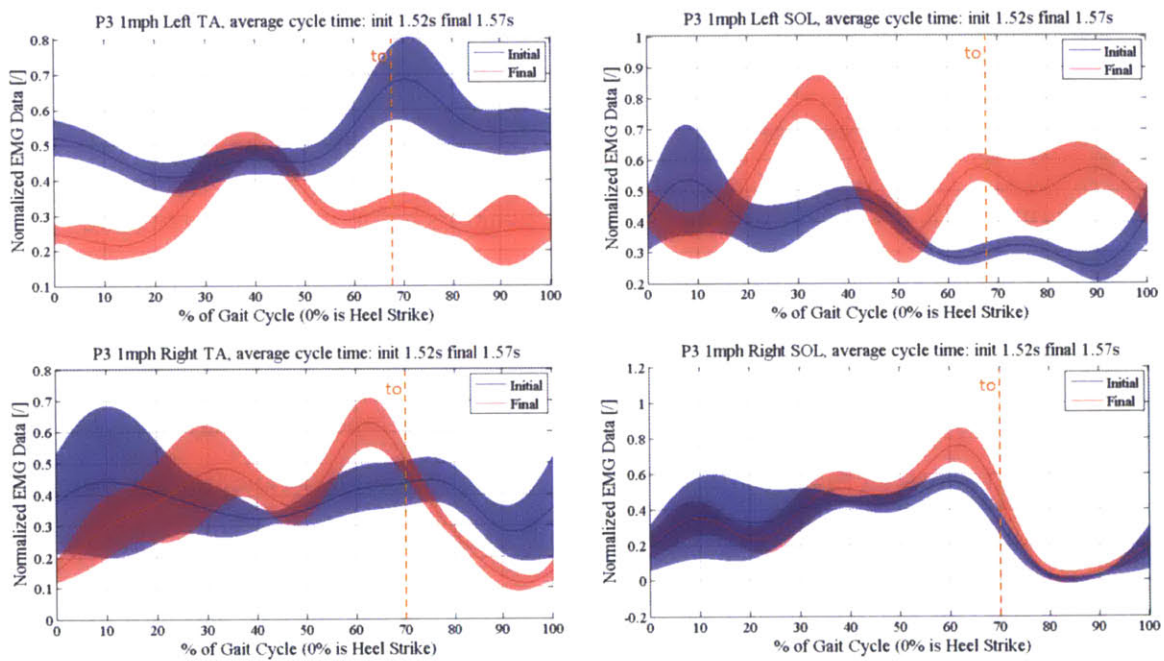
Figure 7-33: P3 EMG during treadmill walking before and after training

Chapter 8

Conclusions, Discussion and Future Work

8.1 Conclusion

The Skywalker-γ system shows promise as a rehabilitation system. We have shown that it can be operated safely with patients affected by neurological injuries and have observed meaningful gait changes. During the study, each of the participants made gains in mobility and each participant's individual improvement was unique. This bodes well for the Skywalker system, being a flexible solution for the vast spectrum of neurological gait disorders. The distinctive nature of this machine as compared with existing robotic gait rehabilitation systems is in its ability to foster self-directed movement without prescribing motion. This is achieved by (1) a mechanical design that lacks a rigid connection to the legs or foot of the patient and (2) programming that relies on human-in-the-loop control via the vision system. No other robotic or manual method of walking therapy allows the same freedom patients will experience on the Skywalker system.

P1 was fast and on the high functioning end of the cerebral palsy gait spectrum. Skywalker was able to train her to be faster, enabling her to train for faster gait with the rhythmic program. The discrete program was reported to be her most challenging program and may have been the program that improved foot scuffing during walking,

allowing her to practice individual steps.

P2 was on the low functioning side of the cerebral palsy community ambulator scale. If there was greater impairment, it would be unlikely that he would be walking alone in the community. For P2, we were able to modify the original protocol, using the frontal plane perturbations to train balance without the added difficulty of walking while they were being applied. We were able to start to train rhythmicity by focusing on a single leg, though we only did this on the fourth session. The discrete program trained P2 to stand more upright while taking individual steps at his own pace.

P3 was our only stroke patient, displaying many of the stereotypic pathological gait characteristics such as drop foot, hip hiking and a bit of circumduction. The drops within the rhythmic program allowed her gait to become rhythmic once again, eliciting the feeling of healthy walking that she had not felt in 5 years. The discrete program let her practice individual steps which may have improved her sagittal plane x-y trajectory afterward.

8.2 Future work

The work described in this thesis outlines a system with great potential but also opens up many questions regarding the mechanism responsible for the gait alterations and the optimal way to train. This study was a feasibility test to ascertain the practicality of using the Skywalker in its three primary modes (rhythmic, discrete and balance) with neurologically impaired individuals and thus was not fit to scientifically test the efficacy of any one program on any one outcome measure. We felt that it was necessary to set forth a set of experiments and future directions from which the machine and rehabilitation programs could be better understood. Section 8.3 will detail efforts to correct step-length assymmetry and compare the method of training to other published work. Section 8.4 will explore the effect of training on rhythmic walking cycle variance and compare it to existing literature. Finally, section 8.5 will offer brief recommendations for the next revision of this machine.

8.3 Step-Length Symmetry

Step-length symmetry was significantly improved for P1 (defined by equation 8.1 where LSL and RSL represent the left and right step length respectively). P1 trained for 16 sessions, 9 of which were rhythmic training. 6 of these were designed to specifically target step-length asymmetry. Each of the 6 symmetry programs was unique in structure, which proved the feasibility of creating and implementing each program with a patient but made it impossible for us to make concrete assessments on the long-term effects of training with each program for multiple sessions. For this, a well-designed pilot study is needed. However, we can look to the data to suggest which of the programs provided immediate symmetry adjustments via the pre-post diagnostic programs run at each training session. Additionally, data was continuously collected during training, allowing us to observe right and left step lengths during the training period.

$$SLasm = \frac{2 * (LSL - RSL)}{LSL + RSL} \tag{8.1}$$

As previously stated, specific programs were built to targeted step-length symmetry but we will examine the pre-post diagnostics of all training programs. Figure 8-1 shows the step-length asymmetry of the gait before and after training. Programs are coded as such: R = Rhythmic, D = Discrete, B = Balance. The digit that follows is the number of each session in chronological order. B2 was omitted from this chart because the diagnostic data became corrupt. Statistically significant changes in step length symmetries occurred in R2, R4, D3, R6, and R9. R2 and R6 implemented asymmetric treadmill speeds and R2 was a rhythmic speed training program and R9 combined the two strategies. The first set of bars in figure 8-1 represents the evaluation done on a standard treadmill before and after the month long training program. Notice that P1 began the study with -11% asymmetry score which indicates a longer right step-length. By the time that the first asymmetry program was run (R3) the symmetry had already flipped (to a longer left step-length) while walking on the Sky-walker system. This (longer left step) type of symmetry was present at the initial

241
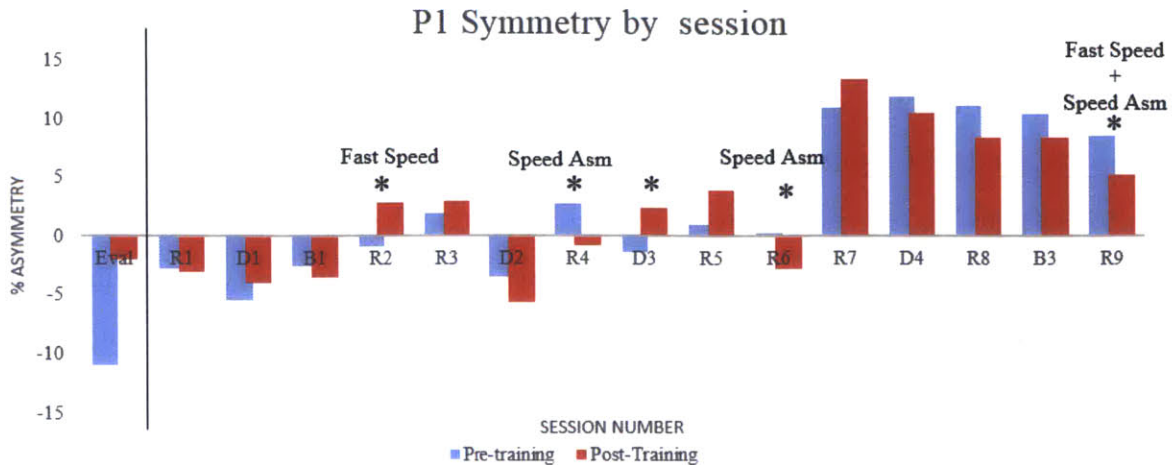
Figure 8-1: Pre-post diagnostic asymmetries by training session

diagnostic program during all symmetry-based programs and as such, the Skywalker attempted to induce a longer right step length and a shorter left leg post training. After R6, there was a substantial jump in step-length asymmetry such that the asymmetry score increased to positive 11% (reversing the original asymmetry seen in the evaluation) The following subsections detail each training routine.

8.3.1   Rhythmic Training Programs

The rhythmic training paradigm is designed to remove the floor during swing phase such that patients can focus on feeling the rhythm of walking. Additionally, we are able to tailor the training to modify step-length symmetry or increase walking speed. Table 8.1 highlights the features of each rhythmic training routine. Most of our training sessions for P1 included 5 blocks of 5 minute training between the two diagnostic programs. R7 is the only program that deviated by running 7 blocks of 3-4 minutes each.

Step-Length Symmetry Programs

Two basic classes of symmetry programs were created for this study. The first is a speed distortion program that creates an asymmetry in the speed of the two treadmill belts to augment step-length asymmetries, something that has been shown to

improve asymmetry in stroke patients[7][90]. The second is a vision program that displays a step length game (as shown in figure 7-8). The basic premise of the game is to ask participants to equalize the two bars that represent the left and right step-length. Within the vision program, we can distort the length of the bars to distort the perceived symmetry, either augmenting the asymmetry or correcting it. Kim et al. showed that healthy subjects will change step-length asymmetry in response to a similar type of implicit visual distortion [97] and that implicit visual distortion may be stronger than explicit [98]. Our vision game can be combined with the speed program (as done in program R3) to allow the patient to view step lengths in real-time while the treadmill speeds are altered.

Table 8.1: Participant 1 Rhythmic Training Protocol by session

	Date	Speed distortion	Step-length game	Training speed
R1	9/3			1 mph
R2	9/10			1.6 mph
R3	9/11	7%	Enabled, no distortion	1 mph
R4	9/15	7%		1 mph
R5	9/18		Distortion 10%	1.2 mph
R6	9/19	33%		1 mph
R7	9/22			2.0 mph
R8	9/25		Reverse Distortion	1.2 mph
R9	9/29	5%		2.2 mph

R1

R1 was P1's first experience on the Skywalker. It was run at 1mph the whole time and only utilized the right side for drops to get P1 comfortable with the machine. There was no attempt to improve symmetry or increase speed and thus analysis for this program was excluded.

R2

The initial diagnostic found an initial asymmetry score of -0.9% (right step-length longer than left). This training program worked on increasing the speed of P1 utilizing small drops on both tracks. The training speed was 1.6mph (faster than her 1.3mph

243
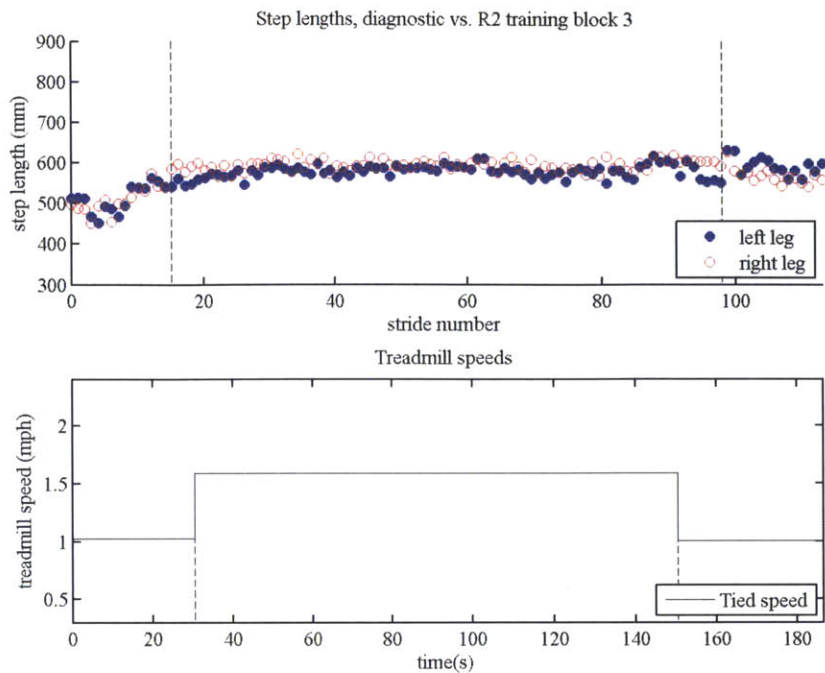
Figure 8-2: R2 step-lengths: initial—training—final

self selected speed on the initial treadmill evaluation). After the program there was a statistically significant difference in step length. Figure 8-2 depicts the right and left step lengths before, during and after training.

R3

The initial diagnostic found an initial asymmetry score of 1.9% (left step-length longer than right). This training program utilized both the step-length game and the speed asymmetry. The speed asymmetry was gradually increased to 7% (Left track speed 1.07mph, Right track speed 0.93mph). P1 was naïve to the changes in speed. Small drops for both the right and left tracks were used. Her instructions were to equalize the two bars on the vision game. Figure 8-3 shows sequential step lengths during the initial diagnostic, within training block 5 of R3 and during the final evaluation. Notice that both the left and right step-lengths increase during training. P1 developed a strategy to equalize her gait despite the changes in the speed of the treadmill. She took very large steps (easily seen in figure 8-3) while holding her left leg (faster belt)
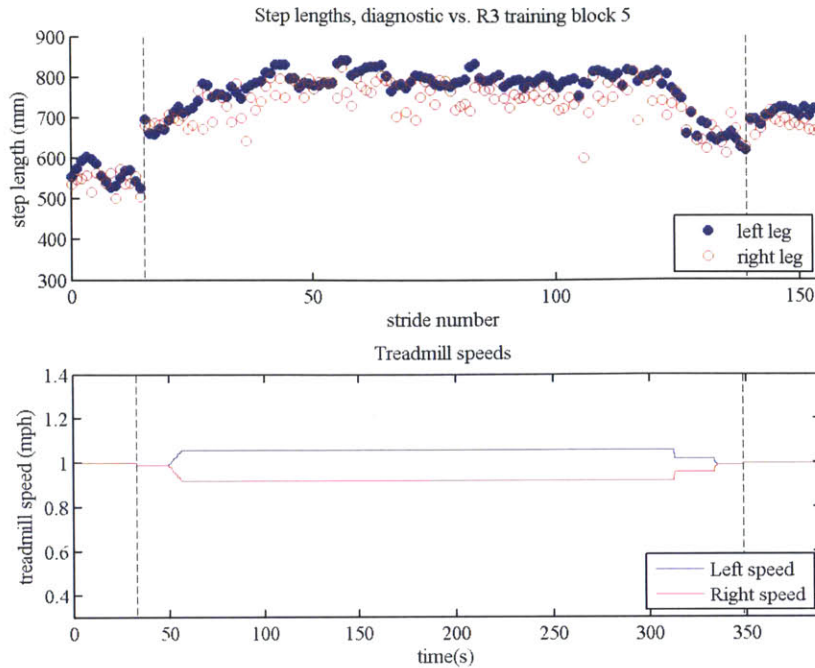
Figure 8-3: R3 step-lengths: initial—training—final

above the track for a split second before allowing it to drop to the track.

This program made P1 consciously work to equalize gait which was being pulled apart by the split belt speed. The final diagnostic showed a non-significant increase in step-length asymmetry.

R4

The initial diagnostic found an initial asymmetry score of 2.7% (left step-length longer than right). This training program utilized only the 7% speed distortion without the game display. In both R3 and R4, 7% speed distortion was used because it was enough to distort the gait but not enough that it was immediately apparent to the participant. It should be noted that the participant indicated that she thought we were changing the speed of the tracks but was not sure. Figure 8-4 shows the 5th block of training for this program. Here, in contrast to R3, we see a larger separation between the left and right leg. This is a result of the split-belt speed asymmetry. In R3, the subject had vision information and was instructed to equalize the right and
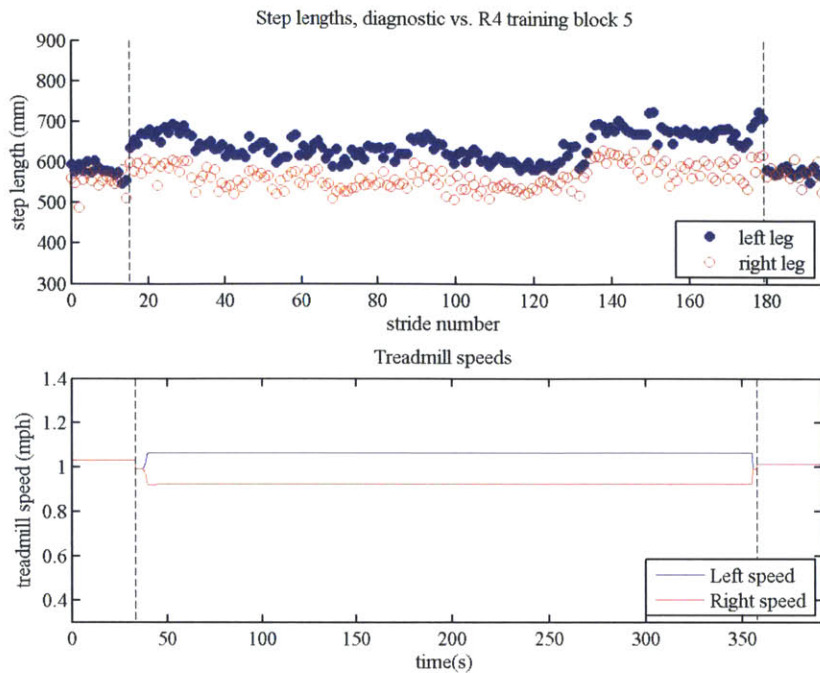
Figure 8-4: R4 step-lengths: initial—training—final

left step-length. Here, the subject is asked to simply walk normally during training. R4 significantly changed the step length symmetry, ending with an asymmetry score of -0.8% indicating a slightly longer right step length.

R5

The initial diagnostic found an initial asymmetry score of 1% (left step-length longer than right). This program utilized the step-length game to distort the visual feedback associated with each step-length while keeping the treadmill speed constant at 1.2 mph. This program would decrease the left bar length and increase the right bar length by a scaling factor. In this program, the scaling factor was gradually increased to 10%. This resulted in a left bar that displayed 90% of the actual length and a right bar that represented 110% of the actual measured length (depicted in figure 8-5). The participant was instructed to equalize the two bars. In order to do this, P1 needed to increase her left step length to augment the initial asymmetry further. Figure 8-6 show the left and right step-lengths during R5 and the associated diagnostics. This
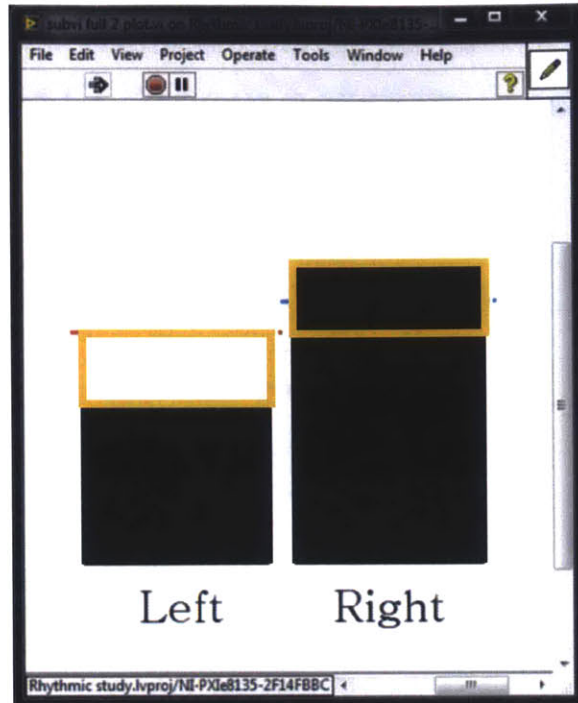
Figure 8-5: Exaggerated step-length visual distortion

program resulted in a non-significant asymmetry increase at the final diagnostic.

R6

The initial diagnostic found an initial asymmetry score of 0.2% (left step-length longer than right). This program split the treadmill belt speeds such that the left treadmill moved twice as fast as the right. We did this by setting a nominal 1mph treadmill speed before splitting the tracks by 33% (setting a left speed of 1.33mph and a right speed of 0.67mph). Because of the obvious change in treadmill speeds, the participant was aware of the protocol. The step-length game was not displayed and the participant was given no specific instructions other than to walk on the device. Figure 8-7 shows the 5th block of training compared to the initial and final diagnostic. Here we notice a large step-length increase in the left (fast) leg and similar contralateral decrease. R6 resulted in a statistically significant change in the step-length symmetry, yielding a final asymmetry score of -2.8% (right step-length longer than right).

This program was developed based on the split-belt training of Reisman, et
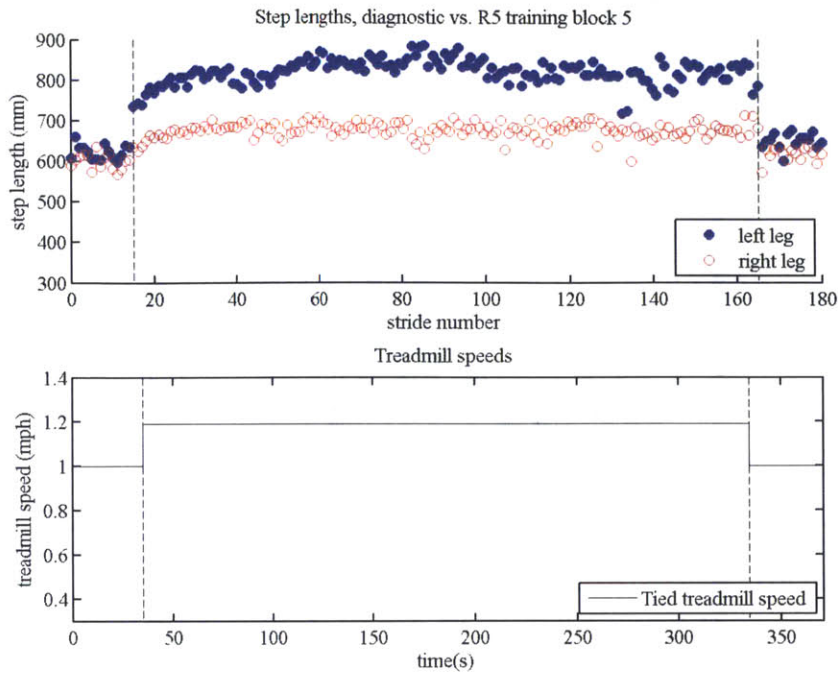
Figure 8-6: R5 step-lengths: initial—training—final

al.[7][90] that reported reductions in step-length symmetry for stroke patients with a similar protocol that also augmented the step-length asymmetry. One key difference that we saw with P1 and healthy subjects was a consistent increase in step-length of the fast leg. This was the opposite observation made by Reisman, et al. (see figure 8-8, taken from [7]) who observed the fast leg decrease in step-length during training. Our hypothesis is that our body weight support, which fixes the subject's position on the treadmill, is the cause, but further testing is needed to confirm this suspicion.

R7

The initial diagnostic found an initial asymmetry score of 10.9% (left step-length longer than right). This program was meant to train P1 for maximum walking speed, while assessing the value of using drops for less-impaired individual. 7 blocks were run in total. For each block, P1 was asked to walk at the maximum speed that was comfortable for three to four minutes. Blocks 1,3,5 and 7 were run without track drops and the even blocks were run with drops. P1 chose 1.55mph for her first blcok
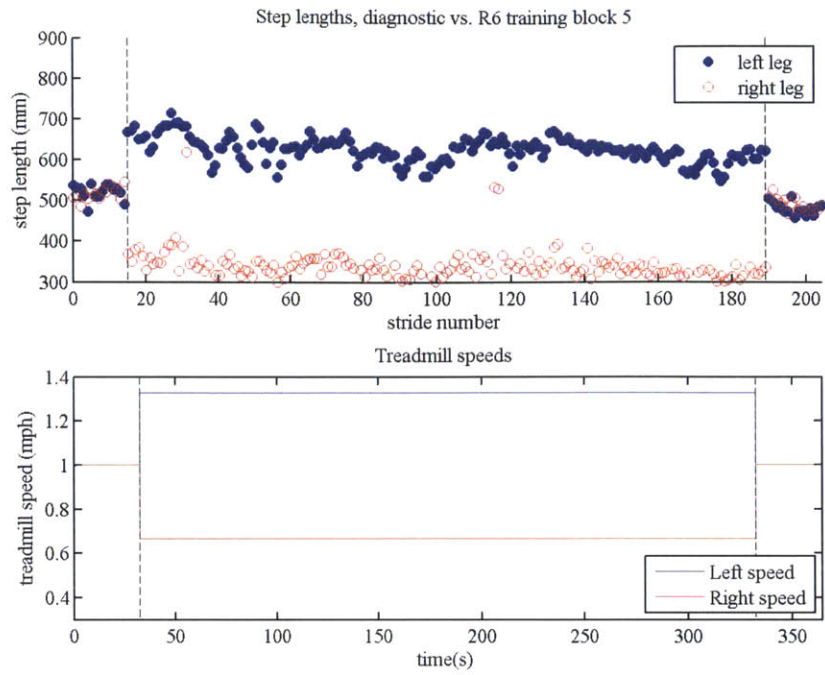
Figure 8-7: R6 step-lengths: initial—training—final
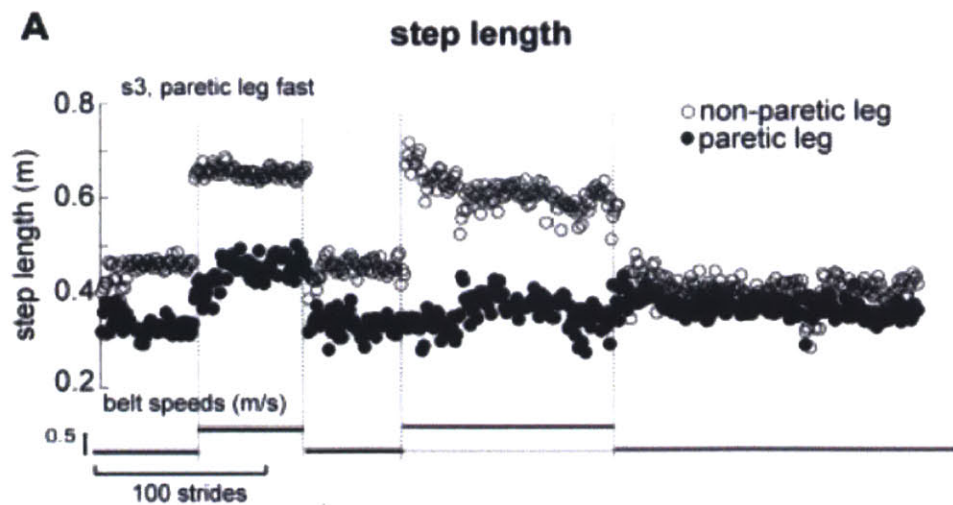
Figure 8-8: Step-length changes of stroke patients from [7]
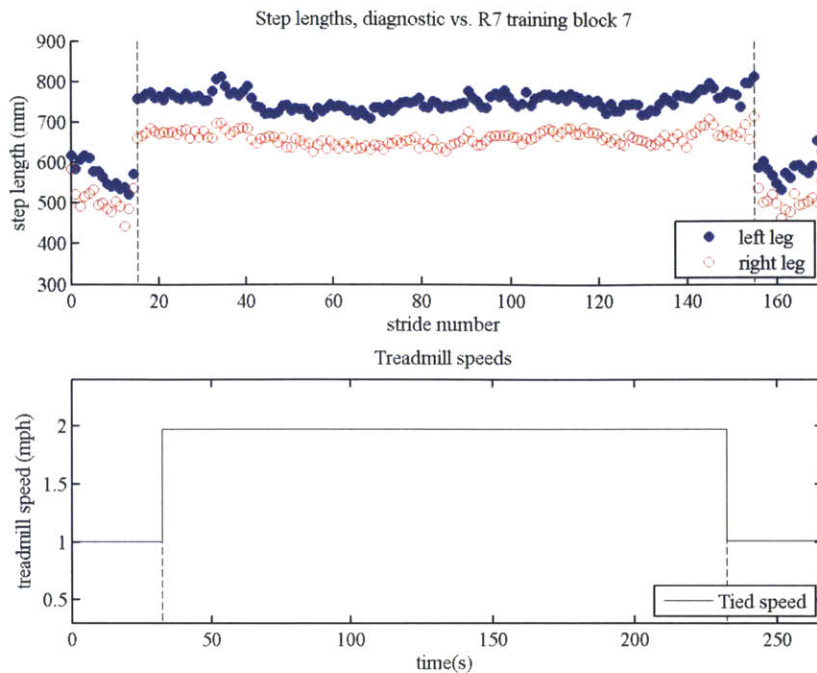
Figure 8-9: R7 step-lengths: initial—training—final

but kept increasing the speed each block until 2mph was reach in blocks 6 and 7. She found little difference in the experience of walking with drops at lower speeds (1.55-1.7mph) but at higher speeds, she reported feeling more comfortable with drops and she noted that it was hard to keep her balance at 2mph without drops. Without the drops, we noticed that she scuffed her feet on the treadmill (which could be the cause of the balance difficulty). The drops allowed her to focus on moving her legs without the worry of tripping. Figure 8-9 shows block 7 of training, where there were no drops and a speed of 2.0mph. Initial asymmetries were exaggerated at the final diagnostic.

R8

The initial diagnostic found an initial asymmetry score of 11% (left step-length longer than right). This program used the opposite strategy as program 3, thus we call it the reverse vision program. The initially longer left step was depicted by a bar that showed an even longer step length and the shorter right step length was shown to be even shorter. The instructions to the participant were to equalize the two bars.

250
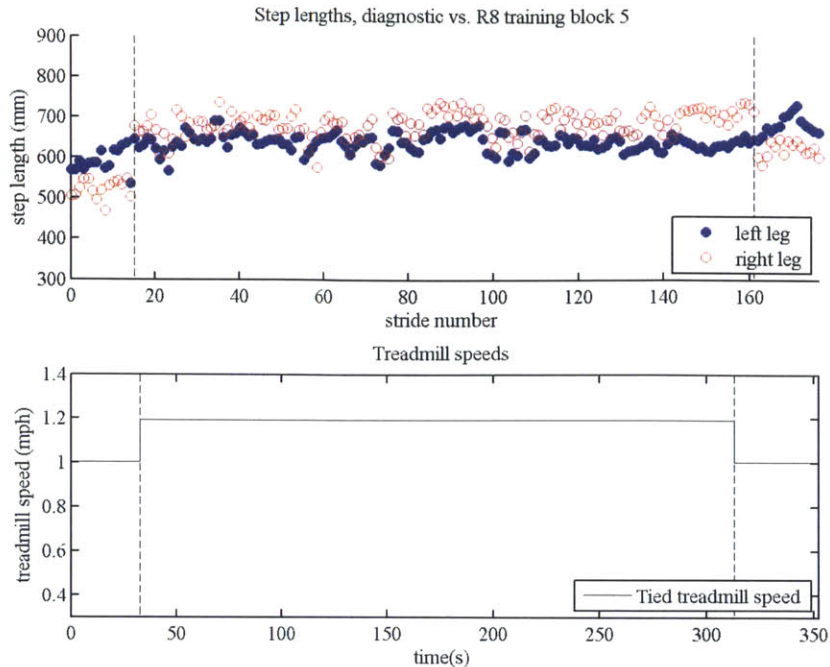
Figure 8-10: R8 step-lengths: initial—training—final

She would do so by accentuating the correction, making the right leg longer than the initially long left step. Figure 8-10 shows P1 attempting to equalize the bars in R8. The visual distortion was set to 5%. It should be mentioned that this program exhausted P1 and after block 3, she was not able to equalize the bars. R8 program resulted in a decreased asymmetry but it was not statistically significant.

R9

The initial diagnostic found an initial asymmetry score of 8.5% (left step-length longer than right). This program blended speed asymmetry training with speed training. The training speed was set at 2 mph for the first two blocks and then was increased to 2.2mph for the final three blocks of training. Each block of training also split the speeds by a factor of 5%. Figure 8-11 depicts the effects of training in this manner. Afterward, step-length asymmetry was decreased.

The advantage of training with speed is well documented. Fast-speed body weight supported treadmill training for stroke patients has been shown to increase self-

251
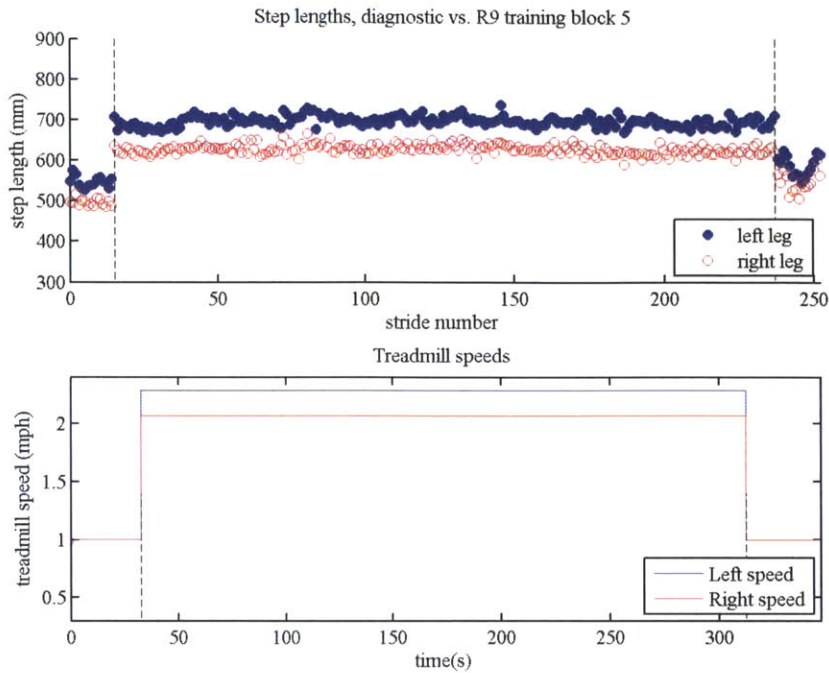
Figure 8-11: R9 step-lengths: initial—training—final

selected overground walking velocities[99][100], a standard measure for gait improvement. R9 demonstrates a hypothesis that we can combine symmetry and speed training in a way that has a statistically significant change in step length symmetry.

8.3.2 Discrete and Balance Training Programs

Of the remaining programs completed by P1, 4 were discrete trainings and 3 were balance programs. Of these 7 programs, only D3 resulted in a statistically significant change in step length asymmetry. Balance programs resembled rhythmic speed programs but included waves in addition to the dual-side drops. P1 operated on level 6 (the highest level) of the balance game. B1 was conducted at a speed of 1.2mph. B2 was run at speeds increasing from 1.3 to 1.4mph. B3 was run at speeds increasing from 1.4mph to 1.9mph. For P1, the waves were intense enough to disturb balance slightly during walking.

8.3.3 Summarizing P1's Asymmetry Study

P1's symmetry on the initial evaluation showed a longer right step length. The many different training programs gradually shifted the asymmetry to a longer left step-length on the Skywalker. After R6, there was a dramatic change to a much longer left step length on the Skywalker system. The reason for this is unknown. The final evaluation on a treadmill showed a slightly longer right step that was significantly reduced from the initial evaluation.

8.3.4 Resulting Future Work

Studying the effects on symmetry from the various training programs used with P1 has illuminated the need for future work. The following pages will offer example protocol for three testable hypotheses arising from this work.

Assessing the effects of speed and split-belt distortion level in symmetry training

Rationale

> R9 showed a statistically significant change in walking symmetry when combining the speed distortion training with high speed training. High speed training has been shown to increase overground walking speed [99][100] and split-belt speed distortion training has been documented to improve step-length asymmetry in stroke patients. Utilizing Skywalker's track drops, we can uniquely work on increasing the maximum training speed of participants while implicitly distorting the speeds of the treadmills to augment asymmetries. Published split-belt work has been done in a similar fashion to R6[7][90] in which one of the treadmills is running at twice the speed of the other. It is unclear if this very apparent disparity in treadmill speeds is the best way to train for step-length symmetry. As shown in R9, splitting the treadmill by a total of 10% (5% speed increase on one track and a 5% decrease on the other) still allows a patient to

train for speed and resulted in a statistically significant decrease in step-length asymmetry.

Protocol

Recruit 15 chronic stroke patients (or adult cerebral palsied patients in a separate protocol) with an symmetry score greater than 10% or less than -10%. Randomize the population into three groups of 5. Each group will receive 24 sessions of therapy done over two months. Group 1 will receive a program similar to R6 with belts split such that the longer step side is at twice the speed of the shorter step side. Group 2 will receive a program similar to R4 with a total distortion of 10%. Group 3 will receive a program similar to R9, attempting to train speed with drops while distorting the split-belt speeds by 10%. Main outcome measures will be self-selected walking speed and the step-length asymmetry score.

Hypothesis

High speed training with a slight distortion will result in the greatest gait speed change but will improve symmetry less than the R6-style split-treadmill training.

Assessing the effects of the body weight support on step-length during split-speed walking

Rationale

Reisman et al. [7] reported that the fast leg responds with a shorter step length. All of our speed asymmetries sessions showed that the fast leg responds with a longer step length. It is unclear what causes the discrepancy but this occurs with and without the drops.

Protocol

6 healthy subjects will walk with the left belt at 2 mph and the right belt at 1mph. The experiment will be done in two blocks of 5 minute walking. One block of training will use the current body weight support and the other will use a loose-fitting safety harness that allows the center of mass to freely float on the treadmill. The order of testing will be randomized. 50% of the subjects will use the BWS in the first block and the other half will use the safety harness in the first block to negate the effect of test ordering.

Hypothesis

The body weight support system will flip the effect of the split-speed paradigm.

Computer simulations to determine the effects of spatial and temporal symmetry parameters on gait stability and efficiency

Rationale

In this feasibility study, we sought to decrease step-length asymmetry but symmetry can be also be defined by temporal parameters such as double stance asymmetry or single stance asymmetry. In one study, 33% of stroke patients exhibited spatial (step-length) asymmetry and over 50% exhibited temporal asymmetry[101]. It seems intuitive that a more symmetric gait is beneficial (for appearances, energy efficiency, etc.) but proof is absent. If we can quantify the benefits to either spatial or temporal symmetry, we can justify a heavier research thrust to improve these types of symmetry.

Protocol

A dynamic computer model will be developed to mimic literature of stroke and

cerebral palsy patients ([102] and [103]). A simulated perturbation will then be applied in the frontal plane and sagittal plane to asses stability. A standard measure of efficiency such as cost of transport quantitatively will be used to assess energetic costs of both temporal and spatial asymmetry.

Hypothesis

Both step-length and temporal symmetry enhance stability and efficiency.

Assessing the value of drops for high speed training for adults with cerebral palsy

Rationale

We found in R7 that the rhythmic drops were useful for P1 to walk at high speeds, removing the floor, which normally made her feel unstable. P1's increase of over 30% in self-selected overground walking clearly indicates a change in her ability to walk quickly. A study should be done to assess the effects of the drops in overground walking speed changes.

Protocol

10 adults with cerebral palsy with self selected overground walking speeds between 1.5 and 2.5 mph will be split into two groups. Each group will receive 24 sessions of therapy on the Skywalker system. The first group will walk on the Skywalker without drops. The second group will walk on the Skywalker with drops. The instructions and protocol will be the same for both groups. Walk for 5 blocks of 5 minutes at the highest speed you feel comfortable. Subjects will be informed that during training, their goal is to walk as quickly as possible without feeling unsafe. The body weight support system will be used for all groups.

Hypothesis

Greater gains will be made in self-selected overground walking speed during and after the study by the group using drops.

8.4 Variance changes by training program

As shown in section 7.3, we noticed a significant decrease in most of the participants' cycle variances (described in section 7.4.2). Of the three participants, P3 showed the greatest change in variance and displayed statistically significant decreases in all cycle variables analyzed (left hip, left knee, and both x-positions of the heel). As an extension to this finding, this section outlines the variance changes seen on the initial and final diagnostics of our three types of programs. It should be noted that during the evaluations, P3 walked at 1mph on a standard treadmill and during the diagnostics, her walking speed was 0.5mph on the Skywalker. These speeds were her self-chosen walking speed on the first session walking with each device.

Figure 8-12 shows the initial and final cycle standard deviations of the hips, knees and x-position of both heels taken from the diagnostic walking programs before and after each training session. The thick bordered columns represent the three types of programs run with P3. Blue boxes represent those that showed a statistically significant decreases in standard deviation after training. The light orange blocks represent those that showed a statistically significant increases in standard deviation after training and the white boxes were not significantly changed. It is clear from this figure that the rhythmic program seems to have a greater immediate effect on the variance of P3's gait than either the discrete or balance.

Left Hip	Eval	Rhythmic				Discrete				Balance			
		R1	R2	R3	R4	D1	D2	D3	D4	B1	B2	B3	B4
Date		9/9	9/15	9/22	9/29	9/10	9/17	9/24	10/1	9/12	9/19	9/26	10/2
Initial	2.21	2.23	1.90	1.79	1.82	2.27	1.33	1.78	1.25	1.91	1.78	2.41	2.06
Final	1.5	2.45	1.15	1.74	1.92	1.95	1.39	4.27	2.20	1.57	1.66	2.17	1.39
Right Hip													
Initial	N/A	2.03	1.59	2.27	2.34	2.12	1.81	2.04	1.66	2.04	1.60	2.26	2.23
Final	N/A	1.80	1.78	1.32	1.70	2.14	1.54	2.96	2.16	2.09	1.97	2.27	2.35
Left Knee													
Initial	2.86	4.08	2.36	2.52	3.37	2.87	1.72	2.16	2.32	2.32	2.45	2.87	2.48
Final	2.29	2.47	1.79	2.22	1.87	2.66	1.94	6.16	3.05	3.08	3.03	3.73	2.31
Right Knee													
Initial	N/A	2.76	2.51	3.60	3.86	2.61	2.85	3.78	2.32	2.96	2.59	3.45	3.87
Final	N/A	2.33	2.31	2.25	2.30	2.35	2.01	4.54	3.82	3.88	3.50	4.05	3.53
Left x													
Initial	29.2	35.2	27.5	23.1	23.8	28.2	17.9	25.2	12.8	22.9	23.6	36.5	28.3
Final	23.7	38.3	17.4	27.8	22.2	21.9	17.5	70.6	31.5	22.3	25.3	30.7	23.1
Right x													
Initial	32.2	26.6	31.2	26.8	30.1	36.9	23.0	27.2	18.9	32.2	23.6	27.6	23.8
Final	25.7	25.3	23.7	15.9	18.3	30.1	22.0	35.1	27.5	28.5	24.9	30.6	23.7

Statistically Significant Decrease

Statistically Significant Increase

Figure 8-12: P3's diagnostic program cycle standard deviations broken down by program type

Figure 8-13 shows the variance at each session taken during the initial diagnostic prior to training. The left joint angles and both heel cycle variances show a decreasing trend-line while the right joint angles show an increasing trend-line. Data for the right hip and knee angles was not taken during the treadmill evaluations before and after the complete training program, so we cannot report the effect of training on those angles.

8.4.1 Resulting Future Work

From the single subject, we see that the rhythmic program has the strongest immediate positive effect on the cycle variances. It is not obvious that the rhythmic program was the cause of the decreased variance at the evaluations after the month-long training period. Future work is needed to separate the three programs. Below, we list sample studies that can be done to assess the effects of decreasing gait variance and separating the training routines.

Determining the effects of rehabilitation training on cycle variance

Rationale

As mentioned in section 7.4.2, if all impaired patients started with a higher cycle variance, decreased the variance after training in the direction of a healthy variance, logic would contend that cycle variance is correlated to walking proficiency if we make the assumption that each participant's walking proficiency improved after training. First, we need a larger study to assess whether a decreasing cycle variance occurs in a larger sample of patients post training with Skywalker and with another rehabilitation device.

Protocol

20 acute hemiplegic stroke patients are recruited and split into two groups. One group receives 12 sessions of rhythmic therapy with the Skywalker. The other

Left Hip Std by Training Session

$y = -0.0275x + 2.0575$
$R^2 = 0.0826$

Right Hip Std by Training Session

$y = 0.0166x + 1.8908$
$R^2 = 0.0494$

Left Knee Std by Training Session

$y = -0.0395x + 2.8842$
$R^2 = 0.0538$

Right Knee Std by Training Session

$y = 0.0857x + 2.5398$
$R^2 = 0.2846$

Left x-pos Std by Training Session

$y = -0.4956x + 28.63$
$R^2 = 0.0744$

Right x-pos Std by Training Session

$y = -0.7307x + 32.081$
$R^2 = 0.3004$
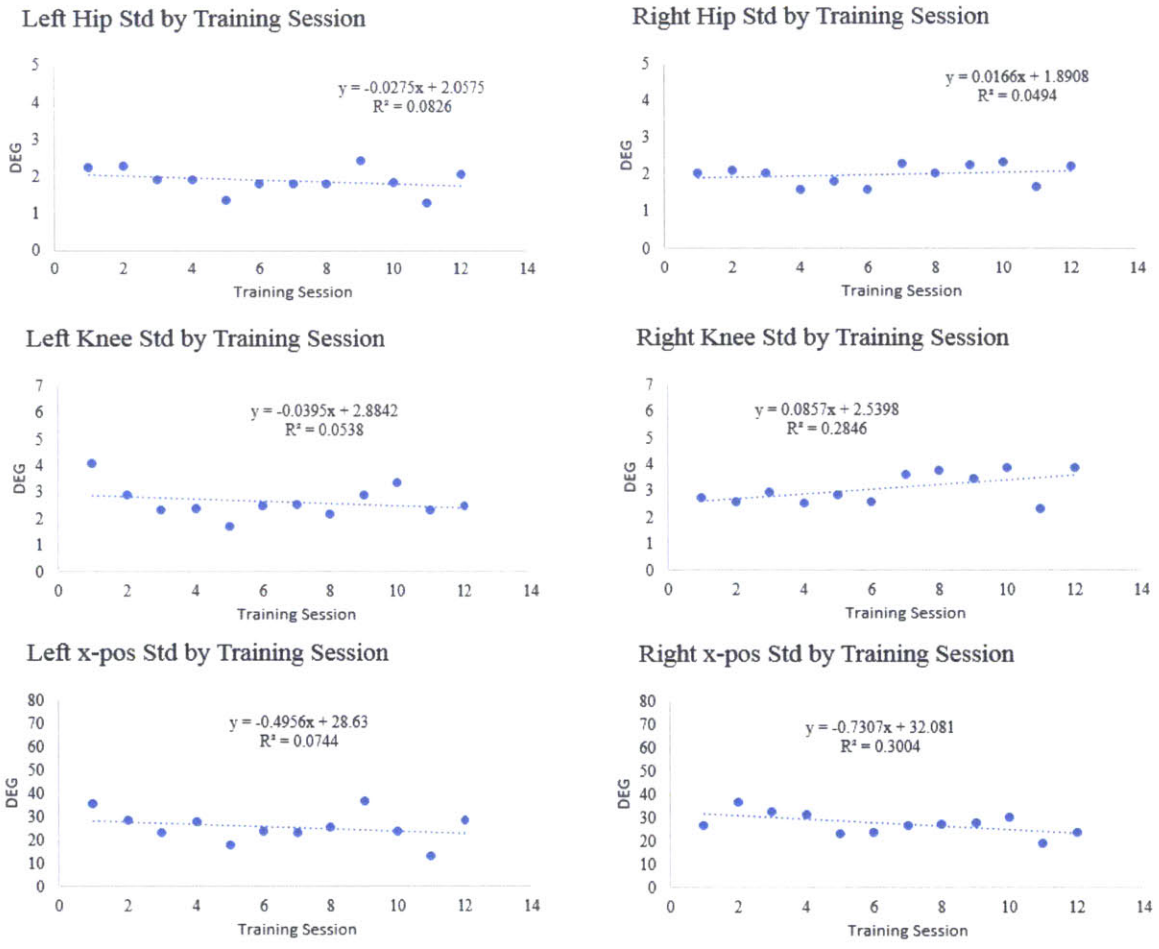
Figure 8-13: P3's initial diagnostic program cycle standard deviations by Skywalker session

group receives 12 session of Anklebot training[87][61]. Patients will be evaluated before and after training on a standard treadmill using the 3D Guidance trakSTAR system(Ascension Technology Corporation, Milton, VT). Primary evaluation measures will be self selected over-ground gait speed and cycle variance on the treadmill.

Hypothesis

The Skywalker group will make a greater improvement in both self-selected overground gait speed and will experience a greater decrease in gait variation than the Anklebot group.

Assessing the effects of a low variation gait

Rationale

In P3's words, "after training with the Skywalker, I walk much better". However, we saw no change in walking speed or stamina on our clinical evaluations. Her major changes after our study included a decreased cycle variance in all variables tested and a more healthy appearing x-y sagittal plane trajectory. The outlying question is: what are the underlying changes that result in decreased cycle variance? In control theory, increasing the proportional gain in a controller will cause a system to respond more quickly to disturbances (in the stable region). Is it possible that a decrease in variance of gait is an indicator of a more responsive control system? In the context of motor primitives, are we able to more closely follow a rhythmic limit cycle or are we generating a more repeatable limit cycle? If the ability to respond to disturbances is improved, we can suggest that a decreased variance corresponds to a more responsive control system. If not, we can suggest that perhaps and unperturbed limit cycle is more repeatable during unperturbed walking.

Protocol

10 acute stroke patients train with the rhythmic program of the Skywalker system for 12 sessions. Before and after training, two separate evaluations are done. The first is a standard cycle variation evaluation outlined in this thesis. The second is a walking test in which the patients are asked to walk on the Skywalker system while random perturbations occur in the frontal and sagittal plane. The sagittal plane kinematics will be recorded during purturbations.

Hypothesis

Patients with a decreased cycle variations are able to respond more quickly to perturbations, which may indicating a more responsive control system.

8.5 Hardware Modification Recommendations

The mechanical design of the Skywalker was proven to be robust during the 1 month trial. It lasted for the full 40 hour training schedule without any problem. Figure 8-14 shows the robotic hardware. As mentioned in section 2.1.4, I recommend reducing the size of the treadmill. This will decrease the mass of the track, increase the robustness of the design by reducing the max distances from the track supports and will decrease the footprint of the machine in a rehabilitation hospital setting. Dimension (a) should be reduced from 60" to 55" and dimension (b) should be reduced from 20" to 18". Dimension (c) is referencing the maximum track drop. In this version, we define small, medium and large drops (see section 7.1.1). Large drops make use of the full drop shown here, however during training, a large drop was never used and a medium drop was used in only 2 of the 40 trials for P3 in early rhythmic sessions. Future use of the machine with a larger population of impaired individuals (stroke patients preferably) can be used to define the maximum angle of drop. A lower maximum drop angle will decrease the height of the machine, making it easier to mount a patient onto the system. Finally, I recommend welding the frame (d) rather than assembling
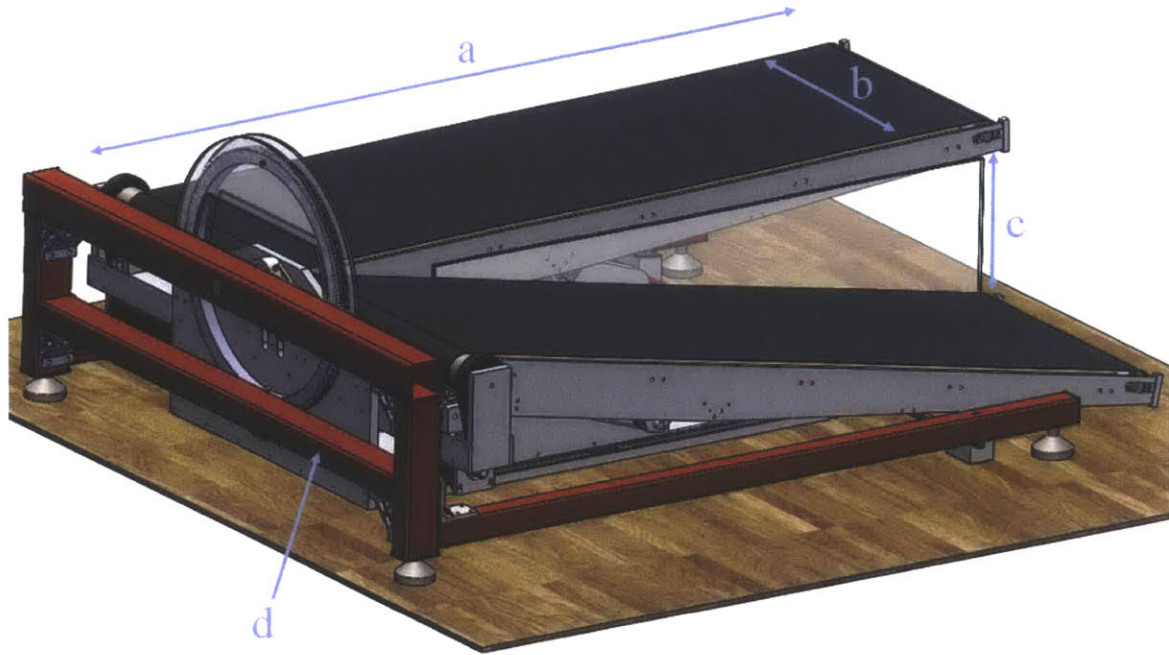
Figure 8-14: Hardware Recommendations

it with brackets. I used fasteners and slots such that I could adjust the machine if needed, however, fastening through tubes is unattractive and access to internal nuts is difficult for assembly. Fixturing and welding will produce a more finished look and result in easier installation.

Appendix A

Setup and Running the Training Programs

The Skywalker-γ is a fairly complex system and while measures were taken to simplify the machine as much as possible, it is still a one-of-a-kind prototype and thus requires careful operation. Prior to a participant coming for a training session, the average set-up time would take 20-30 minutes. The time included the tasks written on the following pages and also included the preparation of other materials such as replacing the batteries on the leg markers, putting a new logging sheet in the clipboard, taking a waterbottle out of the refrigerator for the participant or sweeping up the lab.

The following pages detail the setup and operation of this machine.

SKYWALKER TRAINING MODE PROCEDURES

RHYTHMIC 1&2

Prior to participant's arrival:

Power up Computer and PXI box – connect computer to the real time system

Remove central support beam from the rear of the system (if it is in place)

Open electrical box – engage all treadmill and sagittal plane drives & power up robot

Open *engage robot.vi* and engage robot drives – leave this program running throughout session

Open *individual homing.vi* and home sagittal plane drives

Disable drives via *engage robot.vi*

Open *newvisionoffset2.vi* and run twice to initialize the camera setup – check with frame rate – leave open

Open diagnostic and main program and name files as follows: *diagnostic* ("P#" rd "month day") ("P#" r "cycle #" speed "month day") or ("P#" r "cycle #" vision "month day")

Open video program with the webcam, open *subvi full 2 plot.vi* and place it appropriately

Session procedures:

Fit subject with markers, ask patient to move to door frame to get general measurements, enter measurements and record here: (note: shin measurement should be from knee to heel)

P1n _____thi_____shin_____w_____   P2n _____thi_____shin_____w_____

P3n _____thi_____shin_____w_____   P4n _____thi_____shin_____w_____

Run *potentiometer check.vi*, input weight

Assist participant onto machine and into the body weight support device, adjust BWS to provide 50% WS

Run *newvisionoffset2.vi* – stop and close

Engage drives via *engage robot.vi*

Open *Diagnostic.vi*, and have patient walk at a self-selected speed for 3 minutes

Rest for 2 minutes, lower BWS to allow patient to sit

Open main program (*Split speed training.vi or vision distort rev 4.vi*) – open *subvi full 2 plot.vi* game and move to center of large screen

Relocate BWS to desired % with *potentiometer check.vi*

Run main program – Be diligent in timing of the program 5 minutes training, 2 minutes of rest for 5 cycles

Disengage drives via *engage robot.vi* and help patient down from robot, ask patient to be seated while removing markers, offer a bottle of water, ask about the training – health, feeling of program, progress, any areas of soreness?

Post Procedures:

Convert Data files to .csv format, save to a folder titled with Patient #, training type, date – Write notes for session

SKYWALKER TRAINING MODE PROCEDURES

DISCRETE

Prior to participant's arrival:

Power up Computer and PXI box – connect computer to the real time system

Place central support beam in the rear of the system

Open electrical box – engage both treadmill drives, disable others & power up robot

Open *engage robot.vi* make sure that drives are <u>disabled</u>– leave this program running throughout session

Open *camera initialization.vi* and run twice to initialize the camera setup – check with frame rate – close

Open *subvi game picture.vi* and position it properly (the black portion touches bottom of screen, middle of up-down arrow to right side of screen)

Open *potentiometer check.vi*, input weight, power up the projector

Open *Diagnostic.vi,* name file ("P#" rd "month day")

Open *Discrete3.vi*, name file ("P#" d "cycle number" t "month day")

Session procedures:

Fit subject with markers

P1n _____ w_____   P2n _____ w_____   P3n _____ w_____   P4n _____ w_____

Assist participant onto machine and into the body weight support device, adjust BWS to provide 5% WS – <u>loose</u>

Run *newvisionoffset2.vi* for the diagnostic programs and *Discrete Offsets3.vi* for discrete– stop and close

Engage drives via *engage robot.vi*

Begin training (5 minutes)

Rest for 2 minutes, lower BWS to allow patient to sit

Relocate BWS to desired % with *potentiometer check.vi*

Run again – Be diligent in timing of the program 5 minutes training, 2 minutes of rest for 5 cycles

Disengage drives via *engage robot.vi* and help patient down from robot, ask patient to be seated while removing markers, offer a bottle of water, ask about the training – health, feeling of program, progress, any areas of soreness?

Post Procedures:

Convert Data files to .csv format, save to a folder titled with Patient #, training type, date – Write notes for session

SKYWALKER TRAINING MODE PROCEDURES

BALANCE

Prior to participant's arrival:

Power up Computer and PXI box – connect computer to the real time system

Remove central support beam from the rear of the system (if it is in place)

Open electrical box – engage all drives (decide on Sagittal plane before training, initially have them ready) & power up robot

Open *engage robot.vi* and engage robot drives – leave this program running throughout session

Open *individual homing.vi* and home all drives

Run *center frontal plane. Vi* and disable drives

Open *newvisionoffset2.vi* and run twice to initialize the camera setup – check with frame rate – leave open

Open *subvi balance game.vi* and place is properly on the screen with webcam output

Session procedures:

Fit subject with markers, ask patient to move to door frame to get general measurements, enter measurements and record here: (note: shin measurement should be from knee to heel)

P1n _____thi_____shin_____w_____   P2n _____thi_____shin_____w_____

P3n _____thi_____shin_____w_____   P4n _____thi_____shin_____w_____

Run *potentiometer check.vi*, input weight

Assist participant onto machine and into the body weight support device, adjust BWS to provide 50% WS

Run *newvisionoffset2.vi* – stop and close

Engage drives via *engage robot.vi*

Open *Balance trainer.vi*, name file ("P#" b "cycle #" t "month day") and have patient walk at a self-selected speed on level 1 for 3 minutes

Rest for 2 minutes, lower BWS to allow patient to sit

Relocate BWS to desired % with *potentiometer check.vi*

Run with next levels, saving each run as ("P#" b "cycle #" t "month day")

Run main program – Be diligent in timing of the program 5 minutes training, 2 minutes of rest for 5 cycles

Disengage drives via *engage robot.vi* and help patient down from robot, ask patient to be seated while removing markers, offer a bottle of water, ask about the training – health, feeling of program, progress, any areas of soreness?

Post Procedures:

Open *Center frontal plane.vi* and center tracks

Convert Data files to .csv format, save to a folder titled with Patient #, training type, date – Write notes for session

Appendix B

System Wiring

The following page details the wire connections from the National Instruments PXI breakout boxes (source) to the Kollmorgen AKD motor drivers (drive). Communication between the two devices was accomplished by simple analog or digital signals. Figure B-1(a) shows the cables (a) that split into individual wires (b) and connect to their assigned pins in the NI breakout boxes (c). Figure B-1(b) illustrates the cables entering the controller box (1) and splitting into individual wires (2) before connecting to their respective driver pins(2).
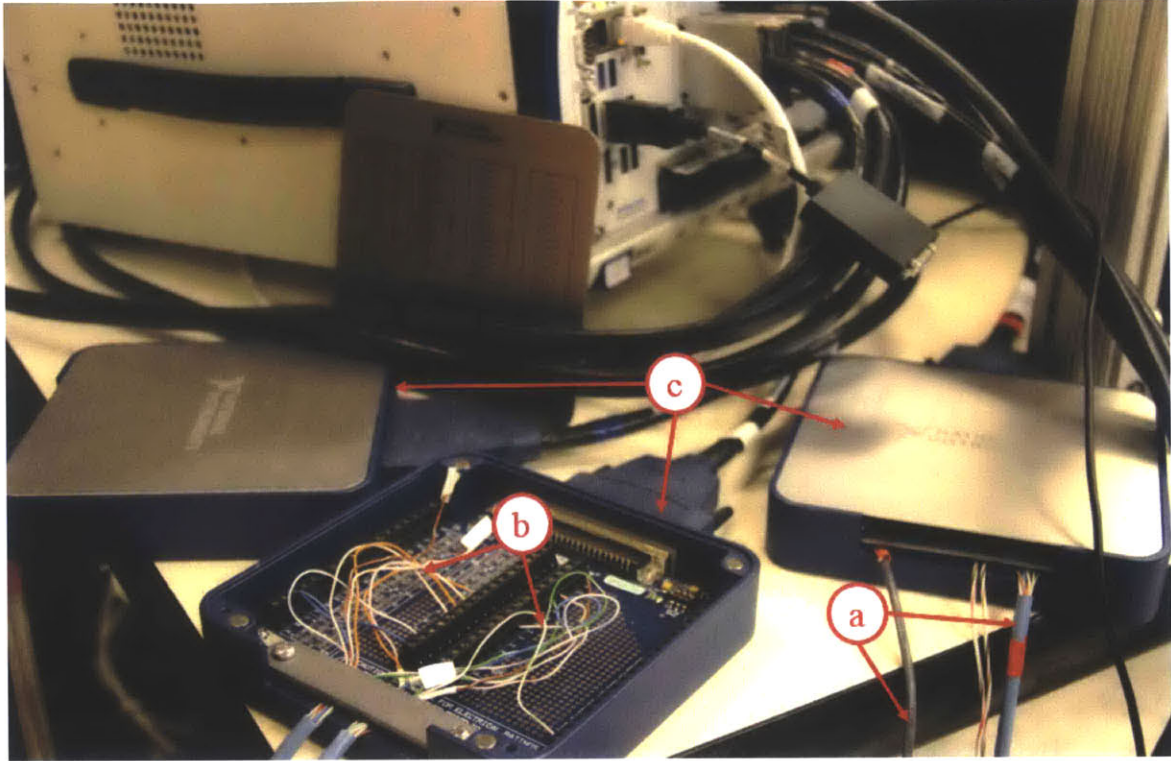
(a) Source (NI PXI breakout boxes)
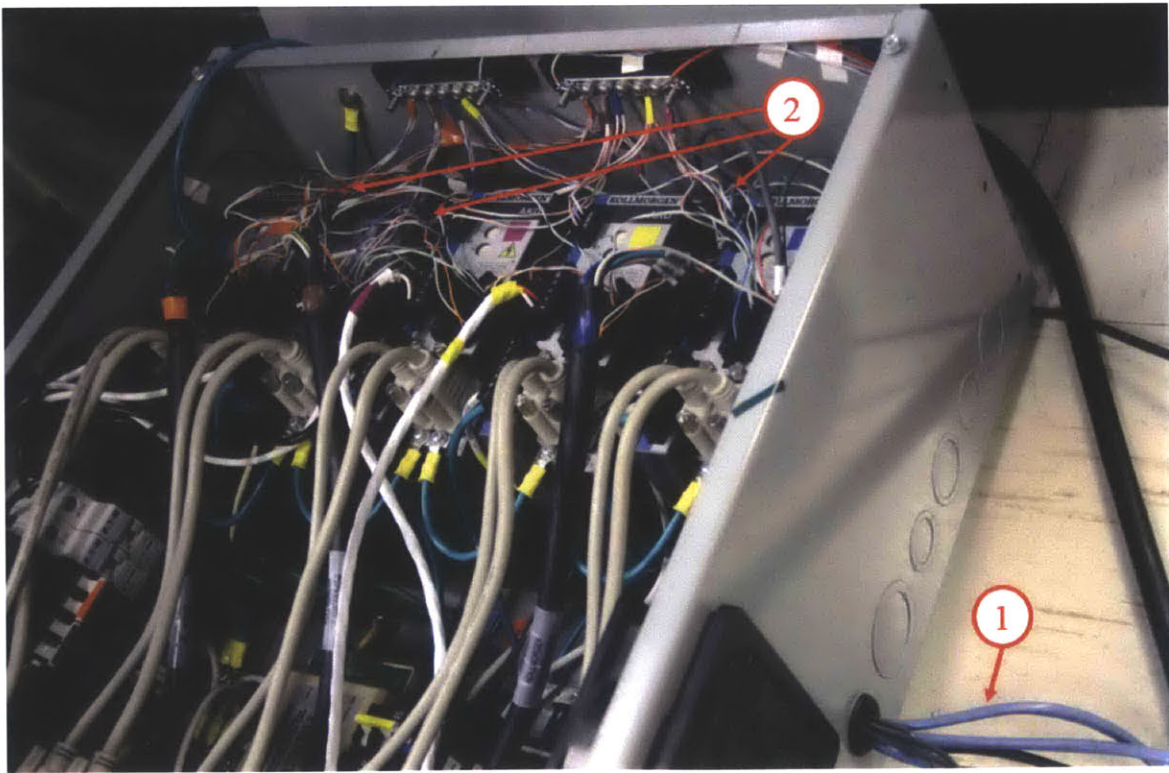
(b) Controller box drivers

Figure B-1: Wire Source and Driver Pictures

Drive	Function	Connector	Pin Name	Pin	Cable	Wire	Source	Control Box	Pin Name	Pin
			Drive			Wire			Source	
Left Treadmill	Ain+	X8	Analog-in+	10	Blue/White	Orange	Control Box	White	AO 2	22
Left Treadmill	Ain-	X8	Analog-in-	9	Blue/White	White/Org	Control Box	White	AO Gnd	55
Left Treadmill	Enable	X8	Enable	4	-	Red	24v P-supply	-	-	-
Left Treadmill	DCOM8	X8	DCOM8	3	-	Blue	24v P-supply	-	-	-
Left Treadmill	DCOM7	X7	DCOM7	1	Blue/White	White/Grn	Control Box	White	D GND	9
Encoder										
Left Treadmill	Encoder A	X9	A	1	Beige/Purp	black	Control Box	Blue	PFI 8/P2.0	37
Left Treadmill	Encoder B	X9	B	4	Beige/Purp	orange	Control Box	Blue	PFI 10/P2.2	45
Left Treadmill	Encoder GND	X9	GND	3	Beige/Purp	red	Control Box	Blue	GND	9
Left Treadmill	Encoder Shield	X9	Shield	6	Beige/Purp	green	Control Box	Blue	GND	9
Right Treadmill	Ain+	X8	Analog-in+	10	Blue	Orange	Control Box	White	AO 3	21
Right Treadmill	Ain-	X8	Analog-in-	9	Blue	White/Org	Control Box	White	AO GND	54
Right Treadmill	Enable	X8	Enable	4	-	Red	24v P-supply	-	-	-
Right Treadmill	DCOM8	X8	DCOM8	3	-	Blue	24v P-supply	-	-	-
Right Treadmill	DCOM7	X7	DCOM7	1	Blue/white	White/Grn	Control Box	White	DGND	9
Encoder										
Right Treadmill	Encoder A	X9	A	1	Beige/Yellow	Brown	Control Box	Blue	PFI 3/P1.3	42
Right Treadmill	Encoder B	X9	B	4	Beige/Yellow	Yellow	Control Box	Blue	PFI 11/P2.3	46
Right Treadmill	Encoder GND	X9	GND	3	Beige/Yellow	Orange	Control Box	Blue	GND	12
Right Treadmill	Encoder Shield	X9	Shield	6	Beige/Yellow	Blue	Control Box	Blue	GND	44
Frontal Plane	11-Home Reference	X8	Digital-IN6	5	-	Black	24v P-supply	-	-	-
Frontal Plane	Enable	X8	Enable	4	-	Red	24v P-supply	-	-	-
Frontal Plane	DCOM8	X8	DCOM8	3	-	Blue	24v P-supply	-	-	-
Frontal Plane	Start Home	X7	Digital-IN7	2	Blue	Green	Control Box	White	P0.10	49
Frontal Plane	2-Motion Task 1 (L wave)	X7	Digital-IN4	3	Blue	White/Grn	Control Box	White	P0.11	47
Frontal Plane	2-Motion Task 2 (R wave)	X7	Digital-IN3	4	Blue	White/Blue	Control Box	White	P0.12	19
Frontal Plane	Center position	X7	Digital-IN2	9	Blue	Blue	Control Box	White	P0.8	52
Frontal Plane	DCOM7	X7	DCOM7	1	Blue/white	White/Grn	Control Box	White	DGND	9
Encoder										
Frontal Plane	Encoder A	X9	A	1	Beige/Red	Brown	Control Box	Blue	PFI 0/P1.0	11
Frontal Plane	Encoder B	X9	B	4	Beige/Red	Yellow	Control Box	Blue	PFI 2/P1.2	43
Frontal Plane	Encoder GND	X9	GND	3	Beige/Red	Orange	Control Box	Blue	GND	7
Frontal Plane	Encoder Shield	X9	Shield	6	Beige/Red	Blue	Control Box	Blue	GND	7
Right Sagittal Plane	11-Home Reference	X8	Digital-IN6	5	-	White/Blk	24v P-supply	-	-	-
Right Sagittal Plane	Enable	X8	Enable	4	-	Red	24v P-supply	-	-	-
Right Sagittal Plane	DCOM8	X8	DCOM8	3	-	Blue	24v P-supply	-	-	-
Right Sagittal Plane	Start Home	X7	Digital-IN7	2	Blue/white	Brown	Control Box	White	P0.13	51
Right Sagittal Plane	2-Motion Task 1 (slow)	X7	Digital-IN4	3	Blue/white	White/Br	Control Box	White	P0.14	16
Right Sagittal Plane	2-Motion Task 2 (med)	X7	Digital-IN3	4	Blue/Red	Blue	Control Box	Red	P0.1	17
Right Sagittal Plane	2-Motion Task 3 (fast)	X7	Digital-IN2	9	Blue/Red	White/Blue	Control Box	Red	P0.2	49
Right Sagittal Plane	2-Motion Task 4	X7	Digital-IN1	10	Blue/Red	Green	Control Box			
Right Sagittal Plane	DCOM7	X7	DCOM7	1	Blue/white	White/Grn	Control Box	White	DGND	9
Left Sagittal Plane	11-Home Reference	X8	Digital-IN6	5	-		24v P-supply	-	-	-
Left Sagittal Plane	Enable	X8	Enable	4	-	Red	24v P-supply	-	-	-
Left Sagittal Plane	DCOM8	X8	DCOM8	3	-	Blue	24v P-supply	-	-	-
Left Sagittal Plane	Start Home	X7	Digital-IN7	2	Blue/Red	White/Grn	Control Box	Red	P0.3	47
Left Sagittal Plane	2-Motion Task 1 (slow)	X7	Digital-IN4	3	Blue/Red	Orange	Control Box	Red	P0.5	51
Left Sagittal Plane	2-Motion Task 2 (med)	X7	Digital-IN3	4	Blue/Red	White/Org	Control Box	Red	P0.6	16
Left Sagittal Plane	2-Motion Task 3 (fast)	X7	Digital-IN2	9	Blue/Red	Brown	Control Box	Red	P0.7	48
Left Sagittal Plane	2-Motion Task 4	X7	Digital-IN1	10	Blue/Red	White/Brn	Control Box			
Left Sagittal Plane	DCOM7	X7	DCOM7	1	Blue/white	White/Grn	Control Box	White	DGND	9
All	Enable	X8	Enable	4	Grey	Red	Control Box	Red	P0.0	52
All	DCOM8	X8	DCOM8	3	Grey	Black	Control Box	Red	DGND	18

available wires:

Blue	Brown
Blue	White/Br
Blue/White	Blue
Blue/White	White/Blu
Blue/White	Green
Blue/Red	White/Brn
Blue/Red	Green

Appendix C

Additional Kinematic Plots

Section 7.4 highlighted changes in the sagittal plane and focused on hip, knee and x-position of the heel. This appendix will add to the data by presenting hip, knee and estimated heel positions in the frontal plane, which can tell us information about scissoring and circumduction of the hip during swing. There are a couple pieces of information here that are unique including the vertical position of the top most sensor (attached to the theigh) which will give us an idea for how the hip hiking may have changed before and after training. The x-y heel trajectory of each participant is also shown here. While this is important information, I chose to focus on sagittal plane kinematics for this thesis.

Frontal Plane profiles are not corrected as of now because these videos were taken of the sagittal plane.

C.1   P1
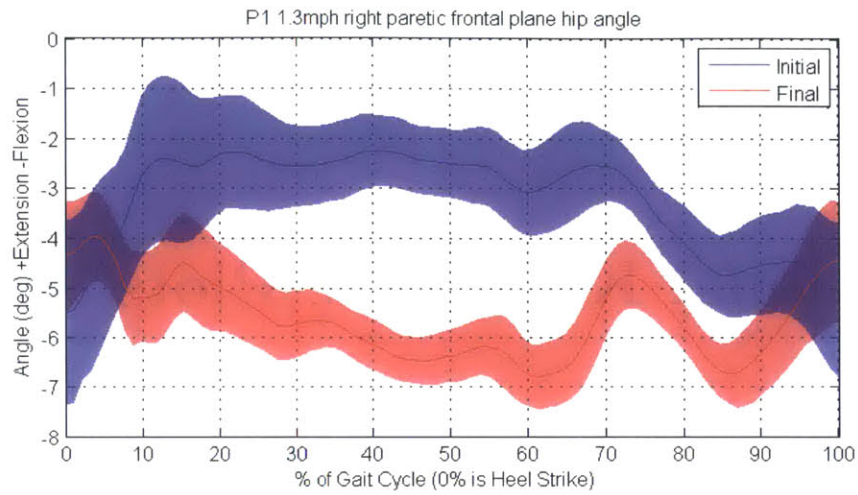
(a) Frontal Plane Hip Angle
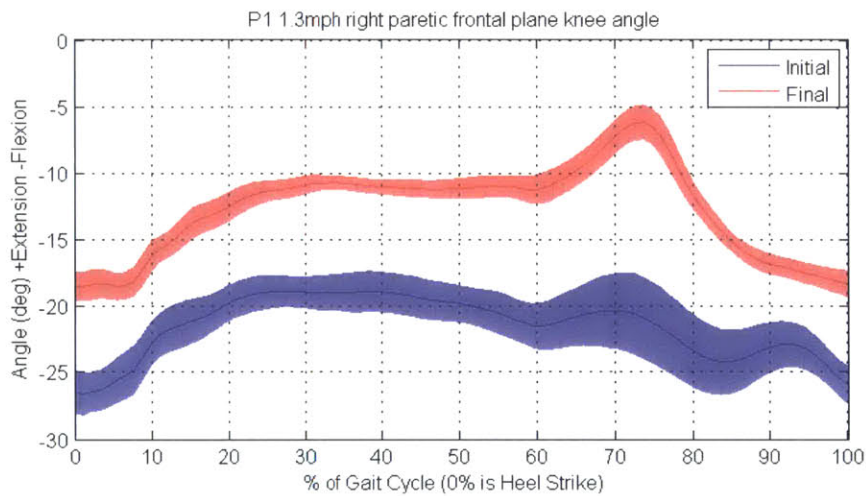
(b) Frontal Plane Knee Angle
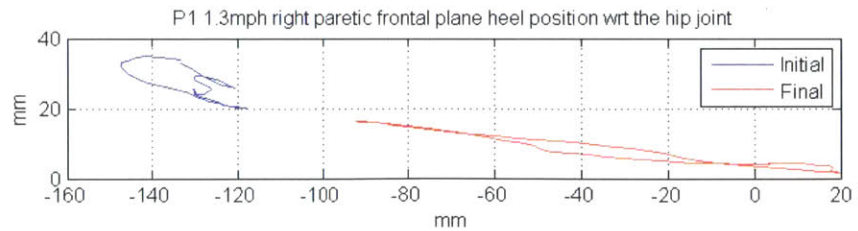
(c) Frontal Plane Average XY Plot

Figure C-1: P1 frontal plane

P1 1.3mph Average Left Heel Trajectory

(a) Left

P1 1.3mph Average Right Heel Trajectory
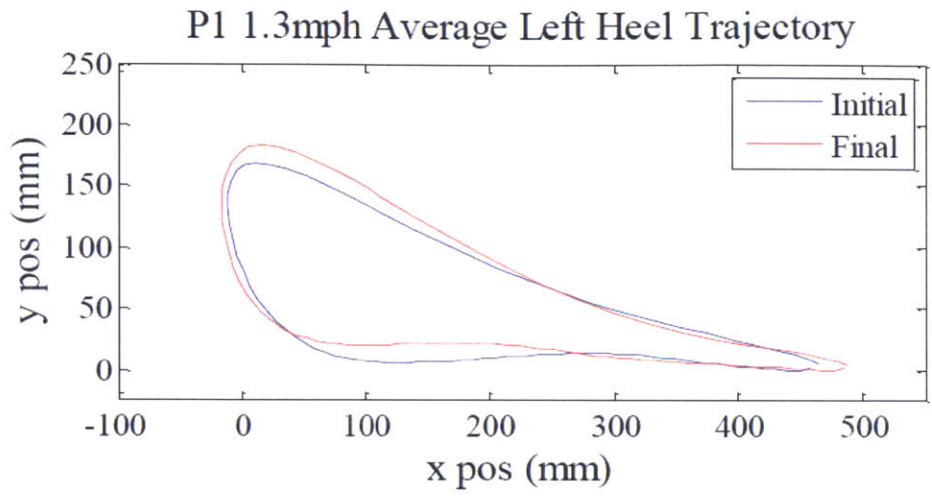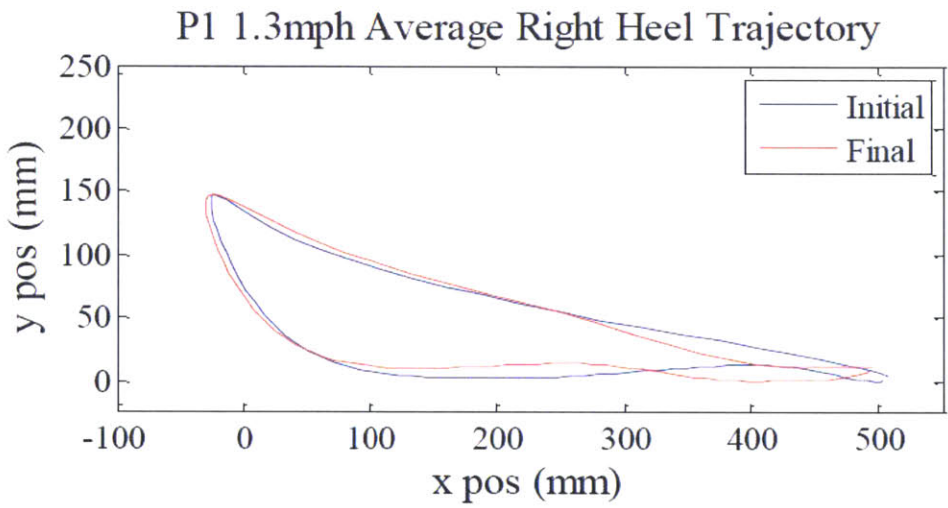
(b) Right

Figure C-2: P1 sagittal plane x-y trajectory (Positive is heel strike)

C.2 P2
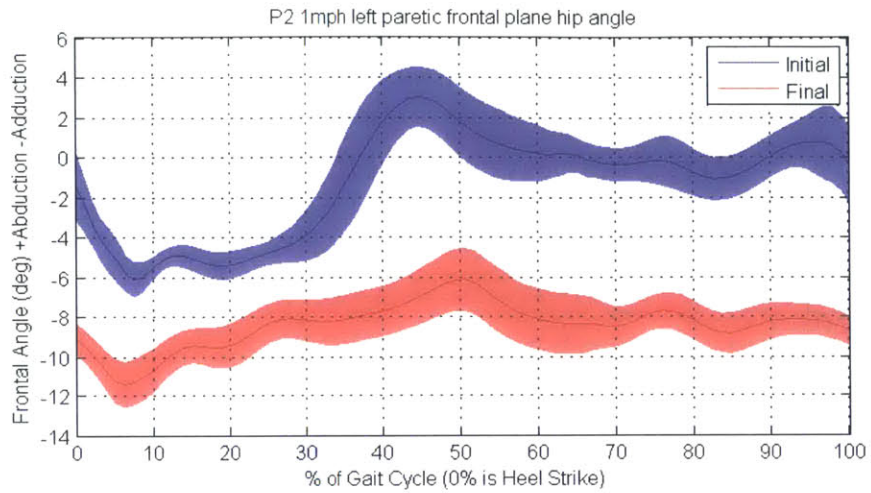
(a) Frontal Plane Hip Angle
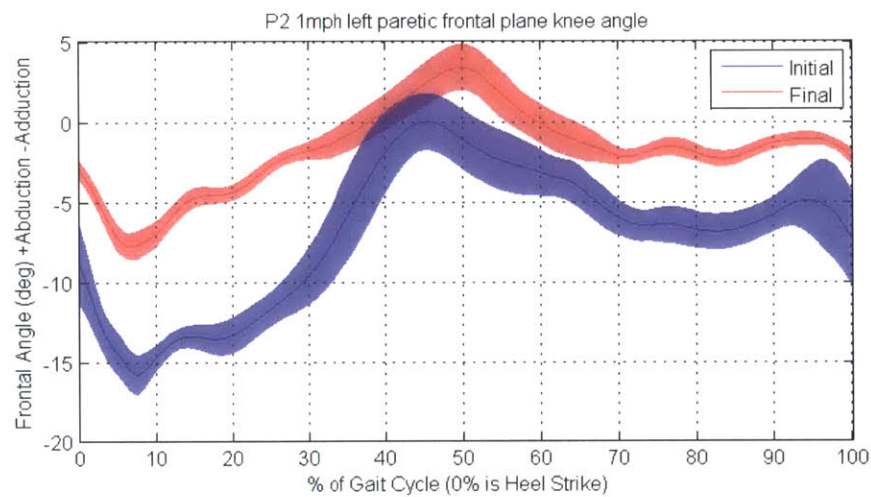
(b) Frontal Plane Knee Angle
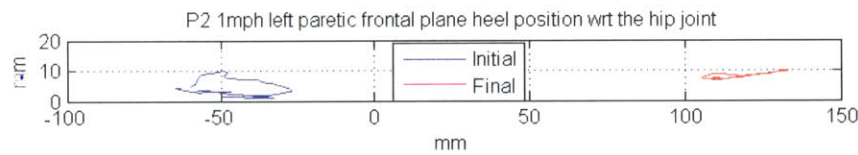
(c) Frontal Plane Average XY Plot

Figure C-3: P2 Frontal Plane
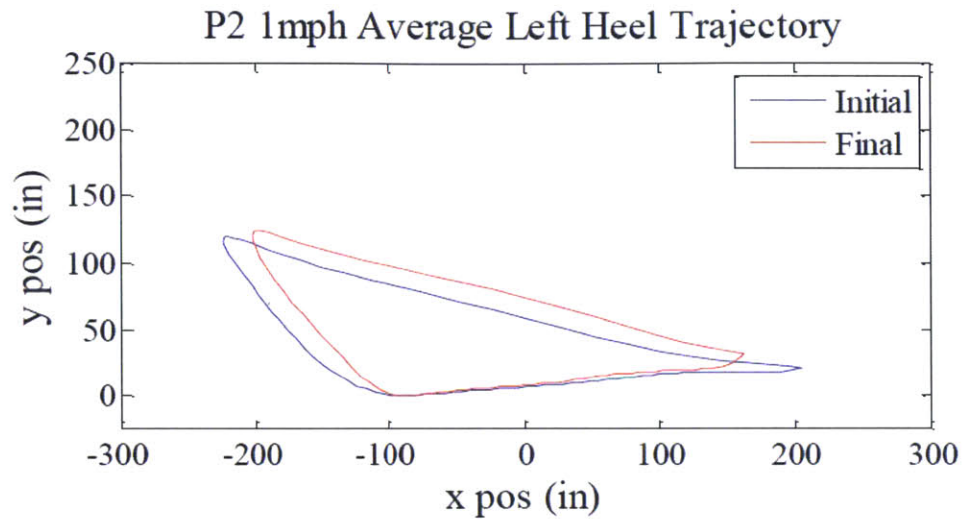
(a) Left
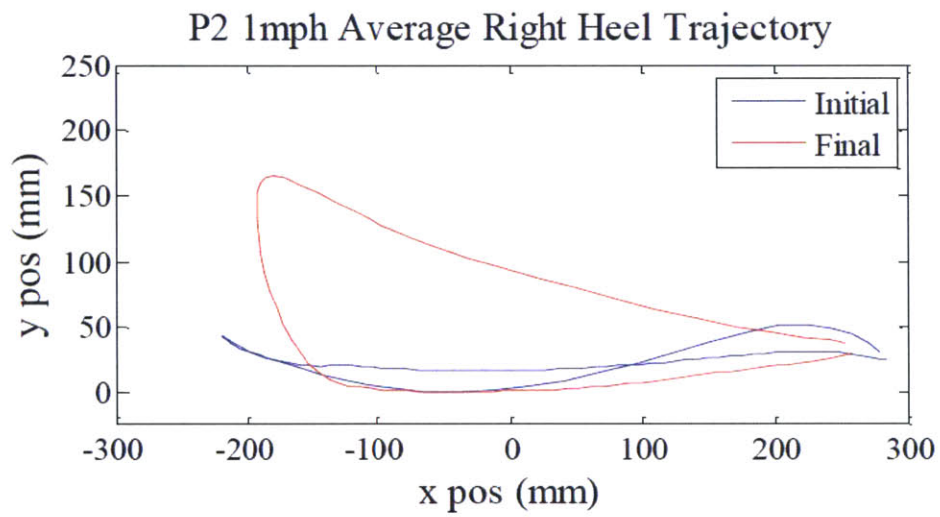
(b) Right

Figure C-4: P2 sagittal plane x-y trajectory (Positive is heel strike)
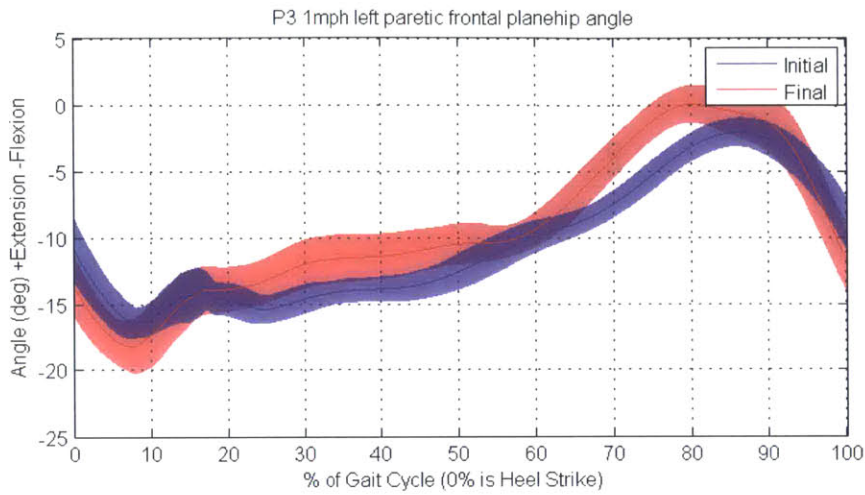
277

C.3 P3

(a) Frontal Plane Hip Angle
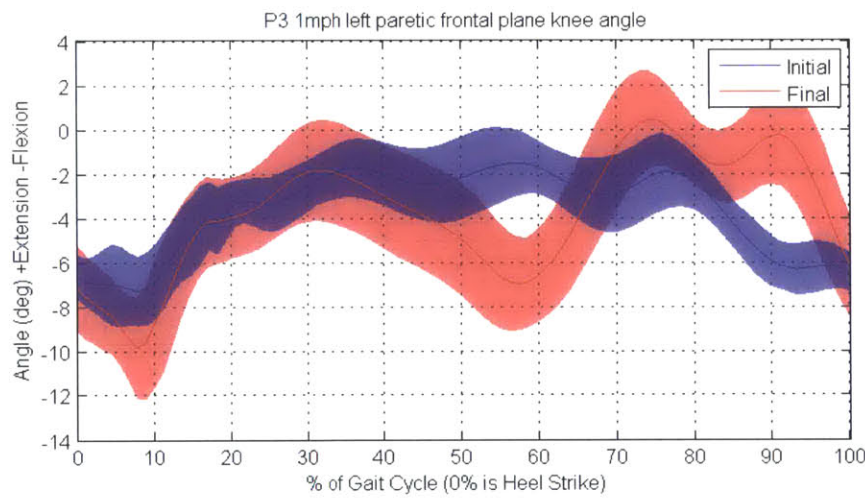
(b) Frontal Plane Knee Angle
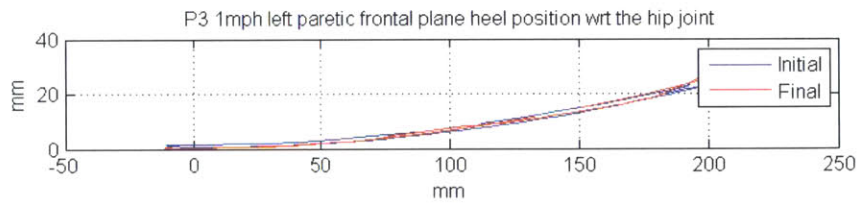
(c) Frontal Plane Average XY Plot

Figure C-5: P3 Frontal Plane
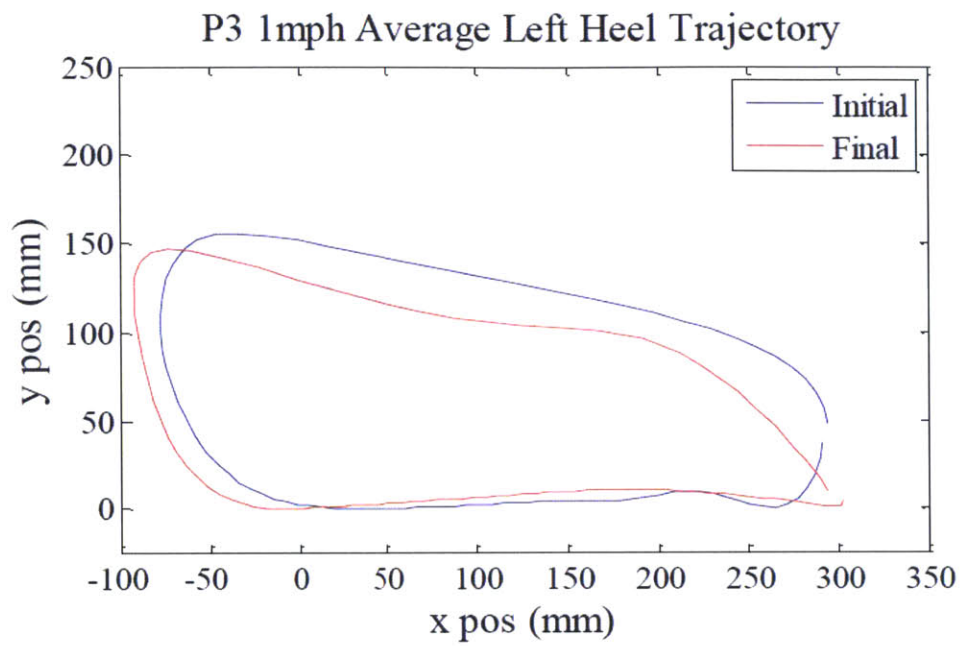
(a) Left
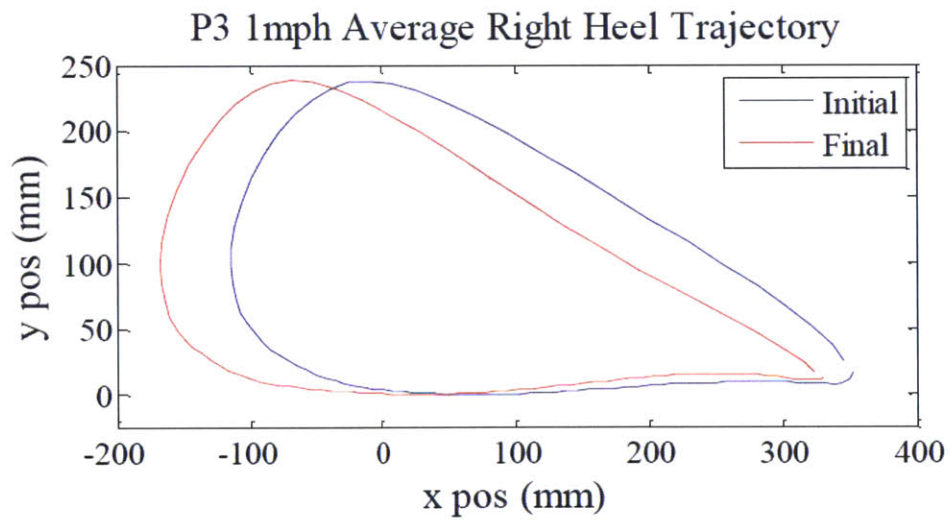
(b) Right

Figure C-6: P3 sagittal plane x-y trajectory (Positive is heel strike)

C.4 Healthy
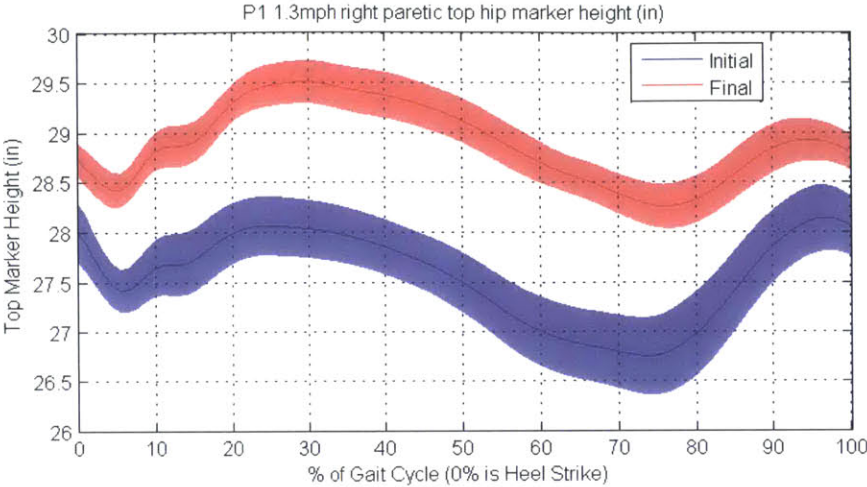
Figure C-7: P1 highest sensor vertical position
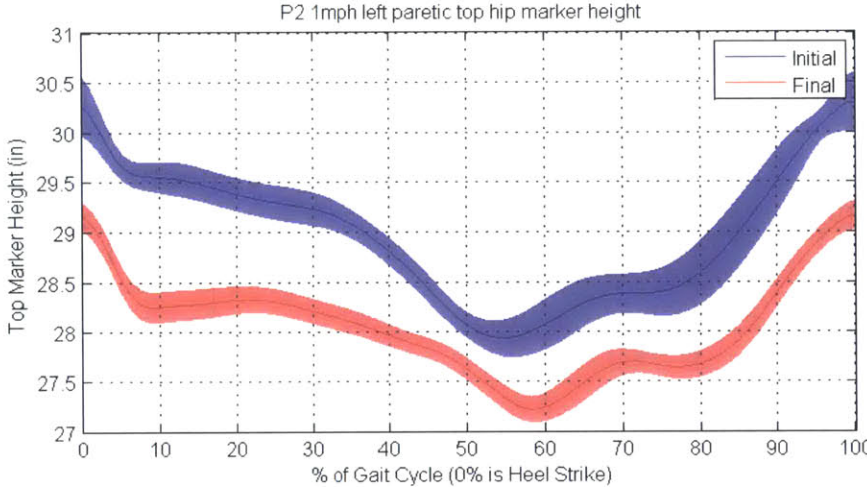
Figure C-8: P2 highest sensor vertical position
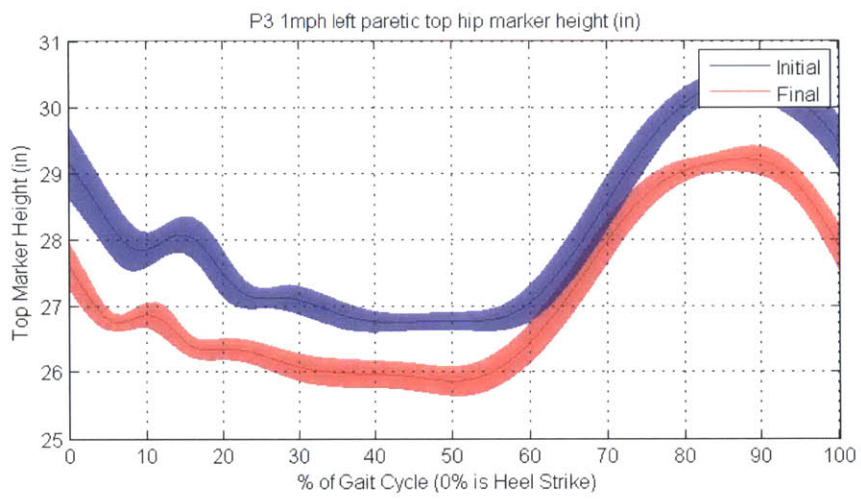
Figure C-9: P3 highest sensor vertical position
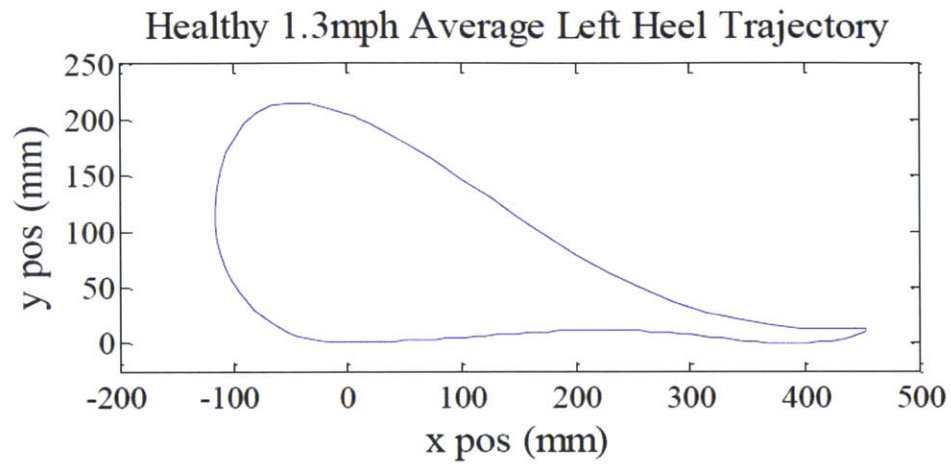
(a) Left
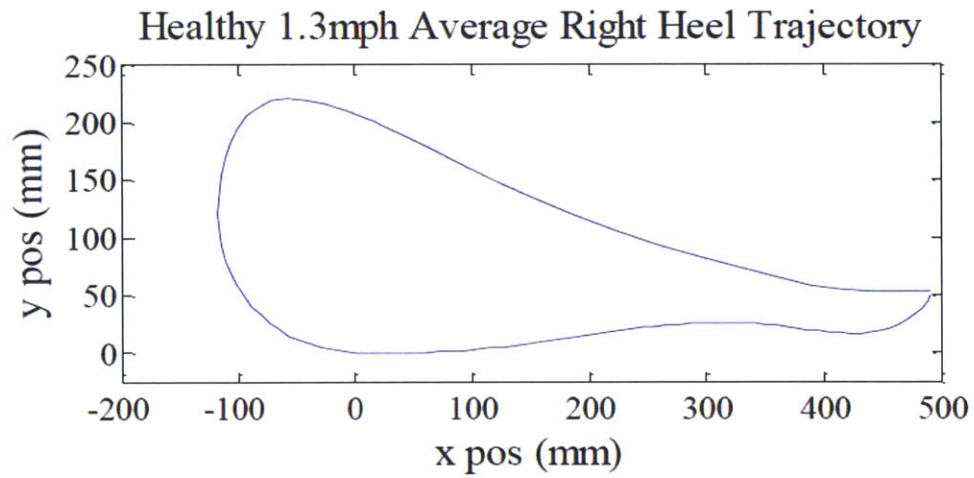
(b) Right

Figure C-10: Healthy sagittal plane x-y trajectory (Positive is heel strike)

Appendix D

Cycle Standard Deviation

Section 7.4.2 introduces the idea of cycle standard deviation as a measure that decreased consistently in all 12 measures studied as part of this thesis. This appendix shows the standard deviation for each gait cycle location. Each cycle standard deviation plot shows the standard deviations of both the ipsolateral and contralateral side of which the data was cut at heel strike. The reader can notice that depending on the side that the data is cut, the cycle standard deviation plot changes, with peaks coming in the contralateral swing phase in most cases. The plots here represent the x-position of the heel on the treadmill only.

The final plots show example histograms of the cycle standard deviation to show the skewness and non-normal profile and how they changed before and after training.
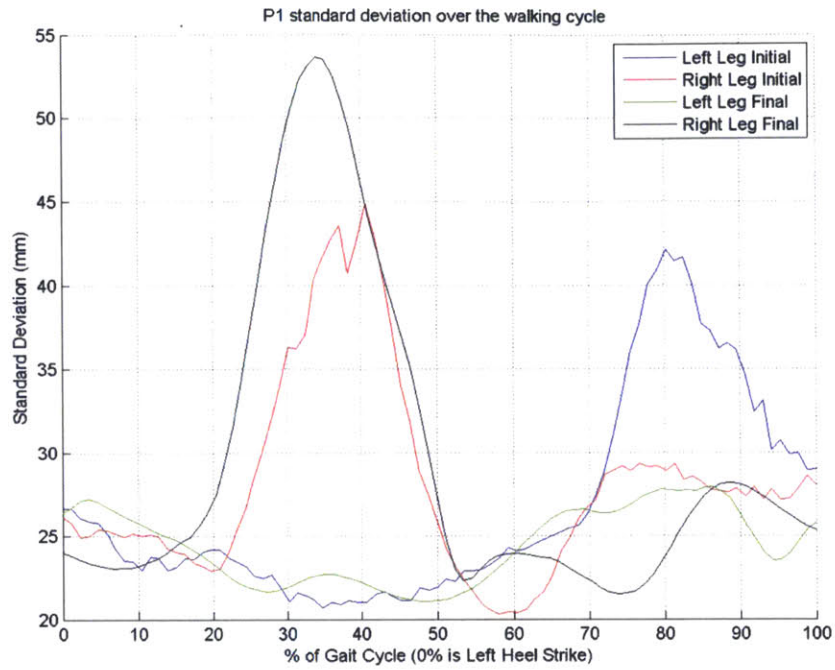
(a) Data cut on the left heel strike
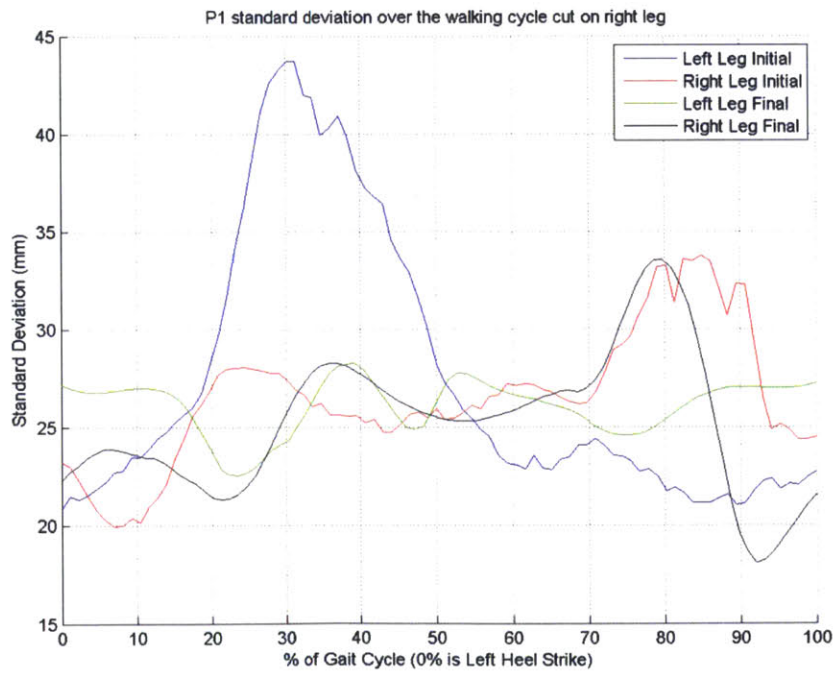
(b) Data cut on the right heel strike

Figure D-1: P1 standard deviation vs. walking cycle location
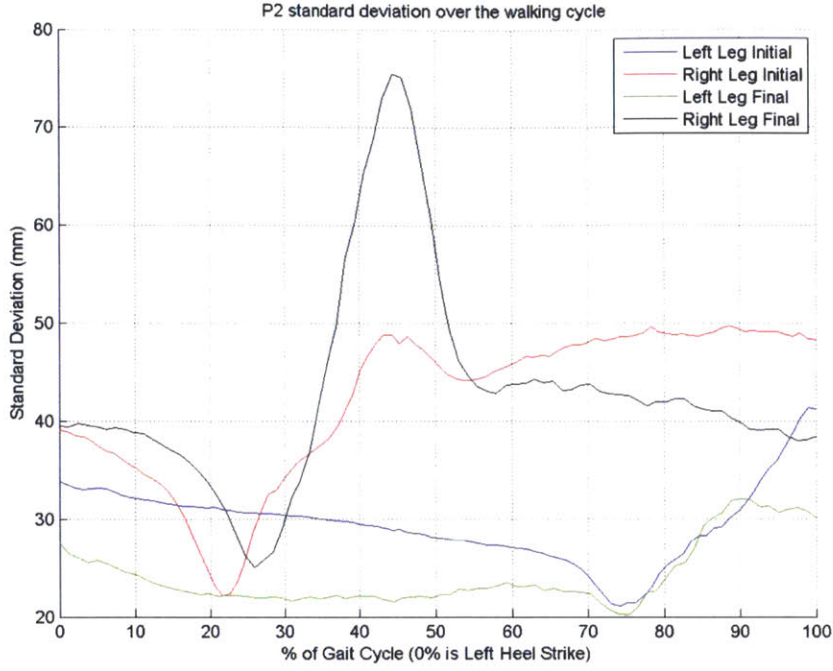
(a) Data cut on the left heel strike
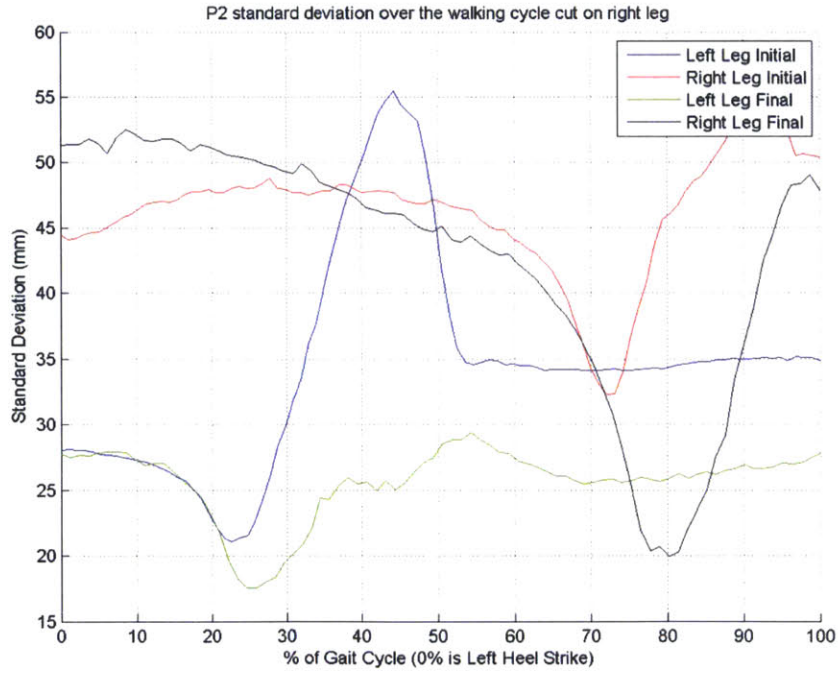
(b) Data cut on the right heel strike

Figure D-2: P2 standard deviation vs. walking cycle location
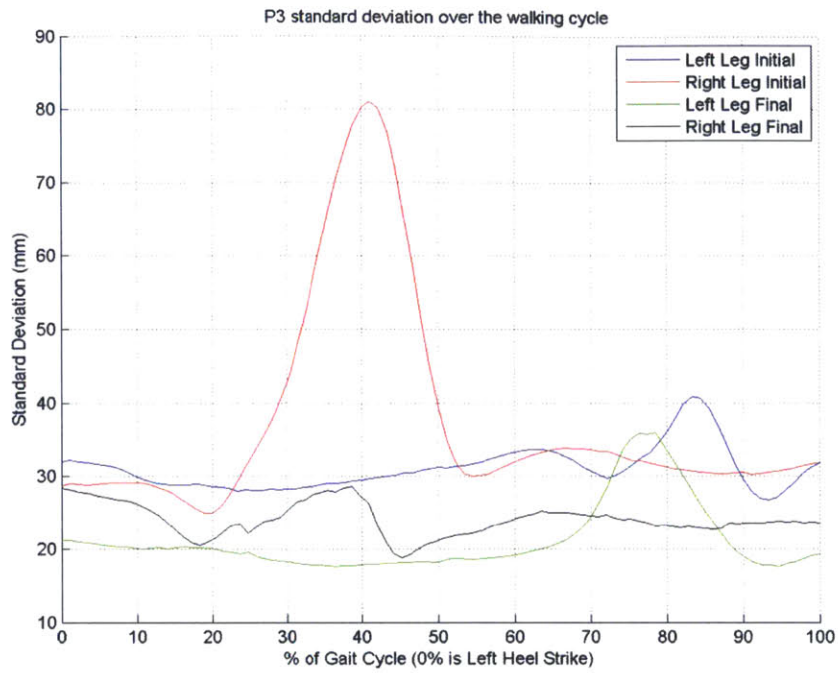
(a) Data cut on the left heel strike
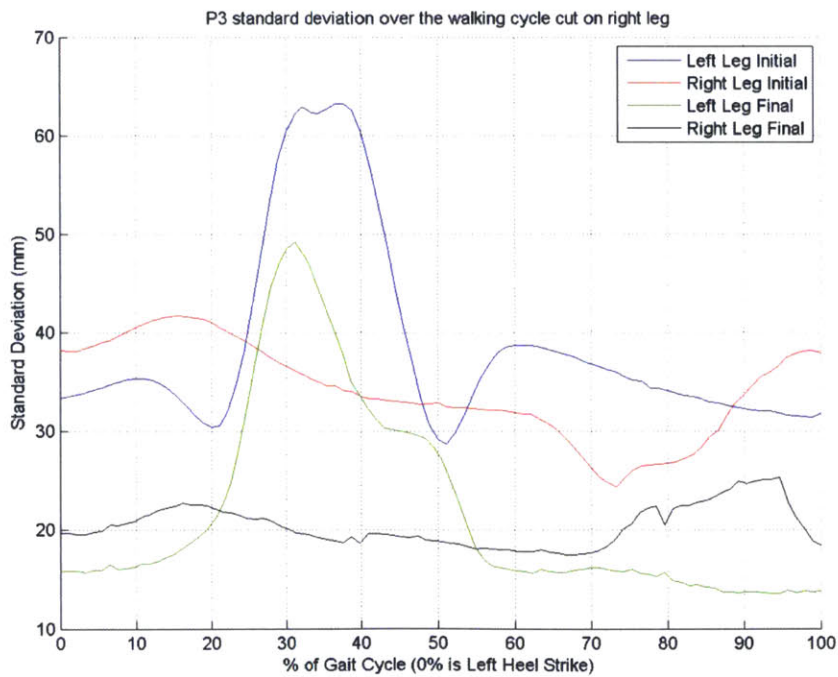
(b) Data cut on the right heel strike

Figure D-3: P3 standard deviation vs. walking cycle location

286
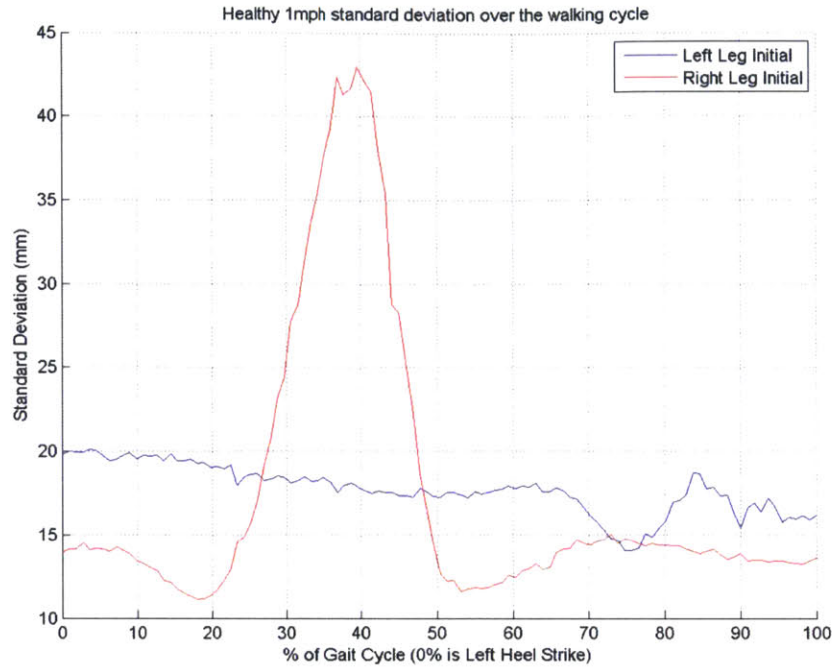
(a) Data cut on the left heel strike
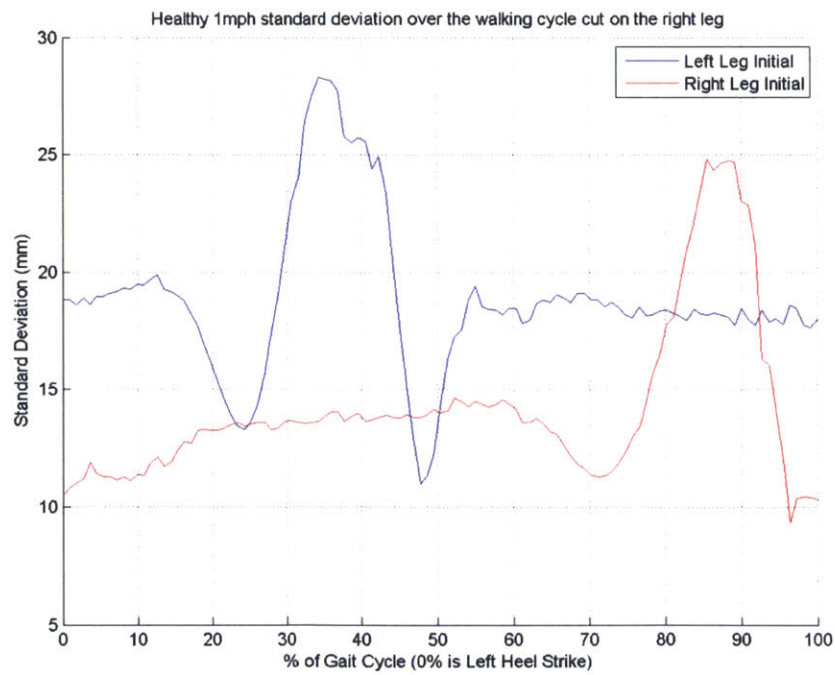
(b) Data cut on the right heel strike

Figure D-4: Healthy 1mph standard deviation vs. walking cycle location

287
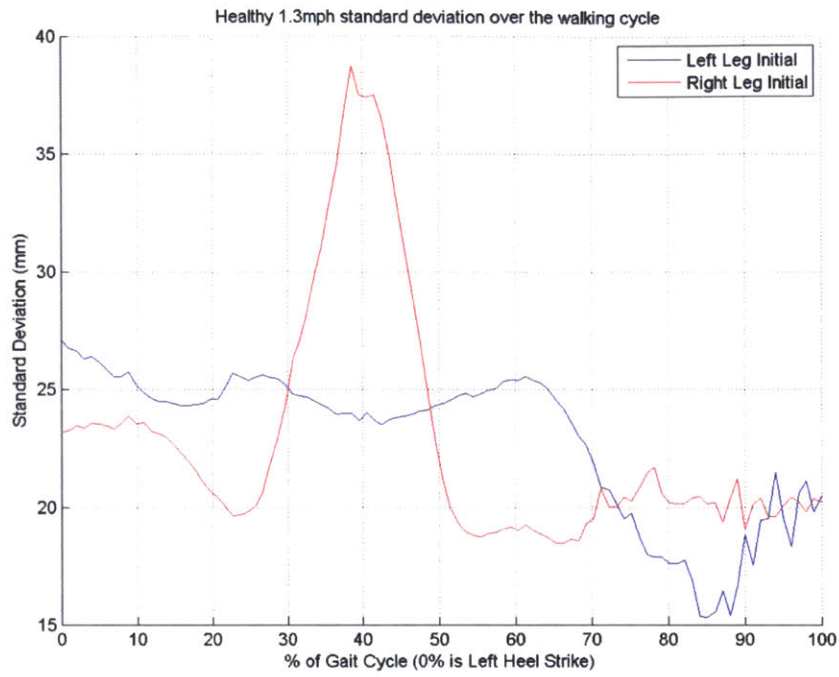
(a) Data cut on the left heel strike

(b) Data cut on the left right strike

Figure D-5: Healthy 1.3mph standard deviation vs. walking cycle location
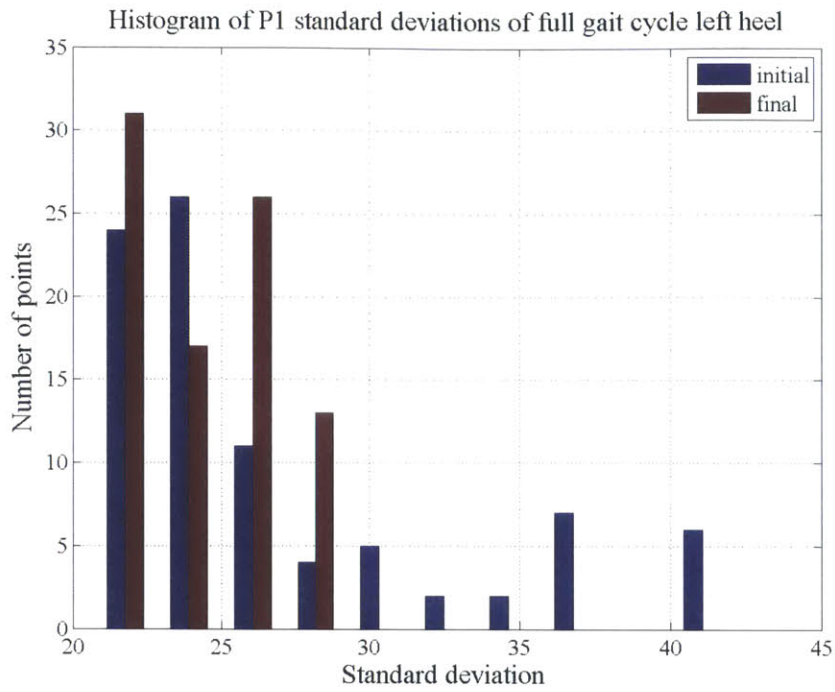
(a) P1 Histogram
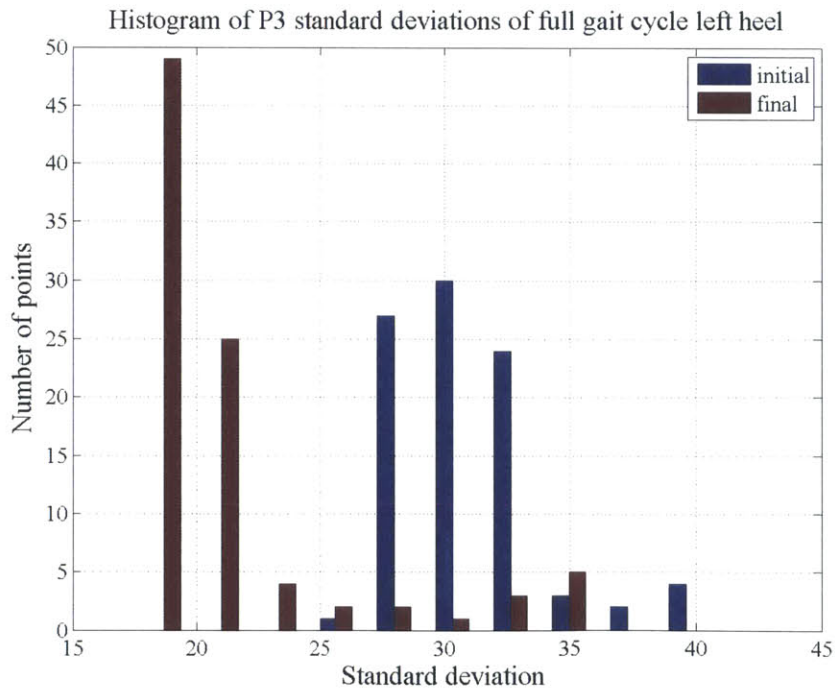
(b) P3 Histogram

Figure D-6: Histograms of the standard deviations over 15 strides

Appendix E

Additional Clinical Evaluation Data

This appendix contains additional clinical evaluations details, previously presented in section 7.3. Specifically, the full manual muscle test, range of motion and the stroke impact scale are reported for each participant. The improved Berg Balance Scale categories only for P2 are shown because he made such a significant improvement on this scale.

E.1 Participant 1 (P1)

Table E.1: P1 Right leg manual muscle test (scale 1-5)

	Initial	Final	Gain	Normal
Dorsiflexion	4	4	0	5
Plantarflexion	5	5	0	5
Ankle Inversion	4	4	0	5
Ankle Eversion	4	5	1	5
Knee Flexion	5	5	0	5
Knee Extension	5	5	0	5
Hip Adduction	5	5	0	5
Hip Abduction	5	5	0	5
Hip Flexion	4	5	1	5
Hip Extension	5	5	0	5

Table E.2: P1 Range of motion (reported in degrees)

		Initial	Final	Gain	Normal
Left ROM	Hip Extension	30	12	-18	30
	Hip Flexion (knee flexed)	90	105	15	100
	Hip Adduction	25	45	20	20
	Knee flexion	125	135	10	150
	Ankle Inversion	30	35	5	30
	Ankle Eversion	25	30	5	20
	Ankle Plantarflexion	40	38	-2	40
	Ankle Dorsiflexion	8	5	-3	20
Right ROM	Hip Extension	28	14	-14	30
	Hip Flexion (knee flexed)	90	107	17	20
	Hip Adduction	35	40	5	40
	Knee flexion	120	130	10	150
	Ankle Inversion	30	35	5	30
	Ankle Eversion	20	25	5	20
	Ankle Plantarflexion	30	40	10	40
	Ankle Dorsiflexion	5	0	-5	20

Table E.3: P1 Stroke Impact Scale by section

	Initial	Final	Gain	Normal
Physical problems	12	13	1	20
memory and thinking	35	35	0	35
Mood and emotions	43	44	1	45
Communication skills	35	35	0	35
Activities	50	50	0	50
Mobility	35	42	7	45
Ability to use affected hand	17	25	8	25
Activities	36	40	4	40
Recovery amount	50	80	30	100

E.2 Participant 2 (P2)

Table E.4: P2 Berg Balance Scale - areas of improvement (scale 0-4)

	Initial	Final	Gain	Normal
Sitting to standing	0	4	4	4
Standing unsupported	0	4	4	4
Standing to sitting	2	4	2	4
Transfers	3	4	1	4
Standing with eyes closed	0	4	4	4
Standing with feet together	0	3	3	4
Reaching forward	0	3	3	4
Retrieving object from floor	0	3	3	4
Turing to look behind	1	2	1	4
Turning 360 degrees	0	1	1	4
Standing with one leg in front	0	1	1	4

Table E.5: P2 Bilateral manual muscle test (scale 1-5)

		Initial	Final	Gain	Normal
Left Muscle tests	Dorsiflexion	5	3	-2	5
	Plantarflexion	4	1	-3	5
	Ankle Inversion	3	1	-2	5
	Ankle Eversion	3	1	-2	5
	Knee Flexion	3	3	0	5
	Knee Extension	5	5	0	5
	Hip Flexion	4	4	0	5
	Hip Extension	5	5	0	5
Right Muscle tests	Dorsiflexion	4	4	0	5
	Plantarflexion	4	4	0	5
	Ankle Inversion	4	2	-2	5
	Ankle Eversion	4	1	-3	5
	Knee Flexion	3	3	0	5
	Knee Extension	5	5	0	5
	Hip Flexion	3	4	1	5
	Hip Extension	5	5	0	5

Table E.6: P2 Range of motion (reported in degrees)

		Initial	Final	Gain	Normal
Left ROM	Hip Extension	3	5	2	30
	Hip Flexion (knee flexed)	90	100	10	100
	Hip Adduction	18	26	8	20
	Hip Abduction	22	28	6	40
	Knee flexion	120	115	-5	150
	Ankle Inversion	1	45	44	30
	Ankle Eversion	1	21	20	20
	Ankle Plantarflexion	40	55	15	40
	Ankle Dorsiflexion	0	2	2	20
Right ROM	Hip Extension	-5	0	5	30
	Hip Adduction	20	28	8	20
	Hip Abduction	32	28	-4	40
	Knee flexion	113	115	2	150
	Ankle Inversion	1	25	24	30
	Ankle Eversion	1	30	29	20
	Ankle Plantarflexion	36	30	-6	40
	Anle Dorsiflexion	0	10	10	20

Table E.7: P2 Stroke Impact Scale by section

	Initial	Final	Gain	Normal
Physical problems	12	15	3	20
memory and thinking	35	35	0	35
Mood and emotions	30	29	-1	45
Communication skills	35	35	0	35
Activities	49	48	-1	50
Mobility	35	38	3	45
Ability to use affected hand	25	25	0	25
Activities	40	40	0	40
Recovery amount	50	50	0	100

E.3 Participant 3 (P3)

Table E.8: P3 Left impaired leg manual muscle test (scale 1-5)

	Initial	Final	Gain	Normal
Dorsiflexion	0	0	0	5
Plantarflexion	0	0	0	5
Ankle Inversion	0	0	0	5
Ankle Eversion	0	0	0	5
Knee Flexion	4	4	0	5
Knee Extension	4	5	1	5
Hip Adduction	4	5	1	5
Hip Abduction	4	4	0	5
Hip Flexion	3	4	1	5
Hip Extension	3	3	0	5

Table E.9: P3 Left impaired leg range of motion (reported in degrees)

	Initial	Final	Gain	Normal
Hip Extension	5	10	5	30
Hip Flexion (knee flexed)	100	107	7	100
Hip Adduction	10	16	6	20
Hip Abduction	20	28	8	40
Knee flexion	90	130	40	150
Ankle Inversion	0	32	32	30
Ankle Eversion	0	28	28	20
Ankle Plantarflexion	0	29	29	40
Ankle Dorsiflexion	0	0	0	20

Table E.10: P3 Stroke Impact Scale by section

	Initial	Final	Gain	Normal
Physical problems	6	7	1	20
Memory and thinking	33	28	-5	35
Mood and emotions	27	29	2	45
Communication skills	31	25	-6	35
Activities	23	29	6	50
Mobility	36	35	-1	45
Ability to use affected hand	5	5	0	25
Activities	13	17	4	35
Recovery amount	10	20	10	100

Appendix F

Participant Exit Interviews

After completing the full month of training, participants were given the following questionnaire to assess their feelings towards the device and their experience.

Skywalker Exit interview   *Name:* **P1**

1. I was comfortable with my Skywalker therapy sessions

   1   2   3   4   (5)

2. I enjoyed doing therapy with the Skywalker system

   1   2   3   4   (5)

3. I believe the robot therapy sessions were beneficial to me

   1   2   3   (4)   5

4. Working with the robot helps me in ways that nobody can

   1   2   3 . (4)   5   .

5. I would like to perform more Skywalker training sessions in the future

   1   2   3   4   (5)

6. The Body weight support system was comfortable

   1   2   3   4   (5)

7. The process of getting on and off the machine would make me less likely to want to use this system in the future

   (1)   2   3   4   5

Please write in how you feel about the following issues of the machine:

Tell us what you liked most about your experience with the Skywalker system.

I liked that I was able to view my gait and try new strategies for fixing it without the fear of falling or ~~~~ stumbling.

Which of the Skywalker training sessions (rhythmic, discrete or the balance) do you think benefitted you the most and why?

I think discrete helped me the most to pick up my feet and dorsiflex ~~~~ which kept me from stumbling

Did you ever experience discomfort or pain due to your activities with the Skywalker system? Please explain.

Just natural soreness from exersize

If you believe you received benefits from training on the Skywalker machine, do you think that training for another month would benefit you to a greater degree?

Yes

Here's your chance to tell us what could be better. We will take this section very seriously so think hard about what we didn't quite get right.

I think the balance part should rock forward and back as well as side to side.

Any additional comments?

I'll miss you guys! Thanks so much

Skywalker Exit interview   *Name:P2*

Please circle the number corresponding with your answer as defined below:

1:Strongly disagree   2:Disagree Somewhat   3:Neutral   4:Agree somewhat   5:Strongly agree

1. I was comfortable with my Skywalker therapy sessions 2

    1   2   3   4   5

2. I enjoyed doing therapy with the Skywalker system 4

    1   2   3   4   5

3. I believe the robot therapy sessions were beneficial to me 3

    1   2   3   4   5

4. Working with the robot helps me in ways that nobody can 4

    1   2   3   4   5

5. I would like to perform more Skywalker training sessions in the future 3

    1   2   3   4   5

6. The Body weight support system was comfortable 2 It triggered spasticity.

    1   2   3   4   5

7. The process of getting on and off the machine would make me less likely to want to use this system in the future 5 The process of getting on/off must be improved.

    1   2   3   4   5

Please write in how you feel about the following issues of the machine:

Tell us what you liked most about your experience with the Skywalker system.

Interacting with Tyler and Igo and learning about their research and the theory of energy conservation in gait mechanics. The Skywalker machine itself is an impressive piece of engineering.

Which of the Skywalker training sessions (rhythmic, discrete or the balance) do you think benefitted you the most and why?

I can't say that any one type of training was most beneficial. I think what I've come away with overall is a greater sense of my own gait mechanics. For example, now I try to remember to stand up straighter while I walk and be more mindful of knee bends and the distance between my feet as ways to conserve energy.

Did you ever experience discomfort or pain due to your activities with the Skywalker system? Please explain.

During Week 1 it took one or two days to get the Body weight settings correct – this is understandable. For moderate/extreme disability I would suggest at least 1 day just getting used to Skywalker.

If you believe you received benefits from training on the Skywalker machine, do you think that training for another month would benefit you to a greater degree?

Not certain.

Here's your chance to tell us what could be better. We will take this section very seriously so think hard about what we didn't quite get right.

Entry/exit onto Skywalker – It took two people to help me get on and off. This should be corrected so that a disabled person can do so independently.

Input from a clinician (PT?) **during** the training sessions might be useful.

Some form of participant incentive (cab voucher/gift card?) should be available.

Any additional comments?

I participated for the sake of science, but in the future I think I would need some form of minimal participant incentive and to be working part-time or not at all (retired). The conversations with Tyler and Igo were very interesting. I'm not sure that the Skywalker had long-term benefits for me – but if it helps others, it's certainly worth developing further.

Skywalker Exit interview

Name: P3

Please circle the number corresponding with your answer as defined below:

1:Strongly disagree   2:Disagree Somewhat   3:Neutral   4:Agree somewhat   5:Strongly agree

1. I was comfortable with my Skywalker therapy sessions

    1   2   3   4   (5)

2. I enjoyed doing therapy with the Skywalker system

    1   2   3   4   (5)

3. I believe the robot therapy sessions were beneficial to me

    1   2   3   4   (5)

4. Working with the robot helps me in ways that nobody can

    1   2   3   4   (5)

5. I would like to perform more Skywalker training sessions in the future

    1   2   3   4   (5)

6. The Body weight support system was comfortable

    1   2   (3)   4   5

7. The process of getting on and off the machine would make me less likely to want to use this system in the future

    (1)   2   3   4   5

Please write in how you feel about the following issues of the machine:

Tell us what you liked most about your experience with the Skywalker system.

Positive attitude of Tyler + Igo was very inspiring for me. Enjoyed the way the machine helped me walk w/ symmetry — I found this very empowering. What a joy to feel like I was walking powerfully as can! purposefully!

Which of the Skywalker training sessions (rhythmic, discrete or the balance) do you think benefitted you the most and why? Rythmic — finding a smooth rythm to my gait made walking easier, seemed more natural — I almost had a sense of "power walking" — balance was difficult — a great exercise — the balance didn't really knock me off balance enough to challenge me —

Did you ever experience discomfort or pain due to your activities with the Skywalker system?
Please explain.

Pain had to do with my own "spasticity" — muscles pulling against each other. Pain always increase w/ exercise... did this before skywalker to.

If you believe you received benefits from training on the Skywalker machine, do you think that training for another month would benefit you to a greater degree?

Yes.

Here's your chance to tell us what could be better. We will take this section very seriously so think hard about what we didn't quite get right.

Can't think of anything! I loved every minute — honostly!

Balance needed to be harder to be a challenge. I didn't feel that it challenged my balance.

Any additional comments?

Skywalker was possibly easier for me because I was fairly fit before I started — I was used to working out (athlete before my stroke) (plus I work out often now) and I enjoyed the physical challenge of the skywalker... found it empowering! ☺

Appendix G

COUHES Study Protocol and Consent Form

The feasibility study was approved following a full board review by the MIT Committee on the Use of Humans as Experimental Subjects (COUHES). The following pages detail the study protocol and consent forms used for this study.

To:	Hermano Krebs 3-137
From:	Leigh Firn, Chair COUHES
Date:	06/24/2014
Committee Action:	**Approval**
COUHES Protocol #:	1406006427
Study Title:	Skywalker - Actuated Split Treadmill with Body Weight Support: A Novel Technology for Gait Rehabilitation of Person with Impairment due to Stroke and Cerebral Palsy
Expiration Date:	06/18/2015

The above-referenced protocol has been APPROVED following Full Board Review by the Committee on the Use of Humans as Experimental Subjects (COUHES).

If the research involves collaboration with another institution then the research cannot commence until COUHES receives written notification of approval from the collaborating institution's IRB.

It is the Principal Investigator's responsibility to obtain review and continued approval before the expiration date. Please allow sufficient time for continued approval. You may not continue any research activity beyond the expiration date without COUHES approval. Failure to receive approval for continuation before the expiration date will result in the automatic suspension of the approval of this protocol. Information collected following suspension is unapproved research and cannot be reported or published as research data. If you do not wish continued approval, please notify the Committee of the study termination.

Adverse Events: Any serious or unexpected adverse event must be reported to COUHES within 48 hours. All other adverse events should be reported in writing within 10 working days.

Amendments: Any changes to the protocol that impact human subjects, including changes in experimental design, equipment, personnel or funding, must be approved by COUHES before they can be initiated.

Prospecitve new study personnel must, where applicable, complete training in human subjects research and in the HIPAA Privacy Rule before participating in the study.

COUHES should be notified when your study is completed. You must maintain a research file for at least 3 years after completion of the study. This file should include all correspondence with COUHES, original signed consent forms, and study data.

CONSENT TO PARTICIPATE IN
BIOMEDICAL RESEARCH

Actuated Split Treadmill with Body Weight Support:
A Novel Technology for Gait Rehabilitation

Stroke and Cerebral Palsy Subjects

You are asked to participate in a research study conducted by Dr. Hermano Igo Krebs and Tyler Susko from the Mechanical Engineering Department at the Massachusetts Institute of Technology (M.I.T). You have been asked to participate in this study because you have known impairments due to a stroke or cerebral palsy. You should read the information below, and ask questions about anything you do not understand, before deciding whether or not to participate.

• PARTICIPATION AND WITHDRAWAL

Your participation in this research is completely VOLUNTARY. If you choose to participate you may subsequently withdraw from the study at any time without penalty or consequences of any kind. If you choose not to participate, that will not affect your relationship with M.I.T.

• PURPOSE OF THE STUDY

Gait impairment is the primary impairment that limits independence of individuals disabled by stroke and cerebral palsy. The actuated, Skywalker split treadmill with body weight support (BWS), used in this study was designed to allow patients to begin gait therapy sooner. The main purpose of this study is to conduct initial safety, tolerability, and training feasibility tests of the device by affected persons. In this phase, we will restrict our research to adult subjects with impairment due to stroke or cerebral palsy to determine comfort using the device and changes in self-selected speed after a 4-weeks 12 session training.

• PROCEDURES

If you volunteer to participate in this study, we would ask you to do the following things:

You will be asked to: 1) walk on the treadmill at a speed comfortable to you (you will determine what is a comfortable speed), 2) walk on the Skywalker with partial body weight support (PBWS) at the speed comfortable to you, 3) allow total weight support and not interfere with the Skywalker while it propels your legs at the speed comfortable to you, 4) self-report of comfort while using the Skywalker with body weight support, and 5) undergo 12 1-hour session in a 4-week period walking on the Skywalker treadmill with body weight support at the speed comfortable to you, and 7) undergo a batch of standard clinical tests.

- **POTENTIAL RISKS AND DISCOMFORTS**
Treadmill

You will be walking on a treadmill. The treadmill is electrically powered and capable of moving independently, but that to minimize the risk of injury it has been equipped with multiple levels of safety protection. First, the Skywalker treadmill meets or exceeds electrical safety standards for clinical use. Second, the proper functioning of all parts of this robotic treadmill, including the software, the computer, the electronics and the mechanism, are independently monitored. In the event that you will want to stop the device you can do so by pressing a button. You also understand that you may stop the robotic treadmill at any time by asking the investigator to do so.

Body Weight Support

The body weight support consists of a bicycle seat and a chest harness. It can be uncomfortable and you might feel some chaffing after an hour use. In the event that you will want to stop the device you can do so by pressing a button. You also understand that you may stop the robotic treadmill at any time by asking the investigator to do so.

Physiological Risks

We will measure your heart rate at enrollment, while walking on a treadmill at your own pace. We will then continuously monitor your heart rate. If your heart rate will go beyond the maximum heart rate observed during the initial measurement, we will stop the training on that day and might have to discontinue the training.

You understand that comparable technology has been used for over two decades in studies at M.I.T. and for over ten years in several rehabilitation hospitals and that a 100% safety record has been maintained.

The treatment or procedure may involve risks that are currently unforeseeable.

- **ANTICIPATED BENEFITS TO SUBJECTS**

You should not expect your condition to improve as a result of participating in this research.

- **ANTICIPATED BENEFITS TO SOCIETY**

The potential benefits to society are significant and substantial. The development of lower extremity robotics devices for the rehabilitation of walking has the potential to serve not only the stroke and cerebral palsy population, but also numerous other clinical patient groups including multiple sclerosis, Parkinson's disease, spinal cord injury, hip fracture, and other orthopedic syndromes. The greatest potential benefit is to include many more patients currently unable to actively participate in exercise-based locomotor

rehabilitation. Related is the opportunity to optimize neurorehabilitation therapies based on massed practice and other motor learning principles. The device will further expand the technology available to serve our aging population.

- **ALTERNATIVES TO PARTICIPATION**

n/a

- **PAYMENT FOR PARTICIPATION**

None. One session of participation will take about 1 hour and 30 minutes.

- **POSSIBLE COMMERCIAL PRODUCTS**

Dr. H. I. Krebs is a co-inventor of the MIT-held patents for the robotic devices used to treat patients in this work. He holds equity positions in Interactive Motion Technologies, Inc., a company that manufacturers this type of technology under license from MIT. If the study demonstrates the robot-mediated movement therapy is beneficial, companies producing this kind of technology, including Interactive Motion Technologies, may point to our results.

- **FINANCIAL OBLIGATION**

Neither you nor your insurance company will be billed for your participation in this research.

- **PRIVACY AND CONFIDENTIALITY**

The only people who will know that you are a research subject are members of the research team and, if appropriate, your physicians and nurses. No information about you, or provided by you during the research will be disclosed to others without your written permission, except: if necessary to protect your rights or welfare, or if required by law.

When the results of the research are published or discussed in conferences, no information will be included that would reveal your identity. If photographs, videos, or audio-tape recordings of you will be used for educational purposes, we will request for your written authorization. Participation in this study does not hinge on you agreeing to be photographed.

Authorized representatives of the Food and Drug Administration (FDA) may need to review records of individual subjects. As a result, they may see your name; but they are bound by rules of confidentiality not to reveal your identity to others.

- **WITHDRAWAL OF PARTICIPATION BY THE INVESTIGATOR**

The investigators may withdraw you from participating in this research if circumstances arise which warrant doing so. If you experience any joint pain or if you become ill during the research, you may have to drop out, even if you would like to continue. The investigators and Dr. Krebs, will make the decision and let you know if it is not possible for you to continue. The decision may be made either to protect your health and safety, or because it is part of the research plan that people who develop certain conditions may not continue to participate.

- **NEW FINDINGS**

During the course of the study, you will be informed of any significant new findings (either good or bad), such as changes in the risks or benefits resulting from participation in the research or new alternatives to participation, that might cause you to change your mind about continuing in the study. If new information is provided to you, your consent to continue participating in this study will be re-obtained.

- **EMERGENCY CARE AND COMPENSATION FOR INJURY**

If you feel you have suffered an injury, which may include emotional trauma, as a result of participating in this study, please contact the person in charge of the study as soon as possible.

In the event you suffer such an injury, M.I.T. may provide itself, or arrange for the provision of, emergency transport or medical treatment, including emergency treatment and follow-up care, as needed, or reimbursement for such medical services. M.I.T. does not provide any other form of compensation for injury. In any case, neither the offer to provide medical assistance, nor the actual provision of medical services shall be considered an admission of fault or acceptance of liability. Questions regarding this policy may be directed to MIT's Insurance Office, (617) 253-2823. Your insurance carrier may be billed for the cost of emergency transport or medical treatment, if such services are determined not to be directly related to your participation in this study.

- **IDENTIFICATION OF INVESTIGATORS**

In the event of a research related injury or if you experience an adverse reaction, please immediately contact one of the investigators listed below. If you have any questions about the research, please feel free to contact:

Principal Investigator: Dr. Krebs at (617)253-8112
Address: 77 Massachusetts Ave (Rm 3-137), Cambridge, MA 02139

- **RIGHTS OF RESEARCH SUBJECTS**

You are not waiving any legal claims, rights or remedies because of your participation in this research study. If you feel you have been treated unfairly, or you have questions

regarding your rights as a research subject, you may contact the Chairman of the Committee on the Use of Humans as Experimental Subjects, M.I.T., Room E25-143B, 77 Massachusetts Ave, Cambridge, MA 02139, phone 1-617-253 6787.

SIGNATURE OF RESEARCH SUBJECT OR LEGAL REPRESENTATIVE

I have read (or someone has read to me) the information provided above. I have been given an opportunity to ask questions and all of my questions have been answered to my satisfaction. I have been given a copy of this form.

BY SIGNING THIS FORM, I WILLINGLY AGREE TO PARTICIPATE IN THE RESEARCH IT DESCRIBES.

_____

Name of Subject

_____

Name of Legal Representative (if applicable)

_____   _____

Signature of Subject or Legal Representative   Date

SIGNATURE OF INVESTIGATOR

I have explained the research to the subject or his/her legal representative and answered all of his/her questions. I believe that he/she understands the information described in this document and freely consents to participate.

_____

Name of Investigator

_____   _____

Signature of Investigator   Date (must be the same as subject's)

SIGNATURE OF WITNESS (If required by COUHES)

My signature as witness certified that the subject or his/her legal representative signed this consent form in my presence as his/her voluntary act and deed.

_____

Name of Witness

_____   _____

Signature of Witness   Date

SIGNATURE OF RESEARCH SUBJECT OR LEGAL REPRESENTATIVE VIDEO or PHOTO RELEASE

In the interest of promoting education, learning, and/or public relations, I agree to be videotaped/photographed in connection with my research participation at the Massachusetts Institute of Technology (MIT) with the agreement of the principal investigator (Dr. Krebs). I understand that I will not be reimbursed for the photos or videotapes.

I further understand that it is not necessary for me to sign the photo or video release to participate in this study. Participation in this study does not hinge on you agreeing to be photographed. I have been given an opportunity to ask questions and all of my questions have been answered to my satisfaction.

BY SIGNING THIS FORM, I WILLINGLY RELEASE PHOTOS or VIDEO-TAPES.

_____

Name of Subject

_____

Name of Legal Representative (if applicable)

_____   _____

Signature   Date

Bibliography

[1] Susan E. Fasoli, Hermano I. Krebs, Joel Stein, Walter R. Frontera, and Neville Hogan. Effects of robotic therapy on motor impairment and recovery in chronic stroke. *Archives of physical medicine and rehabilitation*, 84(4):477482, 2003.

[2] C. Werner, S. von Frankenberg, T. Treig, M. Konrad, and S. Hesse. Treadmill training with partial body weight support and an electromechanical gait trainer for restoration of gait in subacute stroke patients a randomized crossover study. *Stroke*, 33(12):2895–2901, December 2002.

[3] Tyler Susko and Hermano Igo Krebs. MIT-skywalker: A novel environment for neural gait rehabilitation. In *Biomedical Robotics and Biomechatronics (2014 5th IEEE RAS & EMBS International Conference on*, pages 677–682. IEEE, 2014.

[4] Tyler Susko and H.I. Krebs. IR vision system for the estimation of gait phase of the MIT-skywalker. In *Northeast Bioengineering Conference (NEBEC), 2014 40th Annual*, pages 1–2, April 2014.

[5] Brian Armstrong-Hlouvry, Pierre Dupont, and Carlos Canudas De Wit. A survey of models, analysis tools and compensation methods for the control of machines with friction. *Automatica*, 30(7):10831138, 1994.

[6] Ambarish Goswami. A new gait parameterization technique by means of cyclogram moments: Application to human slope walking. *Gait & Posture*, 8(1):15–36, 1998.

[7] Darcy S. Reisman, Robert Wityk, Kenneth Silver, and Amy J. Bastian. Locomotor adaptation on a split-belt treadmill can improve walking symmetry post-stroke. *Brain: A Journal of Neurology*, 130(Pt 7):1861–1872, July 2007.

[8] Jacquelin Perry, Judith M Burnfield, and Lydia M Cabico. *Gait analysis: normal and pathological function*. SLACK, Thorofare, NJ, 2010.

[9] George Chen, Carolynn Patten, Dhara H. Kothari, and Felix E. Zajac. Gait differences between individuals with post-stroke hemiparesis and non-disabled controls at matched speeds. *Gait & Posture*, 22(1):51–56, August 2005.

[10] Deborah S. Nichols. Balance retraining after stroke using force platform biofeedback. *Physical therapy*, 77(5):553558, 1997.

[11] Sarah Winter, Andrew Autry, Coleen Boyle, and Marshalyn Yeargin-Allsopp. Trends in the prevalence of cerebral palsy in a population-based study. *Pediatrics*, 110(6):1220–1225, 2002.

[12] Susan K. Cummins, Karin B. Nelson, Judith K. Grether, and Ellen M. Velie. Cerebral palsy in four northern california counties, births 1983 through 1985. *The Journal of Pediatrics*, 123(2):230–237, August 1993.

[13] Donald Lloyd-Jones, Robert J. Adams, Todd M. Brown, Mercedes Carnethon, Shifan Dai, Giovanni De Simone, T. Bruce Ferguson, Earl Ford, Karen Furie, Cathleen Gillespie, Alan Go, Kurt Greenlund, Nancy Haase, Susan Hailpern, P. Michael Ho, Virginia Howard, Brett Kissela, Steven Kittner, Daniel Lackland, Lynda Lisabeth, Ariane Marelli, Mary M. McDermott, James Meigs, Dariush Mozaffarian, Michael Mussolino, Graham Nichol, Vronique L. Roger, Wayne Rosamond, Ralph Sacco, Paul Sorlie, Randall Stafford, Thomas Thom, Sylvia Wasserthiel-Smoller, Nathan D. Wong, and Judith Wylie-Rosett. Heart disease and stroke statistics - 2010 update a report from the american heart association. *Circulation*, 121(7):e46–e215, February 2010.

[14] Marc Fisher. New approaches to neuroprotective drug development. *Stroke*, 42(1 suppl 1):S24–S27, January 2011. PMID: 21164111.

[15] J. D. Schaechter. Motor rehabilitation and brain plasticity after hemiparetic stroke. *Progress in neurobiology*, 73(1):61, 2004.

[16] Panel, J. P. Mohr, Gregory W. Albers, Pierre Amarenco, Viken L. Babikian, Jos Biller, Robin L. Brey, Bruce Coull, J. Donald Easton, Camilo R. Gomez, Cathy M. Helgason, Carlos S. Kase, Patrick M. Pullicino, and Alexander G. G. Turpie. Etiology of stroke. *Stroke*, 28(7):1501–1506, July 1997. PMID: 9227707.

[17] J. P. Mohr, Louis R. Caplan, John W. Melski, Robert J. Goldstein, Gary W. Duncan, J. P. Kistler, Michael S. Pessin, and Howard L. Bleich. The harvard cooperative stroke registry a prospective registry. *Neurology*, 28(8):754–754, 1978.

[18] Enas S. Lawrence, Catherine Coshall, Ruth Dundas, Judy Stewart, Anthony G. Rudd, Robin Howard, and Charles DA Wolfe. Estimates of the prevalence of acute stroke impairments and disability in a multiethnic population. *Stroke*, 32(6):1279–1284, 2001.

[19] Disa K. Sommerfeld, Elsy U.-B. Eek, Anna-Karin Svensson, Lotta Widn Holmqvist, and Magnus H. von Arbin. Spasticity after stroke its occurrence and association with motor impairments and activity limitations. *Stroke*, 35(1):134–139, 2004.

[20] Thomas K. Tatemichi, D. W. Desmond, Richard Mayeux, M. Paik, Y. Stern, M. Sano, R. H. Remien, J. B. W. Williams, J. P. Mohr, W. A. Hauser, and

others. Dementia after stroke baseline frequency, risks, and clinical features in a hospitalized cohort. *Neurology*, 42(6):1185–1185, 1992.

[21] Bengt Hagberg, Gudrun Hagberg, Eva Beckung, and Paul Uvebrant. Changing panorama of cerebral palsy in sweden. VIII. prevalence and origin in the birth year period 199194. *Acta Paediatrica*, 90(3):271–277, 2001.

[22] D.O. Hebb. *The Organization of Behavior.* Wiley, New York, 1949.

[23] R. J. Nudo and G. W. Milliken. Reorganization of movement representations in primary motor cortex following focal ischemic infarcts in adult squirrel monkeys. *Journal of Neurophysiology*, 75(5):2144–2149, May 1996.

[24] R. J. Nudo, B. M. Wise, F. SiFuentes, and G. W. Milliken. Neural substrates for the effects of rehabilitative training on motor recovery after ischemic infarct. *Science*, 272(5269):1791–1794, June 1996.

[25] Thomas Elbert, Herta Flor, Niels Birbaumer, Stefan Knecht, Scott Hampson, Wolfgang Larbig, and Edward Taub. Extensive reorganization of the somatosensory cortex in adult humans after nervous system injury. *Neuroreport*, 5(18):25932597, 1994.

[26] J. Liepert, W. H. R. Miltner, H. Bauder, M. Sommer, C. Dettmers, E. Taub, and C. Weiller. Motor cortex plasticity during constraint-induced movement therapy in stroke patients. *Neuroscience letters*, 250(1):58, 1998.

[27] Daniel Lynch, Mark Ferraro, Jenifer Krol, Christine M. Trudell, Paul Christos, and Bruce T. Volpe. Continuous passive motion improves shoulder joint integrity following stroke. *Clinical Rehabilitation*, 19(6):594–599, June 2005. PMID: 16180594.

[28] Bruce T. Volpe, Mark Ferraro, Daniel Lynch, Paul Christos, Jennifer Krol, Christine Trudell, Hermano I. Krebs, and Neville Hogan. Robotics and other devices in the treatment of patients recovering from stroke. *Current Neurology and Neuroscience Reports*, 5(6):465–470, November 2005.

[29] E. L. Miller, L. Murray, L. Richards, R. D. Zorowitz, T. Bakas, P. Clark, S. A. Billinger, et al. Comprehensive overview of nursing and interdisciplinary rehabilitation care of the stroke patient. *Stroke*, 41(10):24022448, 2010.

[30] Edward Taub, Gitendra Uswatte, and Rama Pidikiti. Constraint-induced movement therapy: a new family of techniques with broad application to physical rehabilitation-a clinical review. *Journal of rehabilitation research and development*, 36(3):237251, 1999.

[31] Steven L. Wolf, Carolee J. Winstein, J. Philip Miller, Edward Taub, Gitendra Uswatte, David Morris, Carol Giuliani, Kathye E. Light, and Deborah Nichols-Larsen. Effect of constraint-induced movement therapy on upper extremity

function 3 to 9 months after stroke. *JAMA: the journal of the American Medical Association*, 296(17):20952104, 2006.

[32] Catherine E. Lang, Jillian R. MacDonald, Darcy S. Reisman, Lara Boyd, Teresa Jacobson Kimberley, Sheila M. Schindler-Ivens, T. George Hornby, Sandy A. Ross, and Patricia L. Scheets. Observation of amounts of movement practice provided during stroke rehabilitation. *Archives of physical medicine and rehabilitation*, 90(10):1692–1698, October 2009. PMID: 19801058 PMCID: PMC3008558.

[33] Albert C. Lo, Peter D. Guarino, Lorie G. Richards, Jodie K. Haselkorn, George F. Wittenberg, Daniel G. Federman, Robert J. Ringer, Todd H. Wagner, Hermano I. Krebs, and Bruce T. Volpe. Robot-assisted therapy for long-term upper-limb impairment after stroke. *New England Journal of Medicine*, 362(19):17721783, 2010.

[34] Aisen M, Krebs H, Hogan N, McDowell F, and Volpe BT. THe effect of robot-assisted therapy and rehabilitative training on motor recovery following stroke. *Archives of Neurology*, 54(4):443–446, April 1997.

[35] Catherine M. Sackley and Nadina B. Lincoln. Physiotherapy treatment for stroke patients: a survey of current practice. *Physiotherapy Theory and Practice*, 12(2):8796, 1996.

[36] S. Hesse, C. Bertelt, M. T. Jahnke, A. Schaffrin, P. Baake, M. Malezic, and K. H. Mauritz. Treadmill training with partial body weight support compared with physiotherapy in nonambulatory hemiparetic patients. *Stroke*, 26(6):976–981, June 1995. PMID: 7762049.

[37] Ingrid GL van de Port, Sharon Wood-Dauphinee, Eline Lindeman, and Gert Kwakkel. Effects of exercise training programs on walking competency after stroke: a systematic review. *American Journal of Physical Medicine & Rehabilitation*, 86(11):935951, 2007.

[38] Christian Enzinger, Helen Dawes, Heidi Johansen-Berg, Derick Wade, Marko Bogdanovic, Jonathan Collett, Claire Guy, Udo Kischka, Stefan Ropele, Franz Fazekas, and Paul M. Matthews. Brain activity changes associated with treadmill training after. *Stroke*, 40(7):2460–2467, July 2009. PMID: 19461018.

[39] Anne M. Moseley, Angela Stark, Ian D. Cameron, and Alex Pollock. Treadmill training and body weight support for walking after stroke. *Stroke*, 34(12):30063006, 2003.

[40] P. W. Duncan, K. J. Sullivan, A. L. Behrman, S. P. Azen, S. S. Wu, S. E. Nadeau, B. H. Dobkin, D. K. Rose, and J. K. Tilson. Protocol for the locomotor experience applied post-stroke (LEAPS) trial: a randomized controlled trial. *BMC neurology*, 7(1):39, 2007.

[41] P. W. Duncan, K. J. Sullivan, A. L. Behrman, S. P. Azen, S. S. Wu, S. E. Nadeau, B. H. Dobkin, D. K. Rose, J. K. Tilson, and S. Cen. Body-weightsupported treadmill rehabilitation after stroke. *New England Journal of Medicine*, 364(21):20262036, 2011.

[42] Gery Colombo, Matthias Joerg, Reinhard Schreier, and Volker Dietz. Treadmill training of paraplegic patients using a robotic orthosis. *Journal of rehabilitation research and development*, 37(6):693700, 2000.

[43] Michael D. Lewek, Theresa H. Cruz, Jennifer L. Moore, Heidi R. Roth, Yasin Y. Dhaher, and T. George Hornby. Allowing intralimb kinematic variability during locomotor training poststroke improves kinematic consistency: A subgroup analysis from a randomized clinical trial. *Physical Therapy*, 89(8):829–839, August 2009. PMID: 19520734.

[44] R. Riener, L. Lunenburger, S. Jezernik, M. Anderschitz, G. Colombo, and V. Dietz. Patient-cooperative strategies for robot-aided treadmill training: first experimental results. *IEEE Transactions on Neural Systems and Rehabilitation Engineering*, 13(3):380–394, 2005.

[45] A. Duschau-Wicke, J. von Zitzewitz, A. Caprez, L. Lunenburger, and R. Riener. Path control: A method for patient-cooperative robot-aided gait rehabilitation. *IEEE Transactions on Neural Systems and Rehabilitation Engineering*, 18(1):38–48, 2010.

[46] Britta Husemann, Friedemann Mller, Carmen Krewer, Silke Heller, and Eberhardt Koenig. Effects of locomotion training with assistance of a robot-driven gait orthosis in hemiparetic patients after stroke a randomized controlled pilot study. *Stroke*, 38(2):349–354, February 2007. PMID: 17204680.

[47] Andreas Mayr, Markus Kofler, Ellen Quirbach, Heinz Matzak, Katrin Frhlich, and Leopold Saltuari. Prospective, blinded, randomized crossover study of gait rehabilitation in stroke patients using the lokomat gait orthosis. *Neurorehabilitation and Neural Repair*, 21(4):307–314, July 2007. PMID: 17476001.

[48] J. Hidler, D. Nichols, M. Pelliccio, K. Brady, D. D. Campbell, J. H. Kahn, and T. G. Hornby. Multicenter randomized clinical trial evaluating the effectiveness of the lokomat in subacute stroke. *Neurorehabilitation and Neural Repair*, 23(1):513, 2009.

[49] T. George Hornby, Donielle D. Campbell, Jennifer H. Kahn, Tobey Demott, Jennifer L. Moore, and Heidi R. Roth. Enhanced gait-related improvements after therapist- versus robotic-assisted locomotor training in subjects with chronic stroke a randomized controlled study. *Stroke*, 39(6):1786–1792, June 2008.

[50] J.F. Veneman, R. Kruidhof, E.E.G. Hekman, R. Ekkelenkamp, E.H.F. van Asseldonk, and H. van der Kooij. Design and evaluation of the LOPES exoskeleton

robot for interactive gait rehabilitation. *IEEE Transactions on Neural Systems and Rehabilitation Engineering*, 15(3):379 –386, September 2007.

[51] S.K. Banala, S.K. Agrawal, and J.P. Scholz. Active leg exoskeleton (ALEX) for gait rehabilitation of motor-impaired patients. In *IEEE 10th International Conference on Rehabilitation Robotics, 2007. ICORR 2007*, pages 401–407, 2007.

[52] D. Uhlenbrock, T. SarkodieGyan, F. Reiter, M. Konrad, and S. Hesse. Development of a servo-controlled gait trainer for the rehabilitation of non-ambulatory patients. *Biomedizinische Technik*, 42(7-8):196202, 1997.

[53] Stefan Hesse and Dietmar Uhlenbrock. A mechanized gait trainer for restoration of gait. *Journal of rehabilitation research and development*, 37(6):701708, 2000.

[54] Henning Schmidt, Cordula Werner, Rolf Bernhardt, Stefan Hesse, and Jrg Krger. Gait rehabilitation machines based on programmable footplates. *Journal of neuroengineering and rehabilitation*, 4(1):2, 2007.

[55] Stefan Hesse, Andreas Waldner, and Christopher Tomelleri. Innovative gait robot for the repetitive practice of floor walking and stair climbing up and down in stroke patients. *J NeuroEngineering and Rehabilitation*, 7(30), 2010.

[56] S. Hesse, D. Uhlenbrock, and T. Sarkodie-Gyan. Gait pattern of severely disabled hemiparetic subjects on a new controlled gait trainer as compared to assisted treadmill walking with partial body weight support. *Clinical Rehabilitation*, 13(5):401–410, May 1999. PMID: 10498347.

[57] S. Hesse, C. Werner, D. Uhlenbrock, S. V. Frankenberg, A. Bardeleben, and B. Brandl-Hesse. An electromechanical gait trainer for restoration of gait in hemiparetic stroke patients: Preliminary results. *Neurorehabilitation and Neural Repair*, 15(1):39–50, March 2001. PMID: 11527278.

[58] M. Pohl, C. Werner, M. Holzgraefe, G. Kroczek, J. Mehrholz, I. Wingendorf, G. H.lig, R. Koch, and S. Hesse. Repetitive locomotor training and physiotherapy improve walking and basic activities of daily living after stroke: a single-blind, randomized multicentre trial (DEutsche GAngtrainerStudie, DEGAS). *Clinical Rehabilitation*, 21(1):17–27, January 2007.

[59] Stefan Hesse, Christopher Tomelleri, Anita Bardeleben, Cordula Werner, and Andreas Waldner. Robot-assisted practice of gait and stair climbing in nonambulatory stroke patients. *J Rehabil Res Dev*, 49(4):613622, 2012.

[60] Adrian Lees, Jos Vanrenterghem, Gabor Barton, and Mark Lake. Kinematic response characteristics of the CAREN moving platform system for use in posture and balance research. *Medical Engineering & Physics*, 29(5):629–635, June 2007.

[61] Larry W. Forrester, Anindo Roy, Hermano Igo Krebs, and Richard F. Macko. Ankle training with a robotic device improves hemiparetic gait after a stroke. *Neurorehabilitation and Neural Repair*, 25(4):369–377, May 2011.

[62] Larry W. Forrester, Anindo Roy, Amanda Krywonis, Glenn Kehs, Hermano Igo Krebs, and Richard F. Macko. Modular ankle robotics training in early subacute stroke a randomized controlled pilot study. *Neurorehabilitation and Neural Repair*, page 1545968314521004, February 2014. PMID: 24515923.

[63] Ira Khanna, Anindo Roy, M. Rodgers, H. Krebs, R. Macko, and L. Forrester. Research effects of unilateral robotic limb loading on gait characteristics in subjects with chronic stroke. *J NeuroEngineering and Rehabilitation*, 7, 2010.

[64] Jooeun Ahn and Neville Hogan. Feasibility of dynamic entrainment with ankle mechanical perturbation to treat locomotor deficit. In *Engineering in Medicine and Biology Society (EMBC), 2010 Annual International Conference of the IEEE*, pages 3422–3425. IEEE, 2010.

[65] Y. P. Ivanenko, R. Grasso, V. Macellari, and F. Lacquaniti. Control of foot trajectory in human locomotion: role of ground contact forces in simulated reduced gravity. *Journal of neurophysiology*, 87(6):3070–3089, 2002.

[66] Renato Grasso, Yuri P. Ivanenko, Myrka Zago, Marco Molinari, Giorgio Scivoletto, Vincenzo Castellano, Velio Macellari, and Francesco Lacquaniti. Distributed plasticity of locomotor pattern generators in spinal cord injured patients. *Brain*, 127(5):1019–1034, 2004.

[67] Todd H. Wagner, Albert C. Lo, Peter Peduzzi, Dawn M. Bravata, Grant D. Huang, Hermano I. Krebs, Robert J. Ringer, Daniel G. Federman, Lorie G. Richards, Jodie K. Haselkorn, George F. Wittenberg, Bruce T. Volpe, Christopher T. Bever, Pamela W. Duncan, Andrew Siroka, and Peter D. Guarino. An economic analysis of robot-assisted therapy for long-term upper-limb impairment after. *Stroke*, 42(9):2630–2632, September 2011.

[68] Neville Hogan and Dagmar Sternad. Dynamic primitives of motor behavior. *Biological Cybernetics*, 106(11-12):727–739, December 2012.

[69] Tamar Flash and Ealan Henis. Arm trajectory modifications during reaching towards visual targets. *Journal of cognitive Neuroscience*, 3(3):220230, 1991.

[70] S. Schaal, D. Sternad, R. Osu, and M. Kawato. Rhythmic arm movement is not discrete. *Nature neuroscience*, 7(10):11361143, 2004.

[71] Tsuyoshi Ikegami, Masaya Hirashima, Gentaro Taga, and Daichi Nozaki. Asymmetric transfer of visuomotor learning between discrete and rhythmic movements. *The Journal of Neuroscience*, 30(12):4515–4521, 2010.

[72] Karl T Ulrich and Steven D Eppinger. *Product design and development*. McGraw-Hill/Irwin, Boston, 2004.

[73] Caitlyn Bosecker. *Design of a Robot for Gait Rehabilitation*. PhD thesis, Mech Eng., MIT, Cambridge, MA, 2009.

[74] Steven H. Collins, Martijn Wisse, and Andy Ruina. A three-dimensional passive-dynamic walking robot with two legs and knees. *The International Journal of Robotics Research*, 20(7):607–615, July 2001.

[75] Alvin R. Tilley. *The measure of man and woman: human factors in design*. Whitney Library of Design, New York, 1993.

[76] Marion Trew and Tony Everett. *Human Movement: An Introductory Text, 5e*. Churchill Livingstone, Edinburgh; New York, 5 edition edition, December 2005.

[77] P.K. Artemiadis and H.I. Krebs. On the potential field-based control of the MIT-skywalker. In *2011 IEEE International Conference on Robotics and Automation (ICRA)*, pages 1427–1432, May 2011.

[78] Yasuhiro Osaki, Mikhail Kunin, Bernard Cohen, and Theodore Raphan. Three-dimensional kinematics and dynamics of the foot during walking: a model of central control mechanisms. *Experimental brain research*, 176(3):476–496, 2007.

[79] Erik Oberg. *Machinery's handbook: a reference book for the mechanical engineer, designer, manufacturing engineer, draftsman, toolmaker, and machinist*. Industrial Press, New York, 2008.

[80] Joseph Shigley, Charles Mischke, and Richard Budynas. *Mechanical Engineering Design*. McGraw-Hill Science/Engineering/Math, 7 edition edition, July 2003.

[81] Robert L. Norton. *Design of Machinery*. Tata McGraw-Hill, 3rd edition edition, 2004.

[82] Alexander H. Slocum. *Precision machine design*. SME, 1992.

[83] Layton C. (Layton Carter) Hale. *Principles and techniques for desiging precision machines*. Thesis, Massachusetts Institute of Technology, 1999. Thesis (Ph.D.)–Massachusetts Institute of Technology, Dept. of Mechanical Engineering, 1999.

[84] Alexander H. Slocum. *FUNdaMENTALS of Design*. 2007.

[85] TS Keller, AM Weisberger, JL Ray, SS Hasan, RG Shiavi, and DM Spengler. Relationship between vertical ground reaction force and speed during walking, slow jogging, and running. *Clinical Biomechanics*, 11(5):253–259, July 1996.

[86] J. Nilsson and A. Thorstensson. Ground reaction forces at different speeds of human walking and running. *Acta Physiologica Scandinavica*, 136(2):217227, 1989.

[87] Anindo Roy, Hermano Igo Krebs, Dustin J. Williams, Christopher T. Bever, Larry W. Forrester, Richard M. Macko, and Neville Hogan. Robot-aided neurorehabilitation: a novel robot for ankle rehabilitation. *Robotics, IEEE Transactions on*, 25(3):569582, 2009.

[88] Jun Young Yoon and David L. Trumper. Friction modeling, identification, and compensation based on friction hysteresis and dahl resonance. *Mechatronics*, 24(6):734–741, September 2014.

[89] P.K. Artemiadis and H.I. Krebs. On the control of the MIT-skywalker. In *2010 Annual International Conference of the IEEE Engineering in Medicine and Biology Society (EMBC)*, pages 1287–1291, August 2010.

[90] Darcy S. Reisman, Heather McLean, Jennifer Keller, Kelly A. Danks, and Amy J. Bastian. Repeated split-belt treadmill training improves poststroke step length asymmetry. *Neurorehabilitation and Neural Repair*, 27(5):460–468, June 2013.

[91] Thierry Troosters, Rik Gosselink, and Marc Decramer. Six minute walking distance in healthy elderly subjects. *European Respiratory Journal*, 14(2):270–274, 1999.

[92] Richard W. Bohannon. Comfortable and maximum walking speed of adults aged 2079 years: reference values and determinants. *Age and ageing*, 26(1):15–19, 1997.

[93] Robert A Wise and Cynthia D Brown. Minimal clinically important differences in the six-minute walk test and the incremental shuttle walking test. *COPD*, 2(1):125–129, March 2005.

[94] Patricia A. Goldie, Thomas A. Matyas, and Owen M. Evans. Gait after stroke: initial deficit and changes in temporal patterns for each gait phase. *Archives of physical medicine and rehabilitation*, 82(8):1057–1065, 2001.

[95] Jeffrey M. Hausdorff, Merit E. Cudkowicz, Rene Firtion, Jeanne Y. Wei, and Ary L. Goldberger. Gait variability and basal ganglia disorders: Stride-to-stride variations of gait cycle timing in parkinson's disease and huntington's disease. *Movement Disorders*, 13(3):428–437, May 1998.

[96] P. R. Cavanagh and P. V. Komi. Electromechanical delay in human skeletal muscle under concentric and eccentric contractions. *European journal of applied physiology and occupational physiology*, 42(3):159–163, 1979.

[97] Seung-Jae Kim and Hermano Igo Krebs. Effects of implicit visual feedback distortion on human gait. *Experimental brain research*, 218(3):495–502, 2012.

[98] Seung-Jae Kim and Dieudonne Mugisha. Effect of explicit visual feedback distortion on human gait. *Journal of neuroengineering and rehabilitation*, 11(1):74, 2014.

[99] Marcus Pohl, Jan Mehrholz, Claudia Ritschel, and Stefan Rckriem. Speed-dependent treadmill training in ambulatory hemiparetic stroke patients a randomized controlled trial. *Stroke*, 33(2):553–558, February 2002.

[100] Katherine J. Sullivan, Barbara J. Knowlton, and Bruce H. Dobkin. Step training with body weight support: effect of treadmill speed and practice paradigms on poststroke locomotor recovery. *Archives of Physical Medicine and Rehabilitation*, 83(5):683–691, May 2002.

[101] Kara K. Patterson, Iwona Parafianowicz, Cynthia J. Danells, Valerie Closson, Mary C. Verrier, W. Richard Staines, Sandra E. Black, and William E. McIlroy. Gait asymmetry in community-ambulating stroke survivors. *Archives of physical medicine and rehabilitation*, 89(2):304–310, 2008.

[102] Sandra J. Olney and Carol Richards. Hemiparetic gait following stroke. part i: Characteristics. *Gait & Posture*, 4(2):136–148, 1996.

[103] T. F. Winters, J. R. Gage, and R. Hicks. Gait patterns in spastic hemiplegia in children and young adults. *J Bone Joint Surg Am*, 69(3):437–441, 1987.